Quantifying the impact of climate change on power demand and associated CO2 emissions with machine learning methods

Léna Gurriaran

université PARIS-SACLAY

Quantifying the impact of climate change on power demand and associated CO_2 emissions with machine learning methods

Quantifier l'impact du changement climatique sur la demande en électricité et les émissions de CO_2 associées par des méthodes de machine learning

Thèse de doctorat de l'Université Paris-Saclay

École doctorale n°129, Sciences de l'Environnement d'Ile-de-France (SEIF)
Spécialité de doctorat: Géosciences
Graduate School : Géosciences, climat, environnement et planètes.
Référent : Université de Versailles Saint-Quentin-en-Yvelines

Thèse préparée dans l'unité de recherche **LSCE** (Université Paris-Saclay, CNRS, CEA, UVSQ), sous la direction de **Philippe CIAIS**, directeur de recherche CEA au LSCE

Thèse soutenue à Paris-Saclay, le 21 décembre 2023, par

Léna GURRIARAN

Composition du jury

Membres du jury avec voix délibérative

Masa KAGEYAMA Directrice de Recherche, LSCE	Présidente
Jairo CUGLIARI Maître de conférence HDR, Université Lumière 2	Rapporteur & Examinateur
Italia DE FEIS Chercheur Senior, CNR-IAC	Rapportrice & Examinatrice
Philippe DROBINSKI Directeur de Recherche, LMD	Examinateur
Mathilde MOUGEOT Professeure des Universités, ENSIIE	Examinatrice

THESE DE DOCTORAT

NNT : 2023UPASJ031

université PARIS-SACLAY

ÉCOLE DOCTORALE
Sciences de l'Environnement d'Île-de-France (SEIF)

Titre: Quantifier l'impact du changement climatique sur la demande en électricité et les émissions de CO_2 associées par des méthodes de machine learning
Mots clés: réchauffement climatique, énergie, carbone, apprentissage automatique

Résumé: Les activités humaines, à travers l'émission de gaz à effet de serre (GES), en particulier le dioxyde de carbone (CO_2), sont la principale cause du réchauffement climatique. Ce réchauffement a des répercussions significatives sur les activités humaines, notamment dans le secteur de l'énergie et de la production d'électricité. L'augmentation des températures, dépassant déjà 1°C et atteignant localement des valeurs plus élevées, influence directement la demande énergétique. Elle favorise le recours à la climatisation tout en réduisant le besoin de chauffage. Comprendre ces impacts est essentiel pour les décideurs politiques et les acteurs de l'énergie afin d'anticiper les défis liés à la distribution et à la capacité de production. De plus, la production d'électricité à partir de sources fossiles contribue aux émissions de CO_2, créant ainsi une boucle de rétroaction entre production d'énergie et réchauffement climatique.

Pour répondre à ces enjeux, cette thèse vise à développer des modèles de simulation de la demande journalière en électricité à l'échelle nationale en utilisant des modèles de Machine Learning (ML) entraînés sur des données climatiques (réanalyses ERA5) et socio-économiques. Deux cas d'études, le Qatar et le Japon, ont permis de développer la méthode ensuite appliquée à l'ensemble du globe. Au Qatar, un modèle simulant la demande basée sur une régression polynomiale du second ordre de la température journalière a été développé. Au Japon plusieurs modèles utilisant différents régresseurs d'apprentissage automatique, Random Forest, Gradient Boosting et Multivariate Adaptive Regression Spline, ont été testés pour simuler la demande (et l'intensité carbone) journalière, avec un plus grand nombre de variables climatiques. À partir de ces modèles, les variables clés influençant la demande ont été identifiées grâce à des méthodes d'interprétation (Partial Dependence, Local Accumulated Effect, Shapley Values). Ces modèles ont ensuite été utilisés pour projeter la demande en électricité jusqu'en 2100, en utilisant des projections de variables climatiques (CMIP6, ISIMIP3b) et socio-économiques pour différents scénarios futurs. Les émissions de CO_2 associées ont été calculées en faisant des hypothèses sur l'évolution des mix énergétiques des pays.

Cette méthodologie a ensuite été appliquée à une dizaine de pays (Australie, Brésil, Union Européenne, Inde, Chine, Afrique du Sud, Russie, Chili, Mexique, Norvège et Etat Unis) pour lesquels des données de demande en électricité sont disponibles grâce au projet Carbon Monitor, en ajoutant les Modèle Additif Généralisé à la liste des modèles de ML testés. Pour les pays sans données énergétiques, un pays (et modèle) de référence parmi ceux précédemment cités leur a été attribué en se basant sur leurs similitudes climatiques et socio-économiques. Pour ces pays, le modèle de référence a été appliqué avec leur propre projections climatiques et socio-économiques pour estimer l'évolution de leur demande en électricité en réponse au changement climatique. Les émissions de CO_2 issue de la production d'électricité globale ont été calculées en utilisant des projections d'intensité carbone disponibles à l'échelle de grandes régions issues du modèle d'évaluation intégré IMAGE3.2. Enfin, ces émissions de CO_2 ont été ajoutées à un modèle climatique simplifié pour évaluer leur impact sur la température globale.

Les résultats indiquent que dans les hautes latitudes, la baisse de la demande en chauffage peut parfois surpasser l'augmentation liée à la climatisation, tandis que sous les tropiques, l'augmentation de la demande en climatisation est plus marquée. Globalement, les émissions supplémentaires de CO_2 ont un impact faible sur la température globale, bien que localement et ponctuellement pendant certains mois de l'année, des augmentations significatives de la demande en électricité aient été observées.

université PARIS-SACLAY | ÉCOLE DOCTORALE Sciences de l'Environnement d'Île-de-France (SEIF)

Title: Quantifying the impact of climate change on power demand and associated CO_2 emissions with machine learning methods
Keywords: global warming, energy, carbon, machine learning

Abstract: Human activities are the main driver of anthropogenic global warming through the emission of greenhouse gases (GHGs), in particular carbon dioxide (CO_2). The global warming has significant impacts on human activities, particularly in the energy and power generation sectors. Rising temperatures, already +1°C compared to the pre-industrial era and locally higher, have a direct impact on energy demand. It encourages the use of air conditioning while reducing the need for heating. Understanding these impacts is essential for policymakers and energy system planners to prepare for challenges related to distribution and production capacity. In addition, power generation from fossil fuels contributes to CO_2 emissions, creating a feedback loop: human activities → global warming → human activities.

To address these issues, this thesis aims to develop national simulation models of daily power demand using machine learning methods trained on climatic (ERA5 reanalyses) and socioeconomic data. Two case studies, Qatar and Japan, were used to develop the methodology, which was then applied globally. A demand simulation model based on second-order polynomial regression was developed in Qatar. In Japan, several models using different machine learning regressors, including Random Forest, Gradient Boosting, and Multivariate Adaptive Regression Spline, were tested to simulate daily demand and carbon intensity. From these models, the key variables influencing demand were identified using interpretation methods (Partial Dependence, Local Accumulated Effect, Shapley Values, and Feature Importance). These models were then used to project power demand over the course of the century, using daily climate (CMIP6, ISIMIP3b) and socioeconomic projections for different future scenarios. CO_2 emissions from power generation were calculated by assuming fixed energy mixes.

This methodology was then applied to more than ten countries (Australia, Brazil, the European Union, India, China, South Africa, Russia, Chile, Mexico, Norway, and the USA) for which power demand data are available through the Carbon Monitor project. Generalized Additive Models were added to the list of machine learning models tested. For the other countries, a reference country was selected from the above countries using the k-means method based on climatic and socioeconomic similarities. For these countries, the reference model was applied with their own climatic and socioeconomic projections to estimate the evolution of their power demand in response to climate change. CO_2 emissions from global power generation were calculated using regionally available carbon intensity projections from the IMAGE3.2 integrated assessment model.

Finally, these CO_2 emissions were added to a simple climate model ACC2 to assess their impact on global temperature. The results show that in high latitudes, the decrease in power demand due to global warming can sometimes outweigh the increase due to air conditioning, while in the tropics, the increase in air conditioning demand is more pronounced. Overall, these additional CO_2 emissions have very little impact on global temperatures, although locally and temporarily significant increases in power demand are observed.

Les activités humaines, à travers l'émission de gaz à effet de serre (GES), en particulier le dioxyde de carbone (CO_2), sont la principale cause du réchauffement climatique. En retour, le réchauffement a des répercussions significatives sur les activités humaines, notamment dans le secteur de l'énergie et de la production d'électricité. L'augmentation des températures, dépassant déjà 1°C et atteignant localement des valeurs plus élevées, influence directement la demande énergétique. Elle favorise le recours à la climatisation lors des périodes chaudes tout en réduisant le besoin de chauffage dans les pays connaissant des hivers froids. Comprendre précisément l'ampleur de ces impacts est essentiel pour les décideurs politiques et les acteurs de l'énergie afin d'anticiper les défis liés à la distribution et à la capacité de production de l'électricité. De plus, la production d'électricité à partir de sources fossiles relâche des émissions de CO_2 contribuant au réchauffement climatique, créant ainsi une boucle de rétroaction entre production d'énergie et réchauffement climatique.

Pour répondre à ces enjeux, cette thèse vise à développer des modèles de simulation de la demande journalière en électricité à l'échelle nationale en utilisant des modèles de Machine Learning (ML) entraînés sur des données climatiques (réanalyses ERA5) et socio-économiques. Deux cas d'études, le Qatar et le Japon, ont permis de développer la méthode ensuite appliquée à l'ensemble du globe.

Au Qatar, un modèle simulant la demande basée sur une régression polynomiale du second ordre a été développé. Les variables prédictives utilisées pour ce cas d'étude sont la température et les jours de la semaine car on observe une différence significative entre la demande en électricité pendant les jours ouvrés (plus importante) et les week-ends (plus faible).

Le cas d'étude du Japon étant plus complexe, plusieurs modèles utilisant différents régresseurs d'apprentissage automatique; Random Forest, Gradient Boosting et Multivariate Adaptive Regression Spline, ont été testés pour simuler la demande journalière, avec un plus grand nombre de variables climatiques. Ces variables climatiques incluent la température, l'humidité relative, les rayonnements solaires, la vitesse du vent et les précipitations. A partir de la température et de l'humidité relative, des indicateurs de stress thermique représentant l'impact de la combinaison chaleur et humidité sur le corps humain sont calculés et inclus dans les variables prédictives. Les jours de la semaine sont toujours pris en compte dans les modèles. Les modèles de Machine Learning (ML) ainsi développés sont ensuite interprétés avec diverses méthodes (Partial Dependence, Local Accumulated Effect, Shapley Values) pour identifier les variables clés influençant la demande et leur

impact sur la demande journalière. Pour le Japon, l'intensité carbone, qui représente la quantité de CO_2 émise pour chaque unité d'électricité produite, a été simulée de la même manière. L'analyse a été conduite à l'échelle régionale, étant donné que les dix entreprises productrices d'électricité représentant chacune une région rendent les données de demande et de production d'électricité accessibles publiquement.

Les modèles développés au Qatar et au Japon ont ensuite été utilisés pour projeter la demande en électricité jusqu'en 2100, en utilisant des projections de variables climatiques (CMIP6, ISIMIP3b) et socio-économiques pour différents scénarios futurs. Les scénarios futurs utilisés ici sont les Shared Socioeconomic Pathways (SSPs) développés par le Groupe d'Expert Intergouvernemental sur l'Evolution du Climat (GIEC) qui représentent différents futurs possibles et sont associés à des quantités d'émissions de CO_2 résultant en des changements de température plus ou moins importants. Les émissions de CO_2 associées à la demande en électricité ont été calculées en faisant des hypothèses sur l'évolution des mix énergétiques des pays. Au Qatar les hypothèses sont basées sur les ressources du pays en énergies renouvelables et ses engagements communiqués à l'UNFCCC (Convention-cadre des Nations unies sur les changements climatiques). Au Japon ce sont des sorties du modèle d'évaluation intégrée IMAGE3.2 qui ont été utilisées pour calculer les trajectoires de l'intensité carbone de la production d'électricité.

La méthodologie de développement de modèle utilisé pour le Japon a ensuite été appliquée à une dizaine de pays (Australie, Brésil, Union Européenne, Inde, Chine, Afrique du Sud, Russie, Chili, Mexique, Norvège et États Unis) pour lesquels des données de demande en électricité sont disponibles grâce au projet Carbon Monitor, en ajoutant les Modèles Additifs Généralisés (GAM) à la liste des modèles d'apprentissage automatique testés. Des modèles simulant la demande en électricité journalière pour chacun de ces pays ont ainsi été obtenus et utilisés pour projeter la demande dans le futur selon trois SSPs et les émissions de CO_2 ont été calculées avec la même méthode que pour le Japon. Pour les pays sans données énergétiques, un pays (et modèle) de référence parmi ceux précédemment cités leur a été attribué en se basant sur leurs similitudes climatiques et socio-économiques. Les groupes de pays ont été réalisés avec la technique de clustering des k-means. Pour ces pays, le modèle de référence a été appliqué avec leurs propres projections climatiques et socio-économiques pour estimer l'évolution de leur demande en électricité en réponse au changement climatique. Les émissions de CO_2 issues de la production d'électricité globale ont été calculées en utilisant des projections d'intensité carbone disponibles à l'échelle de grandes régions issues du

modèle d'évaluation intégrée IMAGE3.2. Enfin, ces émissions de CO_2 ont été ajoutées à un modèle climatique simplifié (ACC2) pour évaluer leur impact sur la température globale.

Les résultats indiquent que dans les hautes latitudes, la baisse de la demande en chauffage peut parfois surpasser l'augmentation liée à la climatisation résultant en une baisse de demande en électricité. Ce phénomène est particulièrement important pour le Canada et la Russie. Sous les tropiques et pour certains pays déjà fortement consommateurs de climatisation comme les États Unis, l'augmentation de la demande en climatisation est plus marquée et résulte en une hausse annuelle de demande en électricité. Pour les autres pays ou régions tempérées tels que l'Europe ou le Japon la baisse de demande en électricité en hiver compense l'augmentation de la demande en été, résultant en un changement net de demande annuelle en électricité faible, de l'ordre de moins de cinq pourcents d'ici la fin du siècle. En revanche à l'échelle saisonnière et mensuelle des changements importants, jusqu'à +50% pour certains pays d'ici la fin du siècle, ont été observés avec les projections des modèles. Globalement, les émissions supplémentaires de CO_2 dues au changement climatique ont un impact très faible sur la température globale, de l'ordre de moins d'un dixième de degré.

During my Ph.D., I wrote three papers as a first author, presented below. The two first papers have already been published, and the last one is in the review process. The first two papers constitute the major part of Chapter II and III, and the last one constitutes almost all Chapter IV. The supplementary materials of the papers can be found in the Appendix section.

Gurriaran, L., Tanaka, K., Bayram, I. S., Proestos, Y., Lelieveld, J., & Ciais, P. 2023. Warming-induced increase in power demand and CO_2 emissions in Qatar and the Middle East. *Journal of Cleaner Production, 382, 135359,* https://doi.org/10.1016/j.jclepro.2022.135359.

Gurriaran, L., Tanaka, K., Takahashi, K., & Ciais, P. 2023. How climate change may shift power demand in Japan: Insights from data-driven analysis. *Journal of Environmental Management, Journal of Cleaner Production, 345, 118799,* https://doi.org/10.1016/j.jenvman.2023.118799.

Gurriaran, L., Goude, Y., Tanaka, K., Zhu, B., Deng, Z., Song, X., & Ciais, P. 2023. Carbon Monitor Power - Simulators (CMP-SIM v1.0) across countries: a data-driven approach to simulate daily power demand. *Geoscientific Model Development (in review).*

Pour leur encadrement, l'intérêt qu'ils ont porté à ma recherche, l'écriture de mes premiers articles et plus généralement leur aide précieuse pendant la thèse, je voudrais évidemment commencer par remercier mes maïtres de thèse, Philippe, Katsu et Yannig.

Pour leur contribution moins scientifique, mais pas moins importante à ma vie pendant la thèse, merci à mes ami·es de longue date, Cassandre, Marine, Abi, Laure, Matthieu, Inès, Estelle, Hugo, Chiara, Octave, Thomas, Lucie, Corentin, Arthur, Bryan, Léo, Philippe… Merci à Mémé pour son écoute patiente et son support inconditionnel, "t'inquiète ça va le faire". À Isma, Yann et Martin, acolytes tout au long de la thèse et gros support de fin de thèse, sans qui le quotidien au labo n'aurait pas été le même.

Enfin merci à ma famille pour tout ce qu'elle m'a transmis, qui m'a permis de faire de cette thèse ce qu'elle était. Grand-Pa pour son amour de la montagne, Grand-Ma pour ses réflexions sur la société, Lela Toya pour son bon goût et Abuelo pour son humour malicieux qui rend tout plus joyeux. Et par-dessus tout, merci à Pinp, Minm, Bak et Kok qui ont toujours été présents, l'écoute et ont contribué plus que tout à ce que j'en arrive à faire cette thèse.

CONTENTS

I General Introduction **1**

1 General Context . . . 1

2 The Carbon Monitor project . . . 2

3 Climate Sensitivity of Power Demand . . . 6

3.1 Dynamics between Electricity Demand and Climate . . . 6

3.2 Temperature Response Functions with Carbon Monitor data . . . 8

4 Impact of Climate Change on the Energy Sector . . . 11

4.1 Energy Challenges and Issues in the Context of Climate Change . . . 11

4.2 Electricity Demand and Climate Change . . . 13

5 From power demand to CO_2 emissions . . . 16

6 The general framework . . . 18

6.1 The Machine Learning Approach . . . 19

6.1.1 Description of ML models . . . 19

6.1.2 The Significance of Interpretability in Taming ML Model Black Boxes 22

6.2 Description of the Shared Socioeconomic Pathways . . . 23

6.3 General Data Description . . . 25

6.3.1 Description of the ERA5 Climate Input Data . . . 25

6.3.2 Description of the ISIMIP Climate Input Data . . . 25

6.4 What is this Approach Made for? . . . 26

References . . . 28

II Case Study of Qatar **33**

1 Summary . . . 34

2 Abstract . . . 35

3 Introduction . . . 36

3.1 Background . . . 36
3.2 Literature Review . . . 37
3.3 Description of the Case Study . . . 38
4 Material and Methods: Model Development . . . 40
5 Results . . . 44
5.1 Temperature Impact on Electricity Demand in Qatar . . . 44
5.1.1 Annual Average Temperature and Electricity Demand . . . 44
5.1.2 Extreme Annual Temperatures and Electricity Demand . . . 45
5.2 Implication for CO_2 Emissions in Qatar . . . 46
5.3 Generalization of the Study to Gulf Cooperation Council (GCC) Countries . . . 48
6 Discussion . . . 49
7 Conclusion . . . 51
References . . . 52

III Case Study of Japan **55**
1 Summary . . . 56
2 Abstract . . . 57
3 Introduction . . . 58
4 Data and Methods . . . 60
4.1 Training Data . . . 62
4.2 Model Development and Selection . . . 63
4.3 Projections . . . 64
4.4 Socioeconomic Scenarios . . . 66
5 Results . . . 67
5.1 Regional Models: Important Features Explaining Daily Power Demand and Carbon Intensity Variations in Each Region . . . 67
5.2 Impact of Future Climate Change on Power Demand, Carbon Intensity, and CO_2 Emissions . . . 70
5.3 Attribution of the Changes in Power Demand and CO_2 Emissions . . . 72
6 Influence of Socioeconomic Factors . . . 74
7 Discussion . . . 75
References . . . 79

IV Carbon Monitor Power - Simulators **83**
1 Summary . . . 84
2 Abstract . . . 85
3 Introduction . . . 86
4 Data . . . 88
4.1 Predictive Features . . . 88
4.2 Target Features . . . 90
5 Model Development . . . 91
5.1 Partitioning of Input Data Into Learning and Test Subsets . . . 92
5.2 Random Search with Cross-Validation and Evaluating Metrics . . . 93
5.3 Interpretation of the Models with Permutation Feature Importance and ALE Plots . . . 94
5.4 Model Validation . . . 95
6 Output of the Models . . . 97
7 Discussion . . . 102
7.1 Model Inter-Comparison in Different Countries . . . 102
7.2 Validation and Limits of the Models . . . 105
8 Perspective . . . 108
References . . . 110

V Projections **115**
1 Adaptation of CMP-SIMv1.0 . . . 116
2 Projections of Power Demand at the National Scale . . . 117
2.1 Climate and Socioeconomic Features Projections . . . 117
2.2 How to Attribute Each Country to a Reference Country? . . . 119
2.3 Evolution of Power Demand with Global Projections and Representing Countries . . . 121
2.4 Seasonal Evolution of Power Demand . . . 126
3 Carbon Intensity Projections . . . 133
3.1 The IMAGE3.2 Model . . . 133
3.2 National and Regional Projections of Carbon Intensity . . . 135
4 CO_2 Emissions Projections . . . 138
4.1 Additionnal CO_2 Emissions Due to Climate Change . . . 138

4.2 Global CO_2 Emissions . . . 144
4.3 Impact of Carbon Intensity on CO_2 emissions . . . 145
5 Limitations . . . 146
5.1 Machine Learning Models Extrapolation Assumption . . . 146
5.2 Lack of Data to Predict Cooling Demand . . . 148
5.3 Major Energy Data Gaps . . . 150
References . . . 152

VI Conclusion and Perspectives **153**
1 Perspective . . . 153
1.1 Multi-Country Models: a Possible Solution to Adress Data Limitation . . . 153
1.2 Power Demand Extreme Events Models . . . 155
1.3 Feedback on Global Temperature . . . 156
2 General Conclusion . . . 157
References . . . 159

A Appendix A: Case Study Articles **161**
1 Supplementary Material of Article 1 . . . 161
2 Supplementary Material of Article 2 . . . 167

B Appendix B - Power Models Article **181**
1 Supplementary Material of Article 3 . . . 181

C Appendix C - Additional CO_2 maps **221**

CHAPTER I

GENERAL INTRODUCTION

1 General Context

My thesis deals with two of the most challenging topics of recent years: climate change and energy. Climate change refers to the long-term change in the Earth's average weather patterns caused mainly by anthropogenic emissions of greenhouse gases into the atmosphere. The emission of greenhouse gases results in an enhanced greenhouse effect, which traps heat and leads to global warming and associated climate shifts. So far, the global average temperature has risen by +1.1°C compared to the pre-industrial level, with significant regional differences in temperature changes (IPCC, 2023). Energy, on the other hand, is a fundamental driver of human activities and economic development. It encompasses a wide range of sources, including fossil fuels such as coal, oil, and natural gas, as well as renewable sources such as solar, wind, hydro, and geothermal. However, the energy sector faces significant challenges from climate change and societal demands, with a strong focus on sustainability, efficiency, and environmental impact. Climate and energy are inextricably linked and present a tough challenge. This interconnection stems from a feedback loop between these two critical factors. Human activities require energy, and the production of energy often involves the burning of fossil fuels, which emits greenhouse gases into the atmosphere. Carbon dioxide (CO_2) is the most significant greenhouse gas emitted during energy production. CO_2 accounts for a significant portion of total greenhouse gas emissions worldwide. Other gases such as methane (CH_4) and nitrous oxide (N_2O) are also emitted during the extraction, production, or combustion of fossil fuels. Such emissions are undoubtedly responsible for exacerbating climate change (IPCC, 2023). Conversely, the changing climate affects human activities and energy consumption. Extreme weather events, rising sea levels, and changing precipitation patterns, among other

climate-related impacts, directly affect industry, agriculture, and infrastructure. These changes influence the amount of greenhouse gases released into the atmosphere, creating a complex interplay between climate change and energy use.

A key question that garners ongoing attention within the scientific community is about the quantification of the feedback loop between climate and energy. Is it positive or negative? That is, do the interactions between these factors amplify climate change by increasing global temperature and thus exacerbate energy-related challenges, or can they potentially mitigate climate change and its impact on energy infrastructures, or at least neutral?

During my Ph.D. research, I focused on energy demand and CO_2 emissions from power generation. My primary goal was to gain a deeper understanding of the dynamics between electricity demand and climate by analyzing data, conducting simulations, and using different modeling techniques. Second, I wanted to project energy demand throughout the century to explore its evolution with climate change and calculate the associated CO_2 emissions. Finally, my work aimed to determine the impact of these CO_2 emissions on global temperature in order to contribute to ongoing efforts to unravel the complex climate-energy feedback loop and to inform policies that address the urgent challenges posed by climate change.

2 The Carbon Monitor Project: an Opportunity to Have Access to Near Real-Time Energy Data at National and Sub-National Scales

Carbon Monitor is a project launched during the COVID crisis by an international team to provide a near real-time daily dataset of global CO_2 emissions from fossil fuel and cement production. This initiative was motivated, in part, by the opportunity to study the impact of reduced mobility and human activities during lockdowns and related measures. In 2020, the project released its first public database of operational estimates of CO_2 emissions for various sectors (Liu et al., 2020a). With coverage extending to 31 countries, including major economies, Carbon Monitor provides near-global coverage of the Earth's energy-related emissions landscape. The data is regularly updated to maintain a near real-time representation of emissions patterns.

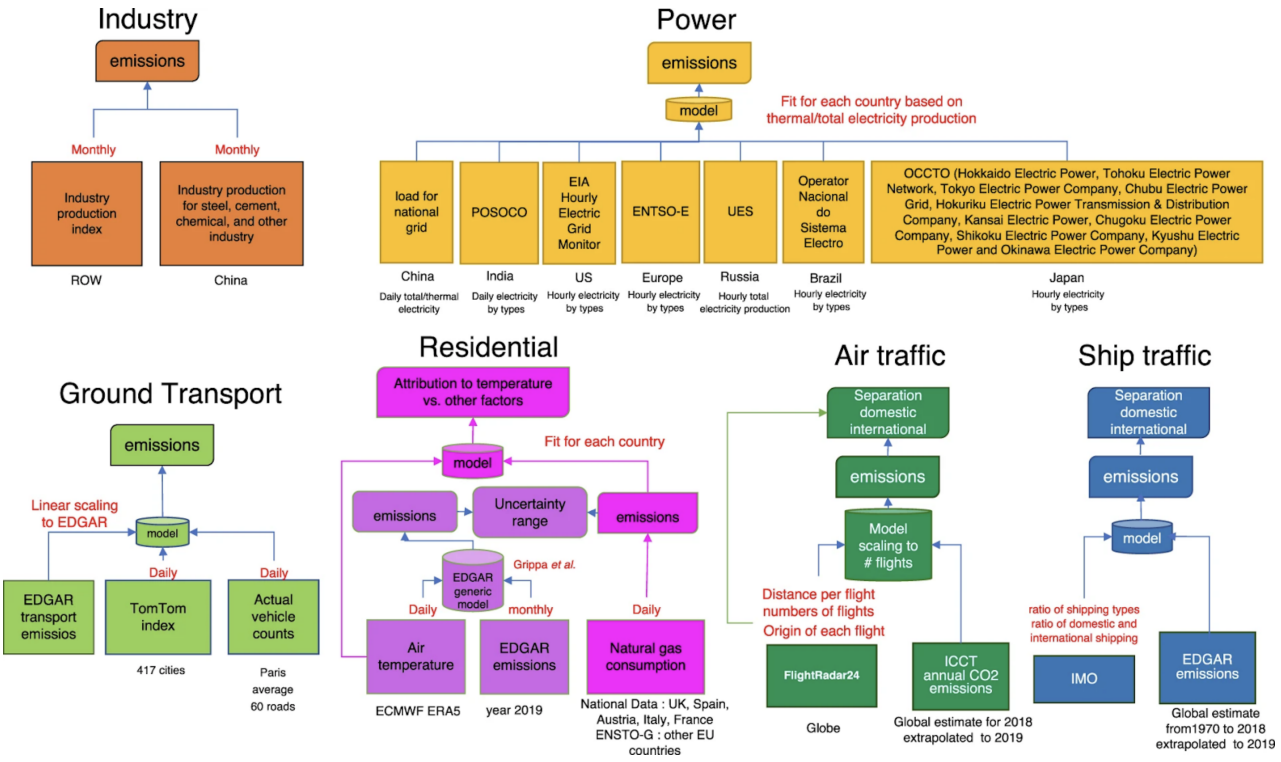

Figure I.1: Carbon Monitor framework for data processing. *Source: (Liu et al., 2020a)*

This Ph.D. research was designed with the core objective of using the daily activity and CO_2 emissions data provided by Carbon Monitor to quantitatively assess the influence of climate and weather variability on energy-related human activities and their associated CO_2 emissions, with a particular focus on electricity demand.

Carbon Monitor's comprehensive dataset includes emissions data for six different sectors: Industry, power, ground transport, residential, air traffic, and ship traffic. While the general framework for calculating CO_2 emissions in each sector involves converting activity data into emissions using models, different data processing chains have been developed for each sector. Details in these processing frameworks and activity data sources are shown in Figure I.1.

The Carbon Monitor dataset spans 2019 to 2023, covering the critical period of the COVID-19 crisis. In particular, the data captures the effects of the lockdown, providing important insights. Liu et al., 2020b, found a 8.8% reduction in global CO_2 emissions, providing a groundbreaking case study. Le Quéré et al., 2020, reported a similar reduction in CO_2 emissions, ranging from -4% to -7%, for the year 2020 compared to 2019 levels, further corroborating the impact of the lockdown measures on global emissions. This finding underscores the utility of Carbon Monitor's daily CO_2 estimates for energy research studies.

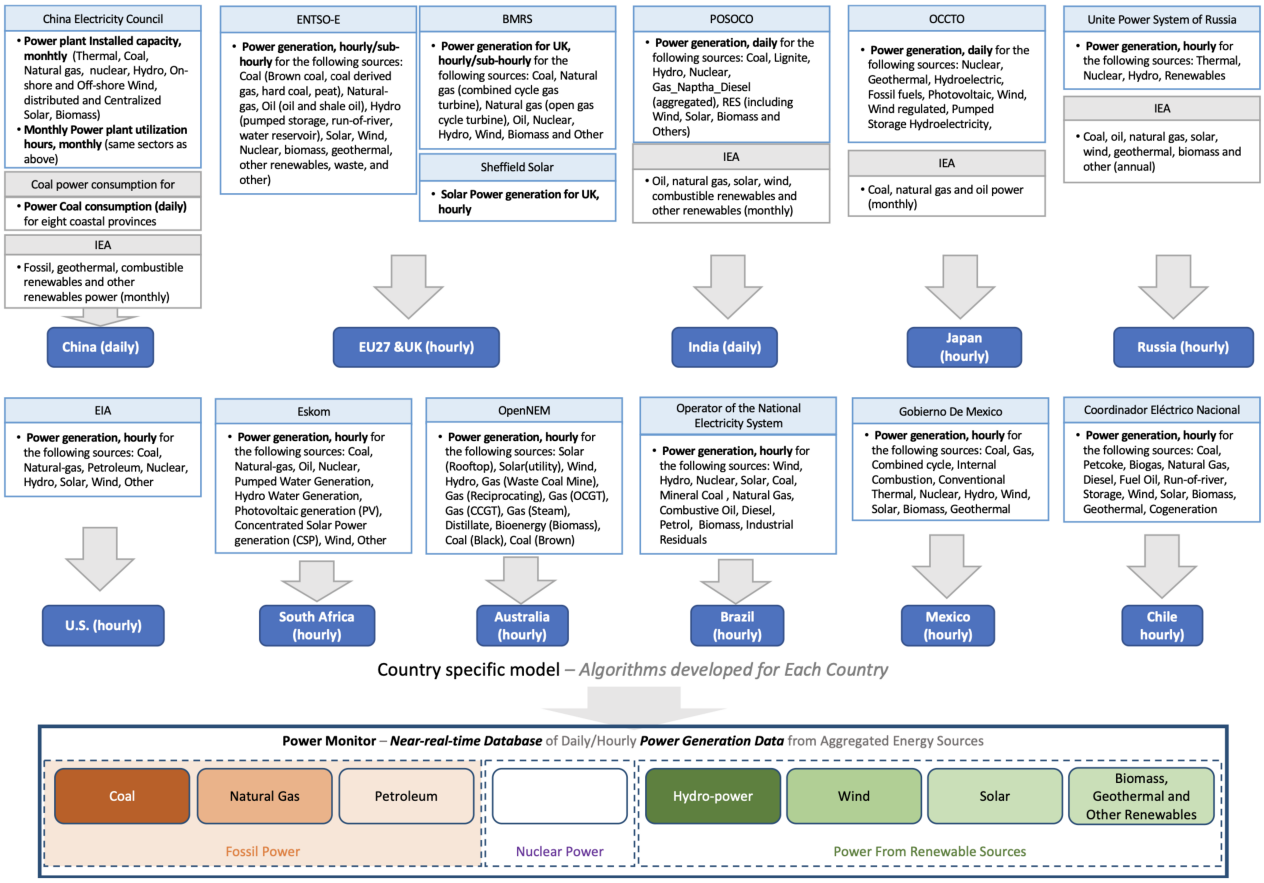

Figure I.2: Carbon Monitor Power data acquisition and processing framework. *Source: (Zhu et al., 2022)*

For my research, I focused specifically on using the Carbon Monitor Power Dataset. This dataset played a pivotal role in my research, allowing me to explore the dynamics of electricity demand and associated CO_2 emissions.

The Carbon Monitor Power dataset provides power generation data for 37 countries since January 2016: the 27 European Union (EU) countries, United Kingdom (UK), Australia, Brazil, China, Chile, India, Japan, Mexico, Russia, South Africa, and the United States (US). Throughout the manuscript, the EU27 & UK are treated as a single ensemble and referred to as a single country for analysis. The dataset provides comprehensive information on total power generation within each country considered, disaggregated by type of supply. The temporal granularity varies depending on the country and is available on either an hourly or daily timescale (see Fig. I.2 for further details). Within the dataset, eight types of supply are represented, covering different energy sources. The fossil fuel category includes data on power generation from coal, natural gas, and oil. In addition, the dataset includes generation from nuclear, hydro, wind, solar, and other renewable sources such as biomass and geothermal. Total generation data is obtained directly from the utilities responsible for generating electricity in each country. In addition, the specifics of energy supply are either obtained from the same companies or de-

rived from estimates provided by the International Energy Agency (IEA) or the International Renewable Energy Agency (IRENA) (IEA, 2022; IRENA, 2022).

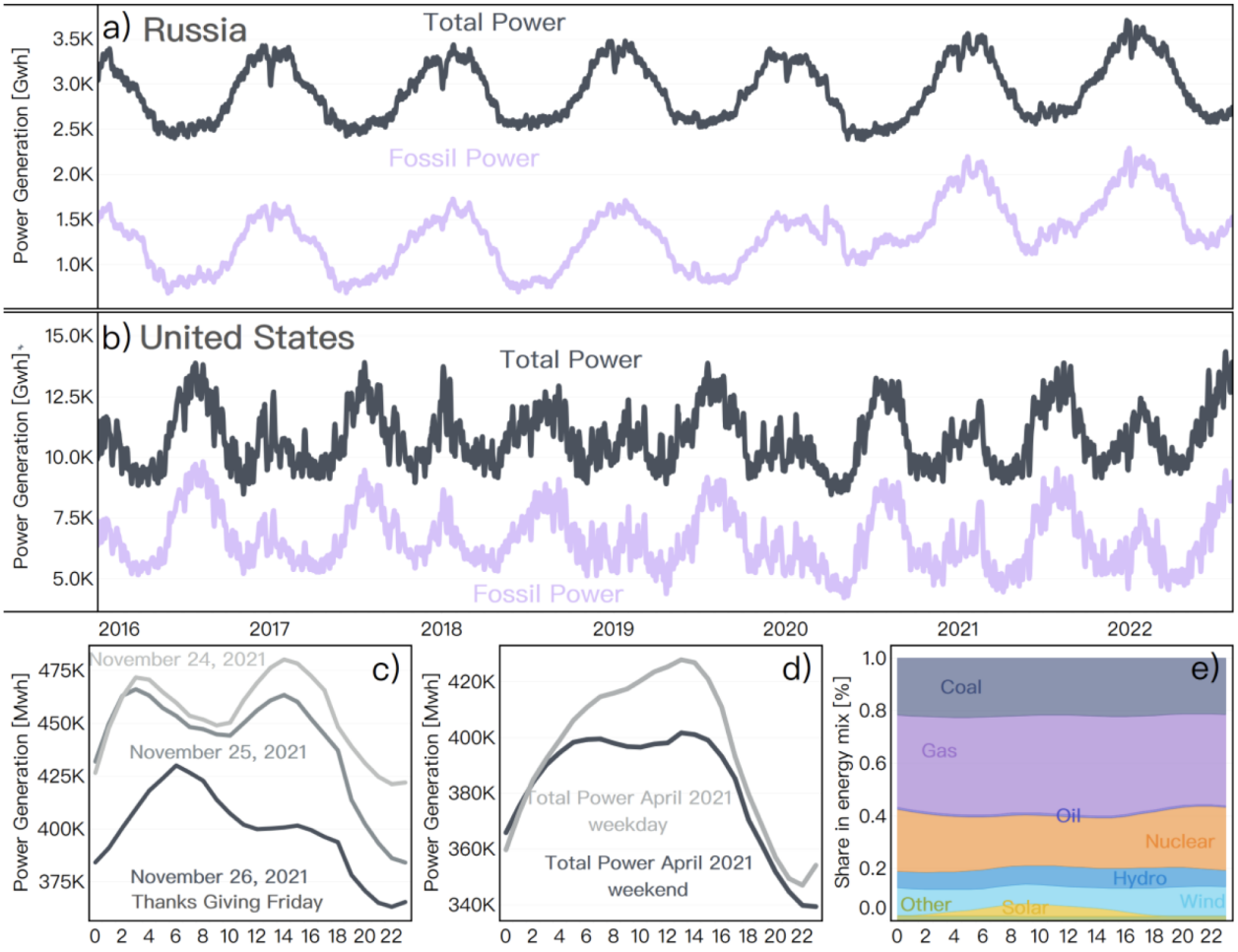

Figure I.3: Example of Carbon Monitor Power data at different temporal granularity: Total and fossil power generation over the whole available period for (a) US and (b) Russia. c) Effect of holidays on diurnal profiles for the Thanksgiving break in the US. d) Difference in power demand between weekends and weekdays in the US. e) Average April diurnal profile of the energy mix of the United States' power system *Source: (Zhu et al., 2022)*

The importance of the Carbon Monitor Power dataset goes beyond capturing the annual or seasonal dynamics of power generation data. It also provides detailed information on the energy structure at both hourly and daily levels. Figure I.3 shows different use cases of the Carbon Monitor Power database and gives an overview of the different data that can be found. For example, panels (a) and (b) show the daily dynamics of total power generation and fossil fuel generation in Russia and the US, providing a clear visualization of the energy production patterns in these countries. The Carbon Monitor Power dataset also captures variations in power demand related to special events or holidays over a daily power generation profile: Panel (c) uses Thanksgiving in the US as an example, showing a notable drop in power generation on

Thanksgiving Friday in 2021. The data also show that power generation is higher on weekdays, especially during peak hours, compared to weekends (panel d). Finally, panel (e) shows the average diurnal profile of the energy mix in the US power system in April. It highlights the share of solar and renewables in the power system at midday, indicating the role of renewables in the energy mix at certain times of the day.

The comprehensiveness and detail of the Carbon Monitor Power dataset make it an invaluable tool for conducting in-depth analyses of power generation patterns, understanding the contributions of different energy sources, and tracking changes in power demand with climate.

3 Climate Sensitivity of Power Demand

3.1 Exploring the Dynamics of Electricity Demand in Response to Meteorological Variability: A Literature Overview

Modeling electricity demand response to temperature has been a research focus for more than two decades in various research fields. For example, in 1994, Peirson et al., 1994, examined the relationship between temperature and electricity load using an economic modeling approach, revealing its dynamic and time-dependent nature. Ignoring this dynamic aspect can lead to biased estimates of the effect of temperature on electricity load. Since then, numerous studies have been published that examine this relationship from different angles, using different approaches, ranging from econometric models to data-driven models, time series analysis, multivariate regression analysis, probabilistic models, and more.

Econometric modeling studies use statistical techniques to analyze historical data and establish the relationship between temperature and electricity demand. These models better capture complex interactions by incorporating relevant factors such as income, population, and energy prices. For example, Harish et al., 2020, used a semi-parametric model in India and found different increases in electricity demand in different regions when temperatures exceeded 30°C (from +11% on average to +30% in some urban areas). Auffhammer et al., 2017, used high-frequency data in the United States to establish temperature response functions (TRFs) with statistical models and found a linear increase in demand at temperatures above 21°C, indicating cooling demand. Li et al., 2018, developed an econometric model for the Yangtze River Delta in China, showing a stronger impact of a +1°C increase in summer on cooling demand (+14.5%) than on cold days (-2.8%). Berkouwer, 2020, found a similar conclusion for South

Africa, with an increase of 8.1% for a +1°C increase above the cooling threshold and only -4.1% for a similar temperature increase below the heating threshold.

With the advancement of machine learning methods, researchers have increasingly used data-driven approaches to study the relationship between temperature and electricity demand in different regions. These studies have provided insights into the dynamic interactions between energy demand and meteorological factors at different scales, from individual cities to larger regions or groups of countries with similar climates, such as hot countries. For example, Moral-Carcedo et al., 2005, used regression techniques to model the nonlinear response of electricity demand to temperature variation in Spain. Bessec et al., 2008, studied the relationship in 15 European countries and confirmed the non-linearity, with more pronounced effects observed in warmer countries. In Serbia, Jovanović et al., 2015, found that average air temperature was the most influential climate variable explaining electricity demand in the city of Kragujevac. Similarly, Gastli et al., 2013, identified the maximum daily air temperature as the main driver of electricity demand in Qatar.

Other approaches, like time series modeling, can lead to similar conclusions. In their study, Ali et al., 2012, used a time series modeling approach to analyze electricity demand in Pakistan. They found that electricity demand is more significant during hot seasons, mainly driven by cooling needs. As a result of climate change, they expected a further increase in electricity demand. They observed a positive correlation by examining the relationship between electricity demand and mean monthly maximum temperature. However, due to inadequate power generation data in the country, they faced challenges in establishing a robust correlation. Nevertheless, their findings revealed that maximum temperature was the most influential factor in the variation of electricity demand.

In addition, some studies have attempted to develop electricity demand simulation models based on local data. A study by Hiruta et al., 2022, used complex machine learning algorithms, specifically the MARS algorithm, to establish TRFs at a sub-national scale in Japan. It is important to recognize that these findings are specific to their respective regions and may not be easily generalized. Anvari et al., 2022, proposed a versatile data-driven load model based on residential electricity consumption data, effectively capturing highly intermittent demand fluctuations. Their study highlighted that the dynamic specification of the temperature response is time-dependent.

While most studies focus on the role of temperature in electricity demand, some studies highlight the importance of other climate features, such as humidity and heat stress measures. In particular, Yan, 1998, demonstrated that heat stress indices could replace weather variables

in residential electricity consumption models, while Maia-Silva et al., 2020, showed an underestimation of up to 15% of electricity demand in US states without accounting for humidity. Miller et al., 2022, got a similar conclusion concerning humidity and found that ignoring cloud cover could overestimate the effect of low temperature.

In addition, most studies focus primarily on the mean response, overlooking the asymmetric nature of electricity demand in response to temperature changes. For example, research by Kumar et al., 2020, in California found that high-intensity electricity demand is more sensitive to temperature increases than normal demand. Neglecting these asymmetries in future projections could potentially lead to an underestimation of the increase in electricity demand during hot periods, with potential deviations as high as 37-43% over a given time period.

Another important aspect is the difference in the electricity demand response to temperature between urban and rural areas. Urban areas are more extensively represented in the literature, mainly due to the significant attention given to the Urban Heat Island Effect (UHI). A review study by Santamouris et al., 2015, found that in urban areas, for each degree of temperature increase, the peak electricity load could vary between 0.45% and 4.6%, and the total increase in electricity demand per degree of temperature increase could vary between 0.5% and 8.5%. On the other hand, rural areas have received less attention in research, leading to a limited understanding of their specific response to temperature changes. For example, a county-level study in rural China (Zhang et al., 2019) showed a very limited impact of temperature change on demand, with a 0.015% increase in cooling demand for a 1 degree Celsius increase in summer, compared to a 0.002% decrease in heating demand for a 1 degree Celsius decrease in winter. A recent study by Cui et al., 2023, examined differences between urban and rural households in air conditioning (AC) adoption and response to temperature changes in Zhejiang Province, China. They found that urban households with AC had steeper response functions at both high and low temperatures than rural households without AC.

Overall, there is a wide range of methodologies and contrasting results across regions, highlighting the need to understand the global balance between electricity demand and temperature on a global and annual scale. The US and European countries have historically been more represented in the literature, while an emerging literature focuses on the Chinese context.

3.2 Temperature Response Functions with Carbon Monitor data

The access to the Carbon Monitor-Power dataset and to the daily mean temperature from the ERA5 reanalysis enables us to plot the relationship between temperature and power demand

for various countries represented in the Carbon Monitor-Power database (Fig. I.4). Some countries show a more or less net U-shaped curve, indicating a demand for electricity for both cooling and heating purposes. These countries include Australia, China, Chile, Japan, and the United States. On the other hand, Brazil, India, and Mexico show an increasing demand for electricity with temperature, indicating a predominant demand for cooling or limited use of electricity for heating.

In contrast, the EU27 & UK, and Russia show a predominant heating demand, although a slight increase in demand is observed for the EU27 & UK at temperatures above 15°C. Notably, most countries show a clear distinction between electricity demand on weekends and weekdays, except for China, India, and the USA. In addition, China shows an anomalous behavior with many data points at very low electricity demand at temperatures below 0°C, which can be attributed to the Chinese New Year holiday period. These different relationships highlight the complex and context-specific nature of the relationship between electricity demand and temperature in different countries, reflecting diverse patterns of energy usage. India, in particular, does not display a clear relationship, which may be linked to the country's relatively limited use of air conditioning, suggesting a connection between the development stage and the observed patterns.

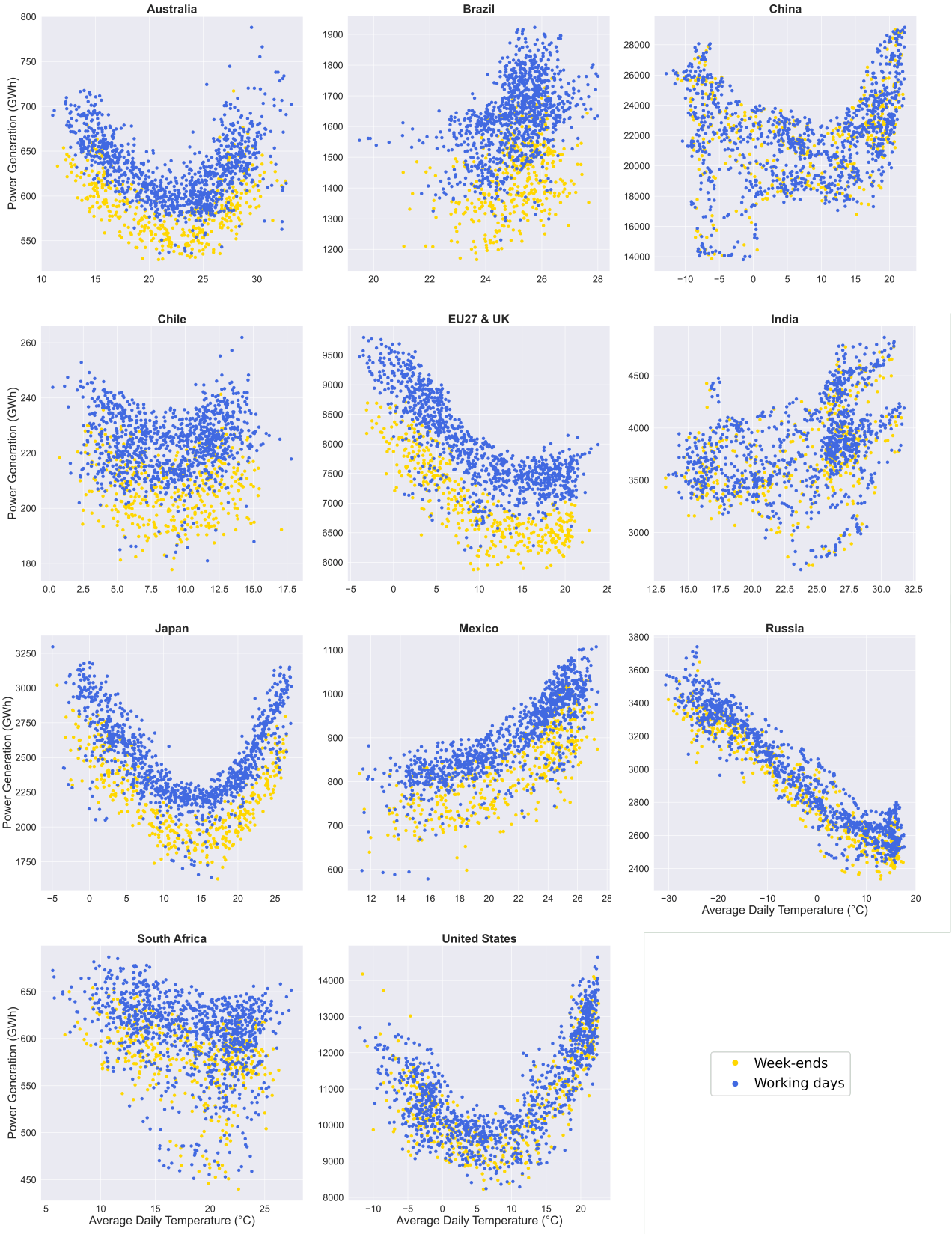

Figure I.4: Power demand from Carbon Monitor versus the daily mean temperature averaged over the countries' territories, obtained from ERA5 reanalysis, for four years of data (2019-2022).

4 Impact of Climate Change on the Energy Sector

4.1 Energy Challenges and Issues in the Context of Climate Change

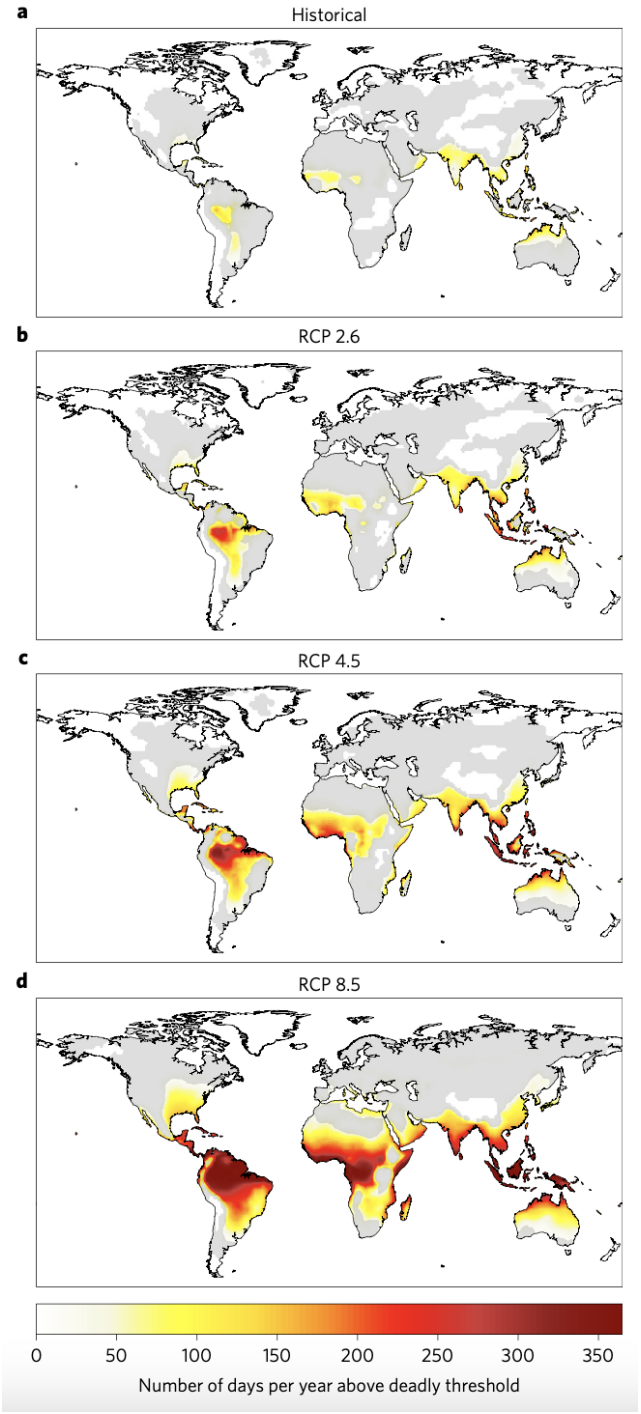

Figure I.5: Geographical distribution of deadly climatic conditions (as defined in Mora, 2017) under different emission scenarios. *Source: (Mora, 2017)*

The impact of climate change on the energy sector is a critical issue that requires attention due to its potential impact on infrastructure and human life in different regions of the world. Extreme heatwaves, as highlighted in Mora, 2017, pose a significant risk to human health, resulting in deadly heat events in areas with specific climatic conditions characterized by certain temperature and humidity thresholds. Currently, such events affect about 30% of the world's population, a number that is projected to increase to 48% by 2100 under the most optimistic scenario and up to 74% under the most pessimistic scenario, RCP8.5 (Fig. I.5). Zittis et al., 2021, looked specifically at the Middle East and North Africa and found that heat waves reaching up to 56°C could last for several weeks in the worst-case scenario. This implies that air conditioning will become an essential means of survival in these regions. This underscores the need for power grids to be equipped to handle the increased demand for electricity to provide cooling during such extreme heat events in the future.

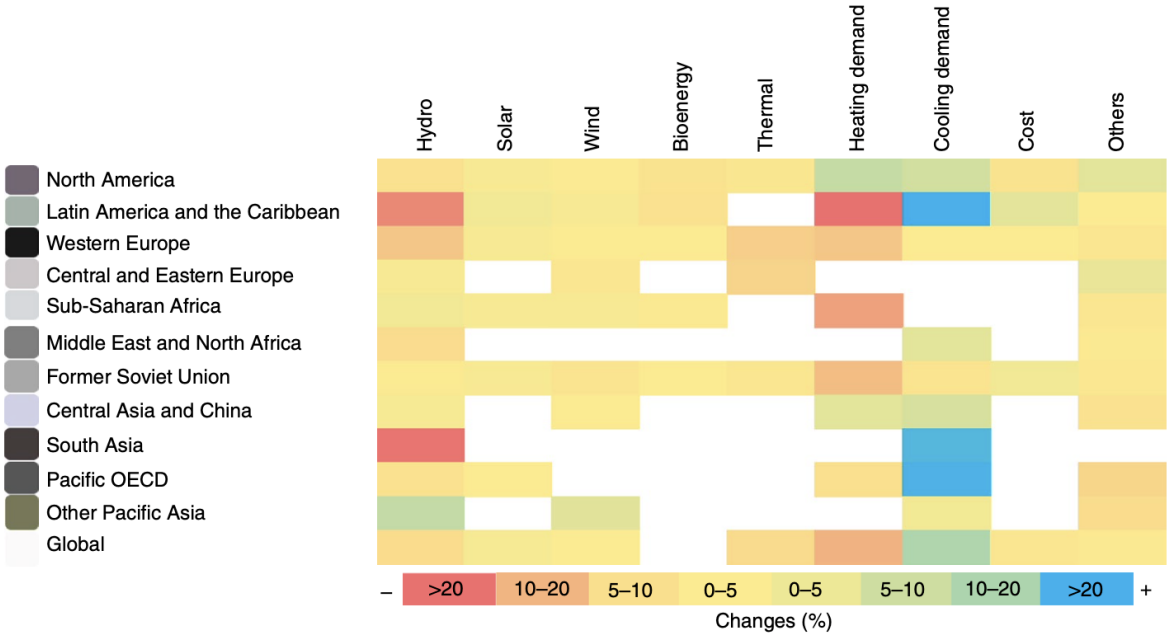

Figure I.6: Climate change impacts on energy systems averaged across 220 studies. *Source: Yalew et al., 2020*

A comprehensive review by Yalew et al., 2020, shows that the impacts of climate change on the energy sector are complex and vary significantly across geographic regions. In general, cooling demand is expected to increase due to rising temperatures, while heating demand may decrease in some areas (Fig. I.6). However, the overall balance of total energy demand will depend on regions. On the supply side, climate change is projected to slightly decrease hydroelectric and thermal energy capacity (Fig. I.6). These changes will likely pose significant challenges to the energy sector, requiring adaptation measures and strategic planning to ensure

a stable and reliable energy supply. Despite the importance of understanding the impacts of climate change on the energy sector, significant uncertainties are associated with these assessments. One of the main reasons for this uncertainty is the lack of harmonized methodologies and data sources across studies and the uneven representation of different parts of the world (Fig. I.6).

4.2 Electricity Demand and Climate Change

The impact of climate change on electricity demand has received significant attention in recent literature, with regional studies revealing different patterns and challenges. As noted in section 3 and Figure I.6, some regions have been studied more than others.

For the United States, several studies have been conducted to assess the impact of climate change on electricity demand. For example, Hadley et al., 2006, used Global Climate Models (GCMs) to drive energy use models, estimating heating and cooling demand changes under different temperature scenarios and comparing the outcomes between 2003-2025 and 1971-2000. They found that under a low deltaT scenario (+1.2°C for a CO_2 doubling), the increase in cooling demand exceeds the decrease in heating demand, resulting in +1.09 quads (quadrillion British thermal units), while under a high deltaT scenario (+3.4°C for a CO_2 doubling), it is the opposite, resulting in -0.82 quads. Similarly, Allen et al., 2016, highlighted variations in the impact of climate change on electricity demand across regions, with more pronounced changes observed in areas with smaller populations. For example, they found that demand in July 2050 could range from +12.5% in Florida to +33.1 in Oklahoma and Arkansas compared to July 2011. Another study by McFarland et al., 2015, used electricity sector models to project changes in electricity demand in response to temperature projections. Their results indicated an increase in electricity demand ranging from 1.6% to 6.5% by 2050, depending on the temperature increase. In addition, Auffhammer et al., 2017, used TRFs combined with 20 downscaled GCMs and found moderate and heterogeneous changes in consumption, with an average increase of 2.8% by the end of the century for RCP4.5. Obringer et al., 2022, for their part, used a statistical machine learning method to simulate electricity demand for air conditioning, revealing substantial increases in future residential air conditioning demand in the U.S., with estimates ranging from 5% to 8.5% (or 13% to 15%) after global warming of 1.5°C (or 2.0°C).

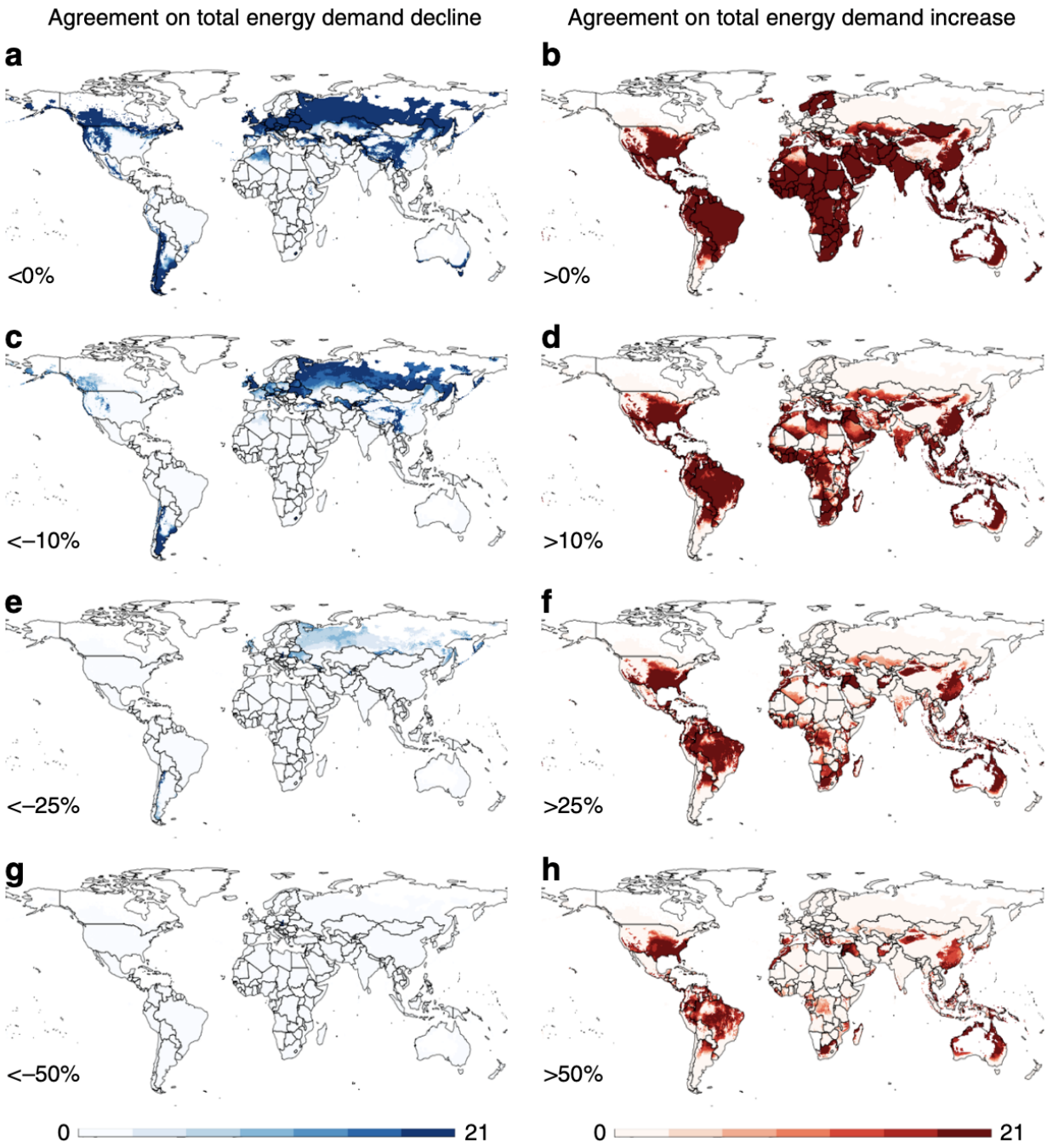

Figure I.7: Maps showing the number of Earth System Models that agree on increases and decreases in total energy demand across various sectors and energy sources by specific percentages: more than 0% (a, b), 10% (c, d), 25% (e, f), or 50% (g, h) by the year 2050 under the RCP 8.5 and SSP5 scenarios. *Source: Van Ruijven et al., 2019*

Emerging literature in China revealed a substantial increase in power demand with rising temperatures. Based on the models they developed for rural and urban areas (Cui et al., 2023), simulate household electricity consumption under different climate change scenarios (RCP4.5 and RCP8.5) and discovered several significant implications: 1) under constant urbanization and AC adoption rates, residential electricity consumption would increase by 5.04-16.37% due

to climate change; 2) as the AC adoption rate increases in both urban and rural areas, residential electricity consumption would continue to increase; and 3) combined with increasing urbanization, the annual residential electricity consumption would experience a further increase. Hu et al., 2023, examined the impacts of daily weather and extremely hot days in Beijing, suggesting that climate change would lead to 5%-7% and up to 29% increases in residential electricity consumption in the near and far future, respectively.

Intra-America regions, particularly those with tropical climates, will also experience significant increases in energy demand per capita due to climate change, according to a study by Angeles et al., 2018. The multi-model ensemble study projects an increase in energy demand per capita by 9.6 and 23 kWh/month in the RCP2.6 and RCP4.5 at the end of the twenty-first century.

At the global level, Labriet et al., 2013, used a macroeconomic perspective to study the adaptation of the energy system to future heating and cooling demand. They found that changes in heating and cooling tended to offset each other, resulting in limited climate feedback at the global level. However, they note that changes at the regional level were more pronounced. Another global analysis (Clarke et al., 2018) focused on the global building sector and found that net energy expenditures were not uniform across the globe. Regions with lower demand for space heating and higher demand for space cooling experienced the largest net expenditures increase. Furthermore, Van Ruijven et al., 2019, combined econometrically estimated responses of energy use to income and extreme weather events with future projections of socioeconomic scenarios and temperature increases to assess climate-sensitive energy demand. Their results showed significant increases in energy demand (+25%) in many regions, particularly in the tropics and southern regions of the U.S., Europe, and China (Fig. I.7).

Although many regional studies have been carried out, there remains a strong need for systematic regional analyses based on a consistent methodology. These analyses can provide a more nuanced understanding of regional variations in the impact of climate change on electricity demand.

5 From Power Demand to CO_2 Emissions: the energy mix in the context of the Paris Agreements

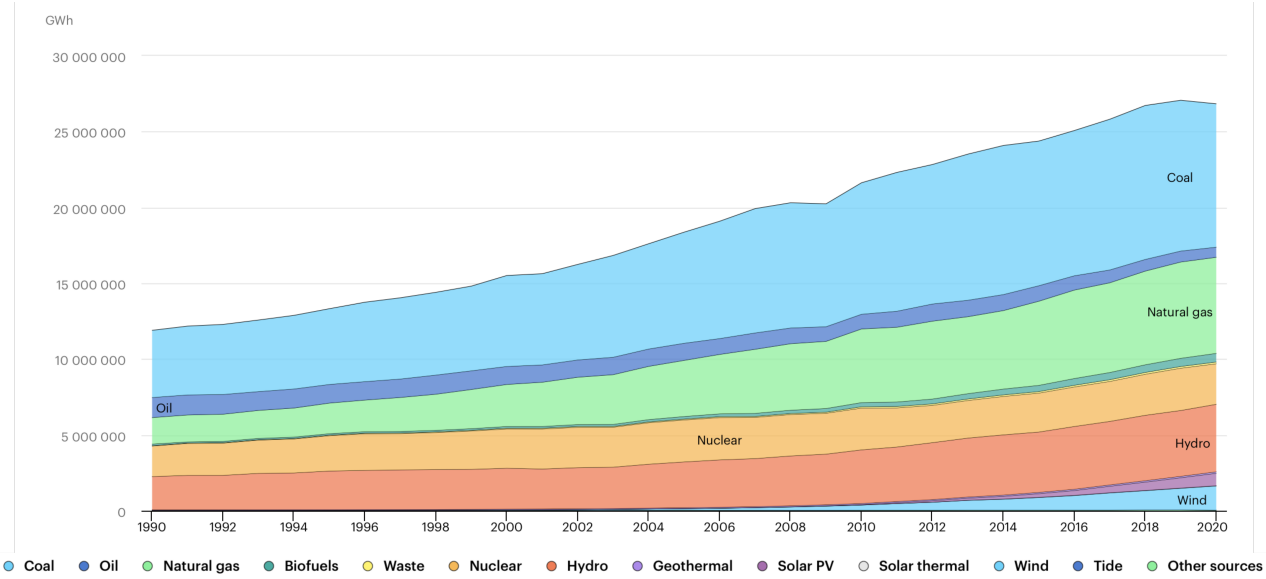

Figure I.8: Gloal power generation by sources from 1990 to 2020. *Source: IEA, 2022*

The composition of the energy mix used to generate electricity directly impacts carbon intensity, which refers to the amount of CO_2 emitted per unit of energy produced. Over the past three decades, global power generation has been on the rise to meet increasing demand. This expansion has been driven by both a growth in fossil fuel production and the emergence of renewable energy sources since the start of the 21st century (Fig. I.8). A higher share of renewables in the energy mix results in lower CO_2 emissions. Because of the different energy mixes in different countries, there are many variations in carbon intensity worldwide.

Figure I.9 shows that each country has a different energy mix for electricity generation. However, in most cases, fossil fuels such as coal, gas, and oil make up at least half of this mix. Brazil stands out, with the majority of its production coming from hydropower. In Chile, renewables, especially hydro and wind, play a significant role, and their shares are increasing over the period. In EU27 & UK, renewables combined with nuclear power account for most of production. In other countries, fossil fuels are dominant, but temporal trends differ. For example, in Australia, the use of fossil fuels is decreasing, while in India, it is increasing. More specifically, coal is the main production source in Australia, China, India, and South Africa. On the other hand, in Japan, Russia, Mexico, and the United States, gas is taking the lead in the energy mix.

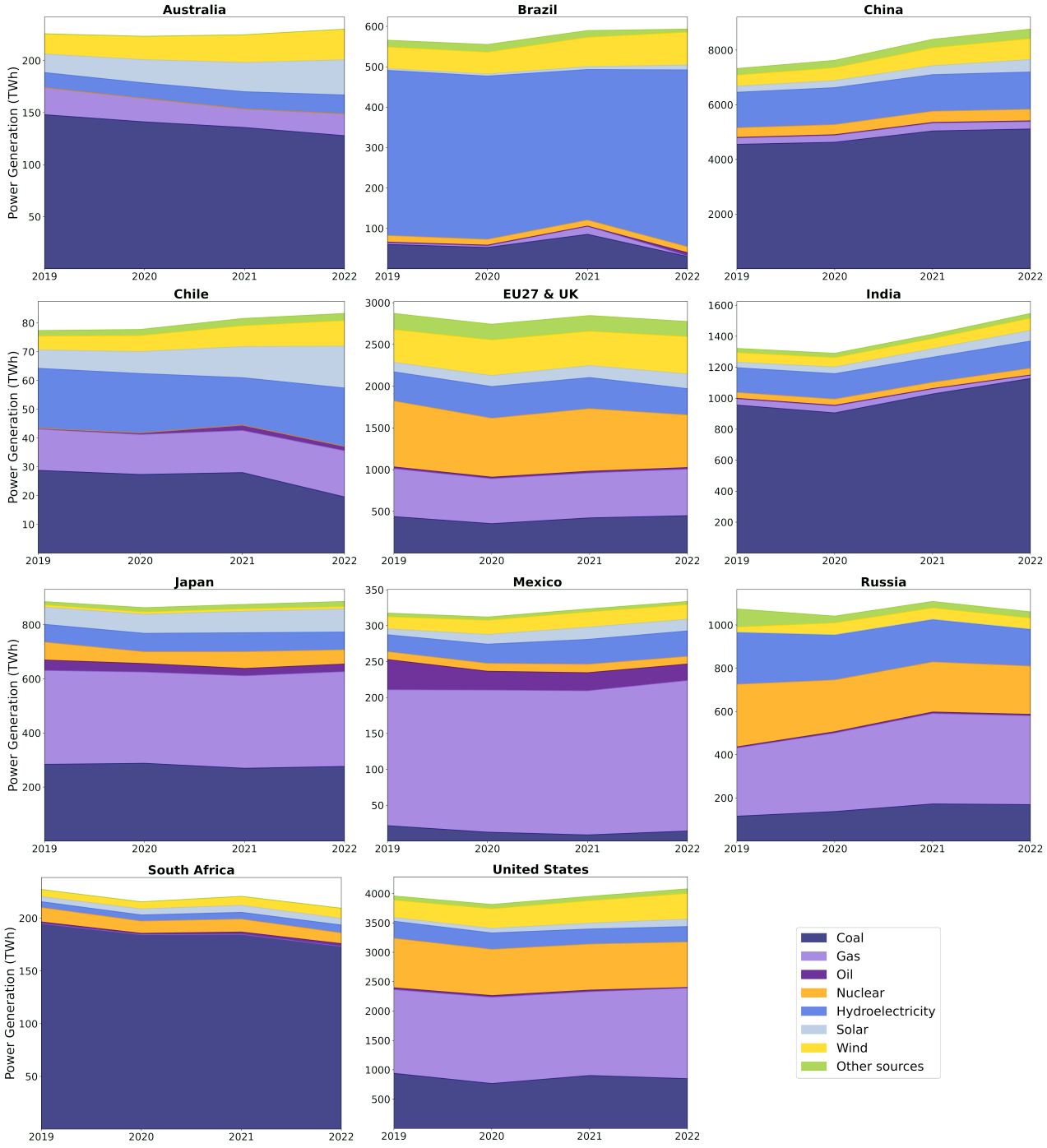

Figure I.9: Average daily energy mix of the countries represented in the Carbon Monitor-Power database over the period 2019-2022.

In addition, the carbon intensity of electricity generation can vary within a single day. This variability is influenced by factors such as the availability of renewable energy sources. As shown in Figure I.3, we can observe fluctuations in the energy mix over the course of a day due to the availability of solar energy. Moreover, when there is high electricity demand, especially during peak hours, power systems often rely more heavily on fossil fuels to meet the increased demand. This reliance on fossil fuels, which have higher carbon emissions, can significantly

increase carbon intensity (Khan et al., 2018).

The landscape of the energy mix is in a state of dynamic transformation, driven by countries' concerted efforts to address the urgent challenges of climate change. Governments around the world have embarked on climate-energy policies aimed at curbing CO_2 emissions and ushering in a new era of sustainability. Central to this national effort are the Nationally Determined Contributions (NDCs) pledged by countries as part of their commitment to the Paris Agreement (UNFCCC, 2016), a historic agreement under the United Nations Framework Convention on Climate Change (UNFCCC). The overall goal of the Paris Agreement is to limit global warming to well below 2 degrees Celsius above pre-industrial levels, with efforts to limit the temperature increase to 1.5 degrees Celsius. This requires efforts from all countries and impacts all sectors of the economy (Falkner, 2016).

The NDCs are a tangible manifestation of a country's commitment to reducing its carbon footprint. They serve as blueprints for action, outlining clear and quantifiable targets for reducing greenhouse gas emissions at the country level. The commitments made in NDCs encompass a wide range of strategies, from energy efficiency measures limiting electricity demand growth to the integration of cutting-edge technologies and innovations that facilitate the decarbonization of the power sector (Stephenson et al., 2019). These commitments are not static. Governments continually update their NDCs with new targets and initiatives that reflect the latest science and global imperatives. As nations move forward on this transformative path, energy mixes will undergo a profound metamorphosis as the imperative to decarbonize the power sector takes center stage as a central component of realizing a low-carbon future (Khan et al., 2018; Santos-Alamillos et al., 2017).

6 The General Framework: From Qatar and Japan Case Studies to a General Approach

The overall idea of this research is to take advantage of the database provided by Carbon Monitor Power and use it as the basis for building national models to simulate daily electricity demand. By using these models, we aim to extend our insights to regions where data is currently lacking. This approach involves integrating machine learning techniques that will be trained using Carbon Monitor Power data, climate information from ERA5 reanalyses, and human activity data accounting for the key socioeconomic factors that influence demand on a daily scale.

The resulting models will then be applied to CMIP6 climate projections, allowing us to project electricity demand into the future and associated CO_2 emissions. This forward-looking analysis will allow us to assess the potential impacts of climate change under different scenarios outlined by Shared Socioeconomic Pathways (SSPs). The framework developed in this research has been rigorously tested and refined through case studies focusing on Qatar and Japan (as detailed in Chapter II and III). Subsequently, this approach was extended to the Carbon Monitor countries (Chapter IV) and eventually to countries worldwide (Chapter V). The final Chapter, Chapter VI, highlights potential improvements to energy demand models and explores potential applications of the approach developed. In particular, it discusses the calculation of the feedback effects of additional CO_2 emissions resulting from electricity demand on global temperatures.

This final section of the introduction serves as a comprehensive guide to the basic elements and concepts that form the core of our approach. The intricacies of the machine learning models used, and the interpretation methods that enhance our understanding of their results are presented. An overview of the distinctive scenarios encapsulated by the common socioeconomic pathways that underpin our projections is proposed. Finally, the additional datasets integral to our analysis alongside the Carbon Monitor Power data are introduced.

6.1 The Machine Learning Approach

6.1.1 From Linear to Ensemble: A Spectrum of Machine Learning Models Employed

Machine Learning (ML) encompasses a diverse set of statistical and mathematical techniques that enable computers to learn from data and discover relationships inherent in that data. This broad field encompasses a spectrum of statistical models, ranging from widely used and intuitive options such as linear regression to more complex implementations such as deep learning models. These models are called "statistical" due to their core principle of minimizing average statistical error. Machine learning is primarily used to solve two types of problems: classification, which involves categorizing data into distinct classes, and regression, which involves predicting a continuous numerical output. The approach taken in this thesis falls into the second category: How to explain electricity demand from other data?

This section describes the various machine learning models used in this study and provides insights into their implementation. The set of models includes three types of linear regression

techniques: the basic Ordinary Least Squares (OLS) regression, the Multivariate Adaptive Regression Splines (MARS) that introduce nonlinearities by using piecewise linear segments, and the Generalized Additive Models (GAM), a generalized linear model. In addition, a broader range of models is explored, including a decision tree-based method known as Random Forest (RF) and a boosting technique known as Gradient Boosting (GB).

The equation of a linear function is (Montgomery et al., 1992) :

$$y = \beta_1 x + \beta_0 \tag{I.1}$$

This equation models the relationship between the target variable y and the predictive feature x with a straight line. β_0 is the intercept and β_1 the slope. If the data points do not fall exactly on the straight line, we can incorporate an error term into Equation (I.1) :

$$y = \beta_1 x + \beta_0 + \epsilon \tag{I.2}$$

Where ϵ is the error between the observation and the value predicted by Equation (I.1). This constitutes a simple linear regression model involving a single predictive feature. For scenarios with multiple predictive features $(x_1, x_2, x_3..., x_k)$ explaining y, a multiple linear regression model is employed, characterized by the equation:

$$y = \beta_0 + \beta_1 x_1 + \beta_2 x_2 + ... + \beta_k x_k + \epsilon \tag{I.3}$$

This equation underpins parametric models like OLS regressions (Pohlman et al., 2003) and semi-parametric models like GAM (Hastie et al., 1986), and MARS (J. Friedman, 1991). The principles of these models are detailed below:

- **Ordinary Least Square (OLS):** OLS is a classic linear regression technique that seeks the best-fitting linear relationship between the input and target variables. It minimizes the squared error (E), *i.e.* the sum of the squared differences between the actual and predicted values:

  $$E = \sum_{j=0}^{k} |p(x_j - y_j)|^2 \tag{I.4}$$

  While OLS assumes a linear relationship, it can also be used for polynomial regressions by transforming the original features into polynomial terms: $y = \beta_0 + \beta_1 x_1^2 + \beta_2 x_2^2 + ... + \beta_k x_k^2 + \epsilon$. OLS regressions are simple and interpretable but may not capture complex nonlinear relationships in the data (Pohlman et al., 2003).

- **Multivariate Adaptive Regression Splines (MARS):** MARS can be conceptualized as linear models in a higher-dimensional basis space that automatically detect interactions

and nonlinear relationships between variables. It employs hinge functions to build a model combining piecewise linear segments (splines). The equation of hinge functions is the following :

$$h(x-t) = \begin{cases} x-t & \text{if } x \ t \\ 0 & \text{if } x \leqslant t \end{cases} \tag{I.5}$$

The MARS model $f(x)$ is a weighted sum of basis function ($B_i(x)$) that are the product of a constant, a linear function of input variables, and hinge functions of input variables. It takes the form $f(x) = \sum_{i=1}^{k} B_i(x)$. MARS models are suitable when relationships are expected to be piecewise (J. H. Friedman, 1993; J. Friedman, 1991; Millborrow, 2012).

- **Generalized Additive Models (GAM):** GAMs also extend the concept of linear regressions to model nonlinear relationships between predictive features and the target variable. They are built as a sum of smooth functions of predictive features, and the smooth functions are constructed using penalized splines. :

$$f(X) = \beta_0 + f_1(x_1) + f_2(x_2, x_3) + ... + f_M(x_N) \tag{I.6}$$

GAMs provide a flexible framework for modeling and interpreting data without requiring a priori assumptions about the functional form of the relationships (Hastie et al., 1986; Wood, 2006).

Two non-parametric ensemble methods are also used, which combine the predictions of multiple individual models to create a more accurate predictive model (Opitz et al., 1999):

- **Random Forest (RF):** RF combines the predictions of multiple decision trees to create a robust and accurate predictive model. Each decision tree is trained on a randomly sampled subset of training data, and predictions from individual trees are averaged to obtain the final prediction. The randomness enhances diversity and helps prevent overfitting (Breiman, 2001; Geurts et al., 2006).

- **Gradient Boosting (GB):**In this study, histogram-based gradient boosting is used, a variant of the traditional Gradient Boosting algorithm that leverages histograms for improved training efficiency. Histogram-Based Gradient Boosting discretizes continuous features into bins and builds trees using bin-level statistics from histograms. The final prediction is a combination of predictions from individual trees in the ensemble (Chen et al., 2016; Ke et al., 2017).

Regardless of the model used, the machine learning approach developed here consists of two phases: a learning phase, in which the model is trained on observations (of electricity demand and demand explanatory variables), and a projection phase, in which the trained model is used to simulate electricity demand in the future.

6.1.2 The Significance of Interpretability in Taming ML Model Black Boxes

Certain ML models lend themselves to simple interpretation, such as linear models (equation (I.3)), which can be visualized with a simple straight-line graph. Similarly, GAMs and MARS combine different functions to capture the effects of different variables. These models are inherently interpretable, as individual functions can be plotted to reveal the influence of a single variable on the final output. However, other models, such as Random Forest (RF) and Gradient Boosting (GB), are more complex, cannot be directly interpreted, and are often referred to as "black boxes".

To address this interpretability challenge, specialized methods come into play that help shed light on the results of complex ML models. Here, I provide a brief overview of the interpretability techniques used in this study:

- **Partial Dependence Plots (PDPs):** PDPs illustrate the marginal effect of one (or two) predictive features on predicted outcomes. They show how the outcome changes with variation of a particular feature, holding other features constant. PDPs provide a global perspective by plotting the average prediction across the marginal distribution. However, they may only partially capture heterogeneous effects, as opposing influences may counteract each other within this technique. PDPs assume feature independence, potentially creating new data points with low actual probabilities (Molnar, 2020).
- **Accumulated Local Effects (ALE) plots:** ALE plots show how features collectively influence the predictions of machine learning models on average. Unlike PDPs, ALE plots remain unbiased and can handle correlated features. By focusing on a given value, ALE plots reveal how changing one feature affects predictions relative to other features (Molnar, 2020).
- **Shapley Values:** Shapley Value is a method based on game theory. Shapley Values assign the contributions of each feature to the final predictions. This method measures the impact of each feature by iteratively adding and removing it from all feature subsets. A feature's Shapley score is a weighted sum of its various contributions, ultimately yielding an overall prediction score (Molnar, 2020).

- **Feature Importance:** Feature importance analysis allows us to understand which features influence the target variable most. Here, permutation feature importance was used, where the importance of a feature is measured by measuring the increase in model prediction error after shuffling its values.

6.2 Description of the Shared Socioeconomic Pathways

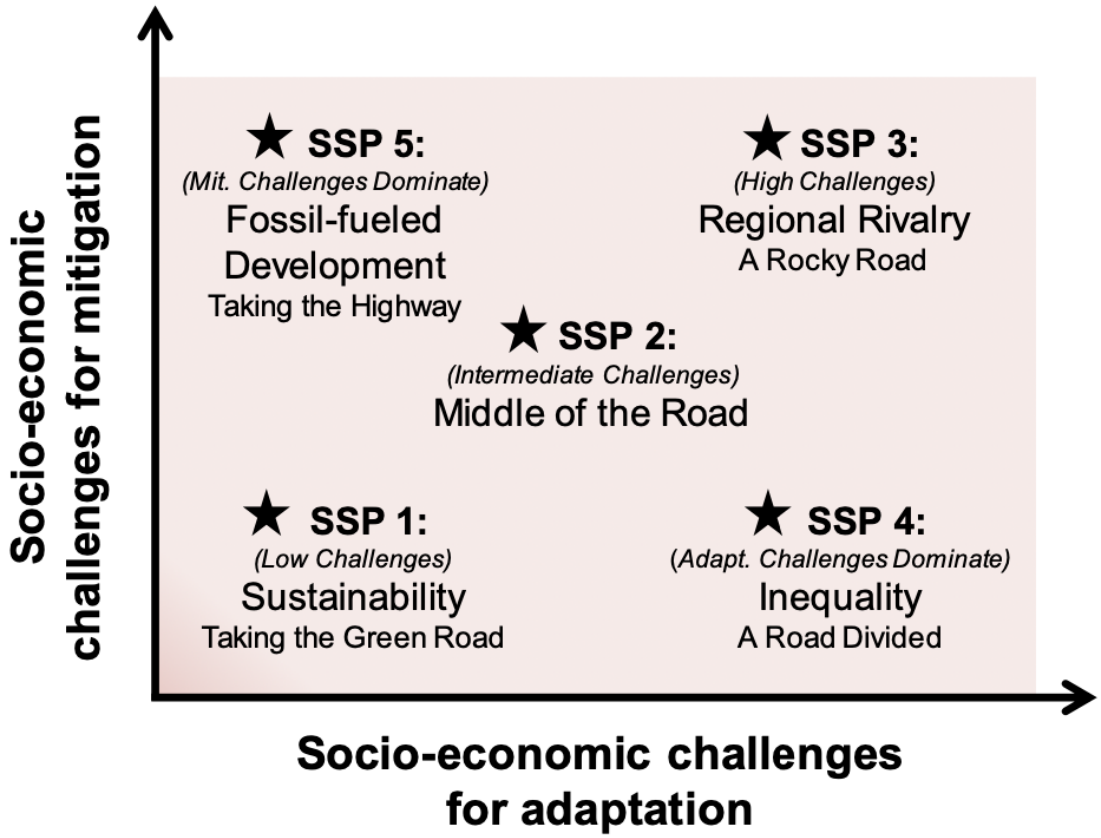

Figure I.10: SSPs and their challenges for adaptation and mitigation. *Source: O'Neill et al., 2015*

The Shared Socioeconomic Pathways (SSPs) were widely used in this study to understand the impacts of different scenarios on power demand and CO_2 emissions. These pathways provide a structured and comprehensive set of future socioeconomic narratives, each representing different development trajectories, technological progress, and societal change. The SSPs serve as critical cornerstones for understanding and projecting potential future scenarios, allowing us to explore the impact of different socioeconomic and policy choices on global development and greenhouse gas emissions. Each SSP describes a unique path that reflects a specific combination of factors such as population growth, economic development, energy use patterns,

technological advances, and environmental policies. These pathways, which range from sustainable, low-carbon futures to fossil-fuel-intensive trajectories, encompass a wide range of plausible global development paths (Fig. I.10). Here is a brief description of each SSP narrative (O'Neill et al., 2015):

- **SSP1 - Sustainability:** SSP1 pictures a world where social, economic, and technological advancements lead to a balanced focus on economic growth, environmental protection, and social equity. It assumes rapid progress in clean and efficient technologies, coupled with a decline in fertility rates, resulting in a global population peak and subsequent decline. This pathway emphasizes sustainable development, reduced inequality, resilient ecosystems, and a low-carbonized energy mix.
- **SSP2 - Middle of the Road:** SSP2 represents a moderate scenario where social and economic trends evolve at a moderate pace. It reflects a world with relatively balanced progress across regions, without extreme shifts towards sustainability or inequality. Population growth slows but remains significant, and technological development follows a moderate trajectory. This pathway assumes a mix of fossil fuels and renewables in the energy mix.
- **SSP3 - Regional Rivalry:** SSP3 portrays a future where regional competition precedes global cooperation. Economic growth is fragmented, and environmental policies are relatively weak. This pathway sees high population growth and relatively slow technological advancements. Fossil fuels continue to dominate the energy mix, leading to higher greenhouse gas emissions and limited climate mitigation efforts.
- **SSP4 - Inequality:** SSP4 presents a world characterized by stark social and economic inequalities. Technological progress is limited, and investments primarily focus on short-term economic gains. Population growth remains high, especially in less developed regions. Energy access is constrained, and the energy mix includes a significant share of fossil fuels.
- **SSP5 - Fossil-Fueled Development:** SSP5 depicts a future where economic growth is prioritized over environmental concerns. Rapid technological advancements and fossil fuel consumption drive high energy demand. Population growth remains significant, and there is little emphasis on climate mitigation. The energy mix is heavily reliant on fossil fuels, resulting in elevated greenhouse gas emissions.

6.3 General Data Description

We always used Carbon Monitor Power data as the target variable to train the models and ERA5 data as climate predictive features. The socioeconomic data used in the training phase depends on the countries and regions considered and are detailed when relevant. The projections of power demand and CO_2 emissions were calculated using ISIMIP climate projection as climate projections.

6.3.1 Description of the ERA5 Climate Input Data

ERA5 data refers to the fifth generation of the European Reanalysis dataset, a comprehensive climate reanalysis product produced by the European Centre for Medium-Range Weather Forecasts and available from the Copernicus Climate Change Service (C3S) Climate Data Store . Reanalysis data combines observations from various sources, such as weather stations, satellites, and buoys, with numerical models to provide a comprehensive and consistent representation of the Earth's climate system over a given time period. ERA5 data include a wide range of atmospheric and surface variables such as temperature, humidity, wind speed, precipitation, pressure, and many others. These variables are available at different vertical levels in the atmosphere and at different temporal resolutions (e.g., hourly, daily, monthly). ERA5 is known for its high spatial and temporal resolution, making it valuable for various research and applications in climate science, meteorology, and environmental studies. For the learning data, hourly data from the "ERA5-Land hourly data from 1950 to present" catalog (Muñoz Sabater, 2019) were used and aggregated at a daily time scale.

6.3.2 Description of the ISIMIP Climate Input Data

The Inter-Sectoral Impact Model Intercomparison Project (ISIMIP) is a collaborative research initiative to assess the potential impacts of climate change across different sectors and regions of the world. The project brings together a global community of scientists and experts to develop and apply a consistent framework for assessing the impacts of climate change on different systems, such as agriculture, water resources, ecosystems, and more. One of the key contributions of the ISIMIP project is the provision of standardized climate input data that can be used as inputs to impact models. These climate input datasets are derived from global climate models (GCMs) and carefully edited to provide consistent and harmonized information for various sectors. The climate input data cover several variables, including temperature, pre-

cipitation, wind patterns, and more, and are typically available at high temporal and spatial resolutions. This thesis used the climate input data provided by the ISIMIP 3b protocol (Lange, 2019, 2021), which provides bias-corrected CMIP6 climate forcing for pre-industrial, historical, SSP1-RCP2.6, and SSP5-RCP8.5 conditions simulated by five ESMs: GFDL-ESM4 (Dunne et al., 2020), IPSL-CM6A-LR (Boucher et al., 2020), MPI-ESM1-2-HR (Mauritsen et al., 2019), MRI-ESM2-0 (Yukimoto et al., 2019), UKESM1-0-LL (Sellar et al., 2019).

6.4 What is this Approach Made for?

This research builds on the premise of previous studies investigating the complex relationship between energy demand, CO_2 emissions, and climate. However, it distinguishes itself by using the cutting-edge capabilities of modern machine learning (ML) techniques and the latest available data, in particular the CMIP6 climate projections. The overarching goal is to achieve greater accuracy and reliability in projecting energy demand and CO_2 emissions than previous studies based on CMIP5 data, focusing on refining seasonal predictions. The foundation for this endeavor is the Carbon Monitor database, a robust resource that facilitates the development of models with near-global coverage. In essence, this research seeks to fill the existing knowledge gaps by combining innovative ML techniques, state-of-the-art climate projections, and an extensive power generation database to advance the understanding of energy demand and CO_2 emissions feedbacks under climate change.

The interaction among the different components of the research is depicted in Figure I.11. This diagram provides an overview of the main stages of the thesis and shows how each chapter aligns with and addresses specific aspects of the research. Chapters II and III lay the foundation through a comprehensive examination of two different case studies: Qatar and Japan. These cases serve as methodological crucibles that allow for the refinement and advancement of the proposed approach. The findings from these studies have already been published (Gurriaran et al., 2023a; Gurriaran et al., 2023b).

Chapter IV represents a central segment of the thesis, detailing the architecture and execution of the developed machine learning approach named CMP-SIMv1.0. This chapter encapsulates the methodological essence, which is intended to be universally applicable to different countries and regions, depending on the availability of the required data. It details ML algorithm training: data partitioning into training and test sets, parameter optimization using techniques such as grid search coupled with k-fold cross-validation, and rigorous evaluation using metrics such as R2 and RMSE. In addition, the interpretability methods discussed earlier are used to gain insights from the complex ML models.

Chapter V describes the changes made to the CMP-SIMv1.0 models to extrapolate electricity demand and CO_2 emission projections globally. This section also analyzes these projections, shedding light on their impacts and implications for a wide range of countries.

Chapter VI is the final part of the thesis dedicated to the perspectives. This section provides a preliminary exploration of the broader implications of changes in CO_2 emissions and global temperature, as calculated by the ACC2 model. At the same time, it opens the door for further investigation, particularly about including climatic extremes and their far-reaching effects.

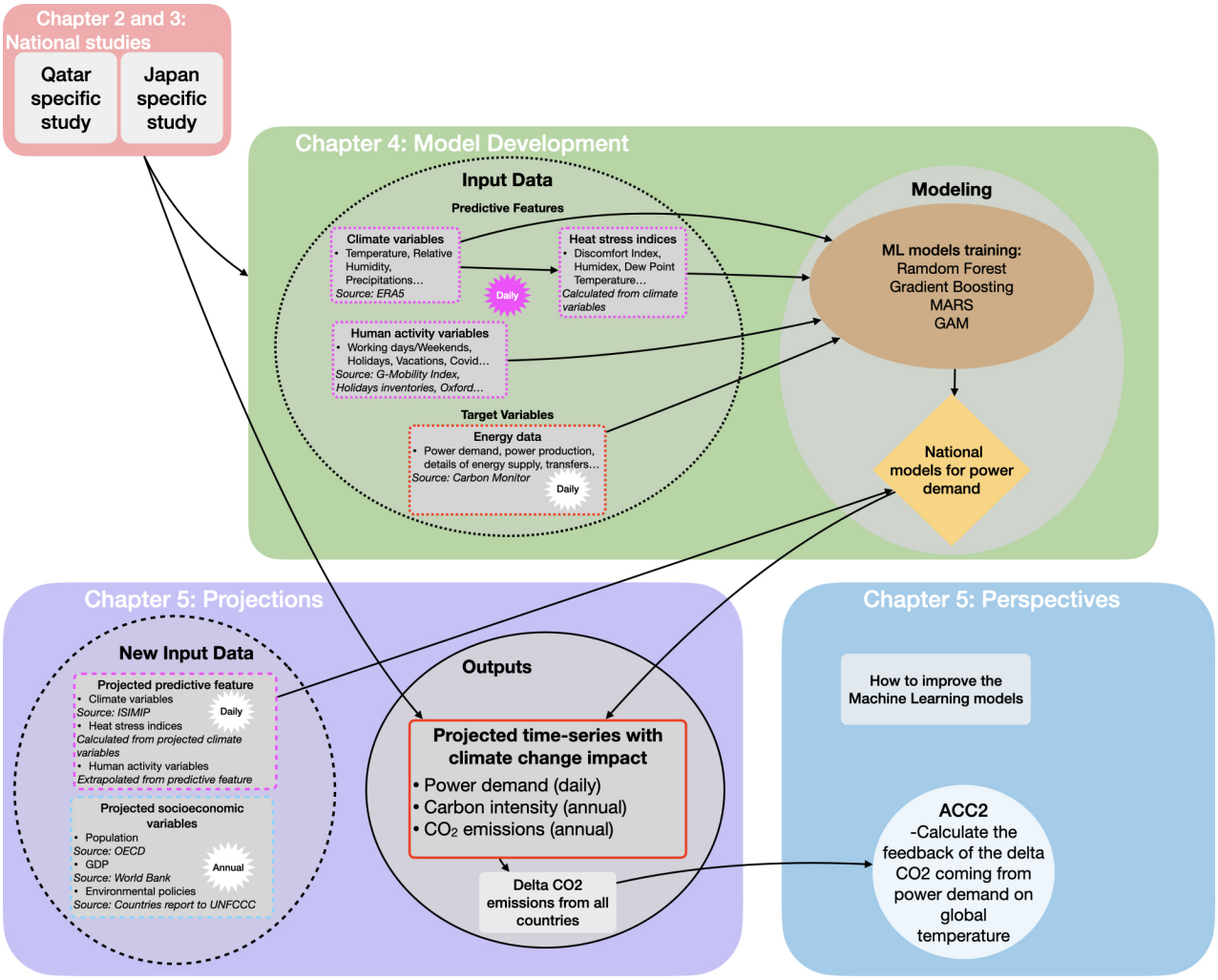

Figure I.11: Flowchart of the broad methodology applied in this thesis.

References

Ali, M., Iqbal, M., Sharif, M., Hussain, M., & Soomro, S. (2012). Relationship between extreme temperature and electricity demand in pakistan. *International Journal of Energy and Environmental Engineering SPRINGER*, *4*. https://doi.org/10.1186/2251-6832-4-36

Allen, M., Fernandez, S., Fu, J., & et al. (2016). Impacts of climate change on sub-regional electricity demand and distribution in the southern united states. *Nature Energy*, *1*, 16103. https://doi.org/10.1038/nenergy.2016.10

Angeles, M., Gonzalez, J., & Ramirez-Beltran, N. (2018). Impacts of climate change on building energy demands in the intra-americas region. *Theoretical and Applied Climatology*, *133*. https://doi.org/10.1007/s00704-017-2175-9

Anvari, M., Proedrou, E., Schäfer, B., et al. (2022). Data-driven load profiles and the dynamics of residential electricity consumption. *Nature Communications*, *13*, 4593. https://doi.org/10.1038/s41467-022-31942-9

Auffhammer, M., Baylis, P., & Hausman, C. H. (2017). Climate change is projected to have severe impacts on the frequency and intensity of peak electricity demand across the united states. *Proceedings of the National Academy of Sciences*, *114*(8), 1886–1891. https://doi.org/10.1073/pnas.1613193114

Berkouwer, S. B. (2020). Electric heating and the effects of temperature on household electricity consumption in south africa. *The Energy Journal*, *0*(4), 209–230.

Bessec, M., & Fouquau, J. (2008). The non-linear link between electricity consumption and temperature in europe: A threshold panel approach. *Energy Economics*, *30*, 2705–2721. https://doi.org/10.1016/j.eneco.2008.02.003

Boucher, O., Servonnat, J., Albright, A. L., Aumont, O., Balkanski, Y., Bastrikov, V., Bekki, S., Bonnet, R., Bony, S., Bopp, L., Braconnot, P., Brockmann, P., Cadule, P., Caubel, A., Cheruy, F., Codron, F., Cozic, A., Cugnet, D., Davini, P., & ... Vuichard, N. (2020). Presentation and evaluation of the ipsl-cm6a-lr climate model. *Journal of Advances in Modeling Earth Systems*, *12*(7), e2019MS002010. https://doi.org/10.1029/2019MS002010

Breiman, L. (2001). Random forests. *Machine Learning*, *45*, 5–32. https://doi.org/10.1023/A:1010933404324

Chen, T., & Guestrin, C. (2016). Xgboost: A scalable tree boosting system. *Proceedings of the 22nd ACM SIGKDD International Conference on Knowledge Discovery and Data Mining*, 785–794. https://doi.org/10.1145/2939672.2939785

Clarke, L., Eom, J., Marten, E. H., Horowitz, R., Kyle, P., Link, R., Mignone, B. K., Mundra, A., & Zhou, Y. (2018). Effects of long-term climate change on global building energy expenditures. *Energy Economics*, *72*, 667–677.

Cui, J., Xie, L., & Zheng, X. (2023). Climate change, air conditioning, and urbanization—evidence from daily household electricity consumption data in china. *Climatic Change*, *176*, 106. https://doi.org/10.1007/s10584-023-03589-y

Dunne, J. P., Horowitz, L. W., Adcroft, A. J., Ginoux, P., Held, I. M., John, V. G., Krasting, J. P., Malyshev, S., Naik, V., Paulot, F., Shevliakova, E., Stock, C. A., Zadeh, N., Balaji, V., Blanton, C., Dunne, K. A., Dupuis, C., Durachta, J., Dussin, R., & ... Zhao, M. (2020). The gfdl earth system model version 4.1 (gfdl-esm 4.1): Overall coupled model description and simulation characteristics. *Journal of Advances in Modeling Earth Systems*, *12*(11), e2019MS002015. https://doi.org/10.1029/2019MS002015

Falkner, R. (2016). The paris agreement and the new logic of international climate politics. *International Affairs*, *92*(5), 1107–1125. https://doi.org/10.1111/1468-2346.12708

Friedman, J. H. (1993). *Technical report no. 110: Fast mars* (tech. rep.). Stanford University Department of Statistics. http://scholar.google.com/scholar?hl=en&btnG=Search&q=intitle:Fast+MARS#0

Friedman, J. (1991). Multivariate adaptive regression splines. *Annals of Statistics*, *19*(1), 1–67. https://doi.org/10.1214/aos/1176347963

Gastli, A., Charabi, Y., Alammari, R., & Ali, M. (2013). Correlation between climate data and maximum electricity demand in qatar. *2013 7th IEEE GCC Conference and Exhibition, GCC 2013*, 565–570. https://doi.org/10.1109/IEEEGCC.2013.6705841

Geurts, P., Ernst, D., & Wehenkel, L. (2006). Extremely randomized trees. *Machine Learning*, *63*(1), 3–42.

Gurriaran, L., Tanaka, K., Bayram, I., Proestos, Y., Lelieveld, J., & Ciais, P. (2023a). Warming-induced increase in power demand and co2 emissions in qatar and the middle east. *Journal of Cleaner Production*, *382*, 135359. https://doi.org/10.1016/j.jclepro.2022.135359

Gurriaran, L., Tanaka, K., Takahashi, K., & Ciais, P. (2023b). How climate change may shift power demand in japan: Insights from data-driven analysis. *Journal of Environmental Management*, *345*, 118799. https://doi.org/10.1016/j.jenvman.2023.118799

Hadley, S., Erickson, D., Hernandez, J., Broniak, C., & Blasing, T. (2006). Responses of energy use to climate change: A climate modeling study. *Geophysical Research Letters*, *33*. https://doi.org/10.1029/2006GL026652

Harish, S., Singh, N., & Tongia, R. (2020). Impact of temperature on electricity demand: Evidence from delhi and indian states. *Energy Policy*, *140*, 111445. https://doi.org/10.1016/j.enpol.2020.111445

Hastie, T., & Tibshirani, R. (1986). Generalized additive models. *Statistical Science*, *1*(3), 297–310.

Hiruta, Y., Gao, L., & Ashina, S. (2022). A novel method for acquiring rigorous temperature response functions for electricity demand at a regional scale. *Science of the Total Environment*, *819*, 152893. https://doi.org/10.1016/j.scitotenv.2021.152893

Hu, Q., Tang, J., Gao, X., Wang, S., Zhang, D., Qin, Y., Wang, Q., Zhou, Y., Huang, N., Penuelas, J., Sardans, J., Canadell, J. G., Ciais, P., Pan, Z., An, P., Xu, L., & Lun, F. (2023). Future hotter summer greatly increases residential electricity consumption in beijing: A study based on different house layouts and shared socioeconomic pathways. *Science of The Total Environment*, *733*, 104453. https://doi.org/10.1016/j.scs.2023.104453

IEA. (2022). Monthly electricity statistics.

IPCC. (2023). *Climate change 2023: Synthesis report. contribution of working groups i, ii and iii to the sixth assessment report of the intergovernmental panel on climate change* (Core Writing Team, H. Lee and J. Romero, Ed.; tech. rep.). IPCC. Geneva, Switzerland. https://doi.org/10.59327/IPCC/AR6-9789291691647

IRENA. (2022). Renewable energy statistics 2022.

Jovanović, S., Savić, S., Bojić, M., Djordjević, Z., & Nikolić, D. (2015). The impact of the mean daily air temperature change on electricity consumption. *Energy*, *88*, 604–609.

Ke, G., Meng, Q., Finley, T., Wang, T., Chen, W., Ma, W., Ye, Q., & Liu, T.-Y. (2017). Lightgbm: A highly efficient gradient boosting decision tree. *Advances in Neural Information Processing Systems 30*.

Khan, I., Jack, M. W., & Stephenson, J. (2018). Analysis of greenhouse gas emissions in electricity systems using time-varying carbon intensity. *Journal of Cleaner Production*, *184*, 1091–1101. https://doi.org/10.1016/j.jclepro.2018.02.309

Kumar, R., Rachunok, B., Maia-Silva, D., & Nateghi, R. (2020). Asymmetrical response of california electricity demand to summer-time temperature variation. *Scientific Reports*, *10*, 10904. https://doi.org/10.1038/s41598-020-67695-y

Labriet, M., Joshi, S. R., Kanadia, A., Edwards, N. R., & Holden, P. B. (2013). Impacts of climate change on heating and cooling: A worldwide estimate from energy and macro-economic perspectives. *SSES Annual Congress 2013*.

Lange, S. (2019). Trend-preserving bias adjustment and statistical downscaling with ISIMIP3BASD (v1.0). *Geoscientific Model Development*, *12*, 3055–3070. https://doi.org/10.5194/gmd-12-3055-2019

Lange, S. (2021). ISIMIP3BASD v2.5.0. https://doi.org/10.5281/zenodo.4686991

Le Quéré, C., Jackson, R., Jones, M., & et al. (2020). Temporary reduction in daily global CO2 emissions during the COVID-19 forced confinement. *Nature Climate Change*, *10*, 647–653. https://doi.org/10.1038/s41558-020-0797-x

Li, Y., Pizer, B., & wu, L. (2018). Climate change and residential electricity consumption in the yangtze river delta, china. *Proceedings of the National Academy of Sciences*, *116*, 201804667. https://doi.org/10.1073/pnas.1804667115

Liu, Z., Ciais, P., Deng, Z., & et al. (2020a). Carbon monitor, a near-real-time daily dataset of global co2 emission from fossil fuel and cement production. *Scientific Data*, *7*, 392. https://doi.org/10.1038/s41597-020-00708-7

Liu, Z., Ciais, P., Deng, Z., & et al. (2020b). Near-real-time monitoring of global co2 emissions reveals the effects of the covid-19 pandemic. *Nature Communications*, *11*, 5172. https://doi.org/10.1038/s41467-020-18922-7

Maia-Silva, D., Kumar, R., & Nateghi, R. (2020). The critical role of humidity in modeling summer electricity demand across the united states. *Nature Communications*, *11*. https://doi.org/10.1038/s41467-020-15393-8

Mauritsen, T., Bader, J., Becker, T., Behrens, J., Bittner, M., Brokopf, R., Brovkin, V., Claussen, M., Crueger, T., Esch, M., Fast, I., Fiedler, S., Fläschner, D., Gayler, V., Giorgetta, M., Goll, D. S., Haak, H., Hagemann, S., Hedemann, C., & Roeckner, E. (2019). Developments in the MPI-M earth system model version 1.2 (MPI-ESM1.2) and its response to increasing CO2. *Journal of Advances in Modeling Earth Systems*, *11*(4), 998–1038. https://doi.org/10.1029/2018MS001400

McFarland, J., Zhou, Y., Clarke, L., & et al. (2015). Impacts of rising air temperatures and emissions mitigation on electricity demand and supply in the united states: A multi-model comparison. *Climatic Change*, *131*, 111–125. https://doi.org/10.1007/s10584-015-1380-8

Millborrow, S. (2012). *Earth: Multivariate adaptive regression spline models* [URL: http://cran.r-project.org/web/packages/earth/index.html].

Miller, J. I., & Nam, K. (2022). Modeling peak electricity demand: A semiparametric approach using weather-driven cross-temperature response functions. *Energy Economics*, *114*, 106291.

Molnar, C. (2020). *Interpretable machine learning*. lulu.com.

Montgomery, D., & Peck, E. (1992). *Introduction to linear regression analysis* (2nd). Wiley.

Mora, C. e. a. (2017). Global risk of deadly heat. *Nature Climate Change*, *7*, 501–506. https://doi.org/10.1038/NCLIMATE3322

Moral-Carcedo, J., & Viceñs-Otero, J. (2005). Modelling the non-linear response of spanish electricity demand to temperature variations. *Energy Economics*, *27*, 477–494.

Muñoz Sabater, J. (2019). Era5-land hourly data from 1981 to present. copernicus climate change service (c3s) climate data store (cds) [Accessed on February 2023]. https://doi.org/10.24381/cds.e2161bac

Obringer, R., Nateghi, R., Maia-Silva, D., Mukherjee, S., CR, V., McRoberts, D., & Kumar, R. (2022). Implications of increasing household air conditioning use across the united states under a warming climate. *Earth's Future*, *10*. https://doi.org/10.1029/2021EF002434

O'Neill, B., Kriegler, E., Ebi, K., Kemp-Benedict, E., Riahi, K., Rothman, D., van Ruijven, B., Vuuren, D., Birkmann, J., Kok, K., Levy, M., & Solecki, W. (2015). The roads ahead: Narratives for shared socioeconomic pathways describing world futures in the 21st century. *Global Environmental Change*, *42*. https://doi.org/10.1016/j.gloenvcha.2015.01.004

Opitz, D., & Maclin, R. (1999). Popular ensemble methods: An empirical study. *arXiv preprint arXiv:1106.0257*, *11*. https://doi.org/10.1613/jair.614

Peirson, J., & Henley, A. (1994). Electricity load and temperature: Issues in dynamic specification. *Energy Economics*, *16*(4), 235–243.

Pohlman, J., & Leitner, D. (2003). A comparison of ordinary least squares and logistic regression. *OHIO J SCI*.

Santamouris, M., Cartalis, C., Synnefa, A., & Kolokotsa, D. (2015). On the impact of urban heat island and global warming on the power demand and electricity consumption of buildings—a review. *Energy and Buildings*, *98*, 119–124. https://doi.org/10.1016/j.enbuild.2014.09.052

Santos-Alamillos, F. J., Archer, C. L., Noel, L., Budischak, C., & Facciolo, W. (2017). Assessing the economic feasibility of the gradual decarbonization of a large electric power system. *Journal of Cleaner Production*, *147*, 130–141. https://doi.org/10.1016/j.jclepro.2017.01.097

Sellar, A. A., Jones, C. G., Mulcahy, J. P., Tang, Y., Yool, A., Wiltshire, A., Stringer, M., Hill, R., Palmieri, J., Woodward, S., Mora, L. D., Kuhlbrodt, T., Rumbold, S. T., Kelley, D. I., Ellis, R., Johnson, C. E., Walton, J., Abraham, N. L., Andrews, M. B., & Zerroukat, M. (2019). Ukesm1: Description and evaluation of the u.k. earth system model. *Journal of Advances in Modeling Earth Systems*, *11*(12), 4513–4558. https://doi.org/10.1029/2019MS001739

Stephenson, S. R., Oculi, N., Bauer, A., & Carhuayano, S. (2019). Convergence and divergence of UNFCCC nationally determined contributions. *Annals of the American Association of Geographers*, *109*(4), 1240–1261. https://doi.org/10.1080/24694452.2018.1536533

UNFCCC. (2016). Paris agreement [United Nations Framework Convention on Climate Change]. https://unfccc.int/sites/default/files/english_paris_agreement.pdf

Van Ruijven, B., De Cian, E., & Wing, I. (2019). Amplification of future energy demand growth due to climate change. *Nature Communications*, *10*, 2762. https://doi.org/10.1038/s41467-019-10399-3

Wood, S. N. (2006). *Generalized additive models: An introduction with r*. CRC press.

Yalew, S., van Vliet, M., Gernaat, D., Ludwig, F., Miara, A., Park, C., Byers, E., De Cian, E., Piontek, F., Iyer, G., Mouratiadou, I., Glynn, J., Hejazi, M., Dessens, O., Rochedo, P., Pietzcker, R., Schaeffer, R., Fujimori, S., Dasgupta, S., & Vuuren, D. (2020). Impacts of climate change on energy systems in global and regional scenarios. *Nature Energy*, *5*. https://doi.org/10.1038/s41560-020-0664-z

Yan, Y. Y. (1998). Climate and residential electricity consumption in hong kong. *Energy*, *23*(1), 17–20.

Yukimoto, S., Kawai, H., Koshiro, T., Oshima, N., Yoshida, K., URAKAWA, S., TSUJINO, H., Deushi, M., Tanaka, T., Hosaka, M., YABU, S., YOSHIMURA, H., SHINDO, E., MIZUTA, R., OBATA, A., ADACHI, Y., & ISHII, M. (2019). The meteorological research institute earth system model version 2.0, mri-esm2.0: Description and basic evaluation of the physical component. *Journal of the Meteorological Society of Japan*, *97*. https://doi.org/10.2151/jmsj.2019-051

Zhang, C., Liao, H., & Mi, Z. (2019). Climate impacts: Temperature and electricity consumption. *Natural Hazards*, *99*, 1259–1275. https://doi.org/10.1007/s11069-019-03653-w

Zhu, B., Song, X., Deng, Z., Zhao, W., Huo, D., Sun, T., Ke, P., Cui, D., Lu, C., Zhong, H., Hong, C., Qiu, J., Davis, S. J., Gentine, P., Ciais, P., & Liu, Z. (2022). Carbon monitor-power: Near-real-time monitoring of global power generation on hourly to daily scales.

Zittis, G., Hadjinicolaou, P., Almazroui, M., et al. (2021). Business-as-usual will lead to super and ultra-extreme heatwaves in the middle east and north africa. *npj Climate and Atmospheric Science*, *4*, 20. https://doi.org/10.1038/s41612-021-00178-7

CHAPTER II

WARMING-INDUCED INCREASE IN POWER DEMAND AND CO_2 EMISSIONS IN QATAR AND THE MIDDLE EAST

In this section, we delve into the detailed case study of Qatar. It is important to note that this initial investigation was conducted without the Carbon Monitor-Power data, as Qatar is not represented in this database.

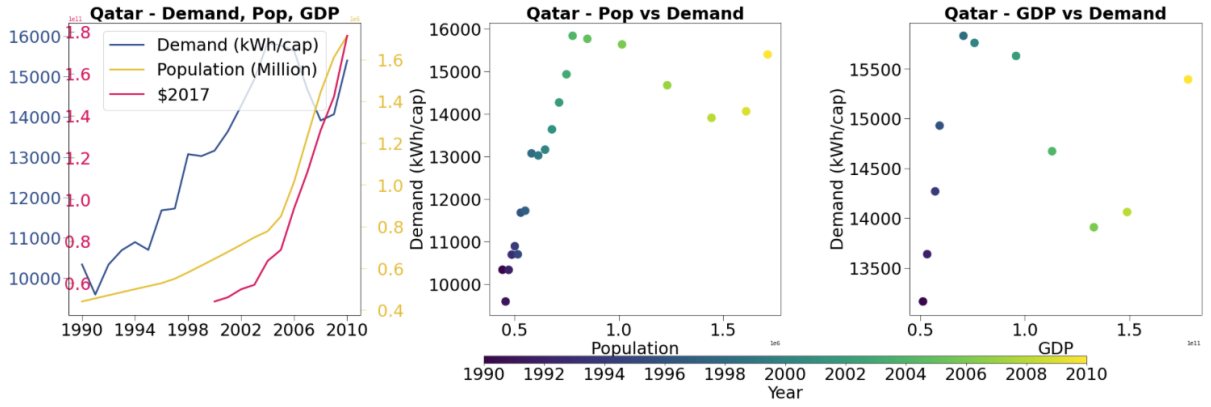

Figure II.1: Comparison and correlation Energy Demand, Population, and GDP Trends for Qatar (1990-2010)

Qatar's study involves projecting CO_2 emissions from electricity demand through the end of the century, considering the effects of evolving GDP and population on that demand. I have assumed a basic linear relationship between electricity demand, population, and GDP to facilitate this. This linear relationship holds up well, especially over the historical period from 1990 to 2010. The evidence from World Bank data (Figure II.1) nicely underscores this point

(World Bank, 2023). However, it is important to note that the financial upheaval of 2007-2008 introduced some deviations from linearity for Qatar toward the end of this historical span.

For future projections, I have chosen to stick with this simple linear framework for estimating electricity demand, incorporating the variables of population and GDP. This choice is deliberate and is intended to maintain clarity and simplicity. However, this approach requires thoughtful consideration, as the linear relationship will not be guaranteed to continue.

1 Summary

Qatar was chosen as the starting point for my thesis for several reasons. Firstly, the Arabian Peninsula region, including Qatar, has been relatively understudied in terms of the impact of climate change on electricity demand. This knowledge gap made Qatar an ideal candidate for comprehensive analysis as we had power demand data for Qatar at our disposal. Secondly, the region is experiencing some of the fastest global warming rates, making it a critical area to investigate in the context of climate change effects. Qatar's climate is particularly characterized by extremely high temperatures, and these conditions have a significant influence on electricity demand. Lastly, Qatar serves as a straightforward and representative case study. The country's power generation predominantly relies on natural gas, and electricity demand highly depends on temperature variations. This simplicity makes Qatar an excellent starting point for understanding the relationship between climate, electricity demand, and CO_2 emissions in a context that can be readily applied to other regions with similar characteristics.

Rising global temperatures in the Arabian Peninsula caused by climate change have increased the demand for air conditioning, resulting in more electricity consumption and CO_2v emissions from electricity production. This paper treats Qatar as a representative country among the six Gulf Cooperation Council (GCC) countries (Bahrain, Kuwait, Oman, Qatar, Saudi Arabia, and the United Arab Emirates) for understanding the effect of future regional warming on electricity demand and CO_2 emissions. We first develop a statistical model that relates daily electricity demand with temperature. Polynomial regressions of a different order (1, 2, 3) between power demand and temperature were tested on different metrics: total or peak daily load combined with daily minimum, maximum, or mean temperature. The second-order polynomial regression was found to be the best model for Qatar. The effect of weekends, working days, and holidays on power demand was accounted for by adding categorical variables to the polynomial model. By combining this model with temperature projections from the CMIP6 database (bias adjusted and statistically downscaled) and population and GDP pro-

jections from four shared socioeconomic pathways (SSPs), we can calculate Qatar's demand for electricity until the end of the century. We worked with SSP1-2.6, SSP2-4.5, SSP3-7.0, and SSP5-8.5, going from the least increase in global temperature to the highest, and we used temperature projections from 10 Earth System Models (ESMs). For each scenario, a projection of the carbon intensity of power production was developed to align with the SSPs' narratives. This was achieved by considering Qatar's communicated commitments and capacity for incorporating renewable energy into its power generation infrastructure.

Our model identifies an average sensitivity of +4.2%/°C for electricity demand and projects an increase in electricity demand by 5–35% due to warming alone at the end of this century, depending on the scenario. The model suggests that under SSP1-2.6, warming-induced CO_2 emissions could be offset by carbon intensity improvements. Furthermore, under SSP5-8.5, assuming no carbon intensity improvement, future warming could add 20–35% of CO_2 emissions per year by the end of the century, with half of the electricity demand related to more frequent hot days. However, when considered alone, the effect of climate change on the power demand and the further effect on CO_2 emissions are small relative to socioeconomic factors, i.e., population, GDP, and carbon intensity.

This work has been published as: Gurriaran, L., Tanaka, K., Bayram, I. S., Proestos, Y., Lelieveld, J., and Ciais, P. (2023). Warming-induced increase in power demand and CO_2 emissions in Qatar and the Middle East, Journal of Cleaner Production, 382, 135359, ISSN 0959-6526. See Appendix 1 for the supplementary materials.

2 Abstract

Rising global temperatures in the Arabian Peninsula region caused by climate change have increased the demand for air conditioning, resulting in more electricity consumption and CO_2 emissions. This paper treats Qatar as a representative country for understanding the effect of future regional warming on the electricity demand and CO_2 emissions. We first develop a model that relates daily electricity demand with temperature. By combining this model with temperature projections from the CMIP6 database (bias adjusted and statistically downscaled)and population and GDP projections from four shared socioeconomic pathways (SSPs), we can calculate Qatar's demand for electricity until the end of the century. The model identifies an average sensitivity of +4.2%/°C for the electricity demand and projects an increase in electricity demand by 5–35% due to warming alone at the end of this century. The model suggests that under SSP1-2.6, warming-induced CO_2 emissions could be offset by carbon intensity

improvements. Furthermore, under SSP5-8.5, assuming no carbon intensity improvement, future warming could add 20–35% of CO_2 emissions per year by the end of the century, with half of the electricity demand related to more frequent hot days. We further found that the temperature effect on power demand and CO_2 emissions is small compared to the effects from socioeconomic factors such as population, GDP, and carbon intensity.

3 Introduction

3.1 Background

The scientific community agrees that fossil fuel CO_2 emissions induce global warming (IPCC, 2021). However, one question that remains unaddressed concerns how rising temperatures will subsequently influence anthropogenic CO_2 emissions. According to the International Energy Agency (IEA, 2019), more than 40% of the global anthropogenic CO_2 emissions in 2018 originated from electricity and heat producers. However, although countries might generate the same amount of electricity, their CO_2 emissions might differ. In Middle Eastern countries, the vast majority of electricity is produced with fossil fuels. In Qatar, for example, 100% of the electricity is currently produced with natural gas (IEA, 2019; Okonkwo et al., 2021). Air conditioning has been identified as consuming the most electricity in Qatar's residential sector (Alrawi et al., 2019); warmer conditions in the future will therefore raise the electricity demand unless decarbonization policies such as the installation of photovoltaics and improvements in building energy efficiency or behavioral changes counteract this response. This work studies how the frequency and intensity of hot days and regional warming in the future may influence electricity demand in Qatar and provides further feedback on electricity-related CO_2 emissions.

3.2 Literature Review

We distinguish two types of studies in the scientific literature related to how climate change relates to energy demand. The first type includes studies that examine relationships between electricity demand and climate from a local point of view, usually on a country, city, district, or household scale. Such studies establish relationships between climate variables and electricity loads, showing that power demand is temperature-dependent. Scientific publications of this type tend to focus on European countries. For example, Valor et al., 2001, showed a nonlinear relationship between temperature and electricity demand in Spain. Jovanović et al., 2015, studied the effect of changing temperature on power demand in Kragujevac, Serbia, which demonstrated similar relationships. Canales et al., 2020, also established these relationships for Poland using data from 19 major cities and studied the impact of temperature on renewable energy capacities. These studies are based on activities and meteorological data and have not yet been used for long-term energy demand forecasting.

The second type of study includes modeling studies that forecast energy demand and electrical loads. As summarized by Mir et al., 2020, there are several methods to forecast loads. For example, bottom-up models can project long-term energy demand by incorporating detailed processes that control load while considering technological progress. In contrast, top-down models such as econometric forecast models can simulate the relationships between socioeconomic drivers of power demand; however, they rarely describe the benefit from technological advances as an endogenous process. Such models are used to understand the impact of policies on electricity demand. Another method relies on time series data to project future values of the loads from previously observed power demand. Finally, some methods incorporate artificial intelligence, ranging from a simple ordinary least square regression (the method used in this study) to artificial neural networks or additive models.

Although these methods use socioeconomic indicators to project long-term power demand, the number of studies considering the impacts of climate is currently limited. At a country level, Auffhammer et al., 2016, established a relationship between power demand and temperature for 166 distinct load zones in the United States. They then projected the impact of climate change on power demand using output from 20 downscaled climate models (GCM). The models projected an increase in peak events in the US in frequency and intensity, which may cause outages if the grid's capacity is not increased. On a global scale, Van Ruijven et al., 2019, used a top-down approach to project future energy demand under two emission scenarios simulated with 21 ESMs. Their approach predicted a 25% increase in energy demand in the tropics, USA, Europe, and China under high warming.

The existence of regional gaps remains one of the major issues unaddressed by the literature. Yalew et al., 2020, highlighted that regions such as South Asia, the Middle East, North Africa, and the Pacific region are under-represented in such studies. No peer-reviewed publications investigate load forecasting in Qatar, with the exception of a conference paper (Gastli et al., 2013) that explored the link between temperature and humidity and power demand in the country during 2012. The question of the climate impact on power demand and its associated CO_2 emissions in Qatar and the Middle East more generally remains unexplored.

3.3 Description of the Case Study

Qatar has one of the highest GDPs per capita in the world ($93,521.4 PPP in 2021, Bank, 2021). Its power generation capacity was 10.5 GW in 2019 (QPSA, 2019). However, power outages have occurred during periods of extreme heat (Bayram et al., 2018) due to the inability of the grid to meet peak demand: the 200% increase in demand between 2000 and 2010 corresponds with the pressure put upon Qatar's electricity grid. Rapid population growth also occurred during the same years, increasing from 600,000 in 2000 to nearly 2 million in 2010, primarily due to immigration (UN, 2021). Relatedly, consumption per capita increased from 9.6 MWh/capita in 1990 to 16.6 MWh/capita in 2018 (IEA, 2019). Three factors can further explain the increase in electricity demand:

1) Qatar's GDP per capita increased dramatically during the 2000s to become one of the highest in the world (9th or 10th according to the International Monetary Fund and the World Bank, respectively (Bank, 2021; IMF, 2021).

2) Electricity prices are highly subsidized by the government and are thus low for the residential sector. The price was 0.032 US$/kWh in Qatar in December 2020 compared to 0.148 US$/kWh in the US in the same period (GPP, 2021).

3) There are no clear incentives from the government to limit the demand for electricity due to its vast amount of fossil fuel resources. Thus, people can financially afford to use large amounts of electricity. The financial accessibility of electricity combined with the very hot climate results in a high demand for cooling and induces an increase in total electricity consumption.

As temperatures in Qatar are rising faster than the global average (IPCC, 2021), it is important to elucidate the effect of increasing hot days on per capita electricity consumption and to assess the further effect on CO_2 emissions under socioeconomic scenarios.

As of 2022, all of Qatar's electricity is produced by gas-fired power plants. Such power plants resulted in emissions of 23 $MtCO_2$ in 2018 (IEA, 2019). In 2008, Qatar published its "National Vision 2030" (GSDP, 2008), where its strategy for developing renewable energy first appeared. In 2017, Qatar announced its first concrete goal: by 2030, 20% of its electricity will be produced from solar energy (OBG, 2017). However, recent studies on the development of renewable energy in Qatar and other Gulf countries argue that actions and commitments on the part of the government, as well as increased public awareness of environmental issues are necessary to develop renewables, reduce per capita electricity consumption, and induce behavioral changes in the energy consumption (Al-Marri et al., 2018; Umar et al., 2020). As stated above, there are currently few incentives to reduce individual energy consumption (Al-Marri et al., 2018), which leads Umar et al., 2020, to conclude that these announced ambitions are unlikely to be realized in a timely manner. With the projected increase in the population of Qatar (Kc et al., 2017) and the future increase in temperatures (IPCC, 2021), the evolution of electricity demand under climate change and the consequences it could have on CO_2 emissions have become increasingly important to understand.

This study investigates how the changes in average daily temperature can influence daily electricity demands, as well as how much the CO_2 emissions related to electricity production in Qatar may increase with warming under changing socioeconomic drivers. These questions are addressed via a novel statistical model that estimates the daily electricity demand and associated CO_2 emissions from temperature data. Section 4 describes the data used to establish the relationship between temperature and electricity demand. This section also discusses how the model considers other factors, i.e., population, GDP, and the carbon intensity of electricity production. Section 5 applies the model to future climatic conditions based on downscaled CMIP6 (Coupled Model Intercomparison Project) temperature projections bias-adjusted for the region of Qatar until the end of the century. Section 5 also presents the results for electricity demand projections and associated CO_2 emissions and estimates the contribution of climatic and socioeconomic factors to the total emissions. Section 6 then draws conclusions on the importance of considering the temperature-emissions feedback in projections of future energy and emissions changes broadly for the Middle East.

4 Material and Methods: Model Development

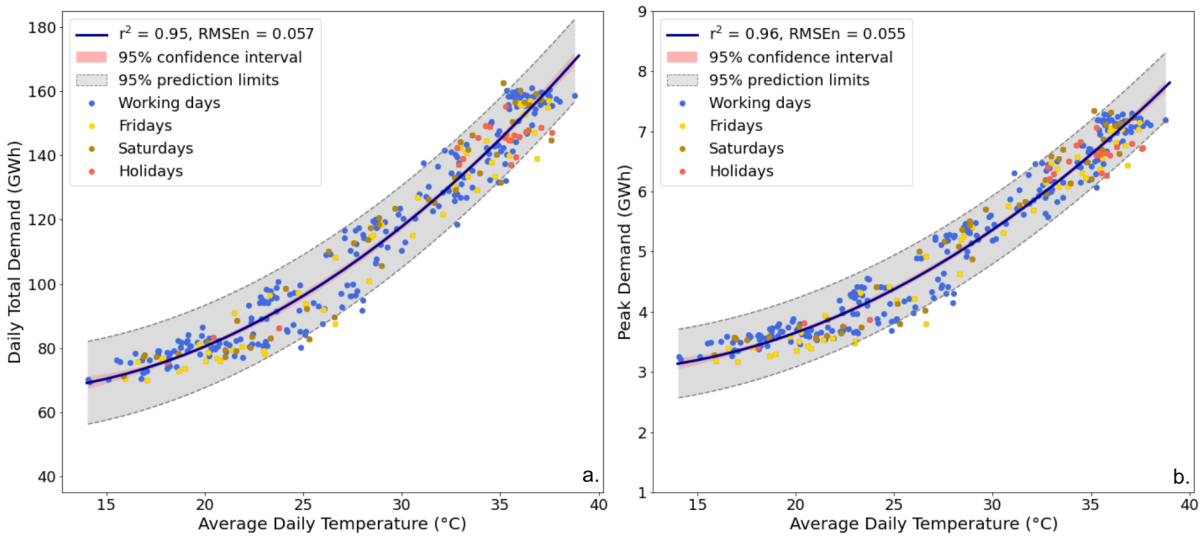

Figure II.2: Relationships between temperature and power demand in Qatar: Daily total electricity demand (a) and peak demand (b) in Qatar as a function of Qatar's daily average temperature for 2016. Blue points represent working days, yellow points represent Fridays, brown points represent Saturdays, and red points represent holidays. The thick blue line is the second-order polynomial regression fit, with its 95% confidence interval in the pink area. The gray area indicates the 95% prediction limits (a 95% chance of finding the value of the electricity demand for a given temperature).

We developed a statistical model describing the temperature dependence of electricity demand using hourly electricity data from Qatar for 2016. Qatar is chosen as a representative country of the Middle East, as good quality data on the country's daily electricity consumption is available for this year (Bayram et al., 2018). Qatar's power company has no legal obligation to publish electricity demand, consumption, or production data regularly. However, as a member of the Gulf Cooperation Council Interconnection Authority (GCCIA), Qatar provides electricity production online in real-time on the GCC website (GCC, 2016). There is no public archive; the data had to be retrieved by the minute from the website. We aggregated the data by hours and days to calibrate our statistical model. Figures II.2a and II.2b present these data at a daily timescale as a function of the daily average temperature in Qatar. Qatar's daily average temperatures are based on hourly temperature values from ERA5 reanalysis (CDS, 2017) at a resolution of 0.25°x0.25° averaged within Qatar's borders. Figure II.2 shows a very strong relationship between electricity demand and temperature. We performed a regression analysis to study the relationship between the electricity demand (daily and peak load) and the temperatures (daily minimum, maximum, and average temperature). We found that the highest correlation can be obtained with the daily average temperature. We fitted polynomial functions with different orders (1, 2, and 3). For the rest of the study, we retained the order of 2, which offers a compromise between a high coefficient of determination and a low normalized RMSE for the total

daily load (r2 = 0.95, RMSE = 0.057) and for hourly loads (r2 = 0.96 and RMSE = 0.055). To account for the effect of weekends and holidays on electricity demand in Qatar, we added two categorical variables to the model for each day: the DOW variable (day of week, i.e., Monday, Tuesday, etc.) and the binary variable holiday (yes or no). Note that what is equivalent to weekends in the West are Fridays and Saturdays in Qatar. A small but statistically significant effect for peak demand was identified for Fridays, but for total daily demand, the same effect was found to be insignificant (p-value is 0.120). No effects were found to be statistically significant on holidays and Saturdays for peak and total demand with p-values higher than 0.1.

To understand the importance of the temperature effect on future CO_2 emissions from electricity production compared to the effects from socioeconomic drivers of population and GDP (Khalifa et al., 2019), we applied the Kaya Identity (Kaya, 1990), as shown in Eq. II.1.

$$E = \frac{E}{TEP} \times \frac{TEP}{GDP} \times \frac{GDP}{pop} \times pop \tag{II.1}$$

where E is the CO_2 emissions from electricity demand, TEP is the total electricity production, GDP is the gross domestic product, and pop is the population. $\frac{E}{TEP} = I$, where I is the carbon intensity of electricity production. We considered the effect of temperature in the term TEP: for each day, TEP is calculated with the quadratic function: $f(T_i) = aT_i^2 + bT_i + c$, where $f(T_i)$ denotes the daily demand and T_i the average temperature of the day i. The quadratic function was fitted to the daily electricity demand and temperature data of 2016. To calculate the annual demand, TEP_y, we summed the daily demand over the year y: $TEP_y = \sum_i f(T_{i,y})$. Then, we adjusted TEP_y with a scaling factor to account for the effect of population growth and GDP on power demand: $\frac{GDP_y \times pop_y}{GDP_{2016} \times pop_{2016}}$. According to Eq. II.1, we multiply TEP_y by the carbon intensity of electricity production to calculate the CO_2 emissions associated with the electricity demand. Hence, we can write:

$$E_y = I_y \times TEP_y \times \frac{GDP_y \times pop_y}{GDP_{2016} \times pop_{2016}} \tag{II.2}$$

We chose to employ this simple approach due to the limitation of data that would be required to capture complex underlying relationships (Mir et al., 2020). More detailed modeling approaches are typically applied only over a short term. For long-term analyses such as this study, we argue that a simple approach is more appropriate, given the difficulty in explicitly describing how the socioeconomic system and the power sector may evolve throughout this century and affect CO_2 emissions. We further assume that temperature, population, GDP, and

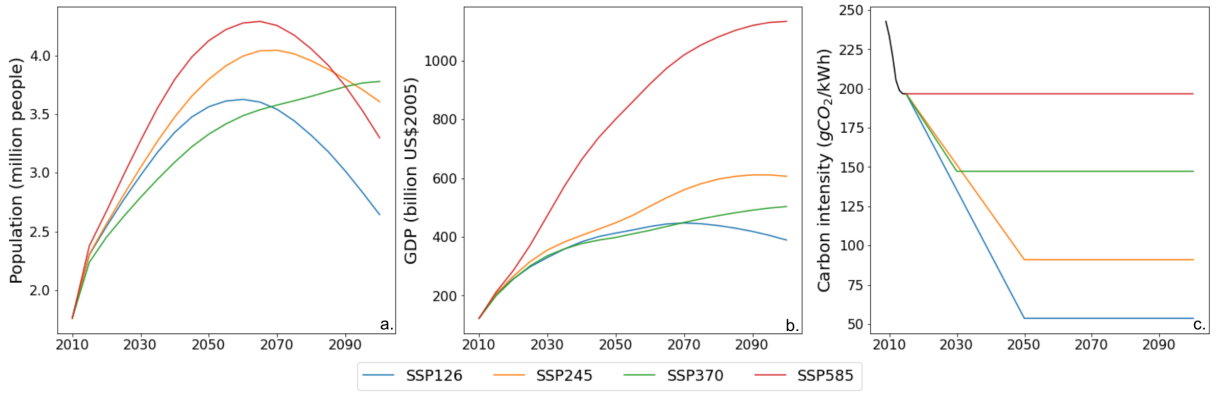

Figure II.3: Projections of socioeconomic data for Qatar under different SSPs: Projections of (a) population, (b) GDP and (c) carbon intensity for Qatar until the end of this century for SSP1-2.6 (blue), SSP2-4.5 (yellow), SSP3-7.0 (green) and SSP5-8.5 (red). Population and GDP data were obtained from the SSP database (Dellink et al., 2017; Kc et al., 2017; Riahi et al., 2017), and carbon intensity values were calculated based on assumptions detailed in the Methods (Section 4).

carbon intensity independently influence the CO_2 emissions from electricity production without cross-interactions.

Finally, Eqs. II.1 and II.2 were applied for projecting the electricity demand and CO_2 emissions using daily average temperature projections from the downscaled CMIP6 database, bias-adjusted for the region of Qatar (Cannon et al., 2015; Cucchi et al., 2020; Werner et al., 2016), from ten General Circulation Models (CESM2-WACCM, CMCC-CM2, EC-Earth3, EC-Earth3-Veg, GFDL-ESM4, INM-CM4-8, INM-CM5-0, MPI-ESM1-2, MRI-ESM2-0, NorESM2). We considered four SSPs (O'Neill et al., 2015): SSP1-2.6, the sustainability scenario; SSP2-4.5, the middle of the road scenario; SSP3-7.0, the regional rivalry scenario; and SSP5-8.5, the fossil-fueled development scenario. We used specific temperature, population, and GDP projections for each SSP. The population and GDP projections (cf. Figs II.3a and II.3b) were obtained from the SSP database (Dellink et al., 2017; Kc et al., 2017; Riahi et al., 2017). These quantitative projections for different storylines are developed by the Integrated Assessment Modeling community. The population projections were converted from the SSP storylines for 195 countries, considering age, gender, and level of education (Kc et al., 2017). Considering the level of education allows a better understanding of socioeconomic issues that can influence demographics. These projections are available at the country level, hence, we used specific projections for Qatar. GDP projections were also developed from the SSP storylines for 184 countries, including Qatar (Dellink et al., 2017). Here we use them as an indicator of possible futures rather than a prediction since it is inherently impossible to make a long-term prediction of the socioeconomic system.

In 2011, Qatar released its Initial National Communication to the UNFCCC, in which national GHG emission factors for the power sector and water desalination (14.9 tC/TJ) were

reported. These emission factors were used in this study. Concerning the evolution of carbon intensity, we made assumptions based on the literature and SSP storylines as follows:

- SSP1 — the "road for sustainability": Qatar will fully exploit its renewable energy potential by 2050. Okonkwo et al., 2021, identified various renewable energy opportunities in Qatar and their potential. Based on that study, we established a scenario in which by 2050, Qatar would produce 92% of its electricity from renewable energies (40% with wind energy, 35% with concentrated solar power, 15% with biomass, and 2% with pumped-storage hydroelectricity); only the remaining 8% would be produced from natural gas. With this assumed energy mix, we obtained a carbon intensity of 50 CO_2eq/kWh in 2050, which represents a decrease of approximately 75% compared to the current value. Then, the carbon intensity is assumed to remain constant for the rest of the century.
- SSP2 — "Middle of the road": Qatar will not fully exploit its renewable energy potential but will still make significant progress in this direction. It will reach 30% of electricity produced from solar PV and 30% from wind energy by 2050. Then, the carbon intensity is assumed to be at the 2050 level for the rest of the century.
- SSP3 — "Regional rivalry": Qatar will keep to its ambitions of 20% of electricity produced by solar energy by 2030, as announced by the government (OBG, 2017). Then the carbon intensity is assumed to be at the 2030 level for the rest of the century.
- SSP5 — "Fossil-fueled development": The emission factors reported by Qatar in their 2011 National Communication to the UNFCCC are assumed for the rest of the century.

Changes in carbon intensity until the end of the century obtained with these assumptions are presented in Figure II.3c. The projected decreases in carbon intensity for SSP1-2.6, SSP2-4.5, and SSP3-7.0 result from assumed environmental policies aiming to decarbonize Qatar's power sector. We made assumptions about the evolution of environmental policies in Qatar, exploiting the data available to be consistent with the SSP narratives. To estimate the CO_2 emissions from solar PV, concentrated solar power, and pumped-storage hydroelectricity, we used standard emission factors from the Base Carbon (ADEME, 2021). The emission factors for biofuels were taken from the IPCC Guidelines for National Greenhouse Gas Inventories (IPCC, 2006). The emission factor for natural gas (14.9 tC/TJ, i.e., 196 gCO_2eq/kWh) was from Qatar's Initial National Communication to the UNFCCC. Validation of the statistical model can be found in the Supplementary Materials (Appendix 1).

5 Results

5.1 Temperature Impact on Electricity Demand in Qatar

5.1.1 Annual Average Temperature and Electricity Demand

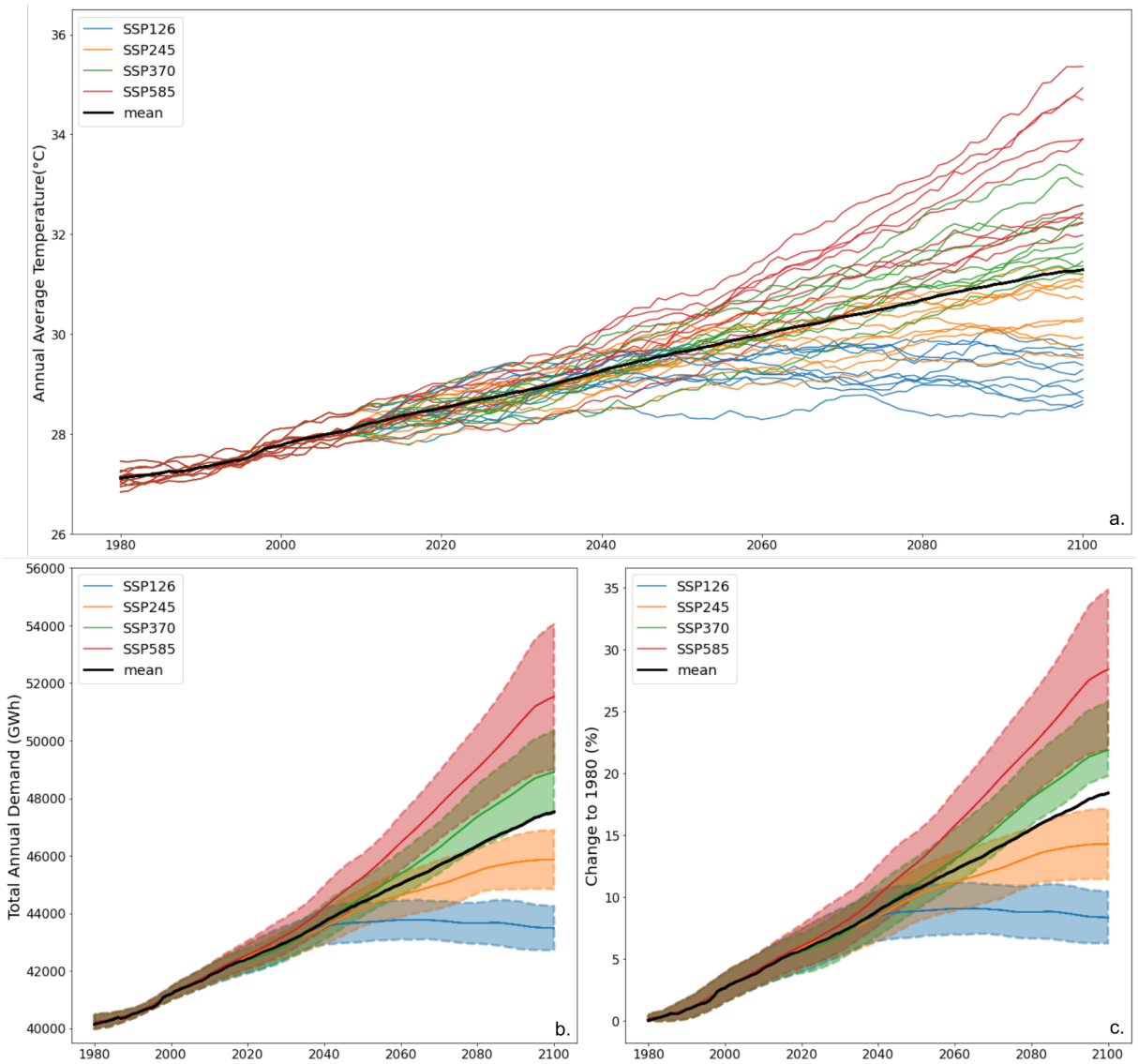

Figure II.4: Projection of electricity demand and average temperature: (a) Bias-adjusted annual average temperature over Qatar from the CMIP6 database for SSP1-2.6 (blue), SSP2-4.5 (orange), SSP3-7.0 (green), and SSP5-8.5 (red) (in 10-year rolling average for the sake of presentation). Each line represents the output of one of the ten CMIP6 GCMs. (b) Total annual demand calculated with the statistical model. (c) Change in demand compared to the year 1980 (in percentage). For (b) and (c), the thick colored lines show the average of the different SSPs and the colored areas with the 1-sigma error ranges.

First, we looked at the effect of temperature on electricity demand. We applied Eq. (2) using mean daily temperature projections while keeping population and GDP constant at their 2016 values. Figure II.4 shows the results for the total daily demand, smoothened with a 10-year rolling average. Projections for the daily maximum hourly demand are shown in the Supplementary Materials (Appendix 1, Fig. S3), as they are very similar in trend and magnitude to the projections obtained for the total daily demand. Figure II.4 shows clear differences between the SSPs during 2040-2050. In Figure II.4c, there is a 15-20% increase in the electricity demand attributable only to the effect of warming. The spreads arising from different climate models are smaller than those from SSPs. Under SSP5-8.5, climate models show increasingly divergent results by the end of the century. Under this scenario, the total annual demand is projected to increase by 35% at the end of the century compared to the 1980 level due to the effect of warming alone, with a mean warming of 4°C in 2080-2100 relative to the current decade. Even under the most optimistic SSP1-2.6 scenario, the additional electricity demand reaches 10% above the current level due to the 1°C warming by the end of this century.

5.1.2 Extreme Annual Temperatures and Electricity Demand

To diagnose the effect of extremely low and high temperatures, we set a low-temperature threshold at the 5th percentile of the 2016 temperature distribution (16.8°C), under which days are categorized as "cold" days. Likewise, we defined hot days with an upper threshold at the 95th percentile of the 2016 temperature distribution (36.8°C). Figure II.5a shows that the number of cold days per year is projected to decrease under all SSPs and even reach zero under SSP5-8.5. In contrast, Figure II.5b shows that the number of hot days per year is projected to increase dramatically under all SSPs (except SSP1-2.6). For SSP1-2.6, the number of hot days remains approximately 50 after 2040. This indicates that the electricity demand during cold periods can decrease over the century and reach very low levels under SSP2-4.5, SSP3-7.0, and SSP5-8.5 (i.e., less than 1% of the annual demand (Fig. II.5c). In contrast, we found that the electricity demand during hot periods would increase and could represent more than half of the annual consumption under SSP5-8.5 (Fig. II.5d). Our results suggest that most of the projected increase in electricity demand is attributable to an increased demand for air conditioning because the average temperature in Qatar is increasing, and heat waves are projected to become more frequent and severe (Zittis et al., 2021).

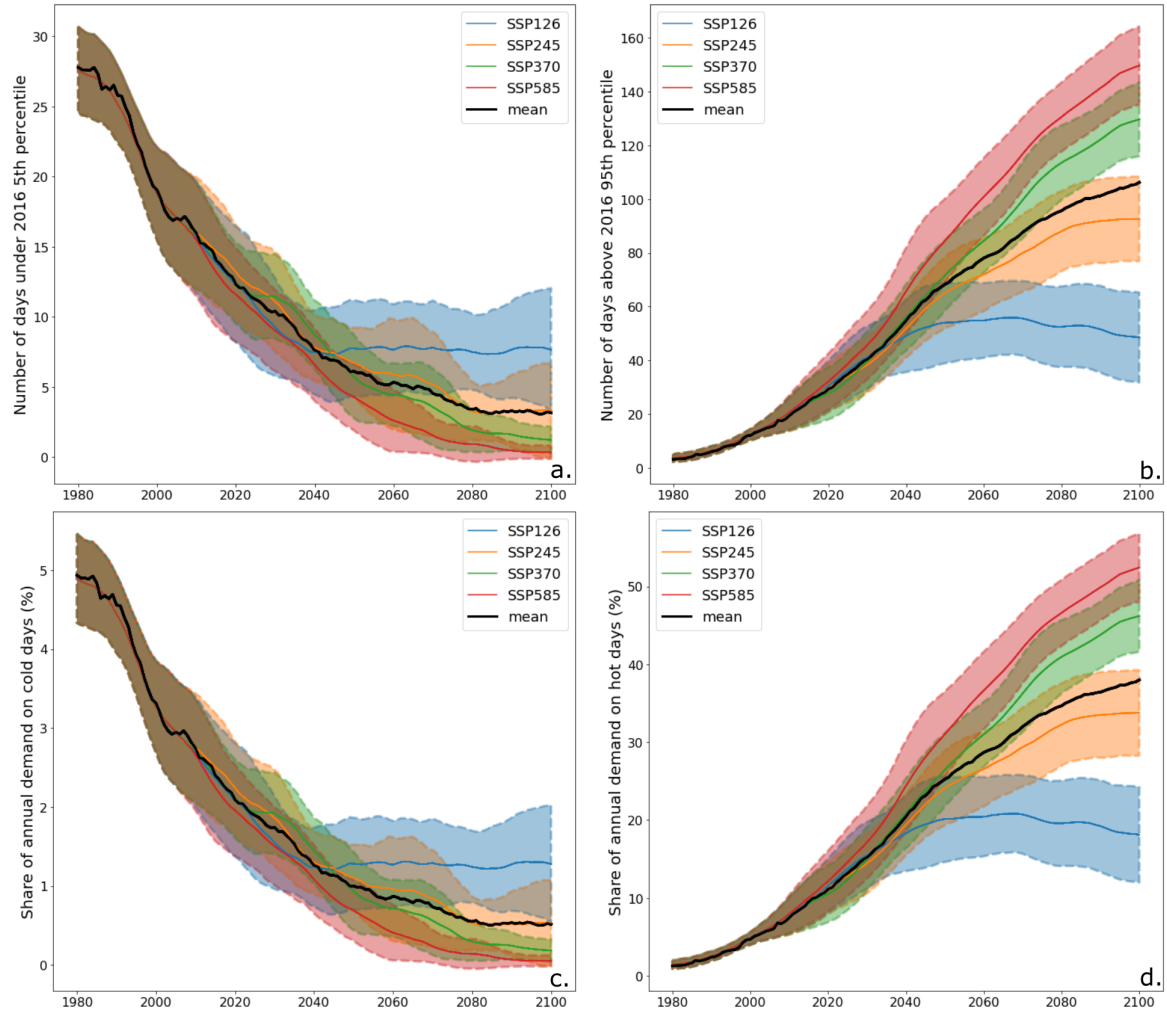

Figure II.5: Electricity demand and extreme temperatures: Year-by-year evolution of the number of cold days (a) and hot days (b) per year and the share of the annual demand during those cold and hot days (c and d). The colored areas represent the 1-sigma error ranges.

5.2 Implication for CO_2 Emissions in Qatar

To calculate the CO_2 emissions associated with the electricity demand, we used Eq. II.2. We calculated the CO_2 emissions for the historical period (2010 - 2020) and the rest of the century. We investigated the contribution of the four independent factors: temperature, population, GDP, and carbon intensity. The results are presented in Figures II.6 and II.7.

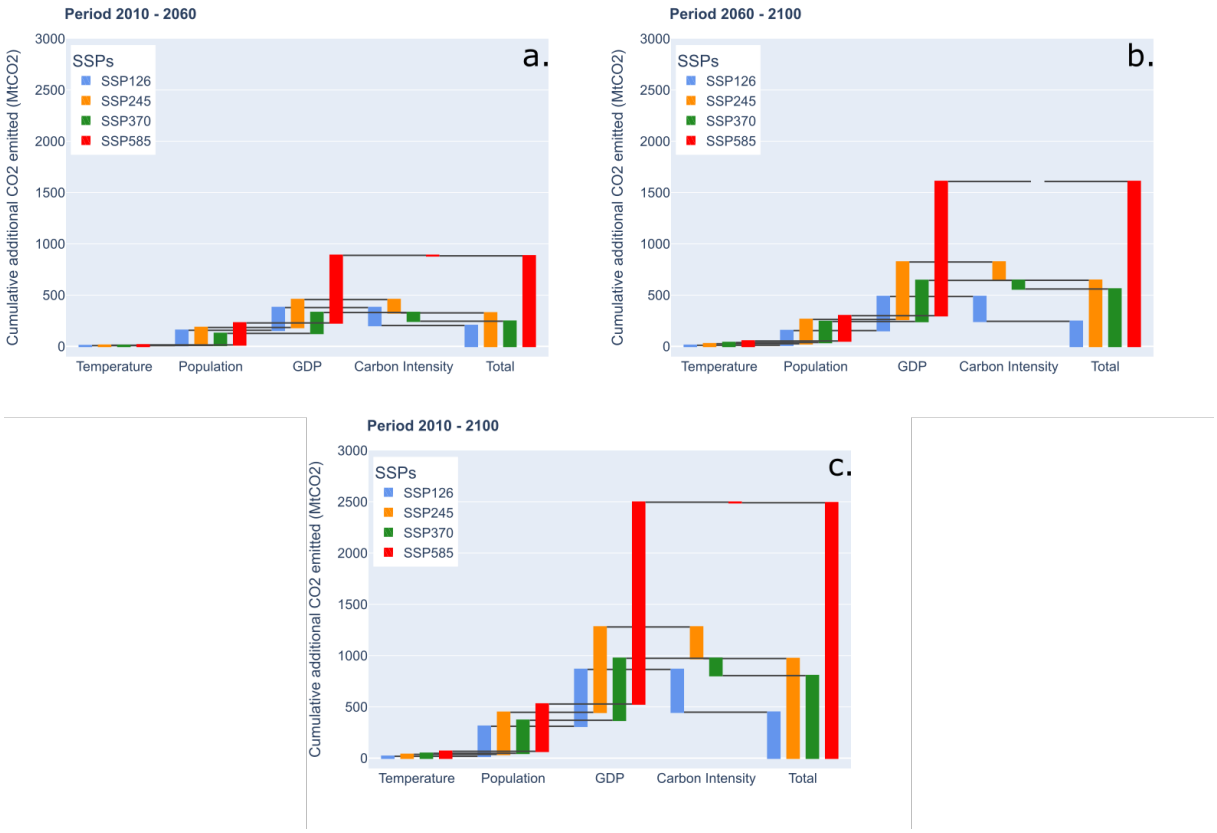

Figure II.6: Attribution of additional CO_2 emissions to different factors: Contributions of changes in climate, population, GDP, and carbon intensity to the changes in cumulative CO_2 emissions from power generation over periods 2010-2060 (a), 2060-2100 (b), and 2010-2100 (c). The figure shows the change in cumulative additional CO_2 emissions due to each factor relative to the level with all other factors kept at current values.

Figure II.6 shows the attribution of the additional cumulative CO_2 emissions to the different factors when only one factor varies, for two periods: the earlier period from 2010 to 2060 (Fig. II.6a) and the later period from 2060 to 2100 (Fig. II.6b). The additional cumulative CO_2 emissions attributed to each factor are obtained by varying only the factor considered and keeping the other factors constant at the level of 2016. Figure II.6 highlights that the importance of the population factor for the total emissions is constant through time and comparable between all SSPs. Thus, it does not explain the difference in emissions over the whole period. Figure II.6 also shows that the GDP effect increase in importance with time and explains almost all of the cumulative emissions changes between the SSPs, especially why emissions in SSP5-8.5 are projected to be more important at this point than those of other scenarios. Indeed, in the second half of the century, the cumulative CO_2 emissions in SSP5-8.5 will be more than twice as large as those in all other SSPs; this occurrence is also visible in the evolution of annual emissions (Fig. II.7). Furthermore, the results for the entire period (Figure II.6c) show that when temperature alone is considered, it is not an important factor compared to other factors in determining the additional CO_2 emissions.

Figure II.7 gives a more nuanced picture by representing the annual CO_2 emissions with and without the effect of temperature change for all SSPs. This result highlights that when combined with the effect of socioeconomic factors, climate change accentuates the changes in annual emissions. The difference in annual emissions between the two scenarios (with and without temperature change) increases over time and with the level of global warming. Under SSP5-8.5, the difference in emissions due to a warmer climate reaches more than 10 $MtCO_2$ per year, while under SSP1-2.6, it is hardly perceptible. This emphasizes the importance of considering the effect of climate change when following a given economic scenario with high warming. Otherwise, the impact on CO_2 emissions may be underestimated.

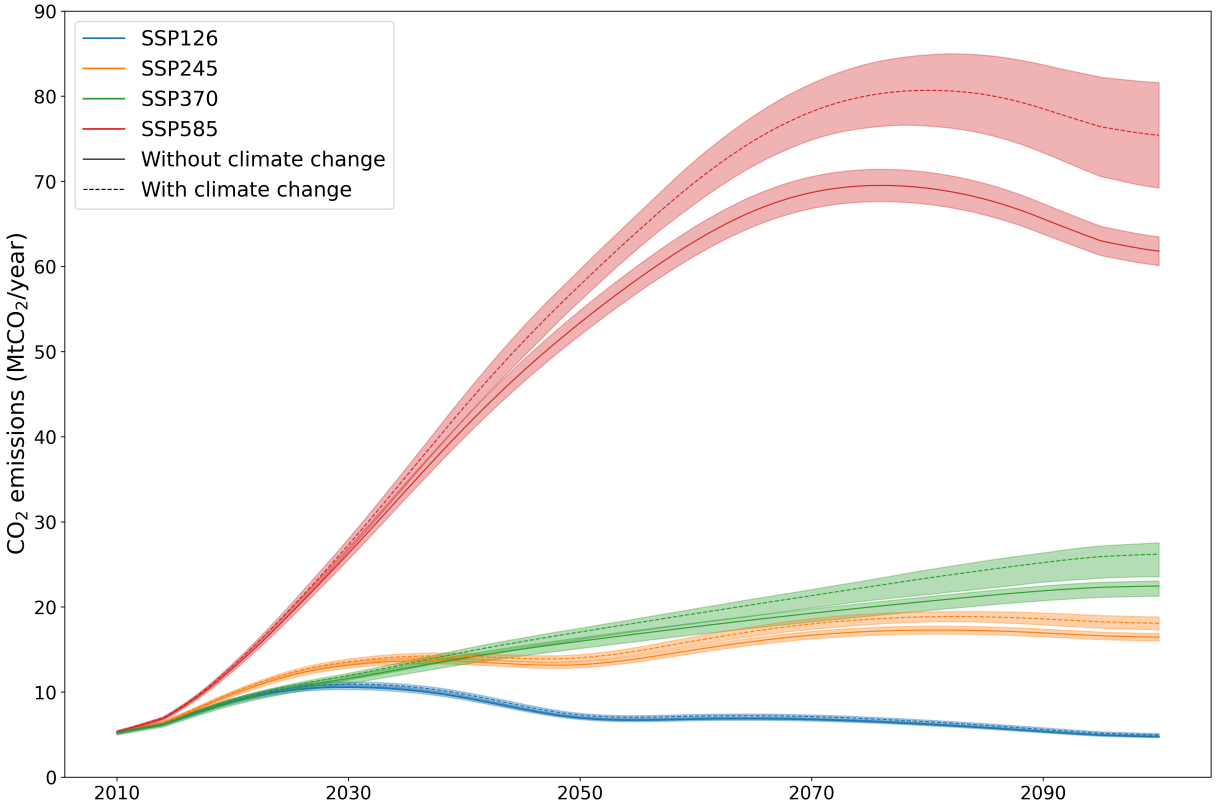

Figure II.7: Projection of CO_2 emissions with socioeconomic effects and with or without climate change effect: Projection of the evolution of CO_2 emissions through the century from socioeconomic changes with no climate change (straight lines) and with the effect of socioeconomic changes and climate change (dashed lines). The colored areas represent the standard 95% confidence intervals.

5.3 Generalization of the Study to Gulf Cooperation Council (GCC) Countries

The Arab states around the Gulf form a regional union, with the aim of intergovernmental and economic cooperation, known as the GCC. This organization brings together the following six countries: Bahrain, Kuwait, Oman, Qatar, Saudi Arabia, and the United Arab Emirates. In

this study, we developed a statistical model specifically for Qatar using electricity consumption data available for this country. Now, we extend the analysis to all GCC countries to gain insight into what the temperature-emission relationship we obtained for Qatar might mean to all GCC countries.

Since GCC countries have common climatic conditions and share similar socioeconomic and industrial structures, we assume that the relationship between temperature and electricity demand is the same in all these countries. We further assume that the carbon intensity of these countries is at the same level as Qatar due to their vast fossil fuel resources (in all these countries, electricity is produced mainly from natural gas, except for Saudi Arabia, which also uses crude oil in significant amounts (Akhonbay, 2020) and renewable resources (mainly wind and solar). However, these countries do not necessarily have the same potential (Bhutto et al., 2014) for development of renewable energies. The governments of GCC countries have set decarbonization targets for 2030 (Praveen et al., 2020). Still, they are also facing the same challenges regarding the development of renewable energies as Qatar; their major challenge is the reluctance of citizens to switch to renewable energy for financial reasons (Al-Maamary et al., 2017). Here, we upscale our model for Qatar to these countries by linearly adjusting to the population, GDP, and temperature of these countries and project CO_2 emissions based on the electricity production of GCC countries. To quantify the final impact of these additional CO_2 emissions on global temperature, we used the simple climate model Aggregated Carbon Cycle, Atmospheric Chemistry, and Climate model (ACC2) (Tanaka et al., 2021; Tanaka et al., 2007; Tanaka et al., 2018), which allows for estimating the global temperature change caused by the emissions from the electricity production of the GCC countries. The results and further details of the methodology are provided in the Supplementary Materials (Appendix 1, Fig. S4). Depending on the SSP, the temperature-energy demand feedback from the GCC countries shows additional CO_2 emissions that range from 0.303% (SSP1-2.6) to 2.045% (SSP2-4.5) of the total CO_2 emissions generated via the electricity production by the end of this century. The further impact of this feedback in GCC countries on global temperature ranges from 0.082% (SSP1-2.6) to 0.278% (SSP5-8.5) by the end of this century.

6 Discussion

To develop future projections of electricity demand and CO_2 emissions, we made assumptions about the relationship between electricity demand and population and the relationship between electricity demand and GDP. Narayan et al., 2008, show that the relationship between GDP and electricity demand is country-specific and depends on development stage. As there

is no relevant study on Qatar, to our knowledge, we adopted a unidirectional causality from GDP to electricity consumption, i.e., we assume that GDP impacts demand but that the demand does not have any feedback on GDP. This is an initial, simple approach, and deserves discussion. For example, there is evidence of a long-run unidirectional relationship from GDP to electricity consumption for renewable energy consumption (Kula, 2014). However, with fossil fuels, the unidirectional nature of the relationship can be questioned (Alsaedi et al., 2020; Ikegami et al., 2016). Indeed, in a study by Alsaedi et al., 2020, a bidirectional causal relationship between electricity consumption and GDP was found in Saudi Arabia. This country has an energy sector similar to that in Qatar. These studies show that the relationship between GDP and electricity demand is probably not as simple as the unidirectional relationship used in our study.

For the effect of population growth on electricity demand, we adopted a hypothesis similar to that for GDP, i.e., linear growth of the demand for electricity with an increase in population. Although this seems true for domestic demand (Ali et al., 2018), it is not necessarily the case for industrial consumption. However, in our projections of the electricity demand in Qatar, we consider the individual and industrial demand without distinction. This lack of distinction is a limitation of our study.

Several studies create an inventory of the renewable energy sources present in the Arabian Gulf states, evaluate their potential, and review the existing policies of these states for renewable energy development (Al-Maamary et al., 2017; Bhutto et al., 2014; Elrahmani et al., 2021). In the case of Qatar, the potential of renewable energy was quantified by Okonkwo et al., 2021. We used figures from this study to establish our carbon intensity projections. However, the future development of low-carbon energy instead of fossil fuels depends on the government's will. We assumed that this intent is accounted for in the SSPs' narratives. Nevertheless, as these figures are designed for global applications, we had to adapt them for Qatar, which entailed strong assumptions about the future share of renewables in each SSP narrative. For example, for SSP5-8.5, we assumed that the carbon intensity would not experience any changes from the present. This allows us to study what can happen in a very carbon-intensive scenario, which is not in line with the pledge of the Qatari government to achieve a 20% solar energy mix by 2030. Furthermore, there is an ongoing debate on the future likelihood of scenarios such as SSP5-8.5 based on recent emissions trends (Hausfather et al., 2020).

Finally, important aspects that impact electricity demand are not explicitly considered in our study, such as urbanization and income inequalities. Indeed, Al-Bajjali et al., 2018, showed that Jordan has experienced a positive effect of urbanization on consumption, which may be important, and Andrijevic et al., 2021, showed that significant regional inequalities in access to

air conditioning arise from urbanization dynamics and income inequalities.

7 Conclusion

Our study quantified the impact of climate and socioeconomic factors on power demand in Qatar and how the change in power demand can further influence CO_2 emissions. Qatar's hot climate is one of the drivers of its high per capita power demand. Our results show that regardless of scenario, the power demand increases with future climate change: a 4.2% increase in the power demand of GCC countries occurs per degree of warming. When considered alone, the effect of climate change on the power demand and the further effect on CO_2 emissions are small relative to socioeconomic factors, i.e., population, GDP, and carbon intensity. However, when CO_2 emissions are calculated considering the impact of climate change combined with the evolution of socioeconomic factors, CO_2 emissions can be significantly higher. Carbon intensity can be decreased through decarbonization policies, which play an important role in reducing the CO_2 emissions from power generation in Qatar and the Middle East.

References

ADEME. (2021). Documentation base carbone - bilan ges ademe. https://www.bilans-ges.ademe.fr/fr/accueil/contenu/index/page/presentation/siGras/0

Akhonbay, H. (Ed.). (2020). *The economics of renewable energy in the gulf*. Routledge.

Al-Bajjali, S., & Shamayleh, A. (2018). Estimating the determinants of electricity consumption in jordan. *Energy*, *147*, 1311–1320.

Ali, H., & Alsabbagh, M. (2018). Residential electricity consumption in the state of kuwait. *Environment Pollution and Climate Change*, *2*, 1–7.

Al-Maamary, H., Kazem, H., & Chaichan, M. (2017). Renewable energy and gcc states energy challenges in the 21st century: A review. *International Journal of Computation and Applied Sciences*, *2*, 11–18.

Al-Marri, W., Al-Habaibeh, A., & Watkins, M. (2018). An investigation into domestic energy consumption behavior and public awareness of renewable energy in qatar. *Sustainable Cities and Society*, *41*, 639–646.

Alrawi, O., Bayram, I., Al-Ghamdi, S., & Koc, M. (2019). High-resolution household load profiling and evaluation of rooftop pv systems in selected houses in qatar. *Energies*, *12*, 3876.

Alsaedi, Y., & Tularam, G. (2020). The relationship between electricity consumption, peak load and gdp in saudi arabia: A var analysis. *Math. Comput. Simul.*, *175*, 164–178.

Andrijevic, M., Byers, E., Mastrucci, A., Smits, J., & Fuss, S. (2021). Future cooling gap in shared socioeconomic pathways. *Environmental Research Letters*, *16*, 094053.

Auffhammer, M., Baylis, P., & Hausman, C. (2016). Climate change is projected to have severe impacts on the frequency and intensity of peak electricity demand across the united states. *PNAS*, *114*(8), 1886–1891.

Bank, W. (2021). Gdp per capita, ppp. the world bank data. https://donnees.banquemondiale.org/indicateur/NY.GDP.PCAP.PP.CD

Bayram, I. S., Saffouri, F., & Koc, M. (2018). Generation, analysis, and applications of high resolution electricity load profiles in qatar. *Journal of Cleaner Production*, *183*, 527–543. https://doi.org/10.1016/j.jclepro.2018.02.084

Bhutto, A., Bazmi, A., Zahedi, G., & Klemeš, J. (2014). A review of progress in renewable energy implementation in the gulf cooperation council countries. *J. Clean. Prod.*, *71*, 168–180.

Canales, F. A., Jadwiszczak, P., Jurasz, J., Wdowikowski, M., Ciapała, B., & Kaźmierczak, B. (2020). The impact of long-term changes in air temperature on renewable energy in poland. *Science of The Total Environment*, *729*, 138965.

Cannon, A., Sobie, S., & Murdock, T. (2015). Bias correction of gcm precipitation by quantile mapping: How well do methods preserve changes in quantiles and extremes? *J. Clim.*, *28*, 6938–6959.

CDS. (2017). Era5: Fifth generation of ecmwf atmospheric reanalyses of the global climate. https://cds.climate.copernicus.eu/cdsapp#!/dataset/reanalysis-era5-complete?tab=overview

Cucchi, M., Weedon, G., Amici, A., Bellouin, N., Lange, S., Müller Schmied, H., Hersbach, H., & Buontempo, C. (2020). Wfde5: Bias-adjusted era5 reanalysis data for impact studies. *Earth Syst. Sci. Data*, *12*, 2097–2120.

Dellink, R., Chateau, J., Lanzi, E., & Magné, B. (2017). Long-term economic growth projections in the shared socioeconomic pathways. *Glob. Environ. Change*, *42*, 200–214.

Elrahmani, A., Hannun, J., Eljack, F., & Kazi, M.-K. (2021). Status of renewable energy in the gcc region and future opportunities. *Curr. Opin. Chem. Eng.*, *31*, 100664.

Gastli, A., Charabi, Y., Alammari, R., & Ali, M. (2013). Correlation between climate data and maximum electricity demand in qatar. *2013 7th IEEE GCC Conference and Exhibition, GCC 2013*, 565–570. https://doi.org/10.1109/IEEEGCC.2013.6705841

GCC. (2016). Gulf cooperation council interconnection authority - demand now. https://www.gccia.com.sa/

GPP. (2021). Electricity prices. https://www.globalpetrolprices.com/electricity_prices/

GSDP. (2008). *Qatar national vision 2030* (tech. rep.). General Secretariat for Development Planning.

Hausfather, Z., & Peters, G. (2020). Rcp8.5 is a problematic scenario for near-term emissions. *Proceedings of the National Academy of Sciences*, *117*(45), 27791–27792. https://doi.org/10.1073/pnas.2017124117

IEA. (2019). International energy agency - world energy outlook. https://www.iea.org/topics/world-energy-outlook

Ikegami, M., & Wang, Z. (2016). The long-run causal relationship between electricity consumption and real gdp: Evidence from japan and germany. *Journal of Policy Modeling*, *38*, 767–784.

IMF. (2021). Gdp, current prices. imf datamapper. https://www.imf.org/external/datamapper/NGDPD@WEO/OEMDC/ADVEC/WEOWORLD

IPCC. (2006). *2006 ipcc guidelines for national greenhouse gas inventories (ipcc)* [Prepared by the National Greenhouse Gas Inventories Programme, Eggleston H.S., Buendia L., Miwa K., Ngara T. and Tanabe K. (eds).]. IGES, Japan.

IPCC. (2021). *Summary for policy maker - climate change 2021: The physical science basis. contribution of wg1 to the sixth assessment report of the intergovernmental panel on climate change* (Core Writing Team, H. Lee and J. Romero, Ed.; tech. rep.). IPCC. Geneva, Switzerland.

Jovanović, S., Savić, S., Bojić, M., Djordjević, Z., & Nikolić, D. (2015). The impact of the mean daily air temperature change on electricity consumption. *Energy*, *88*, 604–609.

Kaya, Y. (1990). *Impact of carbon dioxide emission control on gnp growth: Interpretation of proposed scenarios (ipcc energy and industry subgroup, response strategies working group)* (tech. rep.). IPCC.

Kc, S., & Lutz, W. (2017). The human core of the shared socioeconomic pathways: Population scenarios by age, sex and level of education for all countries to 2100. *Glob. Environ. Change*, *42*, 181–192.

Khalifa, A., Caporin, M., & Di Fonzo, T. (2019). Scenario-based forecast for the electricity demand in qatar and the role of energy efficiency improvements. *Energy Policy*, *127*, 155–164.

Kula, F. (2014). The long-run relationship between renewable electricity consumption and gdp: Evidence from panel data. *Energy Sources Part B: Econ. Plan. Policy*, *9*, 156–160.

Mir, A., Alghassab, M., Ullah, K., Khan, Z., Lu, Y., & Imran, M. (2020). A review of electricity demand forecasting in low and middle-income countries: The demand determinants and horizons. *Sustainability*, *12*, 5931.

Narayan, P., & Prasad, A. (2008). Electricity consumption–real gdp causality nexus: Evidence from a bootstrapped causality test for 30 oecd countries. *Energy Policy*, *36*, 910–918.

OBG. (2017). Qatar gets serious about solar. https://oxfordbusinessgroup.com/news/qatar-gets-serious-about-solar

Okonkwo, E., Wole-Osho, I., Bamisile, O., Abid, M., & Al-Ansari, T. (2021). Grid integration of renewable energy in qatar: Potentials and limitations. *Energy*, *235*, 121310.

O'Neill, B., Kriegler, E., Ebi, K., Kemp-Benedict, E., Riahi, K., Rothman, D., van Ruijven, B., Vuuren, D., Birkmann, J., Kok, K., Levy, M., & Solecki, W. (2015). The roads ahead: Narratives for shared socioeconomic pathways describing world futures in the 21st century. *Global Environmental Change*, *42*. https://doi.org/10.1016/j.gloenvcha.2015.01.004

Praveen, R., Keloth, V., Abo-Khalil, A., Alghamdi, A., Eltamaly, A., & Tlili, I. (2020). An insight to the energy policy of gcc countries to meet renewable energy targets of 2030. *Energy Policy*, *147*, 111864.

QPSA. (2019). *Chapter iii electricity and water statistics (state of qatar)* (tech. rep.). Qatar's Planning and Statistics Authority.

Riahi, K., van Vuuren, D., Kriegler, E., Edmonds, J., O'Neill, B., Fujimori, S., Bauer, N., Calvin, K., Dellink, R., Fricko, O., et al. (2017). The shared socioeconomic pathways and their energy, land use, and greenhouse gas emissions implications: An overview. *Glob. Environ. Change*, *42*, 153–168.

Tanaka, K., Boucher, O., Ciais, P., Johansson, D., & Morfeldt, J. (2021). Cost-effective implementation of the paris agreement using flexible greenhouse gas metrics. *Science Advances*, *7*(22), eabf9020. https://doi.org/10.1126/sciadv.abf9020

Tanaka, K., Kriegler, E., Bruckner, T., Hooss, G., Knorr, W., & Raddatz, T. (2007). *Aggregated carbon cycle, atmospheric chemistry, and climate model (acc2) – description of the forward and inverse modes* (Reports on Earth System Science). Max Planck Institute for Meteorology, Hamburg.

Tanaka, K., & O'Neill, B. (2018). The paris agreement zero-emissions goal is not always consistent with the 1.5 °c and 2 °c temperature targets. *Nature Climate Change*, *8*, 319–324.

Umar, T., Egbu, C., Ofori, G., Honnurvali, M., Saidani, M., & Opoku, A. (2020). Challenges towards renewable energy: An exploratory study from the arabian gulf region. *Proceedings of the Institution of Civil Engineers - Energy*, *173*, 68–80.

UN. (2021). Revision of world population prospects. https://population.un.org/wpp/

Valor, E., Meneu, V., & Caselles, V. (2001). Daily air temperature and electricity load in spain. *American Meteorological Society*, *40*, 1413–1421.

Van Ruijven, B., De Cian, E., & Wing, I. (2019). Amplification of future energy demand growth due to climate change. *Nature Communications*, *10*, 2762. https://doi.org/10.1038/s41467-019-10399-3

Werner, A., & Cannon, A. (2016). Hydrologic extremes – an intercomparison of multiple gridded statistical downscaling methods. *Hydrol. Earth Syst. Sci.*, *20*, 1483–1508.

World Bank. (2023). World Development Indicators.

Yalew, S., van Vliet, M., Gernaat, D., Ludwig, F., Miara, A., Park, C., Byers, E., De Cian, E., Piontek, F., Iyer, G., Mouratiadou, I., Glynn, J., Hejazi, M., Dessens, O., Rochedo, P., Pietzcker, R., Schaeffer, R., Fujimori, S., Dasgupta, S., & Vuuren, D. (2020). Impacts of climate change on energy systems in global and regional scenarios. *Nature Energy*, *5*. https://doi.org/10.1038/s41560-020-0664-z

Zittis, G., Hadjinicolaou, P., Almazroui, M., et al. (2021). Business-as-usual will lead to super and ultra-extreme heatwaves in the middle east and north africa. *npj Climate and Atmospheric Science*, *4*, 20. https://doi.org/10.1038/s41612-021-00178-7

CHAPTER III

How Climate Change May Shift Power Demand in Japan: Insights from Data-Driven Analysis

In this section, we delve into the detailed case studies of Japan, with a similar approach to what was done for Qatar. Here also, the investigation was conducted without the Carbon Monitor-Power data because of the lower reliability of data for Japan at the time of the study compared to the data we could access through the Japanese utilities.

As for Qatar, the study involves projecting CO_2 emissions from electricity demand through the end of the century, considering the effects of evolving GDP and population on that demand. Thus, I made the same assumptions as for Qatar: a basic linear relationship between electricity demand, population, and GDP. This linear relationship holds up well for Japan, as highlighted by World Bank data (Figure III.1) (World Bank, 2023).

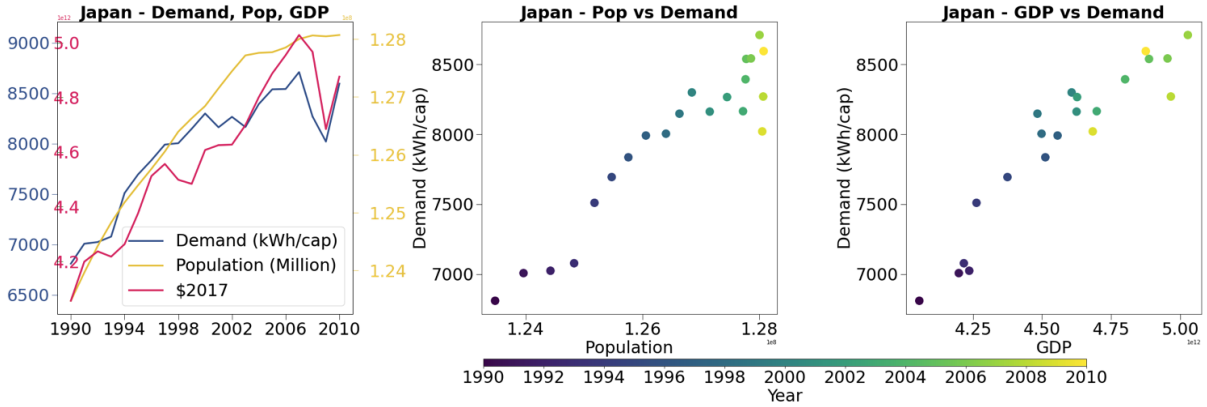

Figure III.1: Comparison and correlation Energy Demand, Population, and GDP Trends for Japan and Qatar (1990-2010)

For future projections, I have chosen to stick with this simple linear framework for estimating electricity demand, incorporating the variables of population and GDP. This choice is deliberate and is intended to maintain clarity and simplicity. However, this approach requires thoughtful consideration, as the linear relationship will not be guaranteed to continue.

1 Summary

Following our exploration of Qatar, which served as a foundational case study, we turned our attention to Japan - a more complex and multifaceted scenario. Japan's diverse climatic regions, ranging from cold to hot extremes, along with its complex power generation landscape, offered a compelling setting to investigate the intricacies of future power decarbonization under the influence of climate change. Unlike Qatar, Japan's electricity power demand can not be explained with a simple second-order polynomial regression accounting only for the temperature effect. We employed Machine Learning (ML) models to solve this and considered various predictive variables.

Three ML models were trained for all ten Japanese regions: Random Forest, Gradient Boosting, and Multivariate Adaptive Regression Splines (MARS). These models were implemented using the scikit-learn (Buitinck et al., 2013; Pedregosa et al., 2011) and pyearth (Liao, 2021) packages, respectively, in Python 3.9. The purpose was to simulate daily power demand from six climate variables, five heat stress measures that quantify the impact of heat and humidity on the human body, and a human activity proxy to account for the level of economic activity on different days of the week. In this study, we also simulated daily carbon intensity with the same approach. Different metrics were used to evaluate the performances of the ML models: the coefficient of determination (R2), the Mean Absolute Percentage Error (MAPE), and the Root Mean Square Error (RMSE). Based on these metrics, we selected Random Forest to make the projections of power demand and carbon intensity in the future.

We used projections of climate variables from six Earth System Models (ESMs) over the period 2020-2100 for three SSPs: SSP1-2.6, SSP3-7.0, and SSP5-8.5. From the climate projection, we calculated the heat stress measure projections. Then, the trained Random Forest model was applied to the projected predictive feature to simulate power demand and carbon intensity until the end of the century. To obtain the daily CO_2 emissions, we multiplied the power demand projection and the carbon intensity projections. The influence of climate change on CO_2 emissions through electricity generation exhibits seasonal and geographical variations. In colder regions, the anticipated reduction in power demand during winters, as a consequence

of future warming, leads to an overall annual decrease in electricity consumption. Conversely, in warmer regions, the decline in winter power demand may be offset by increased demand during the summer, driven by more frequent hot days, resulting in an overall annual increase. Our regional models project that power demand will likely surge the most in various Japanese regions during May, June, September, and October. Overall, our observations suggest that regions with extreme climates exhibit heightened sensitivity to global warming compared to temperate regions. The climate-induced fluctuations in power demand generally lead to a net annual reduction in CO_2 emissions across regions, except for Okinawa, where a substantial summer increase in power demand results in a net annual rise in CO_2 emissions. However, the impact of climate change on carbon intensity may counterbalance this trend in certain regions like Shikoku and Tohoku.

Finally, as in Qatar, we assessed the impact of socioeconomic factors such as population, GDP, and the evolution of the power mix on power demand when combined with climate change. We found that the climate change effect is more important than when considered individually and significantly impacts total CO_2 emissions under SSP5-8.5.

This work has been published as: Gurriaran, L., Tanaka, K., Takahashi, K., and Ciais, P. (2023). How climate change may shift power demand in Japan: Insights from data-driven analysis. Journal of environmental management. 345. 118799. 10.1016/j.jenvman.2023.118799. See Appendix 2 for the supplementary materials.

2 Abstract

The impact of climate change on power demand in Japan and its related CO_2 emissions is a matter of concern for the Japanese authorities and power companies as it may have consequences on the power grid, but is also of global importance as Japan is a significant contributor to global greenhouse gas emissions. In this study, we trained random forest models against daily power data in ten Japanese regions and for different types of power generation to project changes in future power production and its carbon intensity. We used climate variables, heat stress indices, and one variable for the level of human activities. We then used the models trained from the present-day period to estimate the future power demand, carbon intensity, and pertaining CO_2 emissions over the period 2020-2100 under three Shared Socioeconomic Pathways (SSPs) scenarios (SSP1-2.6, SSP3-7.0, and SSP5-8.5). The impact of climate change on CO_2 emissions via power generation shows seasonal and regional disparities. In cold regions, a decrease in power demand during winter under future warming leads to an overall

decrease in power demand over the year. In contrast, the decrease in winter power demand in hot regions can be overcompensated by an increase in summer power demand due to more frequent hot days, resulting in an overall annual increase. From our regional models, power demand is projected to increase the most in most Japanese regions in May, June, September, and October rather than in the middle of summer, as found in previous studies. This increase could result in regular power outages during those months as the power grid could become particularly tense. Overall, we observed that power demand in regions with extreme climates is more sensitive to global warming than in temperate regions. The impact of climate change on power demand induces a net annual decrease in CO_2 emissions in all regions except for Okinawa, in which power demand strongly increases during the summer, resulting in a net annual increase in CO_2 emissions. However, climate change's impact on carbon intensity may reverse the trend in some regions (Shikoku, Tohoku). Additionally, we assessed the relative impacts of socioeconomic factors such as population, GDP, and environmental policies on CO_2 emissions. When combined with these factors, we found that the climate change effect is more important than when considered individually and significantly impacts total CO_2 emissions under SSP5-8.5. The contrasting results observed in the warm and cold regions of Japan can offer valuable insight into the potential future variations in energy demand and resulting CO_2 emissions on a global scale.

3 Introduction

Many studies have investigated the impact of climate change on energy systems. According to the review of Yalew et al., 2020, a slight decrease in hydropower and thermal energy capacity at a global scale is expected. However, the impact of climate on power demand strongly varies across regions (Auffhammer et al., 2017; Van Ruijven et al., 2019).(Van Ruijven et al., 2019) found that the energy demand could increase by 25% in the tropics by 2050 due to increasing hot days, whereas higher latitudes are more prone to a decline in energy demand.

This study focuses on power demand, which comprises a significant percentage of the total energy demand. Power demand is closely related to meteorological conditions, and there is an increasing concern over how it will respond to changing climate. According to Yalew et al., 2020, a global increase in cooling demand and a decrease in heating demand are expected. For example, heat waves are becoming more frequent and intense in hot regions (Zittis et al., 2021), causing increased peak demand during those events. The potential power outages that may result from increased peak demand are a matter of concern for health systems (Patel, 2022). Depending on the scenario of socioeconomic development, 2 to 5 billion people are

at risk of facing deadly heat and are unable to afford air conditioning systems (Andrijevic, 2021; Mora, 2017). CO_2 emissions from power generation constitute a further consequence of climate-induced changes in power demand. An increase in demand for air conditioning and, thus, power generation in subtropical latitudes will subsequently increase the amount of CO_2 emissions from these regions. However, this effect may be counterbalanced at a global scale by a decrease in heating demand in high latitudes leading to lower CO_2 emissions. Our study addresses this phenomenon specifically in Japan.

Japan is one of the largest economies in the world, with the third-largest Gross Domestic Product (GDP) internationally (IMF, 2022). In 2020, power generation reached 987 TWh, i.e., 7.9 MWh per capita (IEA, 2020), ranking the country in the top 20 largest consumers of electricity per capita in the world. The residential sector is the third largest sector for power demand in Japan, after commercial and public services and industry. Japan comprises a territory ranging from 46° to 20° north (2200 km long from northeast to southwest), and de facto includes a wide range of climates, from humid continental to subtropical. The country is divided into ten distinct geographical areas administered by designated power companies. Each region is characterized by a specific climate, population density, urbanization rate, GDP per capita, etc., all factors determining power demand. For example, the adoption rate of household air conditioning is around 90% on a national scale (De Cian et al., 2019), but it varies across regions from north to south. Whereas fewer homes are equipped with cooling systems in Hokkaido, where heating needs are more important, the tropical climate in Okinawa induces a strong demand for air conditioning. Although 80% of the nation's power is produced with fossil fuels (IEA, 2022), some regions use more renewables than others. Each region thus has a specific carbon intensity for power generation depending on the energy mix used by the local power company. We use Japan as a case study to investigate how climate change can influence CO_2 emissions by changing power demand and influencing the carbon intensity of the energy mix. We analyze climate change impacts at national and regional scales and develop regional statistical models to derive monthly and seasonal trends and annual net changes in CO_2 emissions until 2100. These models incorporate the effects of climate change and specific regional socioeconomic factors (population, GDP, and environmental policies aiming to decarbonize the energy mix) to project power demand, carbon intensity, and CO_2 emissions. Detailed energy mix and climate data are available homogeneously for all ten regions. Hiruta et al., 2022a, used similar data to develop a method that acquires regional temperature response functions (TRFs) for power demand and investigates the effect of climate change on power demand. Although our method to obtain regional models projecting power demand is similar to Hiruta et al., 2022a, we use more up-to-date climate data for the projections: our climate variables are from the last phase of the CMIP project, CMIP6, instead of CMIP5 for the Hiruta study. Unlike the Hiruta

study, we further explore long-term changes in CO_2 emissions that can be caused by changes in power demand and carbon intensity under future climate and socioeconomic scenarios. Our proposed method for modeling power demand, carbon intensity, and CO_2 emissions in Japan is of significant local interest as it has the potential to inform policy and decision-making related to energy production and consumption, as well as inform strategies for reducing greenhouse gas emissions. Furthermore, understanding Japan's specific challenges and opportunities in relation to climate change can also contribute to global efforts to address the issue. As the third largest economy in the world and the 11th most populous country, Japan is a major contributor to global greenhouse gas emissions. Our study on Japan will not only provide insight into how energy demand and related CO_2 emissions may evolve under climate change in Japan specifically but will also offer valuable insight into the challenges and opportunities facing larger industrialized nations in transitioning to low-carbon economies. The findings of such a study can inform global efforts to mitigate and adapt to climate change by identifying successful strategies and best practices that can be replicated in other countries. Additionally, with its wide range of climates, Japan is an ideal case study for understanding the possible evolution of power demand under different climatic conditions. Section 4 details the data used and the algorithms tested to develop models that simulate power demand and carbon intensity. It also describes the method to calculate CO_2 emissions under three future scenarios: SSP1-2.6, SSP3-7.0, and SSP5-8.5. Section 5 presents the results; it describes the regional relationships between predictive variables and power demand and carbon intensity, details the regional and temporal impact of climate on power demand, carbon intensity, and CO_2 emissions, compares our results to those of Hiruta et al., 2022b, and discusses the relative importance of climate and socioeconomic factors in determining the power demand, carbon intensity, and CO_2 emissions. Section 7 discusses the results under a broader context, including caveats of our study.

4 Data and Methods

The work presented in this article is built around three main steps (Fig. III.2): i) model development and selection, ii) projections of power demand and carbon intensity under future climate scenarios, and iii) projections of CO_2 emissions under future climate and socioeconomic scenarios. This section details the datasets needed for the different steps (Table III.1), the model development, and the projection stage.

Table III.1: Current (ERA5 for training) and future (ISIMIP3b for projections) climate data used in our analysis.

Variable and description	ERA5		ISIMIP3b	
	name	unit	name	unit
Near surface atmospheric temperature (2m above the surface)	T2M	K	TAS	K
Relative Humidity (water vapor pressure as a percentage of the value at which the air becomes saturated)	RH	%	HURS	%
Surface solar radiation downward (amount of shortwave radiation that reaches a horizontal plane at the surface)	SSRD	$J.m^{-2}$	RSDS	$W.m^{-2}$
Surface thermal radiation downward (amount of longwave radiation emitted by the atmosphere and clouds that reaches a horizontal plane at the surface)	STRD	$J.m^{-2}$	RLDS	$W.m^{-2}$
Wind (speed of horizontal wind 10 m above the surface)	U	$m.s^{-1}$	SFCWIND	$m.s^{-1}$
Precipitation (total amount of water that fall at the surface)	TP	m	PR	$kg.m^{-2}.s^{-1}$

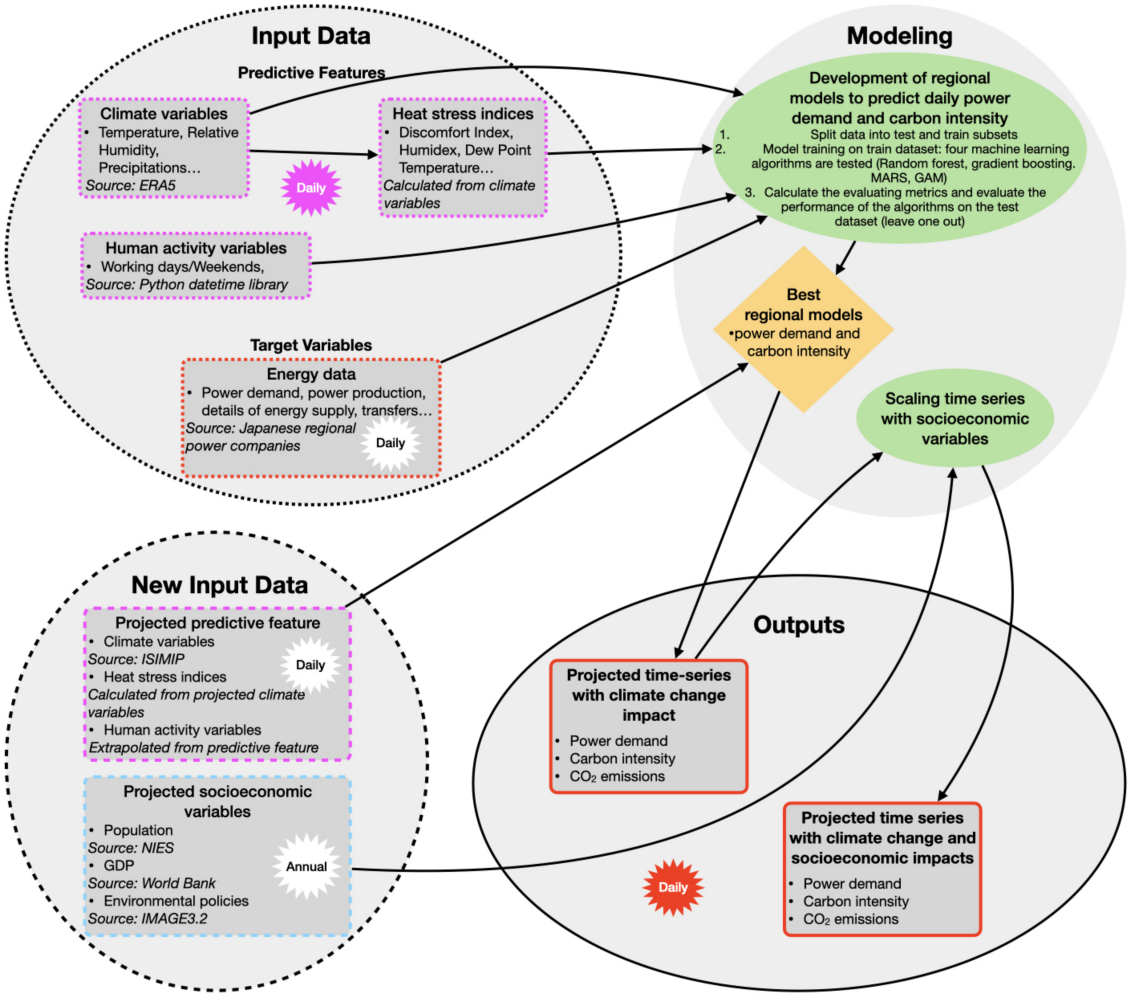

Figure III.2: Flowchart of the methodological procedures used in this study.

4.1 Training Data

We trained a statistical model on climate reanalysis data from the ERA5 project (Muñoz Sabater, 2019) to reproduce the observed daily power demand and carbon intensity for all ten regions. Six raw climate variables were used as predictors: temperature, relative humidity, solar and thermal radiation, wind, and precipitation (Table 1). Those data were downloaded from the Climate Data Store website (CDS, 2017) at an hourly time resolution over the period 2016 - 2020 and a spatial resolution of 0.08°. T2M, RH, SSRD, STRD, and U hourly values were averaged over days, while TP was summed over days. Finally, all these climate variables were regionally averaged. Five human exposure indices were calculated from these climate variables and also used as predictors: the dew point temperature at which the air is saturated with water vapor (Td), the wet bulb temperature (Tw), which is the lowest temperature to which air can be cooled by water evaporation, the discomfort index, which is often used to calibrate air conditioner (DI), the Humidex (Hx), which explains what the temperature feels like for the human body and the Heat Index (HI), which represents what the combination of temperature and relative humidity feels like for the human body. Equations used to calculate these indices (Buzan et al., 2014; Epstein et al., 2006; Maia-Silva et al., 2020; Sohar et al., 1963; Stathopoulou et al., 2005; Thom, 1959) are detailed in Supplementary Materials (Appendix 2, Section S1). We also used the days of the week (DOW) as a proxy for human activity. Each day is assigned a numerical value to quantify its effect in our models: Monday is 0, Tuesday 1,..., and Sunday 6.

Hourly data for power demand and the energy mix was obtained directly from the website of the ten power utilities (Appendix 2, Section S2). Data have been available since April 2016 and provided for eight types of power supply: fossil, nuclear, photovoltaic, wind, hydroelectricity, geothermal, biomass, and pumped-storage hydroelectricity. The energy mix of each region is detailed in Supplementary Materials (Appendix 2, Section S2, Table S1). Further details on the types of fossil fuel (coal, gas, and oil share) are unavailable at the hourly scale. Still, the Japanese Agency for Natural Resources and Energy from the Ministry of Economy, Trade, and Industry (METI) provides monthly fractions of coal, gas, and oil used in the regional energy mixes from 2017 to 2020. The fossil energy mix is relatively constant over these four years, with approximately 50% of gas, 40% of coal, and 10% of oil. The regional daily carbon intensity of power generation was calculated assuming this ratio constant.

4.2 Model Development and Selection

We tested three non-parametric models of daily power demand and carbon intensity; random forest classifier (Breiman, 2001; Ho, 1995), histogram-based gradient boosting (J. Friedman, 1999), and Multivariate Adaptive Regression Spline (MARS) (J. Friedman, 1991). We trained the algorithms for all ten regions with twelve predictors: six climate variables, five human exposure indices, and human activity proxy (DOW), all twelve described in Section 4.1. The training dataset represented 75% of the data, and the test dataset accounted for 25%. We evaluated the performances of the algorithms on both datasets using three metrics: the coefficient of determination (R2), the Mean Absolute Percentage Error (MAPE), and the Root Mean Square Error (RMSE).

Results are very similar between random forest and MARS, and both algorithms perform better than gradient boosting (Appendix 2, Table S2 and Fig. S1, Section S3). As it is faster to optimize random forest hyperparameters, we decided to proceed with this algorithm for the projection stage. Although the methodology used for the model development and selection stage is the same as Hiruta et al., 2022a, we developed our models with a different algorithm and used different evaluation metrics.

We used interpretability methods, including Partial Dependence Plots (PDPs) (J. H. Friedman, 2001; Greenwell, 2017) and Shapley values(Roth, 1988; Winter, 2002), to analyze the effect of predictors on our model predictions. These methods can be distinguished into global and local diagnostics:

- Global diagnostics provide insights into the average behavior of the model, thus giving hints on the mechanisms that influence the prediction. PDPs are part of these diagnostics. Such plots illustrate the marginal effect of a single predictor on the model output (here, power demand or carbon intensity). These plots are generated by averaging the lines of Individual Conditional Expectation (ICE) plots. ICE plots represent the prediction changes for each observation as a predictor varies.
- Local diagnostics, such as Shapley values, explain individual predictions of a machine learning model. The Shapley values are interpreted as follows: "Given the current set of feature values, the contribution of a feature value to the difference between the actual prediction and the mean prediction is the estimated Shapley value"

(Molnar, 2020). One can interpret Shapley values as a way to represent the probability of an impact of a predictor in the projection; a negative Shapley value shifts the predicted value in a negative direction, whereas a positive Shapley value shifts it in a positive direction.

PDPs and Shapley values enable the interpretation of the regional models obtained with random forests, showing how each predictor affects the model outputs. PDPs were calculated from a subsample of fifty observations, and Shapley values were calculated for each observation of each predictor.

4.3 Projections

Once the regional models were calibrated for current climate conditions (i.e., the period 2016-2020), we employed them to project the evolution of power demand and carbon intensity under different climate scenarios over 2020-2100 (Figs. III.3c and III.3d). We worked with three scenarios (SSP1-2.6, SSP3-7.0, and SSP5-8.5) and used bias-corrected and statistically downscaled climate projections from the ISIMIP3b simulation round (Lange, 2021) at a daily timescale as predictors. Those data come from five different Earth System Models from the 6th phase of the CMIP project (CMIP6); GFDL-ESM4, IPSL-CM6A-LR, MPI-ESM1-2-HR, MRI-ESM2-0, and UKESM1-0-LL. Figure III.3a shows the projected temperatures for all ten regions and three scenarios as an example of the projected climate predictors. We calculated human exposure indices (DI (Fig. III.3b), Hx, HI, Td, and Tw) from the projected climate predictors. We checked the consistency of ERA5 data and ISMIP projections over the period 2016-2020 and found good compatibility, with ERA5 values in the range of the ISIMIP projections (Fig. S2 in the Supplementary Materials, Section S5, Appendix 2). Finally, we simulated daily climate-induced CO_2 emission projections by multiplying daily power demand and carbon intensity projections.

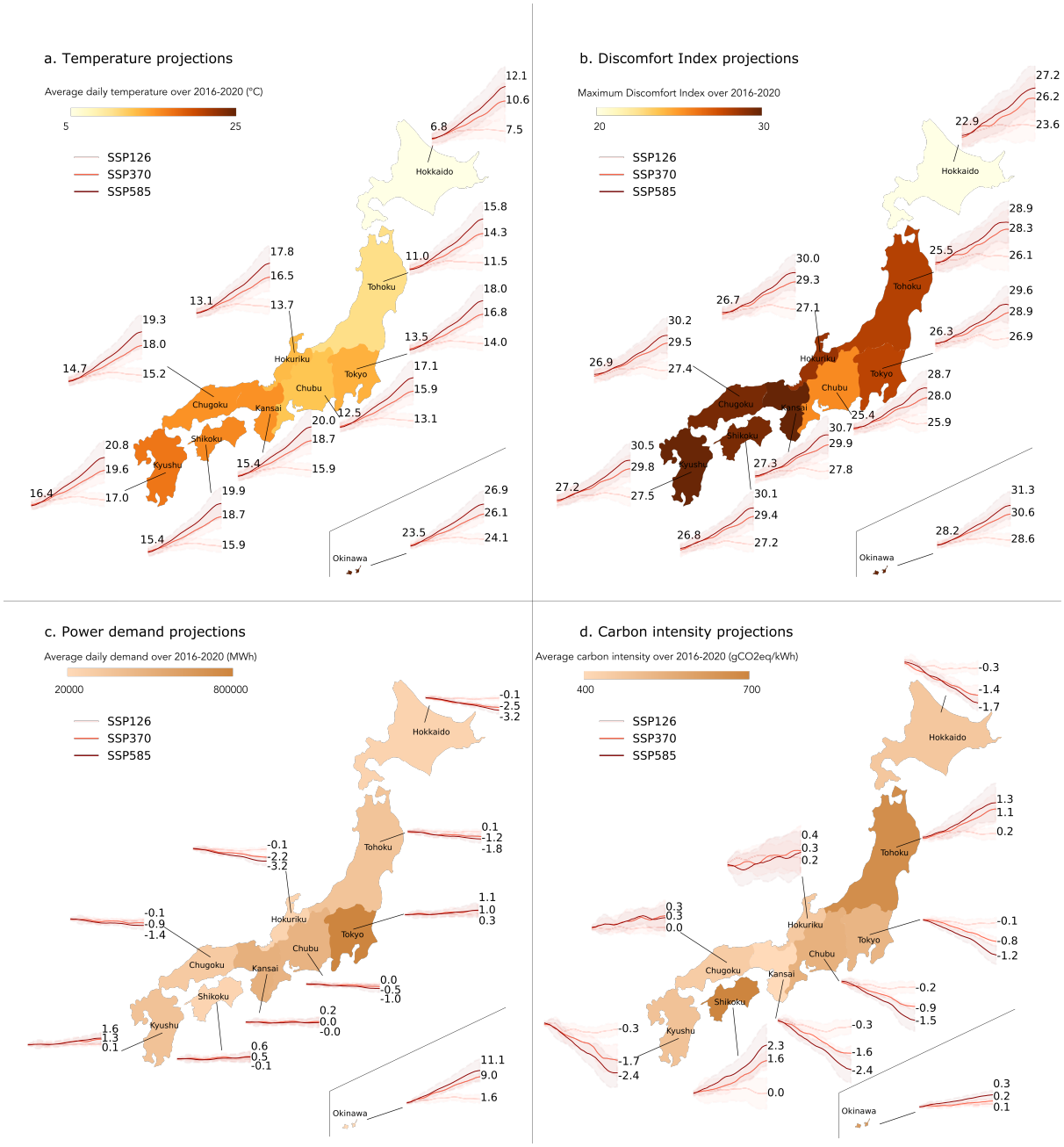

Figure III.3: Current and future projections under climate change of average daily temperature (a), DI (b), power demand (c), and carbon intensity (d) for the ten regions of Japan. The color scale on the maps indicates the level for the period 2016-2020. Projections for the period 2020-2100 are shown in solid bands. Lines give mean values from five models; shaded areas show standard deviations. Future projections in panels c and d are shown in percentage (relative changes to present levels).

4.4 Socioeconomic Scenarios

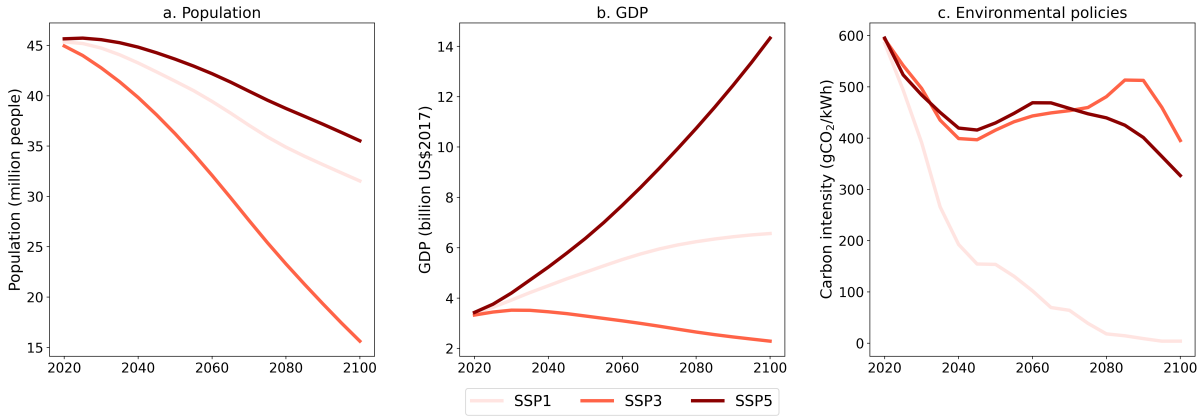

Figure III.4: Socioeconomic projections of (a) population, (b) GDP, and (c) environmental policies aiming to decarbonize the energy mix used for power generation for the region of Tokyo.

The last step of our study was to include the impacts of socioeconomic factors on CO_2 emissions for all three SSPs. The Climate Change Adaptation Information Platform from the National Institute for Environmental Studies (NIES), Japan (A-PLAT, 2022), provides population projections at the prefecture scale. We aggregated such projections at the regional scale. Those data predict a decrease in Japan's population in all SSPs (Fig. III.4a). We obtained regional GDP projections (Fig. III.4b) by scaling Japan's GDP projections provided by the OECD (Dellink et al., 2017; Riahi et al., 2017) with current ratios between Japan's total GDP and regional GDP. Given the absence of regional GDP projections, we assumed that all regional GDP projections follow the same trend. We calculated Japan's carbon intensity projections (Fig. III.4c) based on national projections of the IMAGE3.2 model (Van Vuuren et al., 2021). We downscaled the national carbon intensity projection to regional levels with the same methodology as for GDP. Further details can be found in the Supplementary Material (Appendix 2, Section S4). We quantified the individual influence of each factor (climate change, population, GDP, and environmental policies aiming to decarbonize the energy mix) on total CO_2 emissions by varying one factor at a time. For example to quantify the individual influence of GDP on total CO_2 emissions over the whole period, we varied only the values of GDP when running the models and we fixed all the other variables (climate, population, and carbon intensity) to their 2016 values.

5 Results

5.1 Regional Models: Important Features Explaining Daily Power Demand and Carbon Intensity Variations in Each Region

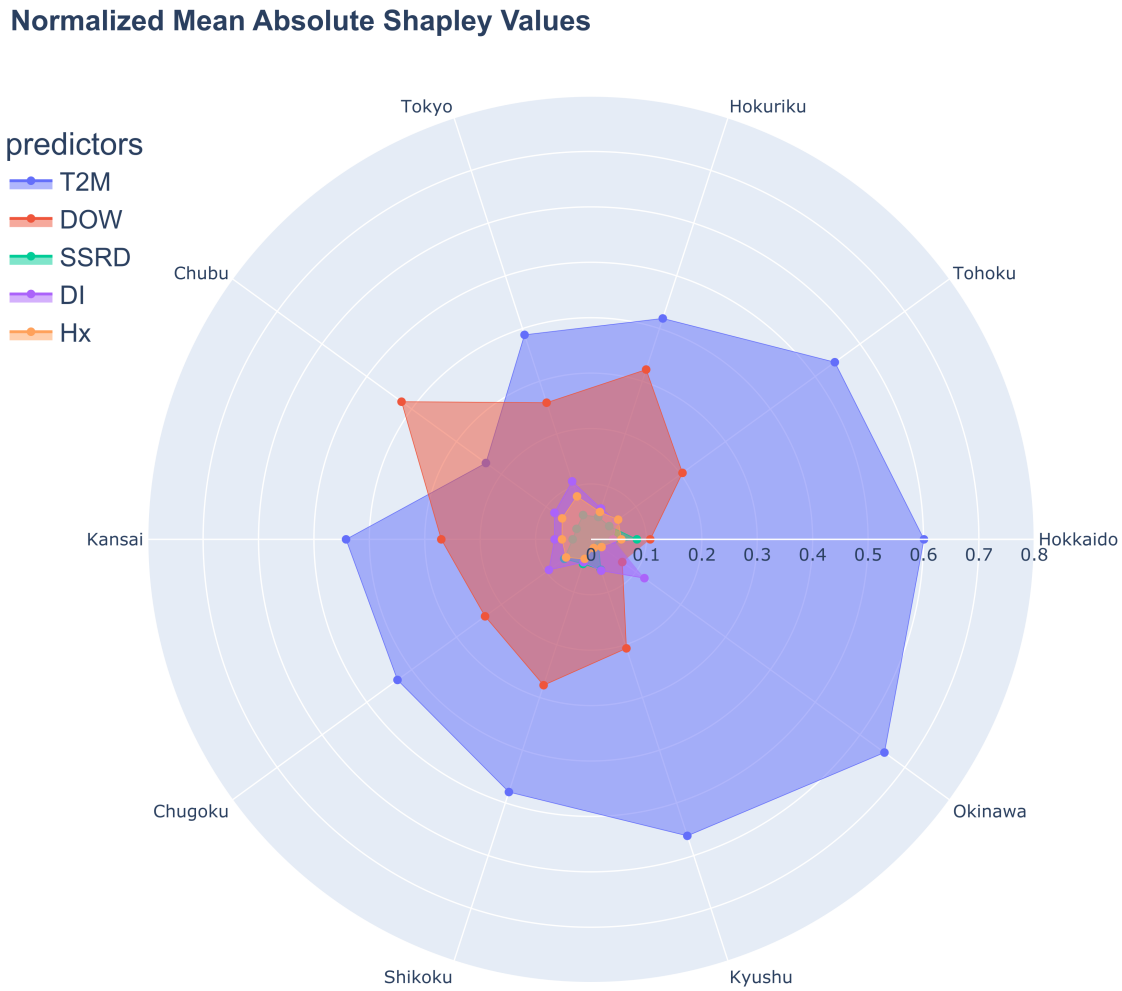

Figure III.5: Radar plot showing the relative importance of the main predictors explaining power demand across regions (T2M, DOW, SSRD, DI, and Hx - see Table 1), obtained from the normalized mean absolute Shapley values of all observations for each predictor. The relative importance of the predictor is calculated for each region by normalizing the mean absolute Shapley value of every predictor.

We calculated Shapley values for all predictors in all ten regions. Of twelve predictors, five consistently appear among the most important to explain the power demand (Fig. III.5): the temperature (T2M), the day of the week (DOW), the solar radiation (SSRD), the discomfort

index (DI) and the Humidex (Hx). T2M is the most important predictor in all regions except Chubu and Okinawa, followed by DOW. The order between T2M and DOW is reversed in Chubu. DI is the second most important predictor instead of DOW in Okinawa (Fig. III.5). The third most important predictor varies by region, but in general, it is DI (for six regions).

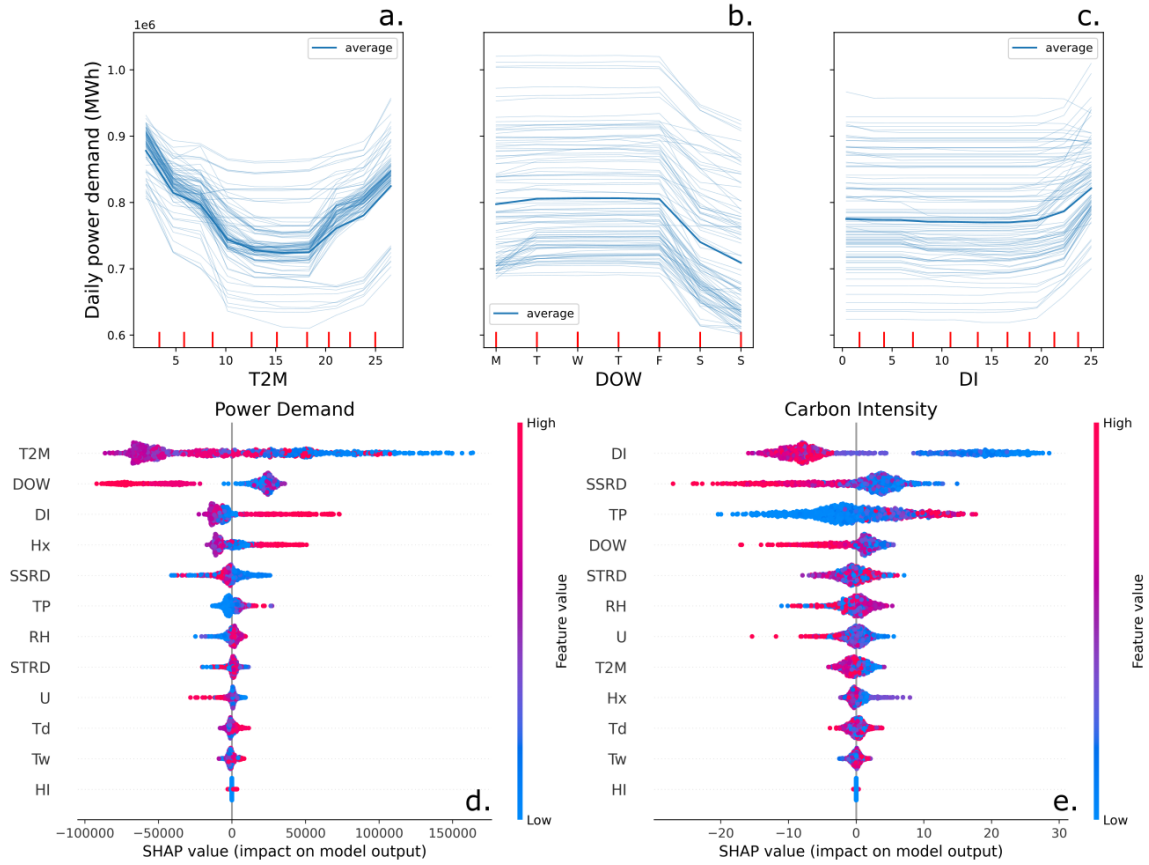

Figure III.6: Partial dependence plot (thick line) and Individual Conditional Expectation plots (thin lines) for 100 model realizations for three main predictors explaining the power demand for the Tokyo region: air temperature at two meters above ground T2M (a), day of week DOW (b - the letters on the x-axis indicate the days of the week) and discomfort index DI (c). The vertical red bars show the predictor values distribution. The lower panels represent the Shapley values for each predictor for power demand (d) and carbon intensity (e). The figures for the other regions can be found in the Supplementary Material, Appendix 2, Section S6.

We looked at the PDPs of the main predictors and the Shapley values (Figs. III.6 and S3, Supplementary Materials, Section S6, Appendix 2) to better understand the non-linear influence of the predictors in our regional models. For example, with the Tokyo region, the PDP for T2M shows a U-shaped dependency of power demand to temperature (Fig. III.6a). Two temperature thresholds can be identified: power demand is increasing under 10 °C for heating purposes and above 18 °C for cooling purposes. The power demand is more or less constant between those two temperatures. Shapley values (Fig. III.6d) show that when temperature values are either high or low (red and blue tones), power demand shifts in a positive direction,

thus confirming the behavior observed with the partial dependence plot. The same relationship between temperature and power demand is also observed in several other regions (Fig. S3, Section S6, Supplementary Materials, Appendix 2). However, Hokkaido and Okinawa show different relationships. Power demand decreases when the temperature increases in Hokkaido and remains constant above 10°C, suggesting that power demand is controlled only by heating demand. The opposite effect is observed in Okinawa; power demand is constant under 24°C and increases once this temperature is exceeded. The specific regional thresholds triggering power demand for heating or cooling reflect households' structure and population behavior.

We also analyzed the dependency of power demand on the days of the week (DOW) with PDP and Shapley Values (Figs. III.6b and III.6d). Power demand is constant from zero to four (Monday to Friday) and decreases above four, reflecting a lower demand during weekends. Figure III.6d highlights the clear separation between weekends and working days. The same relationship is observed for all regions, although the impact of weekends on power demand is larger in Chubu (Fig. S2e and Fig. III.5).

Finally, we analyzed the relationship between the DI and power demand (Figs. III.6c and III.6d). Power demand increases when the threshold of 21 is exceeded. This behavior is observed for all regions having the DI as one of the three most influential predictors (Fig. S3, Supplementary Material, Appendix 2). Previous studies identified 21 as the threshold above which people start to feel heat stress (Stathopoulou et al., 2005; Thom, 1959), and DI is often used to calibrate air conditioners (Buzan et al., 2014; Epstein et al., 2006; Maia-Silva et al., 2020; Sohar et al., 1963), explaining such behavior.

We analyzed the relationships between carbon intensity and all 12 predictors with Shapley values (Fig. III.6e). In the example of Tokyo, DI is the most important predictor. It positively shifts carbon intensity predictions when the predictor values are low, meaning that more fossil fuels are used for power generation when DI is low. Surface solar radiation downward (SSRD) is the second most important predictor. SSRD negatively shifts carbon intensity predictions when the SSRD value is high, probably because solar panels more easily exploit solar energy under a clear sky with much incoming solar radiation than under a cloudy condition. It should be noted that too strong solar radiation can inhibit the efficiency of power production from solar panels. Precipitation (TP) has the opposite effect. Carbon intensity predictions are shifted positively when TP is important, meaning less use is made of renewable energies. The order of importance of predictors for carbon intensity predictions varies more across regions than for

power demand. However, more climate predictors are among the most important predictors, reflecting the dependency of the daily variability of the renewable energy capacity on the daily weather.

5.2 Impact of Future Climate Change on Power Demand, Carbon Intensity, and CO_2 Emissions

Power demand projections for all ten regions and three scenarios (Fig. III.3c, Section 4) show that climate change's impact on power demand differs between regions throughout the century. Such projections show a warming-induced decrease in power demand under SSP3-7.0 and SSP5-8.5 in most regions (up to -3.2% in Hokkaido and Hokuriku). However, the projections reveal a net increase in the daily power demand in Okinawa and Kyushu, the two hottest regions (Fig. III.3a, Section 4). This increase is up to 1.6% in Kyushu and is even more pronounced in Okinawa (+1.6% for SSP1-2.6 and +11.1% for SSP5-8.5). Changes in the power demand across regions (except Okinawa) under SSP1-2.6 are small, ranging from -0.1 to 0.5%. Such results indicate that a decrease in the power demand in winter under future warming leads to an annual decrease in power demand in cold regions like Hokkaido. However, this possible decrease in winter power demand is overcompensated by a summer increase in hot regions such as Okinawa or Kyushu, leading to an annual increase. Climate change's impact on carbon intensity also varies across regions (Fig. III.3d), but results are less significant than for power demand. Carbon intensity projections are less accurately simulated by our models (higher RMSE and lower R2). Nevertheless, the projections show that most regions see their carbon intensity negatively affected by climate change. Tohoku and Shikoku, the regions with the highest average carbon intensity (roughly 600 gCO_2eq/kWh), are the only regions showing a climate-induced increase in carbon intensity under SSP3-7.0 and SSP5-8.5 (+1.3% and +2.3%, respectively). For Chugoku, Hokuriku, and Okinawa, the projected changes in carbon intensity are small and within the models' error range.

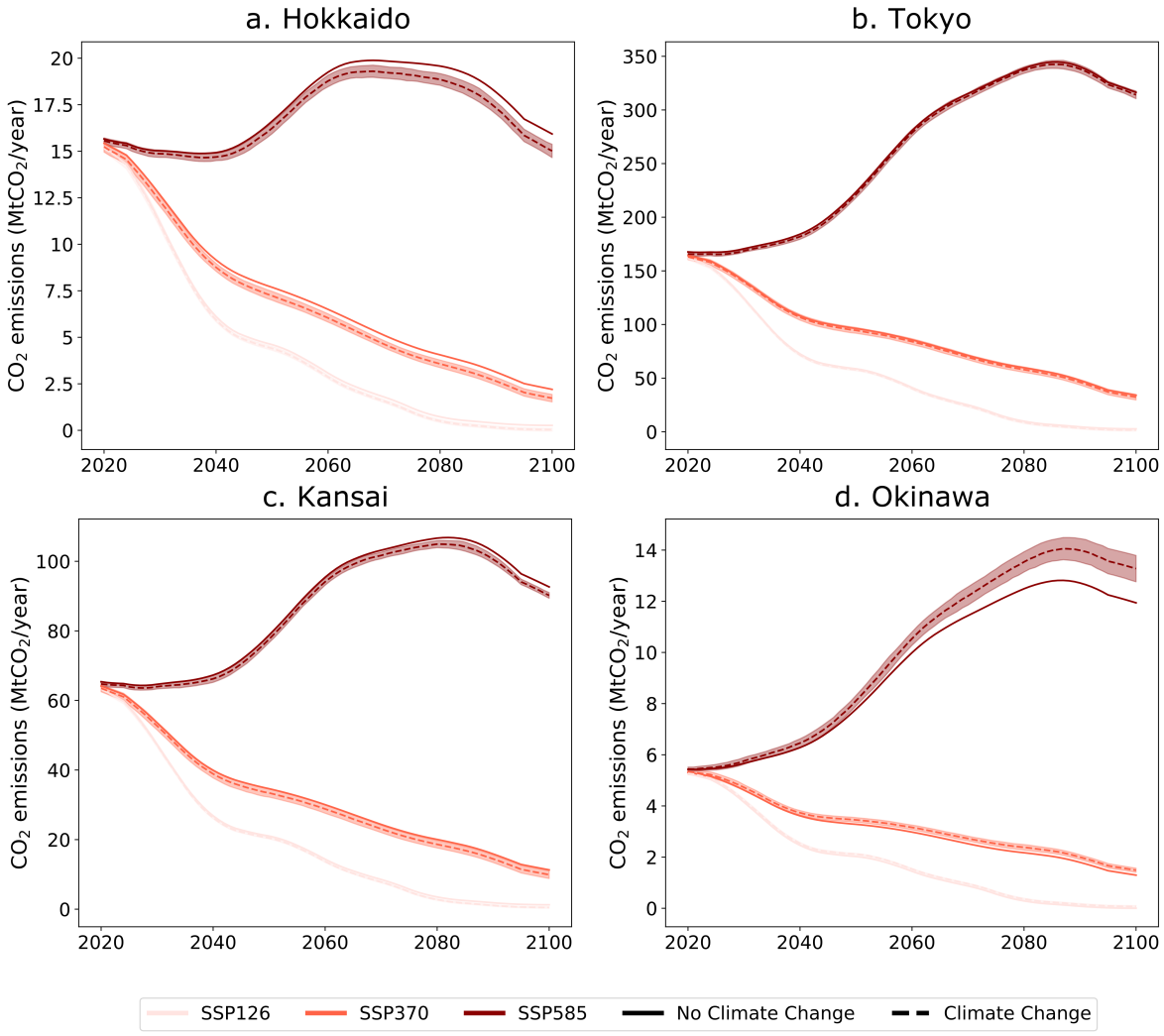

Figure III.7: Annual CO_2 emissions from power generation under SSP1-2.6, SSP3-7.0, and SSP5-8.5, after considering socioeconomic impacts with (dashed line) and without (solid line) climate change impact for four regions: Hokkaido (a), Tokyo (b), Kansai (c) and Okinawa (d). The shaded area represents the 1-sigma standard deviation from the five climate models for the scenario considering climate change impact (dashed line).

Figure III.7 shows how the influence of climate change on power demand and carbon intensity translates into carbon emissions. In the "no climate change scenario" (plain line), climate variables were held constant at their 2016 values. Therefore, are only influenced by changes in population, GDP, and carbon intensity. In the "climate change scenario" (dashed line), we varied all four factors (climate, population, GDP, and carbon intensity) with time. Climate variables values varied according to the ISIMIP projection, and socioeconomic variables according to the projection presented in Figure III.4. The difference between the solid and dashed lines for each region and scenario represents the difference in emissions due to climate change alone. In Figure III.7, we show the results of four regions. Results for the other regions are displayed in Figure S4 (Section S7, Supplementary Material, Appendix 2). The regions with the most ex-

treme temperatures (Hokkaido and Okinawa) indicate the largest differences. Climate change leads to a decrease in CO_2 emissions in Hokkaido but an increase in Okinawa. Okinawa and Shikoku are the only regions with higher emissions from climate change. The power demand is projected to increase strongly in Okinawa, especially under SSP5-8.5, which explains an increase in CO_2 emissions. On the other hand, the CO_2 emissions increase in Shikoku is due to an increase in carbon intensity simulated by the model. In all other regions, climate change leads to an increase in CO_2 emissions. In Kyushu, the CO_2 emissions decrease with climate change because the decline in carbon intensity takes over the increase in power demand. Such an effect can also be found in the Tokyo region, albeit to a lesser extent.

5.3 Attribution of the Changes in Power Demand and CO_2 Emissions

This section analyzes the effect of seasons and hot and cold periods on power demand and their respective contributions to the total annual change in power demand between 2020-2030 and 2090-2100. We divided days into four categories (cold, cool, warm, and hot) based on temperature distributions during 2016-2020. We calculated the number of days in each category under the three SSPs during 2020-2030 and 2090-2100. We attributed the contribution of the change in power demand in each category to the total change in power demand (Fig. S6, Section S8, Supplementary Material, Appendix 2). The number of hot days increases in all ten regions. Increasing power demand during hot days is associated with cooling demand. However, such an increase is counterbalanced by a decrease in power demand in other categories of days. Okinawa is an exception; power demand increases in all categories of days.

Figure III.8 shows the changes in CO_2 emissions between 2020-2030 and 2090-2100 due to changes in power demand and carbon intensity under SSP5-8.5 at monthly and regional levels. This figure allows for comparing our results with those of Hiruta et al., 2022b (see Section 7 for the comparison). Most regions are projected to see a decrease in annual CO_2 emissions from power generation due to climate change, ranging from -0.3% to -5.1%. Shikoku and Okinawa are exceptions; their CO_2 emissions are projected to increase by 2.5 and 10%, respectively. Larger differences emerge at the monthly scale; the largest increases in CO_2 emissions (up to 23% increase in Okinawa) occur during a few transition months before and after the hottest months (i.e., May, June, September, and October) for all regions except Hokkaido and Tohoku. The largest increases occur during the warmest months in these two relatively cold regions. Such results indicate that the "next-warmest months" (May, June, September, and October) are most susceptible to future climate. A threshold temperature above which the demand for air

conditioning starts was identified for each region in Section 5.1 with partial dependence plots. Building on that, we formulate a possible explanation for the observed monthly changes; during July and August, the threshold temperatures triggering cooling demand are already exceeded for most days in all regions (except in Hokkaido and Tohoku). Thus, a further increase in power demand for cooling demand is not expected. However, with future warming, the temperature thresholds could be exceeded earlier in the year (in May or June) and longer (until September or October), explaining why the largest increase in power demand is projected to occur in the "next-warmest months". Similar monthly changes are observed for power demand but not for carbon intensity (Figs. S7a and S7b, Section S9, Supplementary Material, Appendix 2), indicating that monthly changes in regional CO_2 emissions are driven more by power demand than carbon intensity.

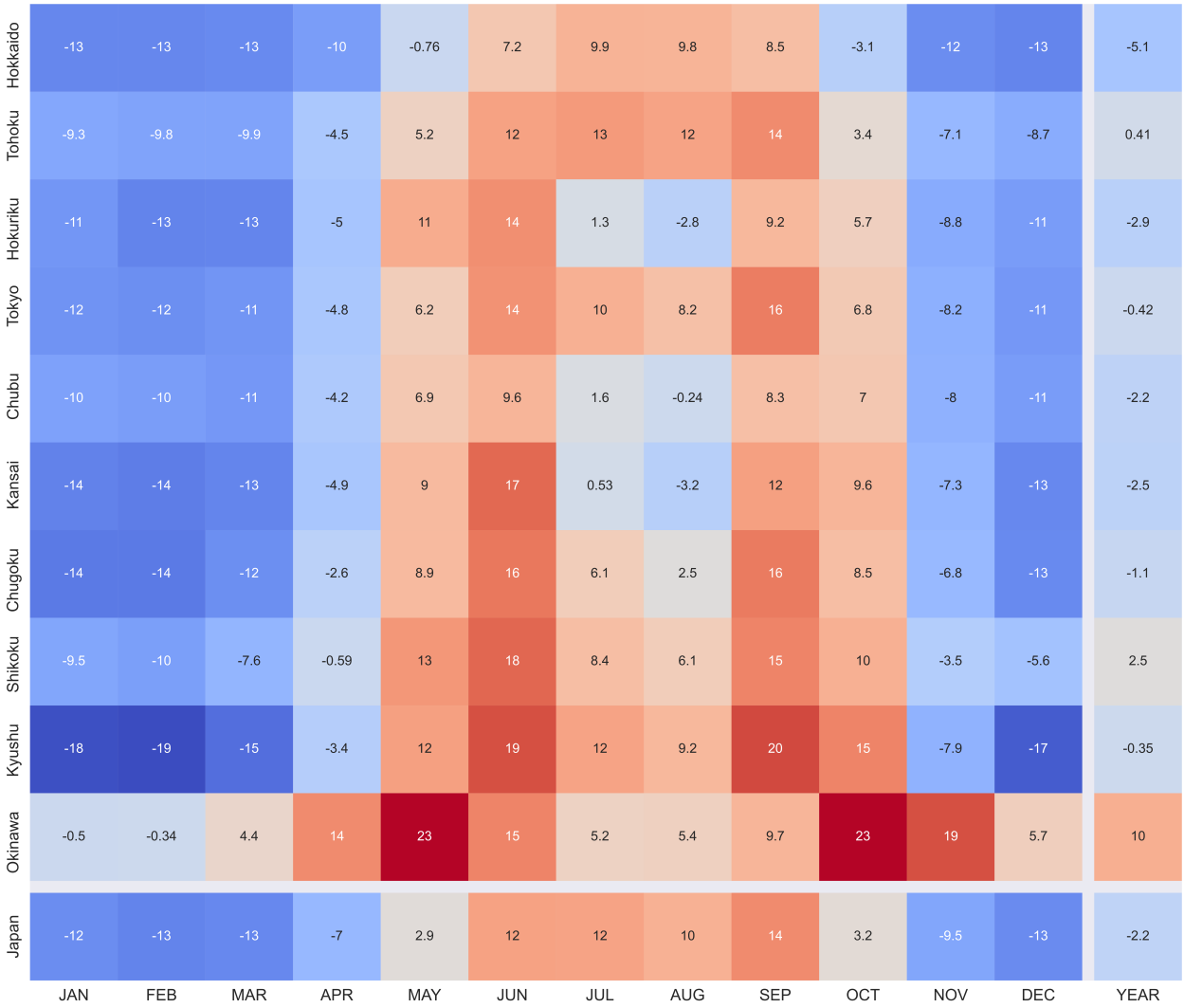

Figure III.8: Monthly and regional changes (in percentage) in CO_2 emissions between the decade 2020-2030 and 2090-2100 due to climate impacts on future power demand. The mean results of the five models for SSP5-8.5 are shown.

6 Comparison of Different Factors Influencing CO_2 Emissions of Power Generation

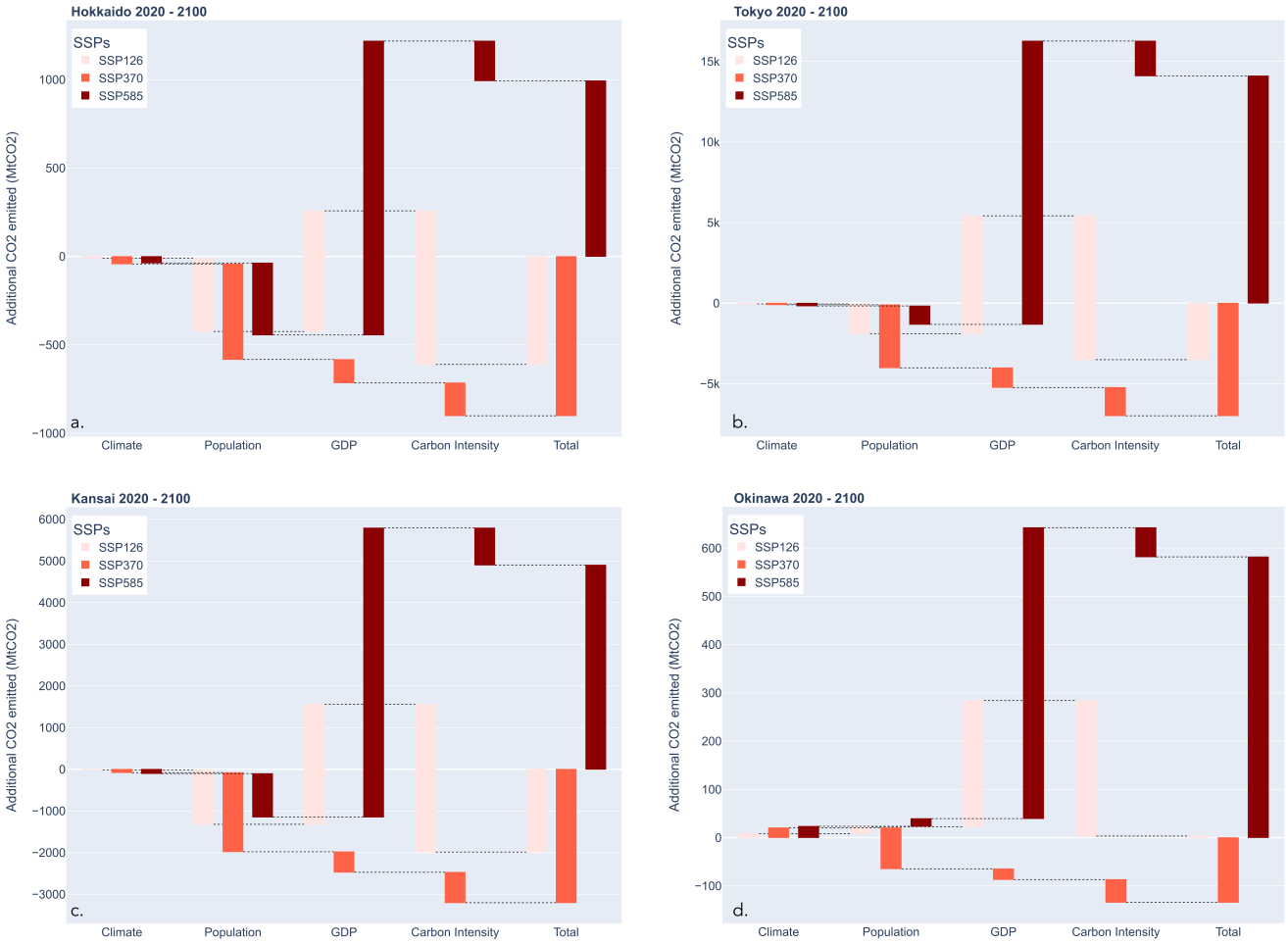

Figure III.9: Individual contributions of changes in climate, population, GDP, and environmental policies to the changes in total CO_2 emissions of power generation over the period 2020-2100. The figure shows the change in CO_2 emissions due to each factor relative to the level with all other factors kept at current values. The figure shows the results for four representative regions from north to south: Hokkaido (a), Tokyo (b), Kansai (c), and Okinawa (d).

Figure III.9 compares the impact of climate change on CO_2 emissions from power generation with those of socioeconomic factors (population, GDP, and carbon intensity). We quantified the amount of CO_2 emitted by each factor individually by varying one factor at a time. Note that the total in Figure III.9 is the arithmetic sum of the individual changes from each factor, which is different from the total (with climate change) in Figure III.7, calculated from

the compounded change from all factors. With such a method, the results show that climate change plays a minor role in determining future changes in CO_2 emissions (Fig. III.9). The decreasing population under all scenarios negatively affects CO_2 emissions in all ten regions. GDP influences emissions in different directions according to scenarios; the GDP effect is negative under SSP3-7.0 due to projected GDP decrease, whereas it is positive under SSP1-2.6 and SSP5-8.5 as GDP grows. Under SSP5-8.5, GDP is by far the most important factor determining CO_2 emissions in all ten regions. The effect of carbon intensity on CO_2 emissions is small under SSP5-8.5 and SSP3-7.0, as carbon intensity is not projected to decrease much in these scenarios. However, carbon intensity is the most important factor under SSP1-2.6, leading to a decrease in CO_2 emissions in most regions.

To summarize, when individual effects of climate, population, GDP, and carbon intensity on CO_2 emissions are considered separately, as in Figure III.9, the climatic factor is overshadowed by the other factors. However, Figure III.7 shows that climate change may have a significant impact when all factors are combined to project CO_2 emissions in certain regions under SSP5-8.5. The importance of the climate change impact on CO_2 emissions depends on the type of climate of the region and future climate scenarios; it also depends on the month of the year, as indicated in Figure III.8.

7 Discussion

Our methodology allows for establishing regional statistical models that adequately reproduce the observations of daily power demand and carbon intensity. Seasonal cycles are well captured by the models for power demand, just as intra-weekly cycles (i.e., the distinction between working days and weekends). Interpretation methods such as partial dependence plots and Shapley values gave insights into understanding underlying mechanisms that control the dependency of power demand and carbon intensity on the predictors. As we are able to understand the impact of predictors on the outputs based on underlying mechanisms, such methods give us confidence in the projections of power demand and carbon intensity obtained using these models. Nevertheless, the models' inherent error is important for carbon intensity.

A well-known default of machine learning models is their bad performance outside their calibration range. For the projection, we calculated the percentage of days that have an average daily temperature outside the training temperature range period: 0.8% for SSP1-2.6, 3.6% for SSP3-7.0, and 5.2% for SSP5-8.5. For the projection period, we argue that the percentage of days

with an average temperature outside the training range is small enough to avoid overfitting.

Hiruta et al. used a comparable methodology (Hiruta et al., 2022a) and also projected regional power demand in Japan with statistical models (Hiruta et al., 2022b). However, we went one step further by modeling the influence of climate on carbon intensity and, eventually, CO_2 emissions. We obtained similar results for regional power demand; a decrease in power demand in cold regions and an increase in hot regions. However, we found a maximal increase in power demand during "next-warmest months" (May, June, September, and October). In contrast, the Hiruta study found it during the warmest months (July and August). This difference between the two studies has important implications for the power grid infrastructure in the future. Projecting the future power demand for air conditioning under changing climate is a critical issue in Japan, as revealed by the power supply situation in the summer of 2022. At the end of June 2022, Japan experienced a serious power deficit during weeks unusually hot for this month but not during equally hot weeks in July or August. The power deficit occurred in June as some thermal power plants were under periodic inspection before the high season and were not being operated (METI 2022). With climate change, there will be an increased risk of having peak demand earlier in the season. Power companies will have to consider it to avoid the problems of June 2022 happening again.

Here we discuss factors that can influence power demand but are not considered in our study. Firstly, the Urban Heat Island effect (UHI) is known to influence power demand. UHI amplifies power demand for air conditioning in densely populated cities in hot regions while it translates into a decrease in the demand for heating in colder regions (Roxon et al., 2020; Xiaoma et al., 2019). Xiaoma et al., 2019, showed that the UHI effect could increase the need for cooling energy by 19% and decrease the need for heating by 18.7% on average. According to the World Bank, 90% of the population lives in urban areas in Japan, with 60% of the country's 126 million inhabitants concentrated in the metropolitan areas of Tokyo, Nagoya, and Osaka. Hence, the UHI effect is probably not negligible and translates into a warming that is already a few degrees higher in cities than in rural areas (Takane et al., 2014; Takaya et al., 2014). The earth system models that generated the climate data we used for projection do not resolve UHI, implying that the future power demand in our projections may be underestimated in densely populated regions.

Secondly, a study by De Cian et al., 2019, predicts that almost 100% of Japanese homes will adopt air conditioning by mid-century for all scenarios. Even though Japan is already among

the countries with the highest air conditioning adoption rate per household, about 90% nationwide in 2011 (De Cian et al., 2019), the effect of increased access to air conditioning was not taken into account in our model. Such an increase could boost power demand if all other factors, such as the efficiency of air conditioning and the housing insulation, are kept the same. Specifically, it could significantly change the climate response functions for power demand in cold regions like Hokkaido as, for now, these regions have fewer houses equipped with cooling systems compared to the rest of the country. However, with our methodology, there is not enough data to model the power demand linked to air conditioner usage in such regions.

Thirdly, human exposure indices use thresholds to account for the level of heat stress felt by the population. For the DI, there is no discomfort below 21; between 21 and 24, less than 50% of the population feels discomfort; between 24 and 27, more than 50% of the population feels discomfort; between 27 and 29, most of the population suffers discomfort; between 29 and 32, everyone feels severe stress; above 32, the state of medical emergency is reached (Stathopoulou et al., 2005). Figure III.3b shows the projection for the annual maximal DI. The threshold of 24 has never been exceeded in Hokkaido for now. By the end of the century, DI could reach 27 in Hokkaido (Fig. III.3b). The maximal DI was 28 in Okinawa in 2020. At the end of the century, it could reach the dangerous threshold of 32. Exceeding such thresholds may lead to an underestimation of the power demand for air conditioning in all regions because there is no data to calibrate human behavior regarding the use of air conditioning when these thresholds are exceeded.

Finally, while our machine learning models developed to simulate the response of power demand to future climate are elaborated, how power demand responds to the future evolution of socioeconomic variables is modeled in a simpler way. Similarly, while we used projections of climate variables with a rather high spatial resolution (CMIP6 data, widely used in the scientific community), the projections used for the socioeconomic variables were only at the national scale for GDP and carbon intensity. Given the data availability, there are differences in the spatial and temporal resolutions of climate and socioeconomic data used in our analysis, which might have affected the accuracy of power demand projections from our model.

In conclusion, our study on Japan has revealed two key findings. The first pertains to the local impact of climate change and highlights the potential for increased power outages and grid saturation during the "next-warmest months" in Japan. The second finding is of global significance and demonstrates the usefulness of Japan as a case study to develop and test a

methodology for assessing the evolution of power demand and CO_2 emissions under the influence of climate change. The selection of Japan as a case study was motivated by its diverse range of climates, which can be representative of various regions of the world and provide insight into potential variations in power demand. Based on the findings from our research, which examined various regions in Japan, it is projected that there will be a decline in demand in cold and temperate regions and an increase in tropical regions. This outcome aligns with previous studies using different modeling methods, such as the research conducted by Van Ruijven et al., 2019, which examined the evolution of energy demand on a global scale.

References

Andrijevic, M. (2021). Future cooling gap in shared socioeconomic pathways. *Environmental Research Letters*, *16*(9), 0940553. https://doi.org/10.1088/1748-9326/ac2195

Auffhammer, M., Baylis, P., & Hausman, C. H. (2017). Climate change is projected to have severe impacts on the frequency and intensity of peak electricity demand across the united states. *Proceedings of the National Academy of Sciences*, *114*(8), 1886–1891. https://doi.org/10.1073/pnas.1613193114

Breiman, L. (2001). Random forests. *Machine Learning*, *45*, 5–32. https://doi.org/10.1023/A:1010933404324

Buitinck, L., Louppe, G., Blondel, M., Pedregosa, F., Mueller, A., Grisel, O., Niculae, V., Prettenhofer, P., Gramfort, A., Grobler, J., Layton, R., VanderPlas, J., Joly, A., Holt, B., & Varoquaux, G. (2013). API design for machine learning software: Experiences from the scikit-learn project. *ECML PKDD Workshop: Languages for Data Mining and Machine Learning*, 108–122.

Buzan, J. R., Oleson, K., & Huber, M. (2014). Implementation and comparison of a suite of heat stress metrics within the community land model version 4.5. *Geoscientific Model Development Discussions*, *7*, 5197–5248. https://doi.org/10.5194/gmdd-7-5197-2014

CDS. (2017). Era5: Fifth generation of ecmwf atmospheric reanalyses of the global climate. https://cds.climate.copernicus.eu/cdsapp#!/dataset/reanalysis-era5-complete?tab=overview

De Cian, E., Pavanello, F., Randazzo, T., Mistry, M., & Davide, M. (2019). Householdsádaptation in a warming climate: Air conditioning and thermal insulation choices. *Environmental Science & Policy*, *100*, 136–157. https://doi.org/10.1016/j.envsci.2019.06.015

Dellink, R., Chateau, J., Lanzi, E., & Magné, B. (2017). Long-term economic growth projections in the shared socioeconomic pathways. *Global Environmental Change*, *42*, 200–214. https://doi.org/10.1016/j.gloenvcha.2016.06.012

Epstein, Y., & Moran, D. S. (2006). Thermal comfort and heat stress indices. *Industrial Health*, *44*, 388–398. https://doi.org/https://doi.org/10.2486/indhealth.44.388

Friedman, J. H. (2001). Greedy function approximation: A gradient boosting machine. *The Annals of Statistics*, *29*(5), 1189–1232. Retrieved June 19, 2023, from http://www.jstor.org/stable/2699986

Friedman, J. (1991). Multivariate adaptive regression splines. *Annals of Statistics*, *19*(1), 1–67. https://doi.org/10.1214/aos/1176347963

Friedman, J. (1999). Stochastic gradient boosting. *Computational Statistics and Data Analysis*, *38*, 367–378. https://doi.org/10.1016/S0167-9473(01)00065-2

Greenwell, B. M. (2017). Pdp: An r package for constructing partial dependence plots. *R J.*, *9*(1), 421.

Hiruta, Y., Gao, L., & Ashina, S. (2022a). A novel method for acquiring rigorous temperature response functions for electricity demand at a regional scale. *Science of the Total Environment*, *819*, 152893. https://doi.org/10.1016/j.scitotenv.2021.152893

Hiruta, Y., Ishizaki, N. N., Ashina, S., & Takahashi, K. (2022b). Regional and temporal variations in the impacts of future climate change on japanese electricity demand: Simultaneous interactions among multiple factors considered. *Energy Conversion and Management: X*, *14*, 100172. https://doi.org/10.1016/j.ecmx.2021.100172

Ho, T. K. (1995). Random decision forests. *Proceedings of the 3rd International Conference on Document Analysis and Recognition*, 278–282. https://doi.org/10.1109/ICDAR.1995.598994

Lange, S. (2021). ISIMIP3BASD v2.5.0. https://doi.org/10.5281/zenodo.4686991

Liao, C. (2021). Pyearth: A python implementation of multivariate adaptive regression splines. https://doi.org/10.5281/zenodo.6368652

Maia-Silva, D., Kumar, R., & Nateghi, R. (2020). The critical role of humidity in modeling summer electricity demand across the united states. *Nature Communications*, *11*, 1686. https://doi.org/10.1038/s41467-020-15393-8

Molnar, C. (2020). *Interpretable machine learning*. lulu.com.

Mora, C. e. a. (2017). Global risk of deadly heat. *Nature Climate Change*, *7*, 501–506. https://doi.org/10.1038/NCLIMATE3322

Muñoz Sabater, J. (2019). Era5-land hourly data from 1981 to present. copernicus climate change service (c3s) climate data store (cds) [Accessed on February 2023]. https://doi.org/10.24381/cds.e2161bac

Patel, L. (2022). Climate change and extreme heat events: How health systems should prepare. *NEJM Catalyst Innovations in Care Delivery*, *3*(7). https://doi.org/10.1056/CAT.21.0454

Pedregosa, F., Varoquaux, G., Gramfort, A., Michel, V., Thirion, B., Grisel, O., Blondel, M., Prettenhofer, P., Weiss, R., Dubourg, V., Vanderplas, J., Passos, A., Cournapeau, D., Brucher, M., Perrot, M., & Duchesnay, E. (2011). Scikit-learn: Machine learning in Python. *Journal of Machine Learning Research*, *12*, 2825–2830.

Riahi, K., van Vuuren, D., Kriegler, E., Edmonds, J., O'Neill, B., Fujimori, S., Bauer, N., Calvin, K., Dellink, R., Fricko, O., & et al. (2017). The shared socioeconomic pathways and their energy, land use, and greenhouse gas emissions implications: An overview. *Global Environmental Change*, *42*, 153–168.

Roth, A. E. (1988). Introduction to the shapley value. *The Shapley value*, 1–27.

Roxon, J., Ulm, F.-J., & Pellenq, R. (2020). Urban heat island impact on state residential energy cost and co2 emissions in the united states. *Urban Climate*, *31*, 100546. https://doi.org/10.1016/j.uclim.2019.100546

Sohar, E., Adar, R., & Kaly, L. (1963). Comparison of the environmental heat load in various part of israel. *Bulletin of the Research Council of Israel*, *10*, 111–115.

Stathopoulou, M., Cartalis, C., Keramitsoglou, I., & Santamouris, M. (2005). Thermal remote sensing of thom's discomfort index (di): Comparison with in situ measurements. *Proc SPIE*, *5983*, 131–139. https://doi.org/10.1117/12.627541

Takane, Y., Kusaka, H., & Kondo, H. (2014). Investigation of a recent extreme high-temperature event in the tokyo metropolitan area using numerical simulations: The potential role of a 'hybrid' foehn wind. *Q. J. R. Meteorol. Soc.* https://doi.org/10.1002/qj.2490

Takaya, A., Morioka, Y., & Behera, S. K. (2014). Role of climate variability in the heatstroke death rates of kanto region in japan. *Scientific Reports*. https://doi.org/10.1038/srep05655

Thom, E. (1959). The discomfort index. *Weatherwise*, *12*, 57–61. https://doi.org/10.1080/00431672.1959.9926960

Van Ruijven, B., De Cian, E., & Wing, I. (2019). Amplification of future energy demand growth due to climate change. *Nature Communications*, *10*, 2762. https://doi.org/10.1038/s41467-019-10399-3

Van Vuuren, D., Stehfest, E., Gernaat, D., & et al. (2021). *The 2021 ssp scenarios of the image3.2 model* (tech. rep. No. 4740). PBL Netherlands Environmental Assessment Agency. https://doi.org/10.31223/X5CG92

Winter, E. (2002). The shapley value. *Handbook of game theory with economic applications*, *3*, 2025–2054.

World Bank. (2023). World Development Indicators.

Xiaoma, L., Yuyu, Z., Sha, Y., Gensuo, J., Huidong, L., & Wenliang, L. (2019). Urban heat island impacts on building energy consumption: A review of approaches and findings. *Energy*, *174*, 407–419. https://doi.org/10.1016/j.energy.2019.02.183

Yalew, S., van Vliet, M., Gernaat, D., Ludwig, F., Miara, A., Park, C., Byers, E., De Cian, E., Piontek, F., Iyer, G., Mouratiadou, I., Glynn, J., Hejazi, M., Dessens, O., Rochedo, P., Pietzcker, R., Schaeffer, R., Fujimori, S., Dasgupta, S., & Vuuren, D. (2020). Impacts of climate change on energy systems in global and regional scenarios. *Nature Energy*, *5*. https://doi.org/10.1038/s41560-020-0664-z

Zittis, G., Hadjinicolaou, P., Almazroui, M., et al. (2021). Business-as-usual will lead to super and ultra-extreme heatwaves in the middle east and north africa. *npj Climate and Atmospheric Science*, *4*, 20. https://doi.org/10.1038/s41612-021-00178-7

CHAPTER IV

CARBON MONITOR POWER - SIMULATORS (CMP-SIM V1.0) ACROSS COUNTRIES: A DATA-DRIVEN APPROACH TO SIMULATE DAILY POWER DEMAND

Building on the lessons learned from the in-depth case studies conducted in Qatar and Japan, the focus of this section shifts to the development of a generalized approach known as CMP-SIMv1.0. This methodology aims to simulate electricity demand while covering a wider range of geographical areas and different climatic conditions. CMP-SIMv1.0 seeks to create a generic framework applicable to different countries and regions worldwide by extrapolating the lessons learned from the Qatar and Japan studies. This section delves into the architecture, methods, and intricacies that underpin CMP-SIMv1.0, shedding light on its potential to simulate accurately power demand under different climates and economies. This approach has been developed for the major countries where data is available in the Carbon Monitor Power database: Australia, Brazil, China, EU27 & UK, India, Russia, South Africa, and the United States. Two prominent machine learning algorithms, Random Forest and Gradient Boosting, were used. These models, implemented with the renowned scikit-learn library (Buitinck et al., 2013; Pedregosa et al., 2011) in Python 3.9, provide a powerful ensemble-based approach to capture complex relationships between climate, socio-economic factors, and energy demand. CMP-SIMv1.0 also includes GAMs implemented with the pygam package (Servén et al., 2018) and MARS models using the pyearth package (Liao, 2021).

1 Summary

Building on the lessons drawn from the case studies conducted in Qatar and Japan, the subsequent focus shifts toward the development of an overarching and generalized approach known as CMP-SIMv1.0. This methodology is crafted to simulate electricity demand on a broader scale, encompassing various geographical regions and distinct climatic conditions. The overarching aim of CMP-SIMv1.0 is to create a versatile and adaptable framework applicable to various countries and regions across the globe, leveraging the insights gleaned from the empirical studies in Qatar and Japan.

This section delves into the architecture, methods, and intricacies that underpin CMP-SIMv1.0, shedding light on its potential to simulate accurately power demand under different climates and economies. This approach has been developed for the major countries where data is available in the Carbon Monitor Power database: Australia, Brazil, China, EU27 & UK, India, Russia, South Africa, and the United States. Two recognized machine learning algorithms, Random Forest and Gradient Boosting, were used. These models, implemented with the renowned scikit-learn library (Buitinck et al., 2013; Pedregosa et al., 2011) in Python 3.9, provide a powerful ensemble-based approach to capture complex relationships between climate, socioeconomic factors, and energy demand. CMP-SIMv1.0 also includes GAMs implemented with the pygam package (Servén et al., 2018) and MARS models using the pyearth package (Liao, 2021).

The significance of assessing the impact of climate change on power demand is underscored by the evolving dynamics of temperature, relative humidity, and other climatic variables, all of which have a substantial influence over cooling and heating demands in domestic and industrial contexts. Accurate power demand predictions assume pivotal importance in energy system planning and management. Moreover, understanding the trajectory of power demand is fundamental in estimating the volume of CO_2 emissions released into the atmosphere.

Artificial intelligence techniques have been harnessed in recent years to explore energy demand responses to external factors across various scales. However, the nexus between climate and weather variability and power demand has remained relatively uncharted. The present study introduces a data-driven approach to model daily power demand, drawing upon Carbon Monitor Power project data. This approach integrates various predictive features encompassing climate variables and human activity indices. The study spans from 2020 to 2022 and focuses on eight countries listed above that collectively account for over 70% of global power consumption.

Evaluation of the models is performed using evaluating metrics, including the coefficient of determination (R2), Mean Absolute Error (MAE), Root Mean Squared Error (RMSE), and Median Absolute Error (MedAE). Additionally, the models are used to identify the most influential variables shaping power demand and elucidate their relationships. The findings offer valuable insights into the variations among countries with respect to key predictive features, shedding light on the distinct roles played by various climate variables and economic activity indicators, such as weekends, working days, vacations, holidays, and the influence of COVID-19.

This work has been submitted as: Gurriaran, L., Goude, Y., Tanaka, K., Zhu, B., Deng, Z., Song, X., and Ciais, P. Carbon Monitor Power - Simulators (CMP-SIM v1.0) across countries: a data-driven approach to simulate daily power demand, EGUsphere [preprint], https://doi.org/10.5194/egusphere-2023-1313, 2023. See Appendix 1 for the supplementary materials.

2 Abstract

The impact of climate change on power demand has become increasingly significant, with changes in temperature, relative humidity, and other climate variables affecting cooling and heating demand for households and industries. Accurately predicting power demand is crucial for energy system planning and management. It is also crucial to understand the evolution of power demand to estimate the amount of CO_2 emissions released into the atmosphere, allowing stakeholders to make informed plans to reduce emissions and adapt to the impacts of climate change. Artificial intelligence techniques have been used to investigate energy demand-side responses to external factors at various scales in recent years. However, few have explored the impact of climate and weather variability on power demand. This study proposes a data-driven approach to model daily power demand provided by the Carbon Monitor Power project by combining climate variables and human activity indices as predictive features. Our investigation spans the years 2020 to 2022 and focuses on eight countries or groups of countries selected to represent different climates and economies, accounting for over 70 % of global power consumption. These countries include Australia, Brazil, China, the European Union (EU), India, Russia, South Africa, and the United States. We assessed various machine-learning regressors to simulate daily power demand at the national scale. For countries within the EU, we extended the analysis to one group of countries. We evaluated the models based on key evaluating metrics: coefficient of determination (R2), Mean Absolute Error (MAE), Root Mean Squared Error (RMSE), and Median Absolute Error (MedAE). We also used the models to identify the most influential variables that impact power demand and apprehend their rela-

tionship with it. Our findings provide insight into variations in important predictive features among countries, along with the role played by distinct climate variables and indicators of the level of economic activity, such as weekends and working days, vacations and holidays, and the influence of COVID-19.

3 Introduction

Climate significantly impacts power demand (Isaac et al., 2009; Lucon et al., 2014), as the changes in temperature, relative humidity, and precipitation patterns affect the cooling and heating demand of households and industries (Mukherjee et al., 2019). Globally, climate change is expected to increase total power demand under low latitudes and decrease under temperate and high latitudes because of warmer winters(Van Ruijven et al., 2019). However, there remain large uncertainties in how climate change will affect power demand (Deroubaix et al., 2021; Romitti et al., 2022; Yalew et al., 2020) due to complexities associated with understanding the precise effects of different variables on power demand, whether they are climatic or socioeconomic. Improving comprehension of the complex interactions between these variables and power demand becomes crucial for accurately predicting and managing power demand across different timescales. Accurate predictions of power demand can help energy providers to optimize generation and transmission, reduce costs, and improve the reliability of power supply at the seasonal scale. This becomes even more critical in the context of climate change, which has already begun to impact power demand and caused power outages in various parts of the world due to high cooling demand associated with exceptional heatwaves and other extreme climate events (Ahmad, 2021; Burillo et al., 2018). Finally, going one step further, understanding the impact of climate change on power demand is essential for managing CO_2 emissions from the power sector, as it is closely related to the development of strategies for reducing greenhouse gas emissions and adapting to changes in energy consumption patterns (Jiang et al., 2020).

While artificial intelligence techniques use has grown to investigate energy demand-side responses at various spatial and temporal scales (Antoniopoulos et al., 2020), literature on the impact of climate and weather variability on power demand using these methods is still limited. Previous studies have primarily been developed for specific regions or countries (Gurriaran et al., 2023a; Gurriaran et al., 2023b; Hiruta et al., 2022a; Hiruta et al., 2022b; Mohammadiziazi et al., 2020). Until recently, there was no comprehensive worldwide dataset for daily power dynamics across multiple countries. This knowledge gap has been filled with the introduction of the Carbon Monitor Power data (Zhu et al., 2023), which provides daily estimates of power

demand at the national level for about forty countries, along with detailed sources of supply. In this study, we use this newly available dataset to develop a machine-learning approach for modeling daily power demand by combining climate variables and human activity indices, considering the impact of climate through cooling and heating demand proxies. In addition, we consider human activity indices, such as working days, weekends, and holidays, as well as the level of stringency of COVID-19 measures, which play a crucial role in determining power demand as they reflect the level of economic activity (Antoniadis et al., 2022; Hiruta et al., 2022b).

Building on our earlier work on Qatar and Japan (Gurriaran et al., 2023a; Gurriaran et al., 2023b), the present study aims to develop data-driven models that simulate daily power demand for a large number of countries with contrasted climates based on the Carbon Monitor Power demand dataset, and a comprehensive set of daily climate variables and human activity indices. Additionally, the study aims to infer the most important variables for each country or region and discuss differences that may arise between the countries. The data we used include total daily power production at a national or regional scale from 15 February 2019 to 15 October 2022, climate variables, and human activity indices to develop models at a national or regional scale. Our study assumes that daily power production is equal to power demand, as transmission losses are assumed to be negligible. The dataset is divided into a learning set and a test set. Different machine-learning regressors are trained on the learning set to develop the models for power demand prediction. The performance of the models is assessed using the test set through error metrics, the evaluation of overfitting, and an analysis of the model's residuals.

The models developed in this study have the potential to be applied in various contexts. The same models could be used to define new responsive power production modules coupled with weather forecast models to enable operational production forecasting. They could also benefit the domain of air quality monitoring; for example, the models could be integrated into data assimilation systems of atmospheric composition, such as the global Copernicus Atmosphere Monitoring Service (CAMS) and regional models, which require interactive emissions fields with weather and human activity variations. Furthermore, our models may be used for adapting power systems to climate extremes. Finally, they may be incorporated into longer-term climate scenarios, assuming that the short-term climate response of power production will remain unchanged. Some of our models can even integrate hypotheses relative to changes in consumption habits.

We present models for eight countries or groups of countries. Those countries represent diverse climates, economies, and populations worldwide: Australia, Brazil, China, the Euro-

pean Union (including the United Kingdom, referred to as EU27 & UK), India, Russia, South Africa, and the United States. Those countries are all significant in terms of population, GDP, power production, and CO_2 emissions. Together they represent about 50 % of the world's total population, 67 % of the global GDP, and 80 % of total power generation in 2021 (IEA, 2022). For the sake of presentation, we present the results for EU27 & UK in the main text as an illustration. The results for other countries are provided in the Supplementary Materials (Sect. 2, Appendix 1).

4 Data

This section describes the input data used to develop the regional or national models simulating power demand: the Carbon Monitor Power – Simulators (CMP-SIM v1.0). Regional power demand refers here to the power demand of EU27 & UK. All the data are at a national or regional level and at a daily timescale. The data were pre-processed to a format suitable for the machine learning approach. We used 32 months of input data from 15 February 2020 to 15 October 2022.

Table IV.1: Input and output dataset for this study

Predictive Features

	Variable Name	Unit	Description	Country/Region	Source
Climate Variable	T2M	°C	Average daily surface air temperature at 2m	All	ERA5
	T2Mmax	°C	Maximum daily surface air temperature at 2m		
	T2Mmin	°C	Minimum daily surface air temperature at 2m		
	Td	°C	Average daily dew point temperature at 2m		
	RH	%	Average daily relative humidity		
	Surface Pressure	Pa	Average daily pressure of the atmosphere on the surface of the land		
	U	m.s-1	Average wind speed and direction at 10m		
	TP	m	Average daily total precipitation		
	SSRD	J.m-2	Surface solar radiation downward		
	STRD	J.m-2	Surface thermal radiation downward		
Human Activities Indices	DOW	-	Day of week – categorical variable from 0 to 6	All	Python repository
	Holidays	-	Categorical variable 0 or 1	All but EU	Manually collected
	Workplace	%	Changes of workplace occupancy compared to a baseline	All but China and EU	Google Community Mobility Reports
	Covid	-	COVID-19 stringency index	All	Mathieu et al., 2020
	TOY	-	Numerical day of year	China and EU	-
	GDP	%	Quarterly GDP growth rate	Only China	China Bureau of Statistic

Target Feature

	Variable Name	Unit	Description	Country/Region	Source
Power Data	Total Demand	GWh	Total daily power demand in the region considered	All	Carbon Monitor - Power

4.1 Predictive Features

The predictive features used to build models predicting power demand, including climate variables and human activity indices (Table IV.1), are described in the following.

Climate Variables: The climate variables include temperature (daily average, max, and min), dew point temperature, surface pressure, relative humidity, wind, precipitation, and solar radiation. These variables are known to impact power demand, as they affect the energy

consumption patterns of households and industries. The climate variables are obtained from the ERA5 reanalysis at a daily timescale (Muñoz Sabater, 2019). All the climate variables were weighted by population density (Center for International Earth Science Information Network - Columbia University, 2018) to give more importance to climate over densely populated areas, as these regions are accountable for a significant proportion of power demand.

Human Activity Indices: Human activity data (Fig. IV.1), such as working days, holidays, and school vacations, also play a crucial role in determining power demand, as they reflect the level of activity influencing the power demand. These indices are obtained from publicly available datasets.

The effect of working days and weekends on power demand is accounted for with the numerical variable DOW (Day Of Week), where the value zero corresponds to Monday, one to Tuesday, and so forth, with six representing Sunday. To account for the effect of holidays, we introduce the variable “Holiday”, which takes the value of one if the day is a holiday and zero otherwise.

Because our data cover the COVID-19 period, we accounted for the impacts of COVID-19-related measures on power demand using the COVID stringency index. We used the COVID stringency index, which aggregates information from various policy sources, including the Oxford COVID-19 Government Response Tracker (Hale et al., 2021) and the ACAPS COVID-19 Government Measures Dataset (ACAPS, 2021). The COVID stringency index is a composite measure comprising nine response indicators, such as school closures, workplace closures, and travel bans. The values of these indicators are rescaled on a scale of 0 to 100, where 100 represents the strictest level of response. The COVID stringency index is available for 207 countries (Mathieu et al., 2020).

Additionally, we used data from the Google Community Mobility Reports to account for the effect of vacations on power demand. Google developed these reports to track the effects of COVID-19 on the frequency of various types of locations and was available from 15 February 2020 to 15 October 2022 (Google, 2020). These reports are constructed by analyzing location data from users who have opted into Location History for their Google account, and the data are aggregated to preserve users’ anonymity. The reports indicate how visits and length of stay in these different location categories have changed over time compared to a baseline period before the COVID-19 pandemic from 3 January 2020 to 6 February 2020. Specifically, we used the "workplaces" metric, which reflects the change in the percentage of people present at their workplaces compared to the baseline reference period. To remove the effects of weekends and holidays in the workplace metric, we applied a running mean on a 7-day basis and replaced

the values of the holiday days to match the value of the previous day. This was done because the effects of weekends and holidays are already represented by the variables "DOW" and "holidays," respectively. However, the Google Community Mobility Reports data are unavailable for China and the EU (Table IV.1). Thus, we employed an alternative variable, namely “Time of the Year” (TOY), to reflect the level of economic activity in the two countries. This variable is defined as the numerical day of the year, ranging from one on January 1st to 365 or 366 on December 31st. TOY is an alternative to Google Mobility data because it can serve as a proxy for economic activity by allowing the possible seasonal variation of power demand throughout the year to be linked to a specific period within that year.

Finally, given the significant reliance of China’s power demand on its industrial sector, it is imperative to consider economic indicators that reflect changes in industrial activity. We hypothesized a strong relationship between GDP and industrial activity and assumed that the fluctuations in GDP could be used as a proxy for changes in industrial activity. Consequently, we added quarterly GDP as a predictive feature for China.

In total, 15 predictive features were used to simulate daily power demand. However, the exact number and combination of predictive features used to simulate power demand vary depending on the availability of human activity data for a particular country and the use of GDP.

4.2 Target Features

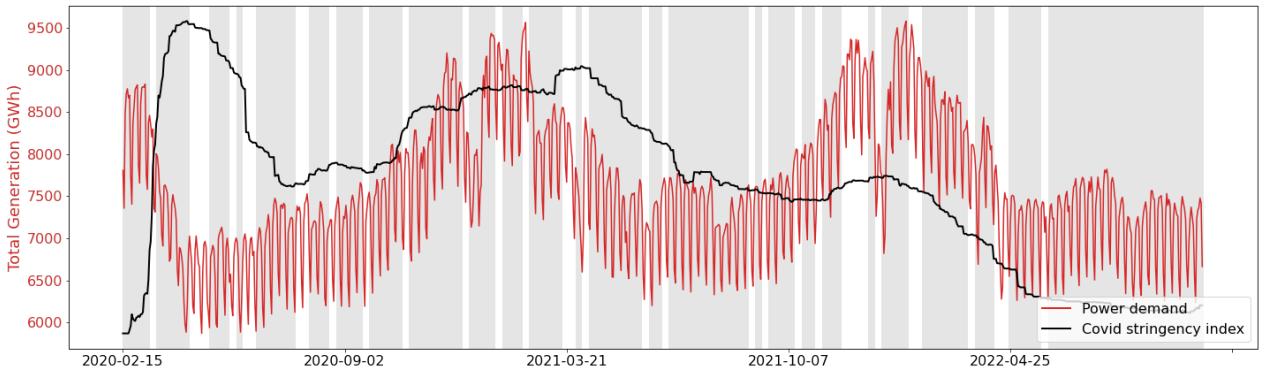

Figure IV.1: Evolution of human activity predictive feature from COVID stringency index for EU27 & UK and power demand over the studied period. The shaded area represents the learning periods, and the blank area the test periods.

The target feature of this study, i.e., the data we aim to simulate, are the total daily power demand at the regional or national scale (Fig. IV.1). This feature is calculated from the publicly

available Carbon Monitor - Power dataset (Liu et al., 2022; Liu et al., 2020; Zhu et al., 2023). This dataset includes daily historical data on electricity generation from 37 countries since January 2019. It gives the electricity generated by different energy sources: fossil (coal, gas, and oil), renewable (solar, wind, hydro, and others including biomass, geothermal, etc.), and nuclear. We obtain the total daily power demand by summing the daily power generation of each source under the assumption that demand is equal to generation. One outlier was detected for India (19 April 2020) and removed from the dataset.

5 Model Development

This section describes the approach we developed for establishing national or regional models simulating daily power demand from the predictive features described in Sect.4.1 (Fig. IV.2). The models have been coded in Python version 3.6.12. Our approach follows machine-learning procedures (Raschka et al., 2019; Raschka, 2020), including the formation of learning and test subsets, random search with cross-validation, regressor training on the learning set and performance evaluation with error metrics on the test set, model interpretation with model agnostic interpretability methods (ALE plots and permutation feature importance), and validation curve analysis to detect potential overfitting or underfitting. Previous studies have applied similar approaches to various countries. For example, in Japan, Hiruta et al., 2022a, used a machine-learning approach to derive temperature response functions at an hourly timescale. In previous works, we have developed data-driven models for long-term predictions in specific regions, namely Qatar (Gurriaran et al., 2023a) and Japan (Gurriaran et al., 2023b) . The approach developed for Japan was more detailed and tailored to the country. It included a separate model for carbon intensity and was conducted on the Japanese regional scale. The approach presented in this study is more generic and can be applied to any country or region worldwide so long as daily data are available.

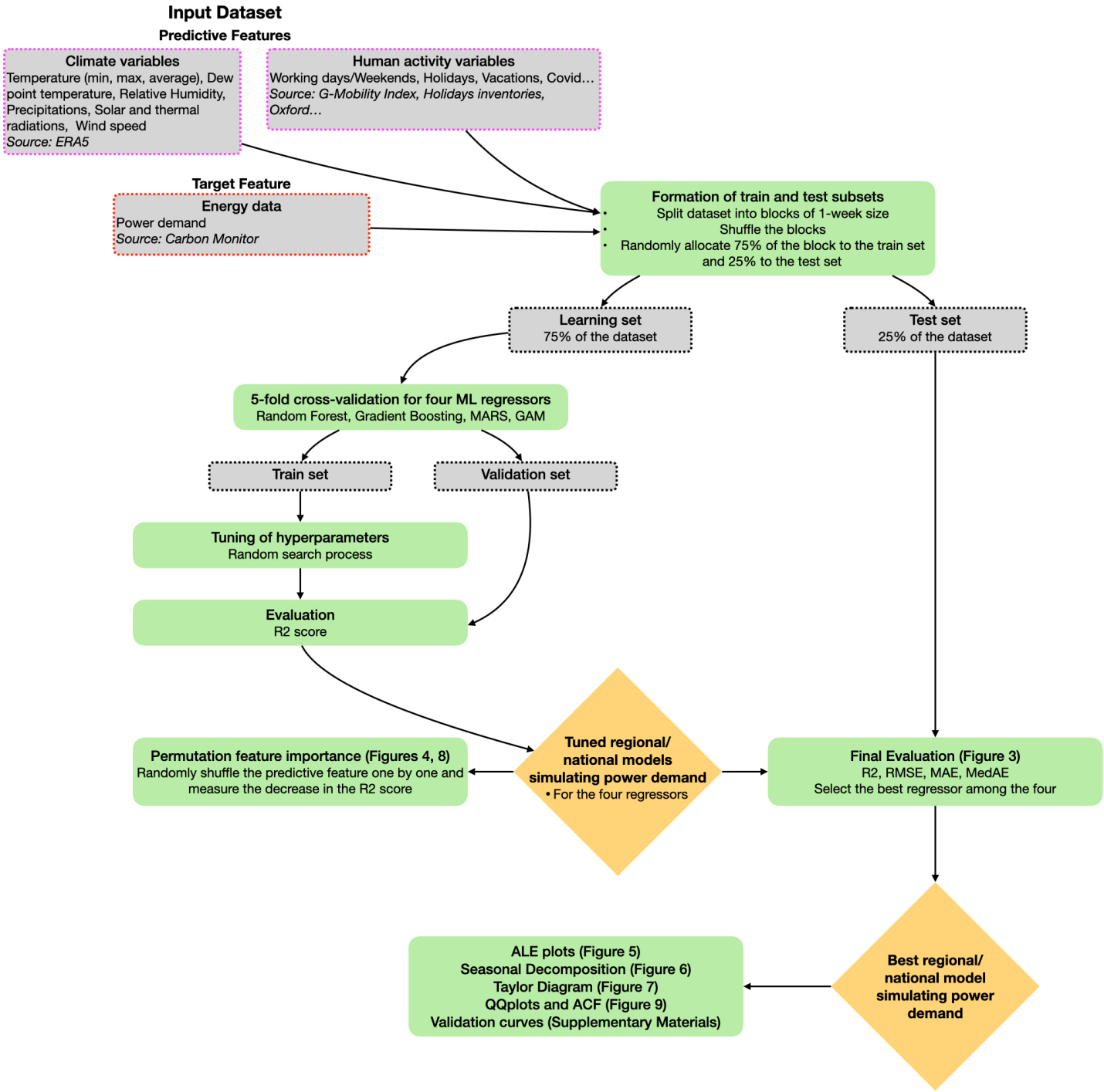

Figure IV.2: Methodological flowchart of this study: CMP-SIM approach.

5.1 Partitioning of Input Data Into Learning and Test Subsets

We followed a consistent procedure for each country or region, as illustrated in Fig. IV.2. The first step is to divide the input dataset into learning and test subsets. This is a necessary step to examine the robustness of the results; machine-learning regressors will be trained on the

learning set, and the performances of the models will be evaluated on the test set. The entire dataset is divided into blocks of one-week size. Then, all these blocks are shuffled randomly. Once the shuffling is done, 25 % of the data are assigned to the testing subset and 75 % to the learning subset (Fig. IV.1). This ratio is common for partitioning the dataset into learning and test subsets (Raschka et al., 2019; Raschka, 2020). This process ensures that both subsets are representative of the whole dataset and that the results obtained are robust and reliable.

5.2 Random Search with Cross-Validation and Evaluating Metrics

We evaluate four machine-learning regressors: Random Forest (RF) (Breiman, 2001), Gradient Boosting (GB) (Chen et al., 2016; Fisher, 1958; Ke et al., 2017), Multivariate Adaptive Regressions Splines (MARS) (Friedman, 1991), and Generalized Additive Model (GAM) (Hastie et al., 1990). RF and GB are two ensemble learning methods. RF combines multiple decision trees to make more accurate predictions. Each decision tree is trained on a random subset of the training data to reduce the risk of overfitting. When making a prediction, RF takes the average prediction of all the decision trees in the ensemble. GB combines weak learners to form a stronger predictor. Each weak learner is trained sequentially to minimize the errors of the previous weak learners. This process is repeated until the error is minimized or a specified number of weak learners is reached. The final prediction is made by combining the predictions of all the weak learners. MARS and GAM are two interpreted machine-learning methods for regression analysis. MARS uses a sum of piecewise linear regressions to model non-linear relationships, while GAM uses a sum of smooth functions such as splines. For GAM, we specified an equation for each country using the backward feature selection process (Wood, 2017). The model was executed using all the predictive features; then, we gradually eliminated all non-significant features until the model's stability was achieved according to a Fisher test. The allocation of a specific number of splines to each feature was accomplished using an integer value approximately one third higher than the degree of freedom estimated by the GAM regressor during the initial run.

All regressors are trained on the learning set, and their hyperparameters are optimized through a random-search process with 5-fold cross-validation on the same subset. The cross-validation process involves partitioning the learning data into multiple subsets (here 5) and uses each subset in turn as a validation set to assess the model's performance. The final evaluation of the model is done on the test set. The hyperparameters are the settings of the regressors that need to be specified before the training phase. They are specific to the type of regressor used and cannot be learned from the data. Optimizing the values of the hyperparameters is

important as they can impact the accuracy and performance of the models. Grid search and random search are two common techniques to tune hyperparameters. Grid search exhaustively searches through all possible combinations of hyperparameters, while random search randomly samples hyperparameters from a specified distribution. In a random search, the number of combinations tried is controlled by a pre-determined number of iterations (n_iter). The high computational cost of grid search led us to choose random search to explore the hyperparameter space for RF, GB, and MARS. Limiting the number of iterations to 200 considerably reduced the computation time while giving satisfying results. For GAM, we optimize only two hyperparameters. The description of the hyperparameters optimized through the random search process can be found in the Supplementary Materials (Sect. 1, Appendix 1).

We calculated various error metrics to evaluate the performance of the models on the test set. These include the coefficient of determination (R2), Mean Absolute Error (MAE), Root Mean Squared Error (RMSE), and Median Absolute Error (MedAE). The objective is to maximize R2 and minimize the values of MAE, RMSE, and MedAE.

5.3 Interpretation of the Models with Permutation Feature Importance and ALE Plots

Permutation feature importance and ALE plots are two methods that allow the interpretation of non-directly interpreted machine learning models such as RF and GB regressors. We use the permutation feature importance to classify the predictive feature by order of importance and the ALE plot to understand the relationship between the predictive features and the target feature. For consistency in our results, we also apply this method to GAM and MARS regressors even though they are interpreted machine learning models.

Permutation feature importance enables a relative classification of features within the models, identifying the most significant predictive features to explain power demand for a particular country. We calculate a permutation score for each predictive feature with the four machine-learning regressors tested. This score is determined by randomly shuffling the feature and measuring the reduction in model accuracy that results. The feature is shuffled five times; then, an average score is calculated.

ALE plots enable interpreting the relationship between the target feature (power demand) and one particular predictive feature (Apley et al., 2020). They represent the influence of the predictive feature on the target feature when the other predictive features are held constant. ALE plots are used to identify the non-linearities between the target feature and predictive fea-

tures. In this study, ALE plots were calculated for all predictive features included in the model that achieved the best evaluation metrics. This calculation involves dividing the range of the feature into intervals, calculating the average power demand for each interval, determining the differences in prediction between adjacent intervals, and integrating to estimate the individual influence of a feature.

5.4 Model Validation: Validation Curves, Quantile-Quantile Diagrams, Autocorrelation, and Seasonal Decomposition

Validation curves are commonly used to detect overfitting or underfitting problems. Overfitting happens when a model is too complex and fitted to the training data to the point that the model cannot be generalized to other data. In this case, the model performs well on the train sets but poorly on the validation set. Two validation curves are calculated, one for the train set and one for the validation set to detect overfitting. Those curves show how the model's performance (here measured with R2) changes for both subsets as a particular hyperparameter value of the model is varied. If the model performs much better on the train set than on the test set or the two curves diverge above a certain hyperparameter value, it indicates overfitting issues. In this study, we also used the validation curves to verify that the correct hyperparameter values were selected during the random search process. Underfitting is detected when the performances of the model are poor on both subsets. The validation curves for all countries considered can be found in Supplementary Materials (Sect. S2, Appendix 1).

Assumptions underpinning statistical methodologies are critical for ensuring the validity of analyses. One of our methodological assumptions is the normality of the residuals obtained from power demand calculations using our statistical models. To verify this assumption, we constructed quantile-quantile (QQ) plots for the residuals obtained from the four regressors (Chambers, 1983). These plots display the quantiles of a dataset as a function of the corresponding theoretical quantiles of a normal distribution. If the points on the QQ plot align closely with the diagonal, it indicates that the residuals follow a normal distribution, supporting the suitability of our methodology for accurately simulating power demand from the given data. Assessing the temporal structure of the residuals of a model is another way to evaluate the validity of a time-series model. Autocorrelation plots represent the correlation between a time-series and its delayed version. We constructed autocorrelation plots for the residuals of our four power demand regression models to identify any remaining temporal structures that the models may not have captured. To ensure the inclusion of weekly information, we chose a maximum time lag of 14 days for our analysis. If the autocorrelation values decrease rapidly

as the lag increases, it suggests that our models have fully explained the temporal information. Conversely, if the autocorrelation values remain high at larger lags, some relevant temporal information may not have been captured.

Finally, we used time-series seasonal decomposition to assess the performances of our models at different time scales. Seasonal decomposition is a statistical technique that decomposes a time-series into different components: trend, seasonality, and residuals (Hyndman et al., 2018). The trend component represents the long-term trend of the data, and the seasonality component captures the periodicity in the data (i.e., weekly, seasonal, or annual cycles). The residuals component is the random variations in the data that cannot be explained by the seasonal decomposition method. For this study, we used a simple decomposition method based on moving average with an additive model: $PD_t = T_t + S_t + R_t$, where PD_t is the power demand time-series, T_t is the "trend" component, S_t is the "seasonality" (here weekly) component, and R_t is the residual component. T_t is estimated using a convolutional filter and then subtracted from PD_t. S_t is obtained by averaging the de-trended series for each period. In this study, we did this analysis with a seven-day period to capture the weekly seasonality. This seasonal decomposition method was applied to the four time-series obtained with our models and to the original power demand time-series to serve as a point of comparison.

6 Output of the Models

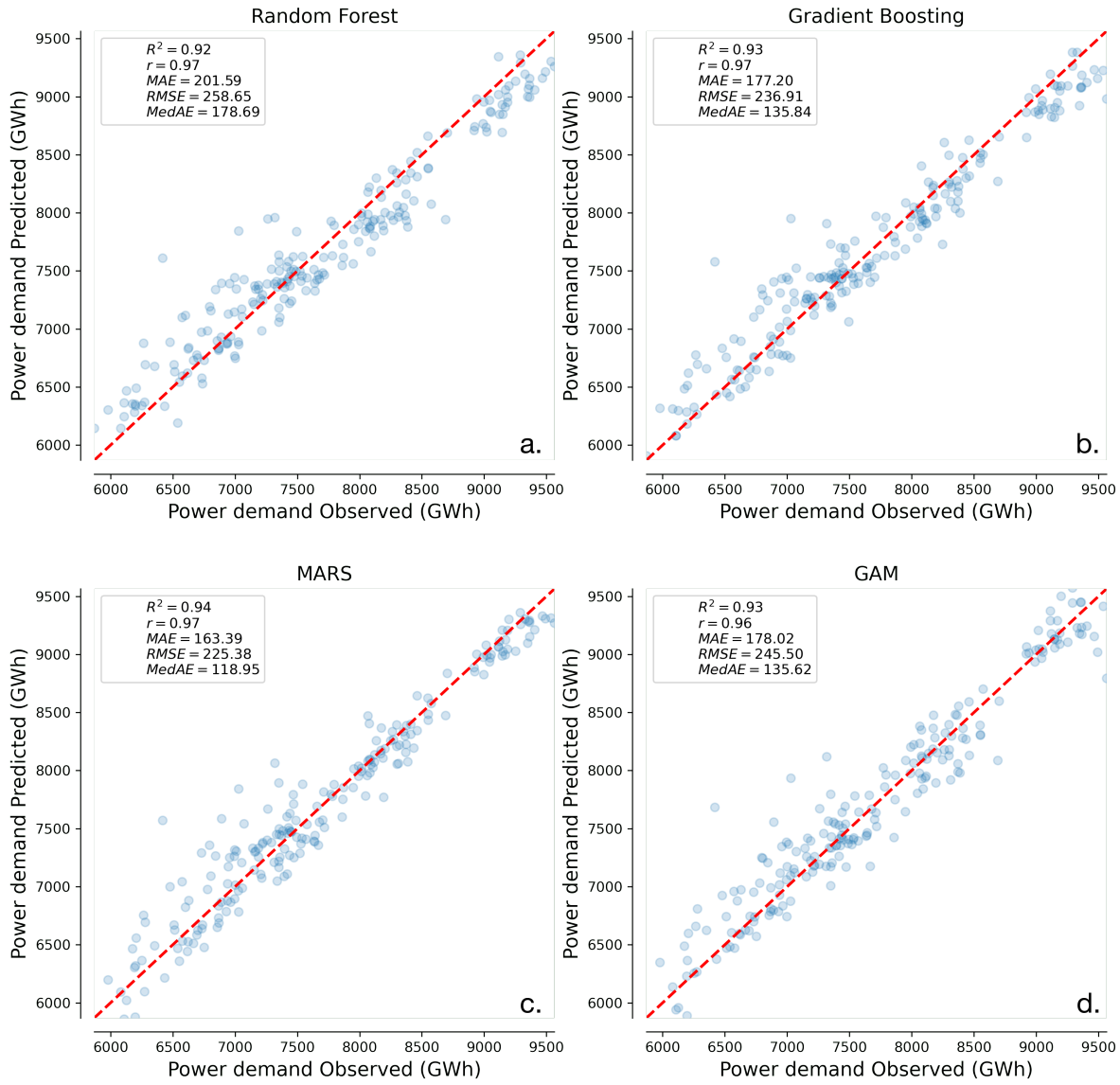

Figure IV.3: Comparison of machine-learning regressors performance for EU27 & UK. Predicted power demand plotted against observed power demand for the four machine-learning regressors tested: (a) RF, (b) GB, (c) MARS, and (d) GAM. The red dashed line represents the 1:1 line of perfect agreement between predictions and observations.

This section presents the main outputs of our machine-learning approach with a focus on EU27 & UK: the performance of the different models tested, the permutation feature importance, and the ALE plots. The results for other countries can be found in the Supplementary Materials (Sect. 2, Appendix 1).

Scatter plots show the modeled vs. observed power demand, with corresponding error metrics displayed on each subplot (Fig. IV.3). In the case of the EU27 & UK, all regressors per-

form similarly in evaluating metrics. Table IV.2 provides a summary of the evaluation metrics for all countries.

Table IV.2: Comparison of the performances of the four machine-learning regressors for the countries studied with the four metrics: R2, MAE, RMSE, and MedAE.

		Australia	Brazil	China	EU27 & UK	India	Russia	South Africa	United States
Random Forest	R2	0.80	0.87	0.75	0.92	0.85	0.96	0.81	0.89
	MAE	12.7	41.5	893.4	201.6	106.9	53.5	13.7	306.2
	RMSE	16.7	59.8	1161.9	258.7	149.1	72.0	18.7	394.1
	MedAE	10.2	29.1	732.1	178.7	76.3	38.6	10.8	250.5
Gradient Boosting	R2	0.84	0.93	0.77	0.93	0.83	0.98	0.77	0.91
	MAE	10.9	33.6	872.5	177.2	112.2	44.6	15.0	280.1
	RMSE	14.6	42.4	1128.6	236.9	159.3	58.7	20.6	361.4
	MedAE	8.4	28.4	666.3	135.8	78.5	35.5	11.7	216.9
MARS	R2	0.83	0.92	0.78	0.94	0.80	0.97	0.83	0.90
	MAE	11.5	36.2	810.3	163.4	121.8	50.3	13.02	309.2
	RMSE	15.1	46.5	1106.6	225.4	173.2	66.8	17.8	388.0
	MedAE	10.3	28.4	635.9	118.9	80.1	42.3	10.4	248.3
GAM	R2	0.81	0.92	0.77	0.93	0.81	0.97	0.83	0.94
	MAE	11.7	37.1	889.8	178.0	127.5	46.9	13.7	22.1
	RMSE	16.2	45.6	1120.1	245.5	171.6	64.1	17.9	292.7
	MedAE	9.0	33.1	753.9	135.6	105.6	34.9	11.4	169.3

Comparing the results of all countries, the models perform best in predicting power demand for Russia, with an R2 of 0.98. In contrast, they exhibit the poorest performance for China, with an R2 always under 0.8 (Table IV.2). The results presented in Table IV.2 do not reveal a single best regressor that consistently outperforms others across all countries.

Figure IV.4 shows the five most important predictive features, as determined by the permutation feature importance. When focusing only on predictive climate features (pink in Fig. IV.4), all regressors recognize temperature as a significant predictor, featuring it within the top five variables. However, the specific temperature-related feature that emerges as significant differs among the models (T2M, T2Mmax, T2Mmin, or Td). Furthermore, the variable SSRD (solar radiation) consistently appears as a crucial predictor, as it is included within the top five predictors for all regressors except MARS. These results underscore the crucial role of climate-related features in predicting power demand. On the other hand, the analysis also highlights the relevance of human activity features, with DOW, Covid, and TOY (blue in Fig. IV.4) always among the top five predictors. It is noteworthy that the order of the top five predictors varies across different models.

ALE plots were generated for the top five predictive features with the MARS regressor, which performed best for EU27 & UK (Fig. IV.5). The ALE plots confirm the strong impact of temperature-related predictors on power demand, with Td, T2Mmax, and T2Mmin being particularly influential. ALE plots for Td demonstrate a positive correlation between power demand and heating (when the temperature is decreasing), and ALE plots for T2Mmax have a positive correlation for cooling (when the temperature is increasing) requirements. ALE plot

for T2Mmin shows both effects. Examining the ALE plot for DOW (day of the week) reveals that power demand holds less significance during weekends than on weekdays. Finally, the ALE plot for TOY shows a decrease in power demand at the end and beginning of the year, corresponding to the holiday season. Overall, our findings here illustrated for EU27 & UK suggest that both climate and human activity factors are crucial in predicting power demand, and a comprehensive approach that considers both these aspects is needed to yield more accurate results.

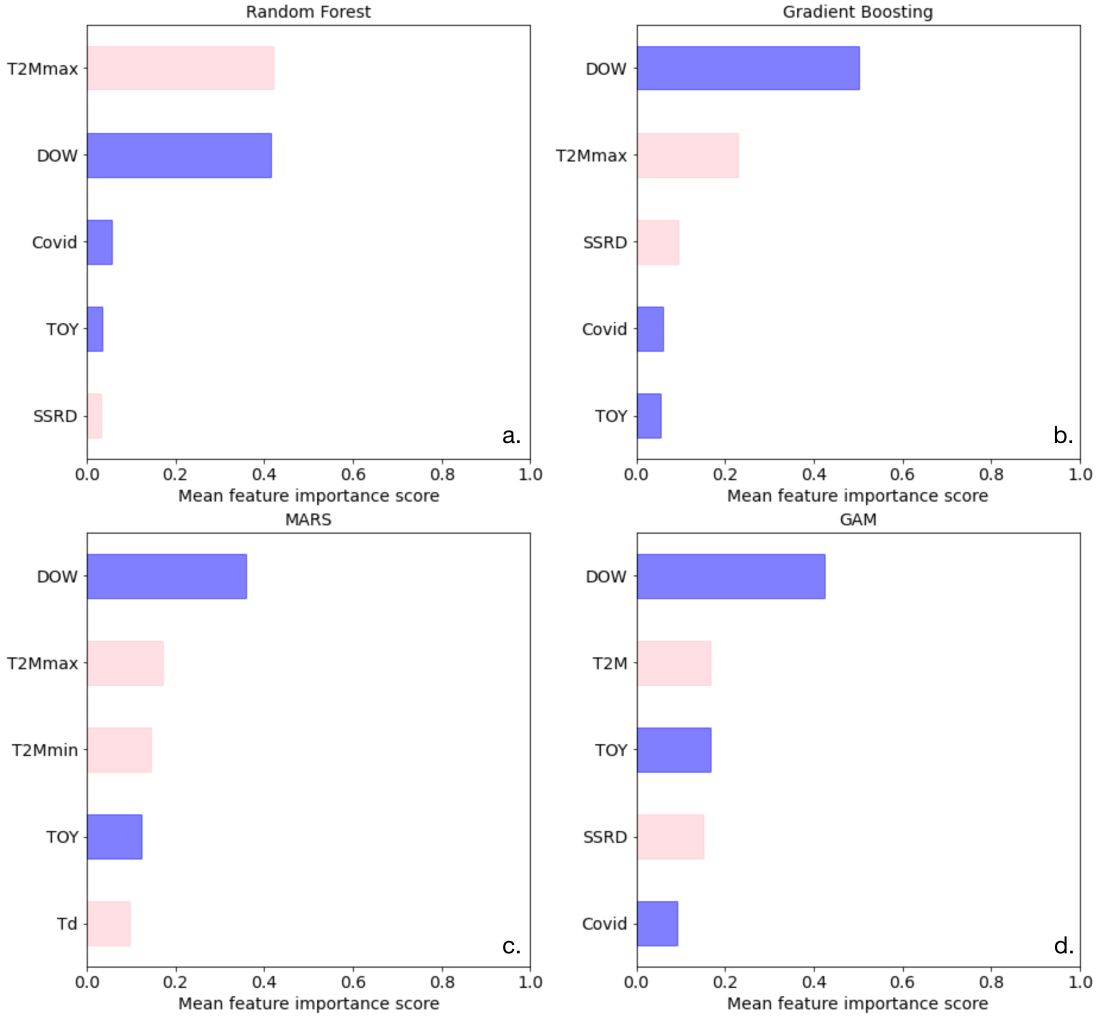

Figure IV.4: Permutation feature importances of the five most important predictive features from four different machine-learning regressors for EU27 & UK: (a) RF, (b) GB, (c) MARS, and (d) GAM.

The comparison of the modeled decomposed times series and the observed decomposed time-series enable assessment of the ability of models to capture the diverse temporal patterns inherent in the data. By decomposing the time-series generated by the models and comparing them with observed electricity demand, it becomes possible to evaluate the models' ability to

accurately replicate the various temporal patterns evident in the observational data. Figure IV.6 focuses on December 2021 to illustrate the negative impact of the Christmas holidays on power demand. Electricity demand remains low at the end of the month, possibly due to the high temperatures observed during this period. The trend component (Fig. IV.6b) indicates that all models successfully capture the decrease in power demand attributed to the Christmas break. Upon comparing the seasonal decomposition of the models with that of the observational data, it demonstrates that GB exhibits the highest accuracy in simulating this decrease in power demand. Additionally, our analysis demonstrates that all models perform well in simulating the weekly component (Fig. IV.6c). Lastly, our investigation reveals a correlation between the residuals of the seasonal decomposition of the models and those of the observations. This finding suggests that the models effectively capture short-term temporal patterns in electricity demand, indicating their potential to be used for generalization.

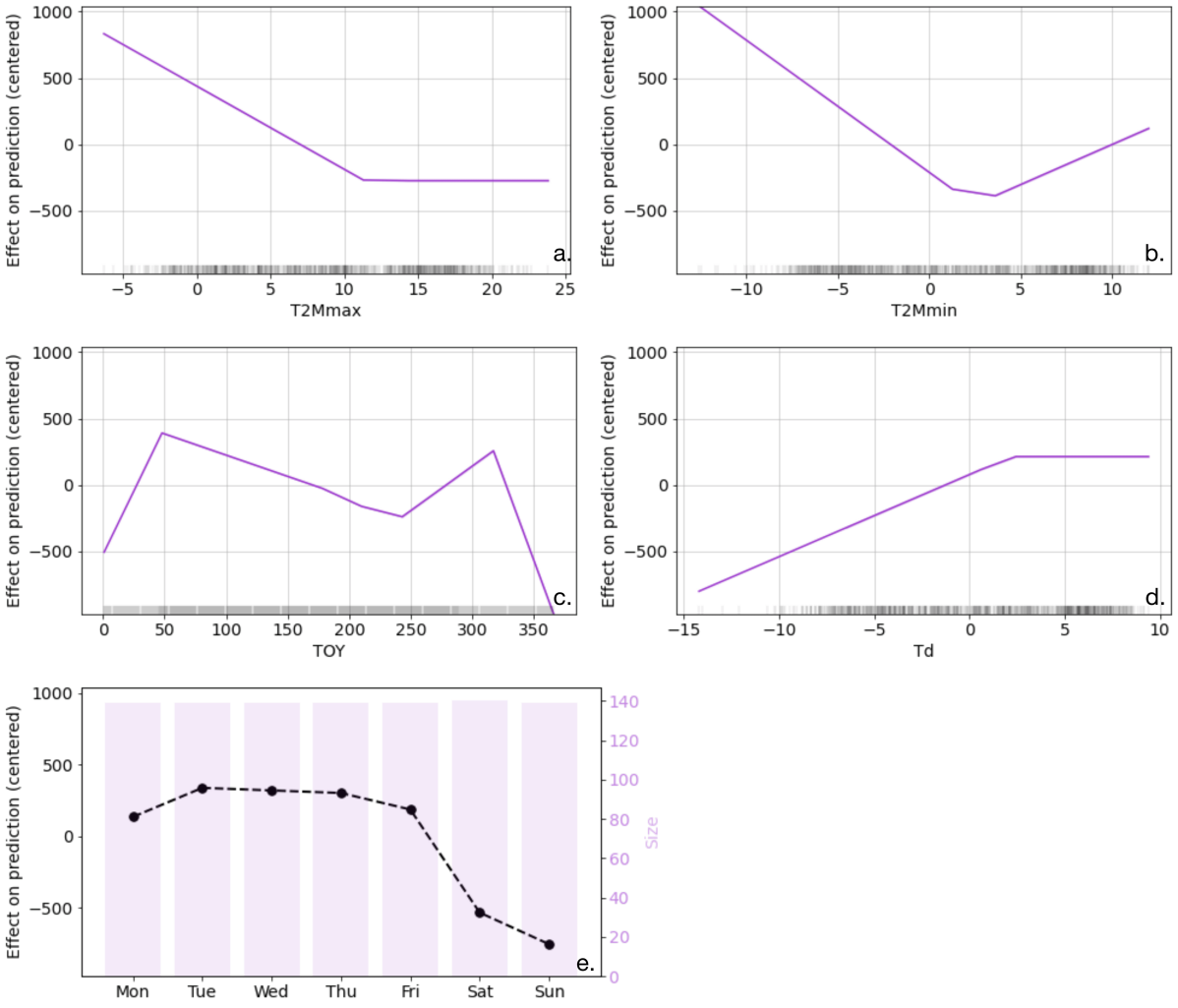

Figure IV.5: ALE plots of the effect of the top-five predictive features from MARS for EU27 & UK: (a) T2Mmax, (b) T2Mmin, (c) TOY, (d) Td, and (e) DOW, where size represents the number of days in each category. Each ALE plot shows the partial dependence of the target feature on a predictive feature while keeping all other features constant. The x-axis represents the values for each feature, and the y-axis represents the corresponding change in the predicted value of the target feature.

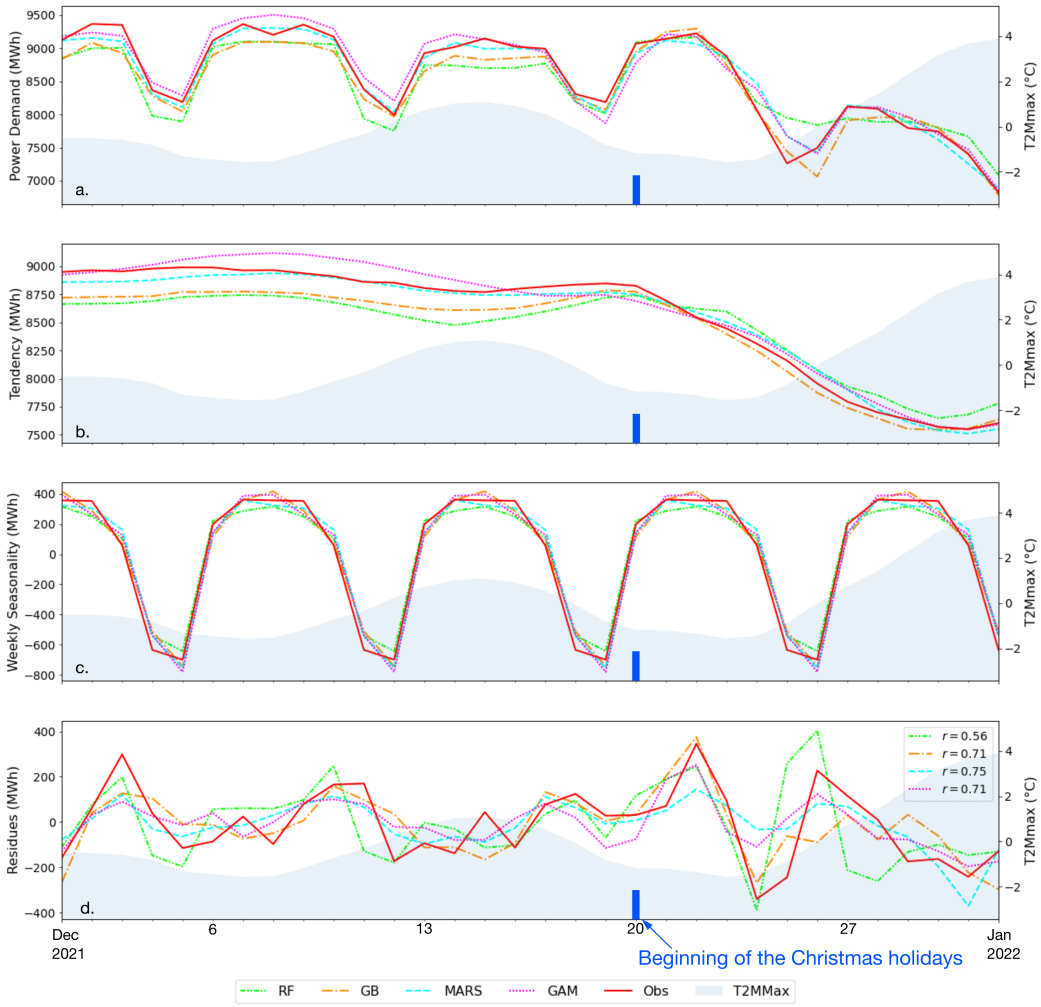

Figure IV.6: Weekly seasonal decomposition analysis of the daily power demand data from four different models (RF, GB, MARS, GAM) as well as the observed data (Obs) for EU27 & UK: (a) Observed and modeled daily times series, (b) trend component, (c) weekly component, and (d) residual component. The legend in panel d represents the Pearson correlation coefficient between the models' residues and the observations' residues. The shaded area in the plots represents the maximum daily temperature (T2Mmax) in a 7-day running mean.

7 Discussion

7.1 Model Inter-Comparison in Different Countries

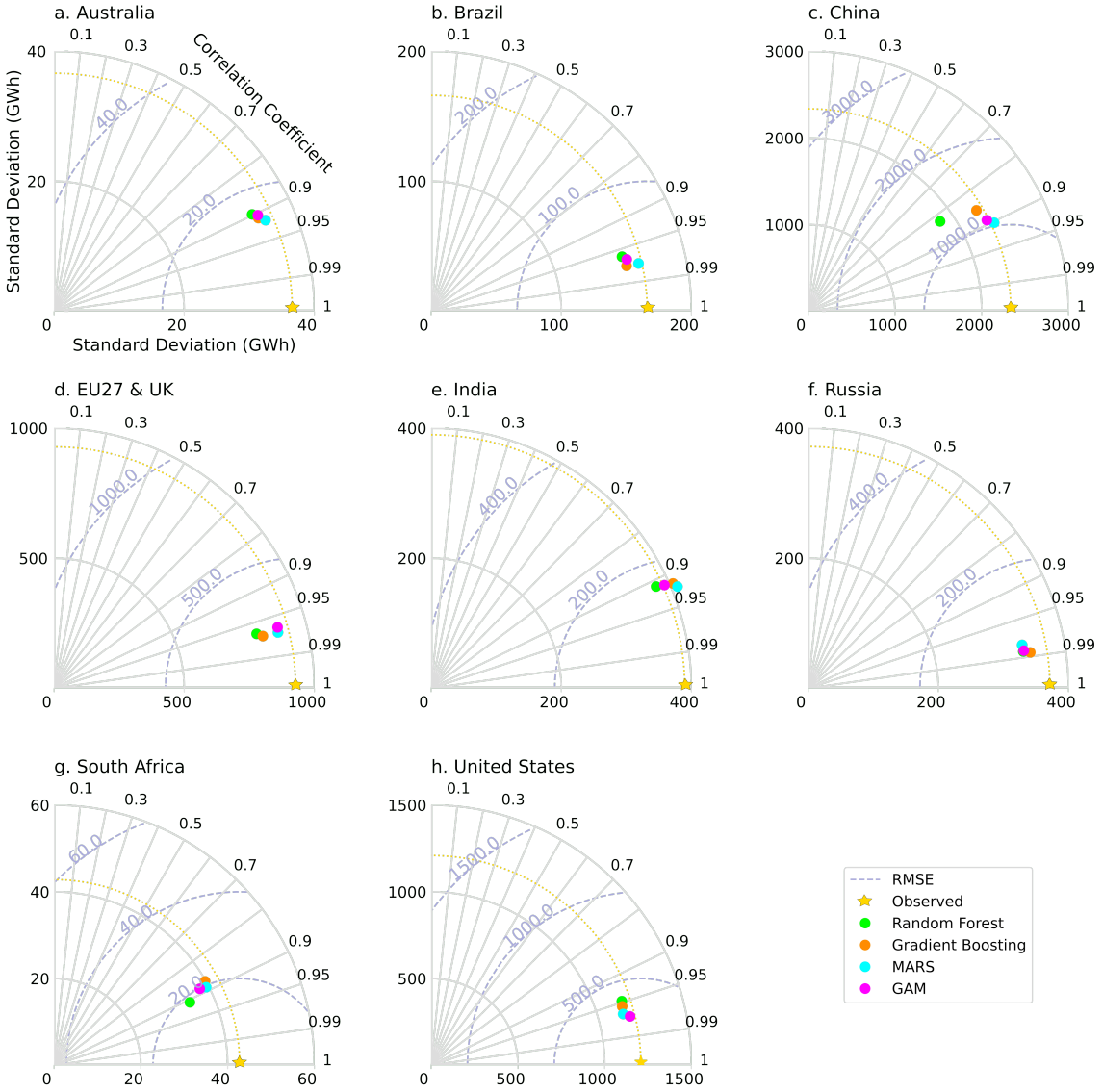

Figure IV.7: Taylor diagram for simulated power demand for the eight countries or regions. The colors indicate the different regressors tested: green, RF; orange, GB; blue, MARS; purple, GAM. The radial axis indicates the standard deviation, the angular axis the coefficient of correlation (R), and the dashed circles the RMSE.

To compare the performance of our models against the (test) observation and across the eight countries or regions, we constructed Taylor diagrams for each country (Fig. IV.7). These diagrams provide a comprehensive visualization of how well the models compare to the refer-

ence data for each country in terms of correlation, RMSE, and standard deviation (Taylor, 2001). The results from the Taylor diagrams confirm what was observed in the previous section with the evaluating metrics (Table IV.2). Specifically, the performance of each model is similar for a given country or region, while it differs across countries. The models exhibit the best correlation with observation for Russia (close to 0.99), closely followed by the United States, EU27 & UK, and Brazil, with a correlation higher or very close to 0.95. For Australia, China, India, and South Africa, the correlation is around 0.90. Except for India, the models underestimate the standard deviation of daily power demand.

One of the objectives of our study is to identify the most influential features on power demand for each country or region and to investigate whether any similarities exist across the different countries. A comparison of feature importance for each country and model (Fig. IV.8) is conducted to achieve this objective. Our results suggest that temperature-related features, including T2M, T2Mmax, T2Mmin, and Td, are always the primary climate drivers of power demand in all examined countries, indicating their significant influence on power demand across different regions. The other climate-related features included in this study do not appear to significantly drive power demand, except for SSRD, which slightly influences power demand for some countries in the RF, GB, and GAM models.

Regarding human activity predictors, we observed significant variations in their importance across different countries and machine-learning regressors. For instance, the DOW feature shows high importance in some countries while insignificant in others, similarly for workplaces activity from Google Mobility data. In general, the different models found the same features to be the most important, even though the value of the feature importance varies across models. Quarterly GDP is a crucial feature for predicting power demand in China. Without quarterly GDP, the evaluating metrics were poor, leading us to conclude that the models for China were unexploitable for generalization. These results highlight the importance of considering economic indicators reflecting the importance of the industrial sector's share in the total power demand, such as quarterly GDP, when developing models for power demand forecasting in China.

Overall, Fig. IV.8 provides insights into the key factors influencing power demand across various countries, highlighting again the crucial role of temperature-related features as a primary driver of power demand. The observed variations in the importance of human activity predictors across different countries and machine-learning regressors suggest the significance of accurately including region-specific characteristics and machine-learning approaches in predicting power demand.

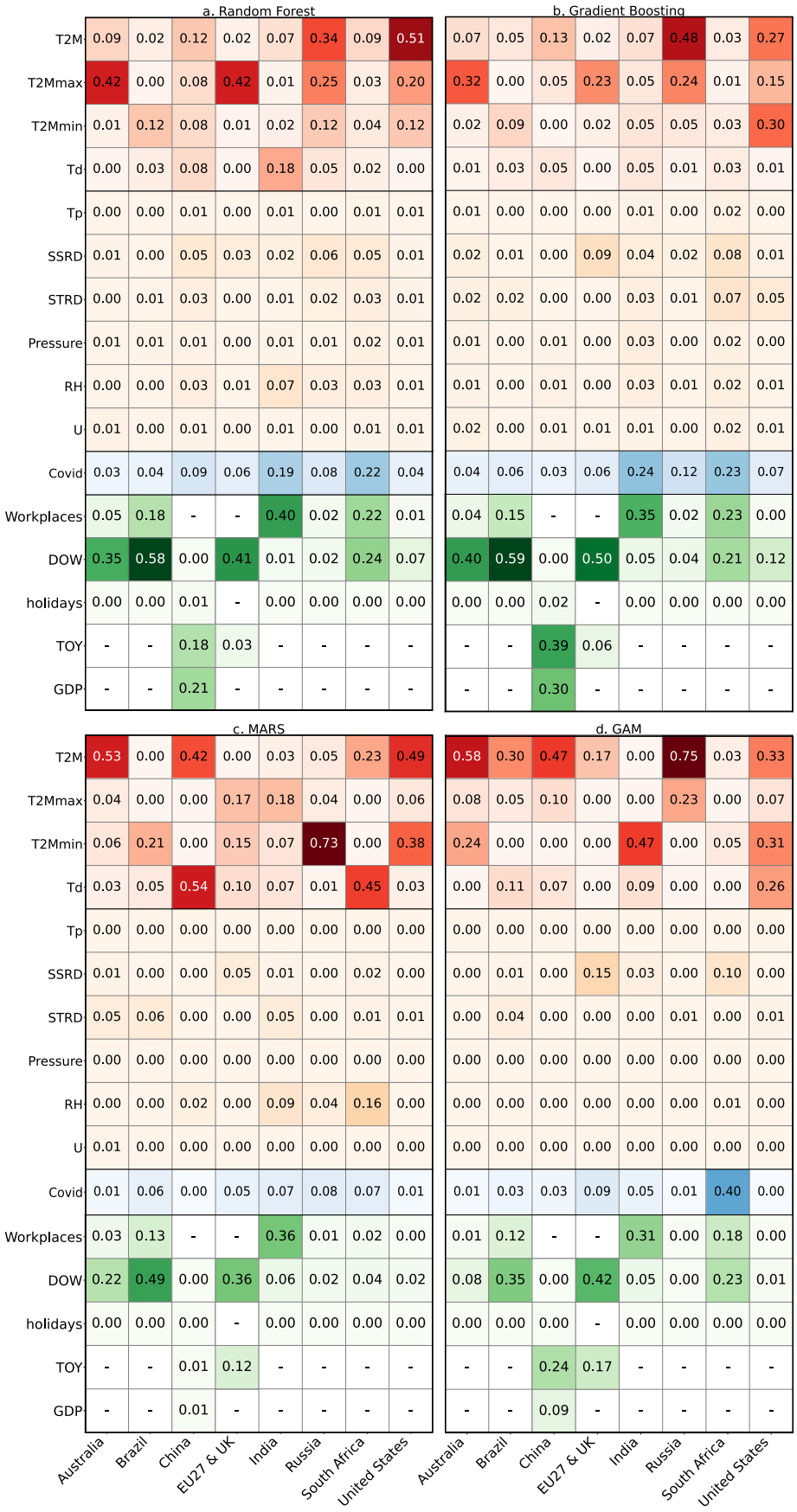

Figure IV.8: Permutation feature importance for four different machine-learning regressors: (a) RF, (b) GB, (c) MARS, and (d) GAM. The colors represent the different types of predictive features: red for temperature-related features, orange for other climate-related features, blue for covid, and green for socioeconomic features. The columns correspond to the countries indicated at the bottom of the figure.

7.2 Validation and Limits of the Models

The analysis of the residuals of the four models provides information on the performance of the models in predicting the statistical distribution of power demand. We analyzed the performance of the four models using residual quantiles compared to the theoretical Gaussian distribution (Figs. IV.9a and IV.9a). This examination is carried out at a global level encompassing all countries and regions (Fig. IV.9a) and at a country-specific level for each model (Fig. IV.10a). This analysis reveals that all models perform similarly, with slight deviations from the expected normal distribution within the intermediate quantiles range (between two and minus two) and higher deviations observed above this threshold. Therefore, the Gaussian hypothesis is confirmed, except for extreme values, for which the dataset contains relatively few observations. Those extreme values are often attributed to periods of unusual economic activity, such as bank holidays or specific public holidays that are difficult to model (Srinivasan et al., 1995; Ziel, 2018). Consequently, our models can underestimate or overestimate very low or high power demand, respectively.

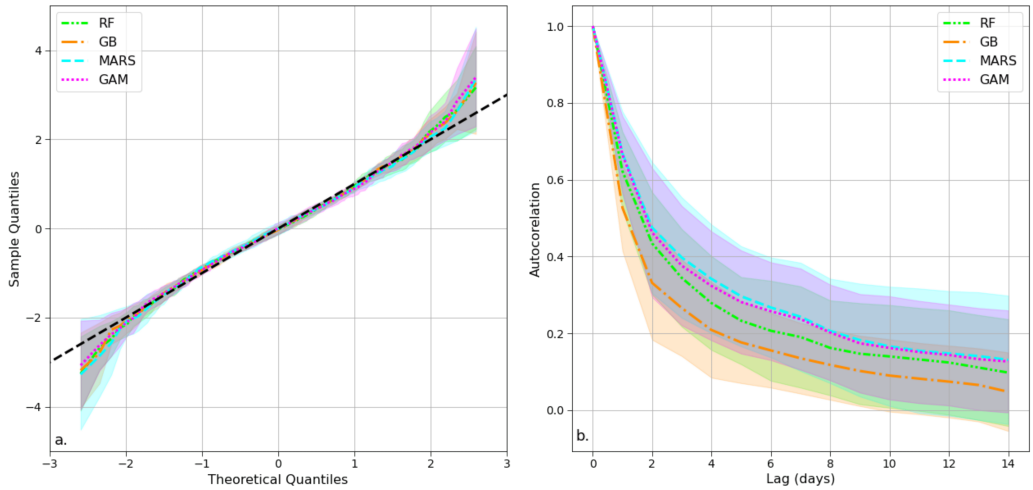

Figure IV.9: (a) Quantile-quantile (QQ) plot displaying the mean and standard deviation (shaded area) of the residuals' quantiles for the four models (RF, GB, MARS, and GAM) across eight European countries during the test period. (b) Autocorrelation plot illustrating the average autocorrelation values across the eight countries or regions studied for each of the four models with a 14-day maximum lag. The shaded area represents the standard deviation across countries.

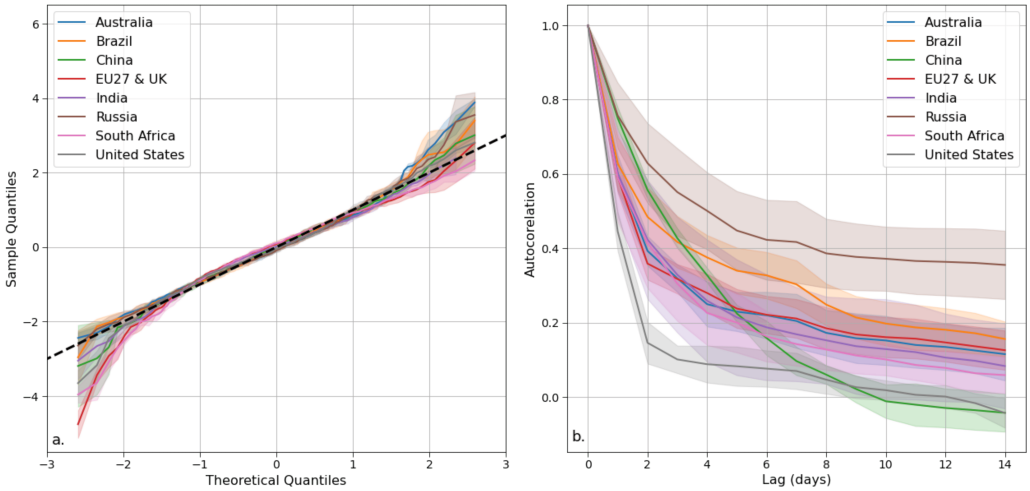

Figure IV.10: (a) Quantile-quantile (QQ) plot displaying the mean and standard deviation (shaded area) of the residuals' quantiles for all countries across the four models during the test period. (b) Autocorrelation plot illustrating the average autocorrelation values across the four models for all countries with a 14-day maximum lag. The shaded area represents the standard deviation across countries.

The autocorrelation plots of the residuals (Fig. IV.9b) reveal differences between the models and countries. In particular, gradient boosting outperforms the other models in this respect, with the lowest autocorrelation values. In contrast, MARS shows the highest values. RF and GAM are in between with very similar results. Some countries exhibit superior performances (Fig. IV.10b). For example, the residual autocorrelation values for Russia decrease with time at a slower pace than for other countries. Despite the differences in autocorrelation values between the models and across countries, it is worth noting that all models exhibit a similar trend. Specifically, the autocorrelations of the residuals are high up to a lag of a few days, as also reported elsewhere. The autocorrelations drop beyond a lag of a few days, indicating that our models did not miss any significant temporal information.

Overall, these findings are encouraging and validate our models. Therefore, the models can be used for the projection of power demand. However, caution should be exercised when considering extreme values. It is possible to improve the modeling of such values by using a class of quantile regression models. Various types of models have been developed that are specifically designed to address extreme quantiles. One such model is the quantile regression forest, which is a generalization of the random forest model (Meinshausen, 2006). Another example is the additive quantile regression model, which has demonstrated promising results in recent studies (Fasiolo et al., 2021). Such models can be applied in future studies to improve the accuracy of power demand projections.

Overall, while the models developed in this study offer valuable insights into predicting power demand, some limitations must be considered. Firstly, our study period included the COVID-19 pandemic, which significantly impacted energy consumption and emissions (Aruga et al., 2020; Garcia et al., 2021; Liu et al., 2022) . While we incorporate this variable in our models, the extent of its impact may not have been fully captured. Training the regressors on periods not affected by covid might give better results.

Additionally, the irregularity observed in the modeling process for China is worth noting, as China necessitates the inclusion of quarterly GDP to attain good results. Although our approach was largely consistent across countries, it did not achieve a perfect "one-fits-all" approach. Consequently, while this work established a modeling framework applicable to multiple countries, further revisions may be required when extending it to countries not encompassed in this study.

Finally, although all models yielded satisfactory outcomes, each model employed the predictive features in distinct ways (Figs. IV.4 and IV.9). Certain predictive features did not exhibit the expected behavior (as shown in Fig. IV.5b, where T2Mmin showed no sensitivity for lower temperatures). Furthermore, the role and impact of the TOY variable, which functions as a corrective factor for countries where Google Mobility data are not available, remain somewhat ambiguous. While it can account for annually recurring phenomena not elucidated by other predictive features, it would require a more extensive dataset spanning several years to refine its precise function.

Addressing these limitations through future research can lead to more accurate and robust models for predicting power demand and related CO_2 emissions.

8 Perspective

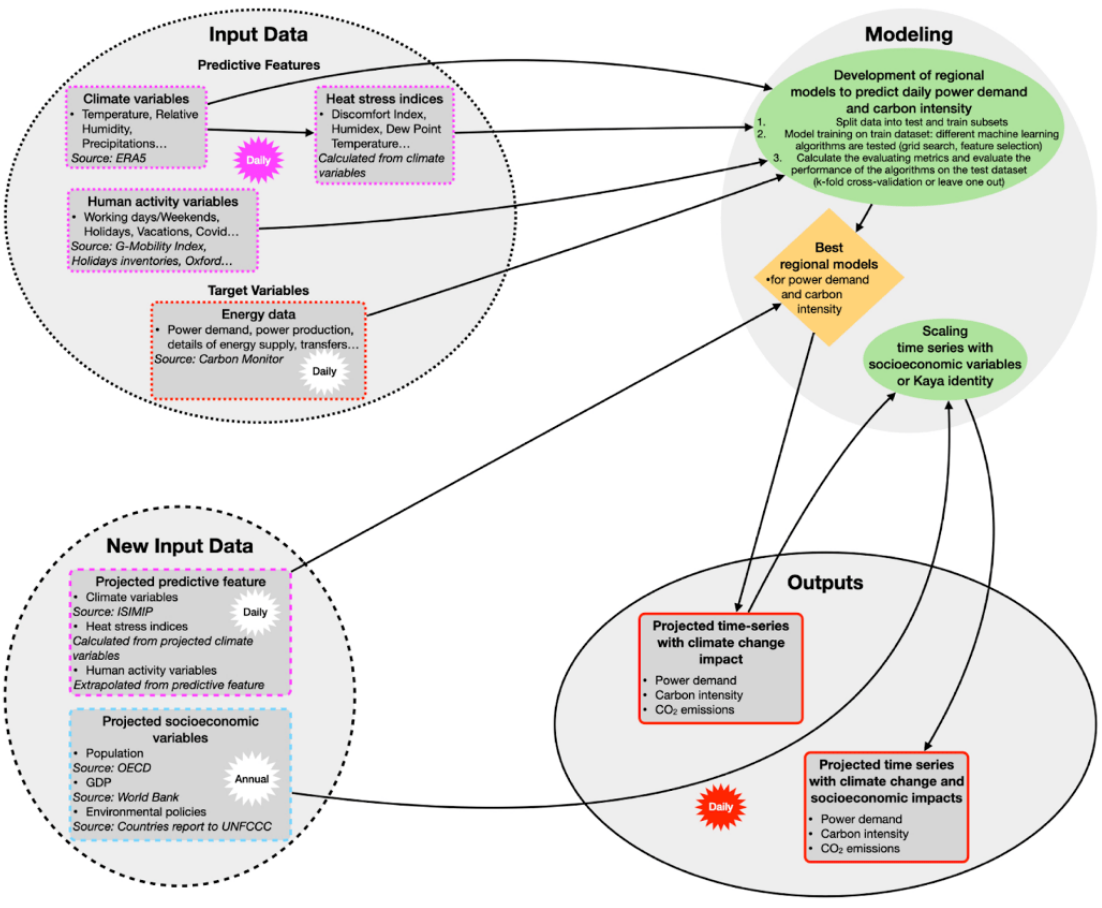

Figure IV.11: Extended methodological flowchart toward CO_2 emission projections.

The present study aims to establish a modeling approach to simulating national daily power demand from climate and human activity features. The proposed approach has the potential to be extended to predict long-term power demand trends under changing climatic conditions and to estimate the corresponding CO_2 emissions resulting from power generation (Fig. IV.11). This extension would involve developing separate models for simulating power demand and carbon intensity. To achieve this, the target variable would be set as the daily carbon intensity rather than power demand, resulting in the development of two parallel models: one for daily power demand and another for daily carbon intensity. CO_2 emissions are calculated by combining the projections from these two models.

To apply this approach, projected climate features obtained from the CMIP6 simulation round, along with projected human activity variables such as DOW (Day of the Week) and Holidays, would be necessary. It should be noted that certain predictive features, such as "workplaces" from the Google Mobility Data, may not be subject to projection. By employ-

ing the two abovementioned models, projections of power demand, carbon intensity, and CO_2 emissions can be obtained. Other socioeconomic factors, such as population growth, GDP, and environmental policies, can be incorporated to enhance the projection of daily power demand and CO_2 emissions (Fig. IV.11). By considering the influence of population growth and GDP, the projections of daily power demand can be scaled accordingly. Carbon intensity projections could be developed based on assumed environmental policies aligned with the SSPs (Shared Socioeconomic Pathways) narratives and used to scale the projection of daily carbon intensity obtained with the data-based models. A similar approach has already been applied to Qatar and Japan with different scenarios in alignment with the SSPs narratives (Gurriaran et al., 2023a; Gurriaran et al., 2023b).

The approach presented in this study has the potential to be extended to evaluate the effectiveness of different policies and initiatives aimed at reducing CO_2 emissions. By considering the influence of changing energy demand under future climate change scenarios, it becomes possible to evaluate the effectiveness of these measures in achieving emission reduction targets. Furthermore, coupling the models developed in this study with simple climate models such as ACC2 (Aggregated Carbon cycle, atmospheric chemistry, and climate model, (Tanaka et al., 2007; Tanaka et al., 2018) enables quantification of the feedback loop between human activity, CO_2 emissions, climate change, power demand changes, CO_2 emission changes, and the impact on climate (precisely, human activity $\rightarrow$ CO_2 emissions $\rightarrow$ climate change $\rightarrow$ human activity).

In conclusion, the models developed in this study provide a valuable tool for analyzing, forecasting and understanding power demand patterns and CO_2 emissions in the context of climate change across various regions worldwide. Applying these models could offer insights into the potential future scenarios and dynamics of power demand, enabling policymakers and stakeholders to make informed decisions and shape effective energy policies.

References

ACAPS. (2021). Covid-19 – government measures dataset [Last accessed on 5 January 2023].

Ahmad, A. (2021). Increase in frequency of nuclear power outages due to changing climates. *Nature Energy*, *6*, 755. https://doi.org/10.1038/s41560-021-00849-y

Antoniadis, A., Gaucher, S., & Goude, Y. (2022). Hierarchical transfer learning with applications for electricity load forecasting. *arXiv preprint arXiv:2111.08512*.

Antoniopoulos, I., Petropoulos, F., & Hatziargyriou, N. (2020). Artificial intelligence and machine learning approaches to energy demand-side response: A systematic review. *Renewable and Sustainable Energy Reviews*, *130*, 109899. https://doi.org/10.1016/j.rser.2020.109899

Apley, D., & Zhu, J. (2020). Visualizing the effects of predictor variables in black box supervised learning models. *Journal of the Royal Statistical Society: Series B (Statistical Methodology)*, *82*(4), 1059–1086. https://doi.org/10.1111/rssb.12377

Aruga, K., Monirul Islam, M., & Jannat, A. (2020). Effect of covid-19 on indian energy consumption. *Sustainability*, *12*(14), 5616. https://doi.org/10.3390/su12145616

Breiman, L. (2001). Random forests. *Machine Learning*, *45*, 5–32. https://doi.org/10.1023/A:1010933404324

Buitinck, L., Louppe, G., Blondel, M., Pedregosa, F., Mueller, A., Grisel, O., Niculae, V., Prettenhofer, P., Gramfort, A., Grobler, J., Layton, R., VanderPlas, J., Joly, A., Holt, B., & Varoquaux, G. (2013). API design for machine learning software: Experiences from the scikit-learn project. *ECML PKDD Workshop: Languages for Data Mining and Machine Learning*, 108–122.

Burillo, D., Chester, M. V., Pincetl, S., Fournier, E. D., & Reyna, J. (2018). Forecasting peak electricity demand for los angeles considering higher air temperatures due to climate change. *Applied Energy*, *236*, 1–9. https://doi.org/10.1016/j.apenergy.2018.11.039

Center for International Earth Science Information Network - Columbia University. (2018). Gridded population of the world, version 4 (gpwv4): Population density, revision 11 [Accessed on 30 May 2023].

Chambers, J. M. (1983). *Graphical methods for data analysis* (1st). Chapman; Hall/CRC. https://doi.org/10.1201/9781351072304

Chen, T., & Guestrin, C. (2016). Xgboost: A scalable tree boosting system. *Proceedings of the 22nd ACM SIGKDD International Conference on Knowledge Discovery and Data Mining*, 785–794. https://doi.org/10.1145/2939672.2939785

Deroubaix, A., Labuhn, I., Camredon, M., Stéfanon, M., & Fantozzi, F. (2021). Large uncertainties in trends of energy demand for heating and cooling under climate change. *Nature Communications*, *12*(1), 5197. https://doi.org/10.1038/s41467-021-25504-8

Fasiolo, M., Wood, S. N., Zaffran, M., Nedellec, R., & Goude, Y. (2021). Fast calibrated additive quantile regression. *Journal of the American Statistical Association*, *116*(535), 1402–1412. https://doi.org/10.1080/01621459.2020.1725521

Fisher, W. D. (1958). On grouping for maximum homogeneity. *Journal of the American Statistical Association*, *53*, 789–798.

Friedman, J. (1991). Multivariate adaptive regression splines. *Annals of Statistics*, *19*(1), 1–67. https://doi.org/10.1214/aos/1176347963

Garcia, S., Parejo, A., Personal, E., Ignacio Guerrero, J., Biscarri, F., & Leon, C. (2021). A retrospective analysis of the impact of the covid-19 restrictions on energy consumption at a disaggregated level. *Applied Energy*, *287*, 116547. https://doi.org/10.1016/j.apenergy.2021.116547

Google. (2020). Google mobility reports, data file.

Gurriaran, L., Tanaka, K., Bayram, I., Proestos, Y., Lelieveld, J., & Ciais, P. (2023a). Warming-induced increase in power demand and co2 emissions in qatar and the middle east. *Journal of Cleaner Production*, *382*, 135359. https://doi.org/10.1016/j.jclepro.2022.135359

Gurriaran, L., Tanaka, K., Takahashi, K., & Ciais, P. (2023b). How climate change may shift power demand in japan: Insights from data-driven analysis. *Journal of Environmental Management*, *345*, 118799. https://doi.org/10.1016/j.jenvman.2023.118799

Hale, T., Angrist, N., Goldszmidt, R., & Kira, B. e. a. (2021). A global panel database of pandemic policies (oxford covid-19 government response tracker). *Nature Human Behaviour*, *5*, 529–538. https://doi.org/10.1038/s41562-021-01079-8

Hastie, T. J., & Tibshirani, R. J. (1990). *Generalized additive models* (Second). Chapman; Hall.

Hiruta, Y., Gao, L., & Ashina, S. (2022a). A novel method for acquiring rigorous temperature response functions for electricity demand at a regional scale. *Science of the Total Environment*, *819*, 152893. https://doi.org/10.1016/j.scitotenv.2021.152893

Hiruta, Y., Ishizaki, N. N., Ashina, S., & Takahashi, K. (2022b). Regional and temporal variations in the impacts of future climate change on japanese electricity demand: Simultaneous interactions among multiple factors considered. *Energy Conversion and Management: X*, *14*, 100172. https://doi.org/10.1016/j.ecmx.2021.100172

Hyndman, R. J., & Athanasopoulos, G. (2018). *Forecasting: Principles and practice* (2nd). OTexts. https://otexts.com/fpp2/

IEA. (2022). Monthly electricity statistics.

Isaac, M., & van Vuuren, D. P. (2009). Modeling global residential sector energy demand for heating and air conditioning in the context of climate change. *Energy Policy*, *37*(2), 507–521. https://doi.org/10.1016/j.enpol.2008.09.051

Jiang, P., Khishgee, S., Alimujiang, A., & Dong, H. (2020). Cost-effective approaches for reducing carbon and air pollution emissions in the power industry in china. *Journal of Environmental Management*, *264*, 110452. https://doi.org/10.1016/j.jenvman.2020.110452

Ke, G., Meng, Q., Finley, T., Wang, T., Chen, W., Ma, W., Ye, Q., & Liu, T.-Y. (2017). Lightgbm: A highly efficient gradient boosting decision tree. *Advances in Neural Information Processing Systems 30*.

Liao, C. (2021). Pyearth: A python implementation of multivariate adaptive regression splines. https://doi.org/10.5281/zenodo.6368652

Liu, Z., Ciais, P., Deng, Z., Lei, R., Davis, S. J., Feng, S., Zheng, B., Cui, D., Dou, X., Zhu, B., Guo, R., Ke, P., Sun, T., Lu, C., He, P., Wang, Y., Yue, X., Wang, Y., Lei, Y., … Schellnhuber, H. J. (2022). Near-real-time monitoring of global co2 emissions reveals the effects of the covid-19 pandemic. *Nature Communications*, *11*(1), 5172. https://doi.org/10.1038/s41467-020-18922-7

Liu, Z., Ciais, P., Deng, Z., Lei, R., Davis, S. J., Zheng, B., Wang, Y., Cui, D., Zhu, B., Dou, X., Ke, P., Sun, T., Guo, R., Zhong, H., Boucher, O., Bréon, F.-M., Lu, C., Guo, R., Xue, J., … Chevallier, F. (2020). Carbon monitor, a near-real-time daily dataset of global co2 emission from fossil fuel and cement production. *Scientific data*, *7*(1), 392. https://doi.org/10.1038/s41597-020-00708-7

Lucon, O., Ürge-Vorsatz, D., Zain Ahmed, A., Akbari, H., Bertoldi, P., Cabeza, L. F., ..., & Vandeveer, S. D. (2014). Buildings. In *Climate change 2014: Mitigation of climate change. contribution of working*

group iii to the fifth assessment report of the intergovernmental panel on climate change (pp. 1–68). Cambridge University Press.

Mathieu, E., Ritchie, H., Rodés-Guirao, L., Appel, C., Giattino, C., Hasell, J., Macdonald, B., Dattani, S., Beltekian, D., Ortiz-Ospina, E., & Roser, M. (2020). Coronavirus pandemic (covid-19). https://ourworldindata.org/coronavirus

Meinshausen, N. (2006). Quantile regression forests. *Journal of Machine Learning Research*, *7*, 983–999.

Mohammadiziazi, R., & Bilec, M. (2020). Application of machine learning for predicting building energy use at different temporal and spatial resolution under climate change in the usa. *Buildings*, *10*(8), 139. https://doi.org/10.3390/buildings10080139

Mukherjee, S., Vineeth, C. R., & Nateghi, R. (2019). Evaluating regional climate-electricity demand nexus: A composite bayesian predictive framework. *Applied Energy*, *235*, 1561–1582. https://doi.org/10.1016/j.apenergy.2018.11.064

Muñoz Sabater, J. (2019). Era5-land hourly data from 1981 to present. copernicus climate change service (c3s) climate data store (cds) [Accessed on February 2023]. https://doi.org/10.24381/cds.e2161bac

Pedregosa, F., Varoquaux, G., Gramfort, A., Michel, V., Thirion, B., Grisel, O., Blondel, M., Prettenhofer, P., Weiss, R., Dubourg, V., Vanderplas, J., Passos, A., Cournapeau, D., Brucher, M., Perrot, M., & Duchesnay, E. (2011). Scikit-learn: Machine learning in Python. *Journal of Machine Learning Research*, *12*, 2825–2830.

Raschka, S., & Mirjalili, V. (2019). *Python machine learning, third edition*. Packt Publishing.

Raschka, S. (2020). Model evaluation, model selection, and algorithm selection in machine learning. *arXiv preprint arXiv:1811.12808*. https://arxiv.org/abs/1811.12808

Romitti, Y., & Sue Wing, I. (2022). Heterogeneous climate change impacts on electricity demand in world cities circa mid-century. *Scientific Reports*, *12*, 4280. https://doi.org/10.1038/s41598-022-07922-w

Servén, D., & Brummitt, C. (2018). Pygam: Generalized additive models in python. https://doi.org/10.5281/zenodo.1208723

Srinivasan, D., Chang, C. S., & Liew, A. C. (1995). Demand forecasting using fuzzy neural computation, with special emphasis on weekend and public holiday forecasting. *IEEE Transactions on Power Systems*, *10*(4), 1897–1903. https://doi.org/10.1109/59.476055

Tanaka, K., Kriegler, E., Bruckner, T., Hooss, G., Knorr, W., & Raddatz, T. (2007). Aggregated carbon cycle, atmospheric chemistry, and climate model (acc2) – description of the forward and inverse modes. *Reports on Earth System Science*, *40*, Max Planck Institute for Meteorology, Hamburg.

Tanaka, K., & O'Neill, B. (2018). The paris agreement zero-emissions goal is not always consistent with the 1.5 and 2°c temperature targets. *Nature Climate Change*, *8*, 319–324. https://doi.org/10.1038/s41558-018-0097-x

Taylor, K. E. (2001). Summarizing multiple aspects of model performance in a single diagram. *Journal of Geophysical Research*, *106*(D7), 7183–7192. https://doi.org/10.1029/2000JD900719

Van Ruijven, B., De Cian, E., & Wing, I. (2019). Amplification of future energy demand growth due to climate change. *Nature Communications*, *10*, 2762. https://doi.org/10.1038/s41467-019-10399-3

Wood, S. N. (2017). *Generalized additive models: An introduction with r, second edition*. Chapman; Hall/CRC. https://doi.org/10.1201/9781315370279

Yalew, S., van Vliet, M., Gernaat, D., Ludwig, F., Miara, A., Park, C., Byers, E., De Cian, E., Piontek, F., Iyer, G., Mouratiadou, I., Glynn, J., Hejazi, M., Dessens, O., Rochedo, P., Pietzcker, R., Schaeffer,

R., Fujimori, S., Dasgupta, S., & Vuuren, D. (2020). Impacts of climate change on energy systems in global and regional scenarios. *Nature Energy*, *5*. https://doi.org/10.1038/s41560-020-0664-z

Zhu, B., Song, X., Deng, Z., Zhao, W., Huo, D., Sun, T., Ke, P., Cui, D., Lu, C., Zhong, H., Hong, C., Qiu, J., Davis, S. J., Gentine, P., Ciais, P., & Liu, Z. (2023). Carbon monitor-power: Near-real-time monitoring of global power generation on hourly to daily scales. *Scientific Data*, *10*, 217. https://doi.org/10.1038/s41597-023-02094-2

Ziel, F. (2018). Modeling public holidays in load forecasting: A german case study. *Journal of Modern Power Systems and Clean Energy*, *6*(2), 191–207. https://doi.org/10.1007/s40565-018-0385-5

CHAPTER V

FROM GLOBAL POWER DEMAND SIMULATIONS TO CO_2 EMISSIONS

The development of the CMP-SIMv1.0 models was followed by the intention to use these models to project global electricity demand to the end of the century under different global warming scenarios. In order to be able to forecast electricity demand, it is necessary to have daily projections of all predictive features over the period under consideration for all countries. The ISIMIP project (section 6.3.2, chapter I) makes this relatively straightforward for climate features by providing daily climate feature projections that are already bias-adjusted and statistically downscaled for the entire globe. However, projections for socioeconomic features previously used in the CMP-SIMv1.0 models are not always available. Therefore, these models need to be adapted to forecast future electricity demand using only predictive features that can be projected.

In addition, the Carbon Monitor Power (CMP) database is not exhaustive as it contains data for only about thirty countries. Therefore, a method needs to be found to model demand for countries not represented in the database and for which specific models cannot be developed. The approach proposed here is based on a classification of countries using a clustering algorithm (k-means clustering), which groups countries based on their climatic and socioeconomic similarities. Each country without data is assigned to a country with data and, thus, to a model. This model becomes the reference model for the country without data, and demand for that country is then projected using this reference model.

Once demand has been projected, it is possible to calculate the CO_2 emissions associated with the electricity generation required to meet that demand. This requires carbon intensity

projections, which are calculated by country or region using data from the Integrated Assessment Model IMAGE3.2. The demand projections are then multiplied by the carbon intensity projections to obtain the CO_2 emission projections.

This section describes these different steps in detail, starting with the adaptation of the CMP-SIMv1.0 models, then the classification of countries, the global electricity demand projection, and the estimation of global CO_2 emissions.

1 National Power Demand Simulations: an Adaptation of CMP-SIMv1.0 Models

The CMP-SIMv1.0 models encompassed ten climate features: T2M, T2Mmax, T2Mmin, Td, RH, Surface Pressure, U, TP, SSRD, and STRD. However, we found that not all of these features significantly affected power demand. We thus retain only six climate features for the power demand projections: the three temperature-related features (T2M, T2Mmax, T2Mmin), RH, and the radiation-related features (SSRD and STRD). Similarly, the socioeconomic features considered in CMP-SIMv1.0 needed reevaluation to keep only those that can be projected in the future. Initially, six features were included: Covid, Workplaces, DOW (Day Of Week), holidays, TOY (Time Of Year), and quarterly GDP (used exclusively for China). Two of these features were eliminated: Workplace and quarterly GDP. This decision was motivated by the small number of years of data available for workplaces (only from February 2020 to October 2022) and the lack of a simple approach to projecting this variable into the future. The TOY feature was used for all countries to address the removal of the workplace feature that ensured a representation of annual cycles in human activities in the machine learning (ML) models. The TOY feature can also account for the impact of specific periods, such as significant vacation periods, on power demand. Without the workplace feature, the Machine Learning (ML) models can be trained for four full years (2019 to 2023) instead of just two and a half years. With this more extended dataset, the annual human activity cycles aimed to be captured with the TOY feature should be better represented than with only two and a half years. Similarly, we hope to compensate for the elimination of the quarterly GDP variable in China by this increase in training data.

Adjusting the predictive features described above were the only modifications introduced during the learning phase. The subsequent steps of model training closely followed the procedures described in the previous Chapter. This training process was applied to a selected set of countries, including those presented in Chapter IV (Australia, Brazil, China, EU27 & UK, India,

Russia, South Africa, and the United States) and countries with available data from the Carbon Monitor Power database (Chile, Japan, Mexico, and Norway). For Japan, we used this new projection process to take advantage of the newly available four full years of data, a significant improvement over the previous analysis (Chapter III).

2 Projections of Power Demand at the National Scale

2.1 Climate and Socioeconomic Features Projections

	Learning (ERA5)	Projection (ISIMIP)
Average Daily Temperature	T2M (K)	TAS (K)
Average Maximum Temperature	T2Mmax (K)	TASmax (K)
Average Minimum Temperature	T2Mmin (K)	TASmin (K)
Solar Radiation Downward	SSRD ($J.m^{-2}$)	RSDS ($W.m^{-2}$)
Thermal Radiation Downward	STRD ($J.m^{-2}$)	RLDS ($W.m^{-2}$)
Relative Humidity	RH (%)	HURS (%)

Table V.1: Climate features used for the learning and training phase for the global projection

As for the first study on Japan (Chapter III), the ISIMIP climate projections (detailed in Section 6.3.2, Chapter I) were used here to represent the daily climate features. These climate projections from the ISIMIP3b protocol are bias-adjusted and statistically downscaled (Lange, 2021) using observational data from WFDE5v2 over emerged land and ERA5 data over the ocean (Cucchi et al., 2020; Lange et al., 2021). The bias adjustment method is described in Lange, 2019. It is designed to reduce biases across all percentiles of the data distribution while preserving the trends within these percentiles. This method, known as parametric quantile mapping, provides a common framework for all variables that can be customized to suit specific needs. The statistical downscaling approach, also detailed in Lange, 2021, is based on the multivariate quantile mapping bias adjustment method developed by Cannon, 2018. In this context, the downscaling problem can be assimilated to a bias adjustment problem: after broadcasting the climate data onto a finer grid, the statistical downscaling process involves adjusting the multivariate distribution of all time series within a coarser grid cell. In the approach proposed by Lange, 2019, an additional step is introduced to preserve the values at the aggregated spatial resolution.

Equivalents of the ERA5 climate features T2M, T2Mmax, T2Mmin, SSRD, STRD, and RH were downloaded from the ISMIP3b climate input database for the projection period on a daily timescale and a spatial resolution of 0.5° (table V.1). All these features have been spatially aver-

aged within the countries' geographical perimeters. The temperature features were converted from Kelvin to Celsius degrees for both the learning and training phases. RSDS and RLDS were converted from $W.m^{-2}$ to $J.m^{-2}$ for the projection phase to match the units of the ERA5 features used for the learning phase.

	Description	Source
DOW	Numerical variable (from 0 to 6)	function .weekday() in the datetime module python 3.9
Holiday	Numerical variable (0 or 1)	module holiday (python 3.9) or webscrapping
TOY	Numerical variable (from 0 to 366)	implemented in python 3.9
Covid	Numerical variable	set to 0 for the projection period

Table V.2: Description of socioeconomic features and their sources.

The socioeconomic features used in this part of the thesis have already been presented in detail in Chapter IV. They are numerical features and their daily projection were generated with Python methods (table V.2).

Thanks to the ISIMIP database and the Python methods used, the climate and socioeconomic features necessary to run the ML models are all available at a daily timescale for every country in the world. However, we miss the target feature, *i.e.* the daily power demand data, for a number of countries. To mitigate the lack of power demand data, each country without such data was paired with a reference country with available power demand data. This approach allows models developed for countries with available data to serve as reference models for countries without data.

2.2 How to Attribute Each Country to a Reference Country?

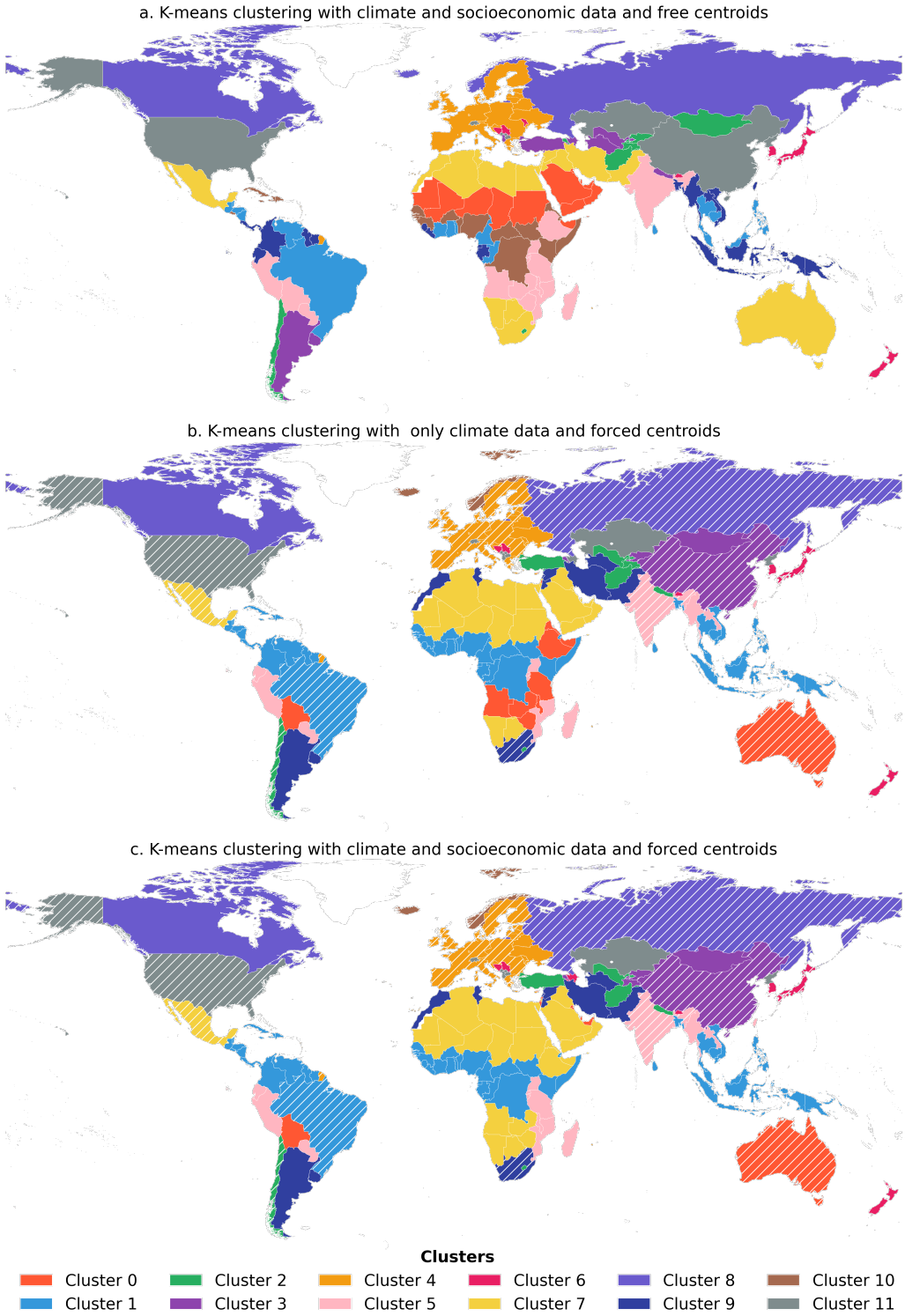

Figure V.1: The different groups of country. The hatched countries are the reference countries against which the models were calibrated.

A set of 12 reference countries is available, and the goal is to assign each of the remaining 131 countries without CMP data to one of these reference countries. The k-means clustering

method was used to achieve this. The k-means method is a widely used clustering technique in data analysis and machine learning. It is based on the principle of dividing a data set into coherent groups, called clusters, while minimizing the distance between data points and the centroids of these clusters.

The main steps of this method, as applied in our study, are outlined below:

- Data Normalization: All climatic data used in the demand simulation models, as well as specific socioeconomic indicators related to the country's electricity sector, are used to define the centroids and data points. These indicators include the percentage of the population with access to electricity, the percentage of people engaged in industrial activities (reflecting a country's level of industrialization), average annual electricity consumption per capita, and GDP per capita. These socioeconomic indicators, taken from the World Development Indicators, a World Bank database (WorldBank, 2023), for 2014 (the most recent year with comprehensive global data), are normalized to ensure comparisons.
- Centroids Initialization: The process begins by specifying the number of clusters, which in this case is set to 12. The initial centroids are constrained to correspond to the 12 reference countries.
- Assignment of Points to Clusters: Each country is assigned to the cluster whose centroid is closest in terms of distance. This step creates preliminary clusters.
- Centroid Updates: After assigning countries to clusters, new centroid positions are calculated by averaging the points associated with each cluster.
- Point Reassignment: Countries are reassigned to clusters based on the updated centroids. This iterative process continues until the centroids converge to stable positions and countries no longer show significant cluster changes.
- Convergence and Results: The algorithm reaches convergence when the centroids stop moving or when changes become negligible. At this point, each point is conclusively assigned to a cluster.

The other two maps demonstrate the validity of the approach and the importance of using both climatic and socioeconomic variables. Map V.1a shows that using the socioeconomic and climatic variables without forcing the centroids converges to similar clusters as the final map, proving that forcing the centroids does not compromise the reliability of the clusters obtained. Map V.1b shows the clusters obtained by forcing the centroids but using only the climatic variables. The difference with the first and the final map shows the importance of adding socioe-

conomic variables for clustering. This avoids reference countries with a much higher level of development being assigned to a country with no data and vice versa. This is well illustrated in Southern Africa, where countries that were assigned to Australia (in red) using the 'climate-only' approach are finally reassigned to Mexico (in yellow) or India (in pink) using the full approach.

2.3 Evolution of Power Demand with Global Projections and Representing Countries

After processing the ISIMIP climate data to ensure the availability of daily data for each country throughout the projection period, and after calculating the projections of socioeconomic variables and using the k-means method to classify countries, daily power demand projections can be calculated for all countries. Projections are calculated for three scenarios (SSP1-2.6, SSP3-7.0, and SSP5-8.5) and five Earth System Models (ESMs) using the four previously trained ML models. This results in a total of 20 projections per scenario for each country. In cases where a reference model is used for a particular country, the demand is scaled using a ratio (r) determined as follows:

$$r = \frac{Dcap_{country} \times pop_{country}}{Dcap_{country_{ref}} \times pop_{country_{ref}}} \tag{V.1}$$

Where $Dcap$ is the per capita demand and pop is the total population of the country.

Electricity demand trends through the end of the century are shown on the maps in Figure V.2a, which show the average annual change in electricity demand between the 2020-2030 decade and the 2090-2100 decade for all 20 projections. Based on the average of the 20 projections, three distinct patterns of electricity demand behavior emerge from the maps presented. First, certain countries, mainly in the tropics, are projected to experience significant increases in electricity demand (shown in purple). This increase is attributed to increased cooling demand due to climate change. Conversely, another group of countries, mostly at high latitudes in the Northern Hemisphere, is projected to experience a decrease in electricity demand (shown in beige). These are primarily Russia and Canada. These countries currently have limited cooling needs due to their relatively cool climates and could experience a decrease in heating demand, explaining the overall decrease in annual electricity demand. Finally, some countries, highlighted in gray, are projected to maintain relatively stable electricity demand levels. These behaviors are evident for SSP3-7.0 and even more pronounced for SSP5-8.5, but the changes are expected to be small for SSP1-2.6. Overall, these results highlight the significant influence

of climate change on electricity demand trends, with tropical regions experiencing increased cooling demand and cold climate countries potentially experiencing reduced heating demand.

Standard deviations were calculated using three different approaches to quantify the uncertainty associated with these projections. The first approach, shown in Figure V.2b, calculates the standard deviation across all 20 projections, providing an overall measure of uncertainty by accounting for variations across all ESMs and ML models. The second approach, shown in Figure V.2c, calculates the standard deviation over the five ESMs while averaging over the four ML models, providing insight into the uncertainty due to the different climate models. Finally, the third approach, shown in Figure V.2d, calculates the standard deviation over the four ML models while averaging over the five ESMs, providing a perspective on the variability introduced by the different ML models. Together, these approaches contribute to a comprehensive understanding of the uncertainty inherent in the average power demand projections shown in Figure V.2a.

Countries with the largest increases in electricity demand, such as Brazil and the countries of Central Africa and Southeast Asia, also tend to have the highest uncertainties. Uncertainties in these countries are significantly higher than in other regions for both ESM and ML model uncertainties. However, the uncertainties are more pronounced when considering ML models, showing that the total uncertainty shown in Figure V.2b is mainly due to the ML models for these countries.

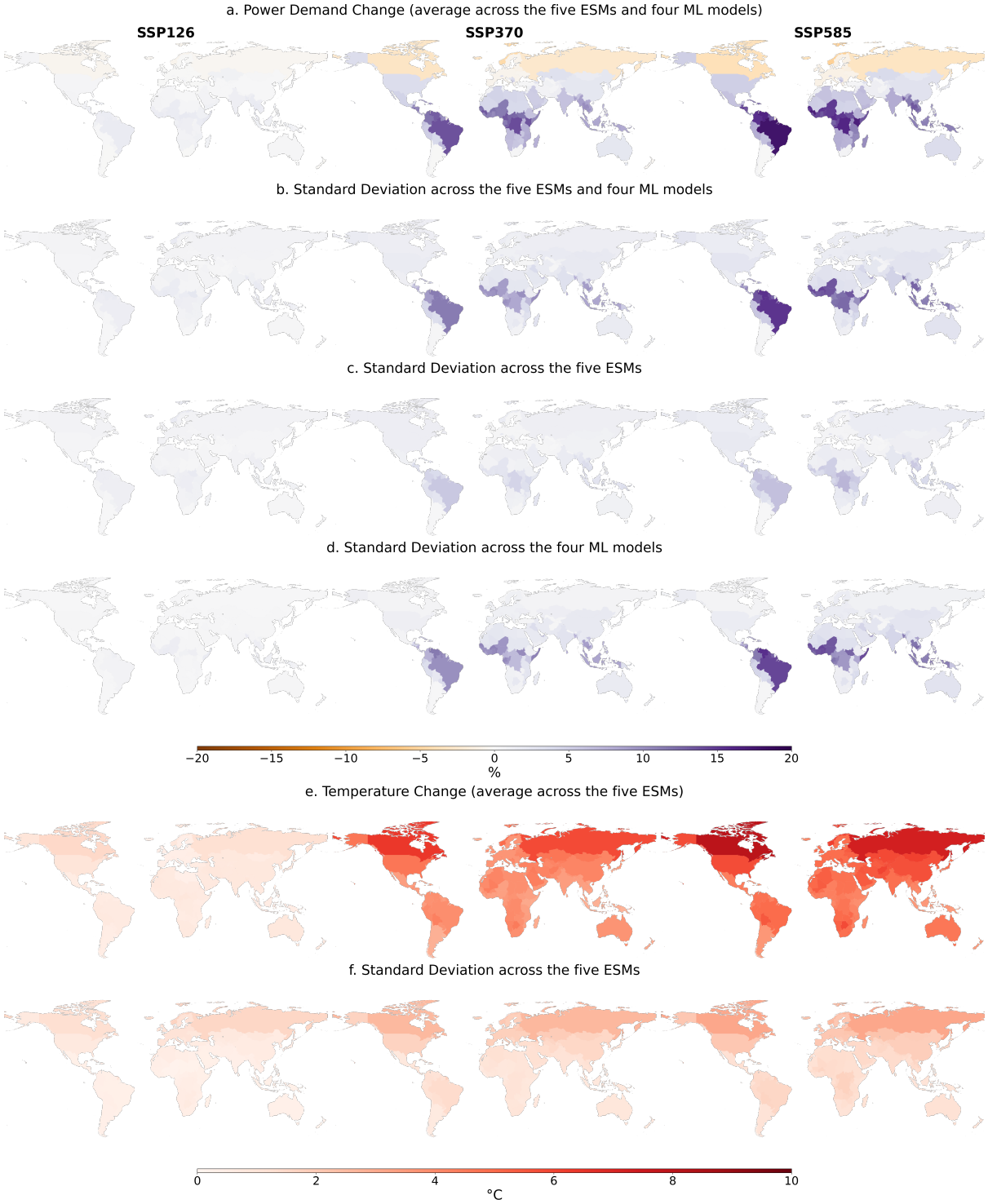

Figure V.2: Annual difference of power demand between the decade 2020-2030 and the decade 2090-2100 in percentage (mean of the 10 years) for SSP1-2.6, SSP3-7.0, and SSP5-8.5, average across the five ESM and the four ML models (a), standard deviation across the five ESMs and the four ML models (b), standard deviation from the five ESM (c), and standard deviation from the ML models (d). Temperature change between these two decades for the three scenarios averaged across the ESMs (e) and standard deviation (f).

A closer look at the behavior of the different projections in the ESM and ML models highlights the contrasting patterns among the projections. The possibility of divergent projections is well illustrated by the case of Europe (Fig. V.3).Specifically, for the SSP5-8.5 scenarios, the GAM model predicts an increase in electricity demand for the two ESMs, UKESM and IPSL. In contrast, the other ML models show an opposite trend, and this increase is not observed for the remaining ESMs. Furthermore, the figure shows that a larger temperature increase projected by the ESMs corresponds to a larger divergence between the projections. This observation is consistent with the earlier finding that countries with significant temperature increases have greater uncertainty about the evolution of electricity demand. In the following figures, which show the cases of the United States (Fig. V.4) and Russia (Fig V.5), while there is variation in the total projected demand, a consistent directional effect is evident. Specifically, all projections indicate an increase in demand for the United States and a decrease for Russia, allowing the direction of the impact to be determined in these regions. Nevertheless, the collective knowledge gained from examining these different projections allows us to identify key trends and potential patterns in the response of electricity demand to changing climate conditions.

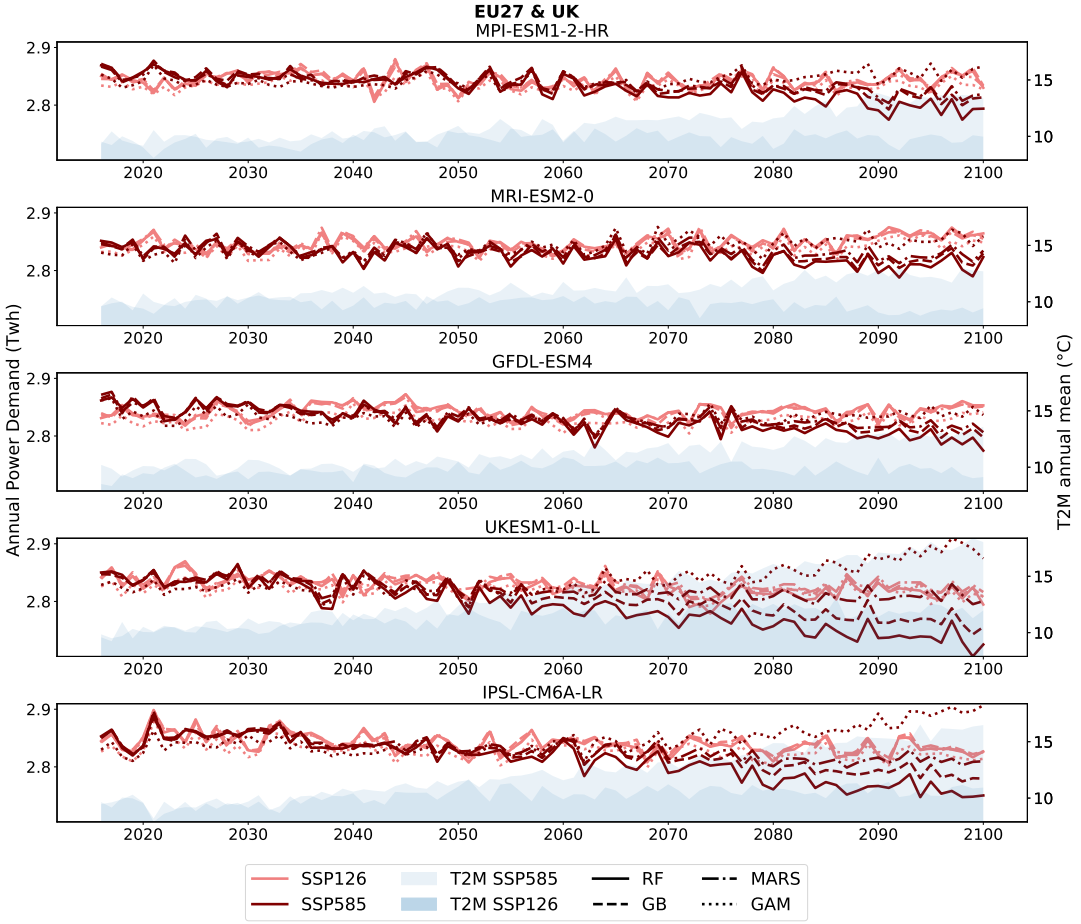

Figure V.3: Power demand projections for the United States under two scenarios, SSP1-2.6 and SSP5-8.5. The projections are generated using the four ML models, with the averages calculated across the ESMs.

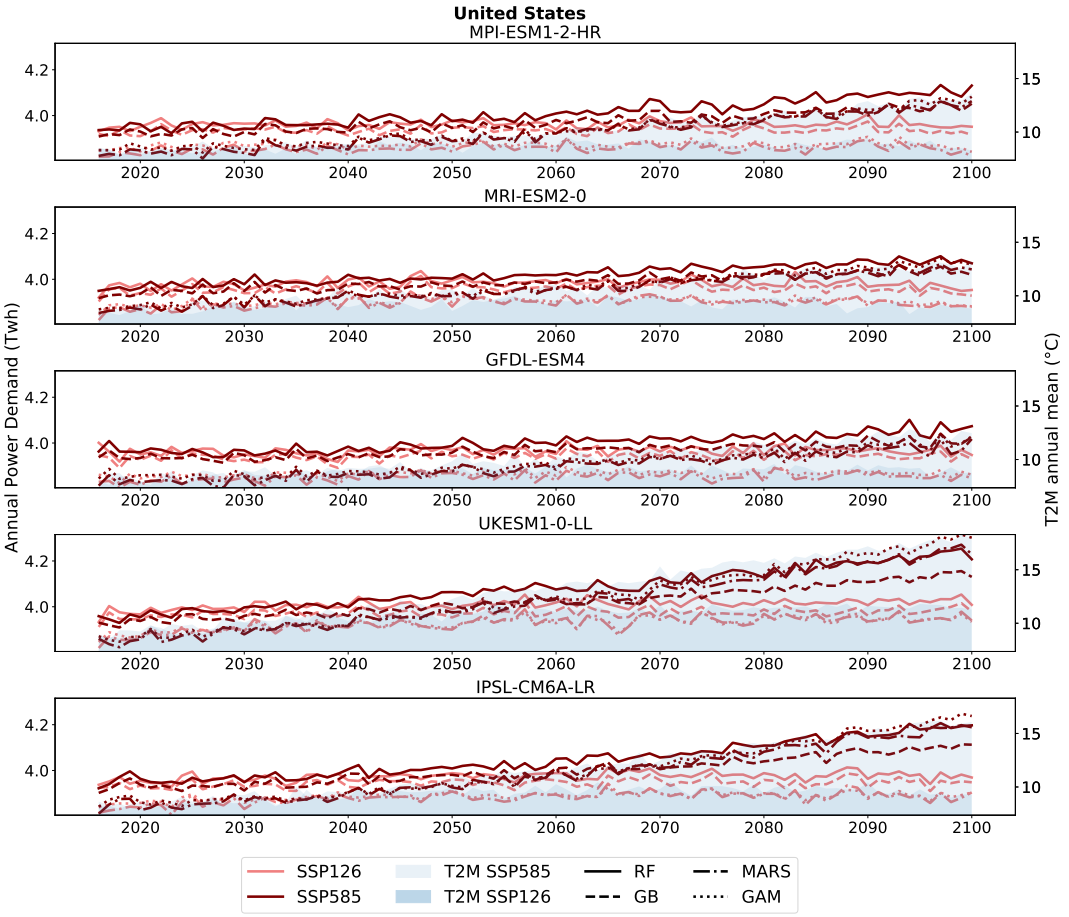

Figure V.4: Power demand projections for the EU and UK under two scenarios, SSP1-2.6 and SSP5-8.5. The projections are generated using the four ML models, with the averages calculated across the ESMs.

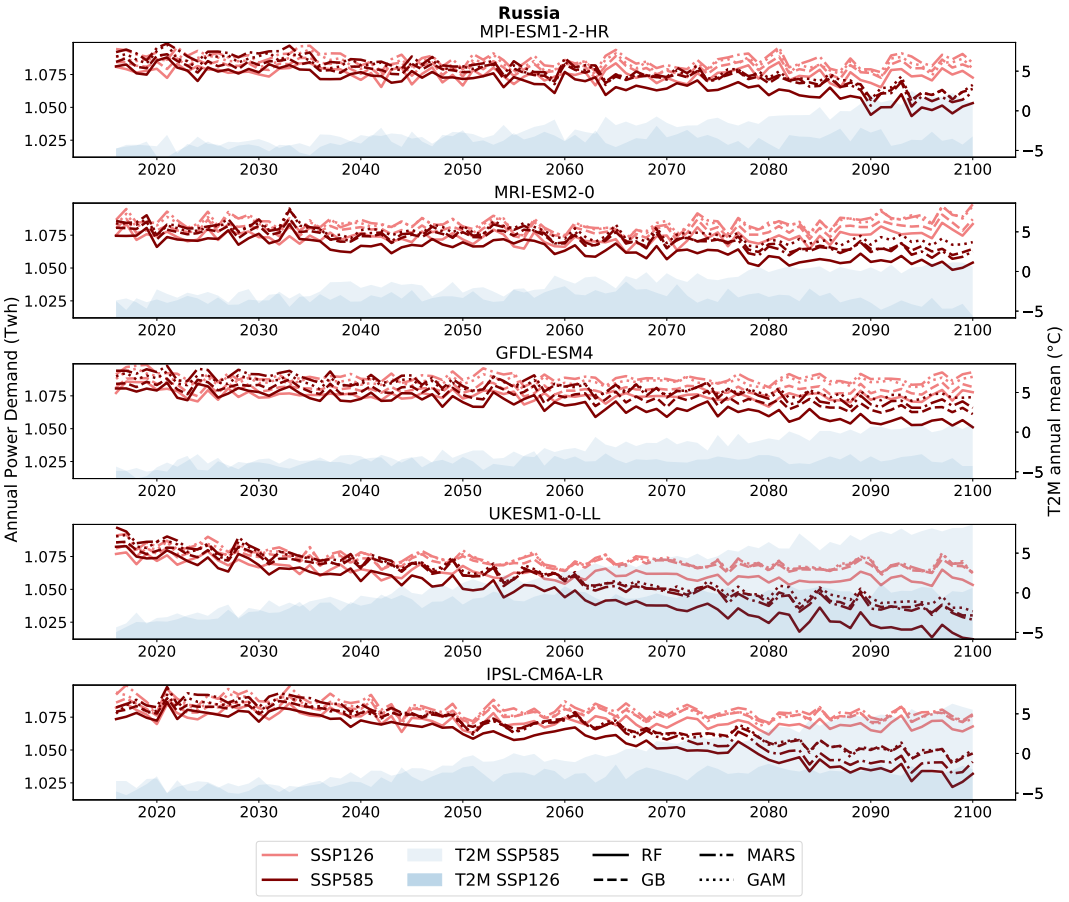

Figure V.5: Power demand projections for Russia under two scenarios, SSP1-2.6 and SSP5-8.5. The projections are generated using the four ML models, with the averages calculated across the ESMs.

2.4 Seasonal Evolution of Power Demand

Another interesting result is the seasonal dynamics of power demand changes. Although annual electricity demand may appear relatively stable, especially in regions like Europe, it is crucial to consider significant shifts that occur on a seasonal timescale. These shifts reflect variations in heating and cooling demand throughout the year.

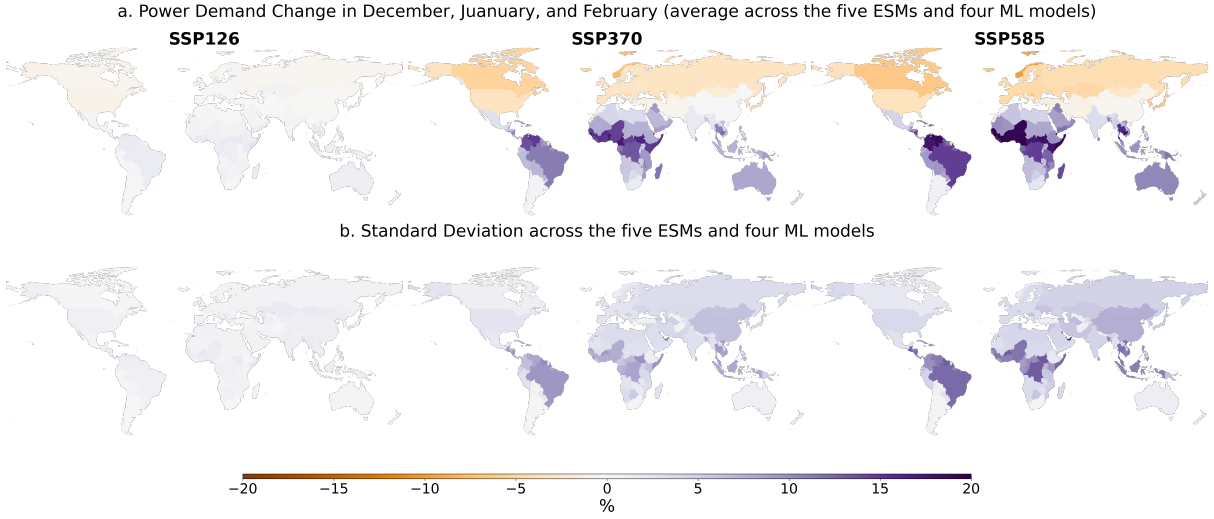

Figure V.6: Total power demand difference over the months December, January, and February between 2090-2100 and 2020-2030 in percentage.

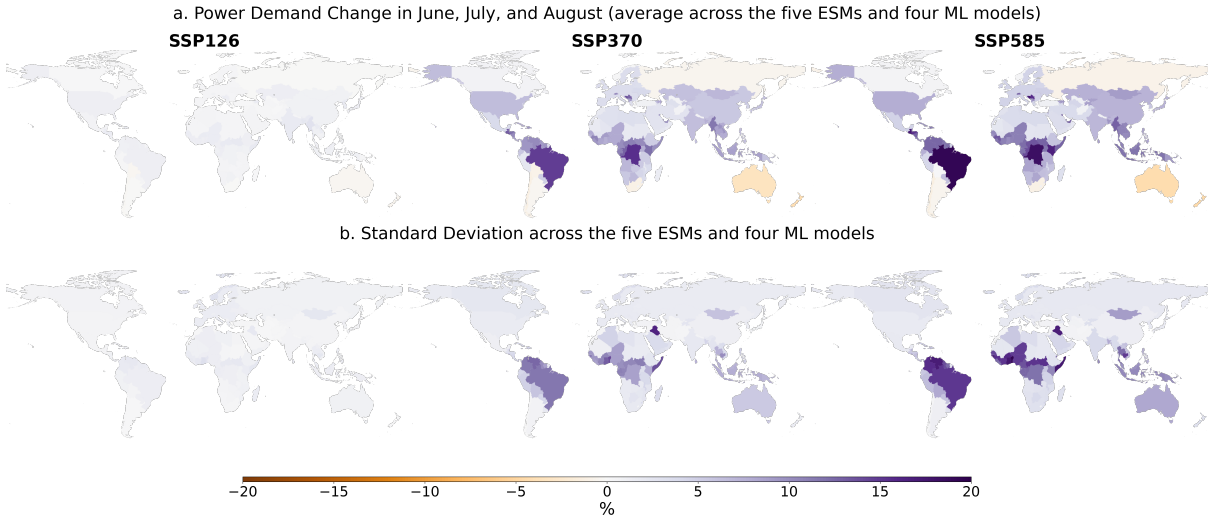

Figure V.7: Total power demand difference over the months June, July, and August between 2090-2100 and 2020-2030 in percentage.

Obtaining daily electricity demand forecasts enables an examination of the seasonal dynamics inherent in demand trends. This reveals underlying patterns that may be obscured by insignificant annual demand trends, such as in Europe. No substantial changes are readily discernible when considering the average of the 20 projections for annual demand growth in

Europe (Fig. V.2). However, a more focused analysis of the trends in the three northern hemisphere winter months (Fig. V.6) reveals a potentially significant decline in demand during this season. Conversely, an evaluation of the three summer months (Fig. V.7) presents an opposing effect characterized by increased demand. This reflects the reduction in heating demand due to warmer winters and the surge in air conditioning usage during the summer, albeit to a lesser extent in Europe compared to regions like the US. Furthermore, the low standard deviation across the 20 projections associated with these projections for both periods instills confidence in their reliability. More generally, Figures V.6 and V.7 demonstrate distinctive seasonal patterns in electricity demand behavior. During the winter months in the northern hemisphere (Fig. V.6), a noticeable reduction in power demand is observed, while demand increases in the southern hemisphere. This contrast confirms that power consumption dynamics are influenced by heating and cooling needs, with northern regions experiencing reduced heating demand. Conversely, when it is winter in the southern hemisphere (Fig.V.7), a decrease in demand is observed in countries such as Australia, New Zealand, South Africa, Chile, and Argentina, while demand increases in regions including Europe, the USA, and China. This inverse relationship highlights the reciprocal nature of seasonal electricity demand fluctuations in different hemispheres. In tropical regions, a consistent upward trend in demand is evident, emphasizing the ongoing growth in energy consumption regardless of the season.

Figures V.8 to V.11 provide a detailed view of these trends each month at the country scale. It shows the monthly change in power demand for countries with different economic and climatic conditions in both hemispheres. These figures show the results for the different ML models, highlighting the nuances of seasonal electricity demand projection depending on the model considered. Taking Europe, the United States, and South Africa as examples - regions known for their distinct seasonal transitions due to their temperate climates - a common pattern emerges: Seasonal patterns show some consistency across models, but the degree of change can vary depending on the model considered. However, the GAM model always shows more distinct patterns from the other models, either with more pronounced changes (in Europe and South Africa) or with months showing the largest changes that differ from the other models (in the US). For Brazil, there is a notable difference between the seasonal variations predicted by the RF and GB models, on the one hand, and those predicted by the MARS and GAM models, on the other. Specifically, the RF and GB models predict a more pronounced increase in demand between May and June. On the other hand, the MARS and GAM models predict a more pronounced rebound around October, especially in the GAM model, where the increase in demand reaches up to +38%, compared to the RF and GB models, where the increase is limited to +13%.

As previously observed, Europe is projected to see an increase in demand during the sum-

mer months, which is offset by a decrease in demand for the rest of the year, except for the GAM model, which predicts a sharp increase in demand in summer. Similarly, the United States mirrors this behavior, echoing previous findings in Japan: there is a notable spike in demand during the "next warmest months", especially May and September V.9. This phenomenon can be attributed to what we call a 'saturation effect.' During the summer months, namely June, July, and August, there is already a substantial demand for air conditioning in the United States. This high demand during the summer months limits any further significant escalation in electricity demand during that period. In contrast, the relatively lower demand for cooling in May and September currently provides an explanation for the possible substantial increase in electricity demand observed during these months. Finally, while Europe and the US experience an increase in demand between May and September, South Africa experiences this trend between October and March, due to opposite season in both hemisphere.

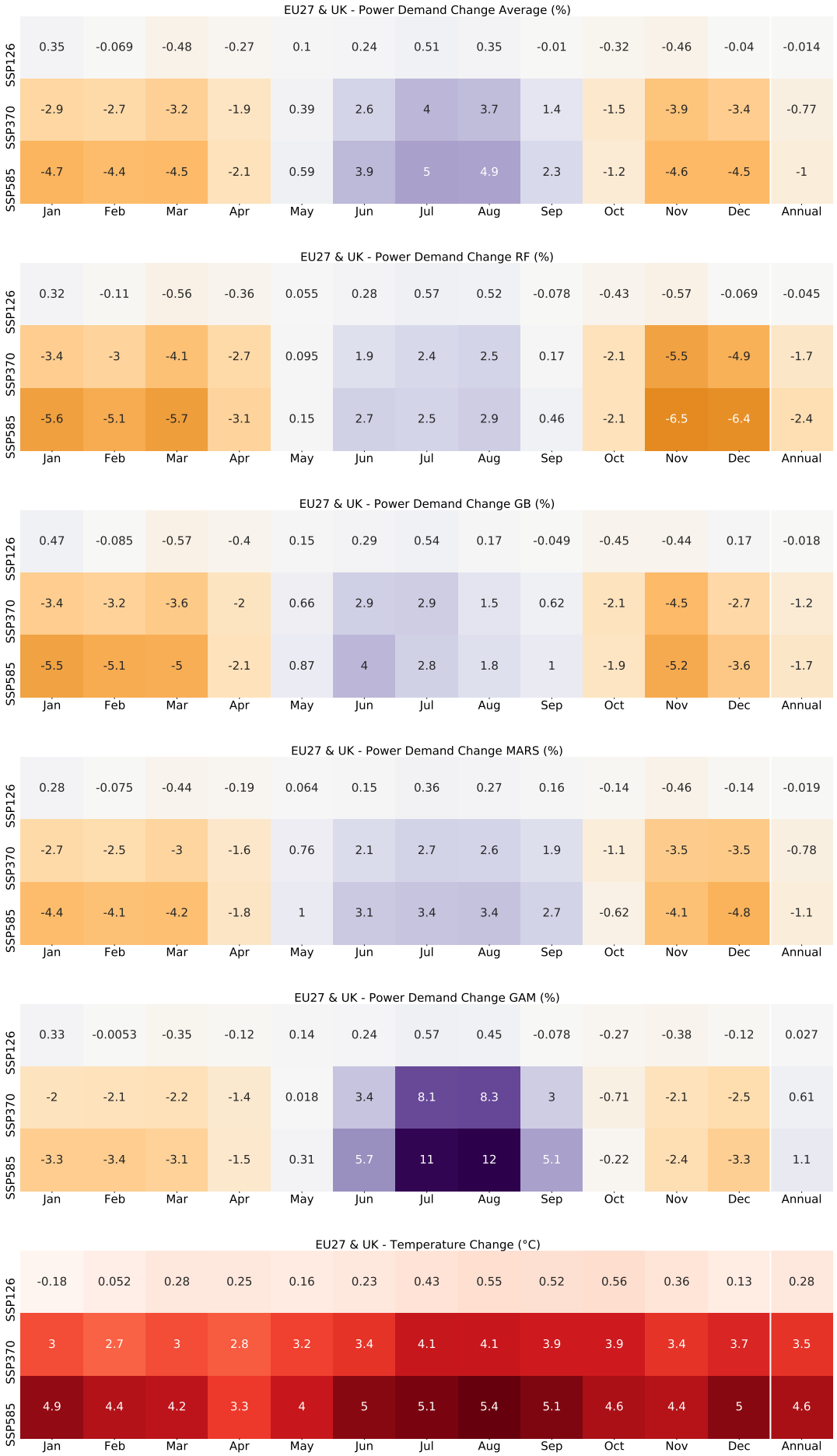

Figure V.8: Monthly power demand difference between 2090-2100 and 2020-2030 for EU27 & UK across ML models in percentage and monthly temperature changes between the same decades in °C.

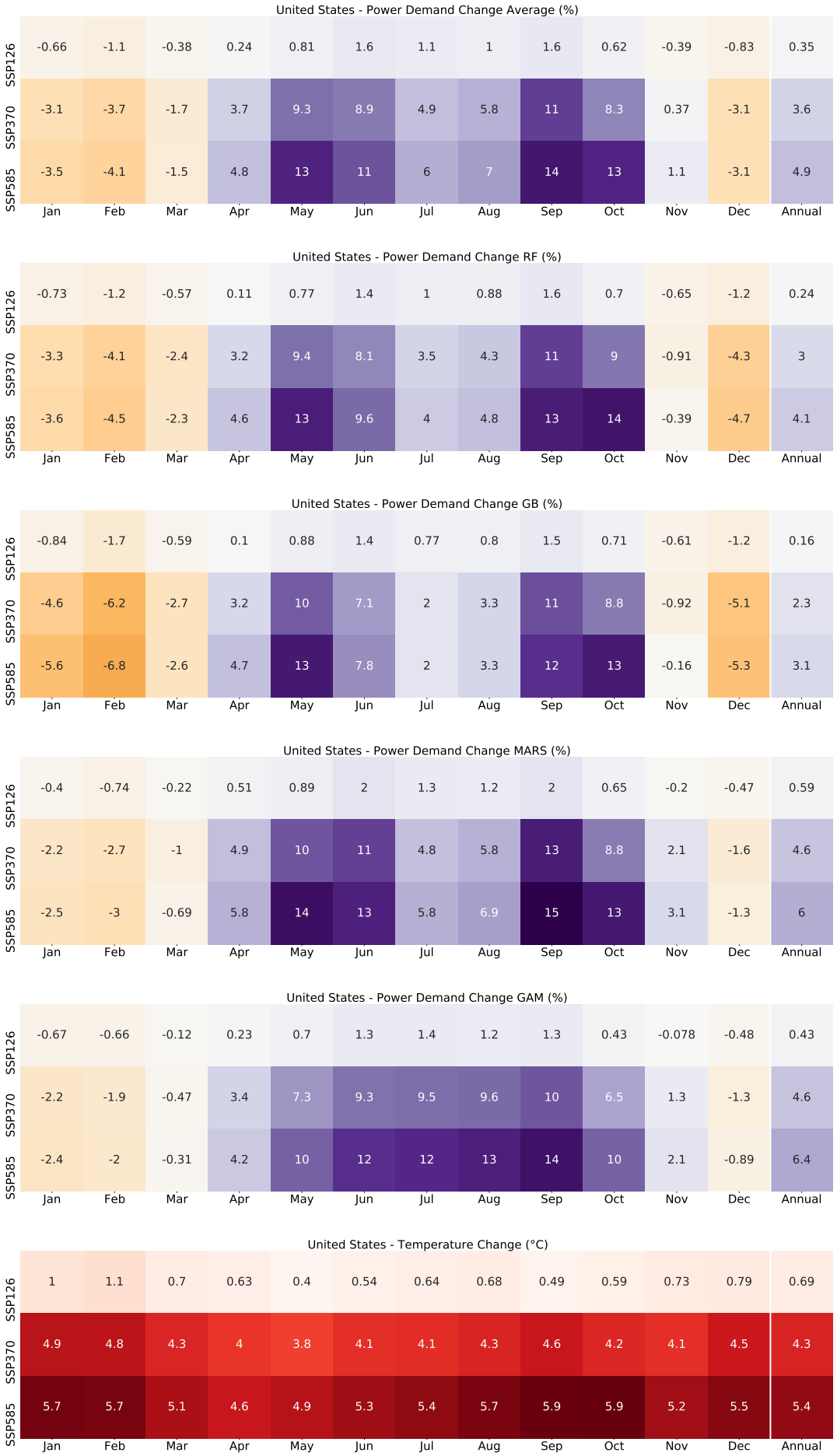

Figure V.9: Monthly power demand difference between 2090-2100 and 2020-2030 for the US across ML models in percentage and monthly temperature changes between the same decades in °C.

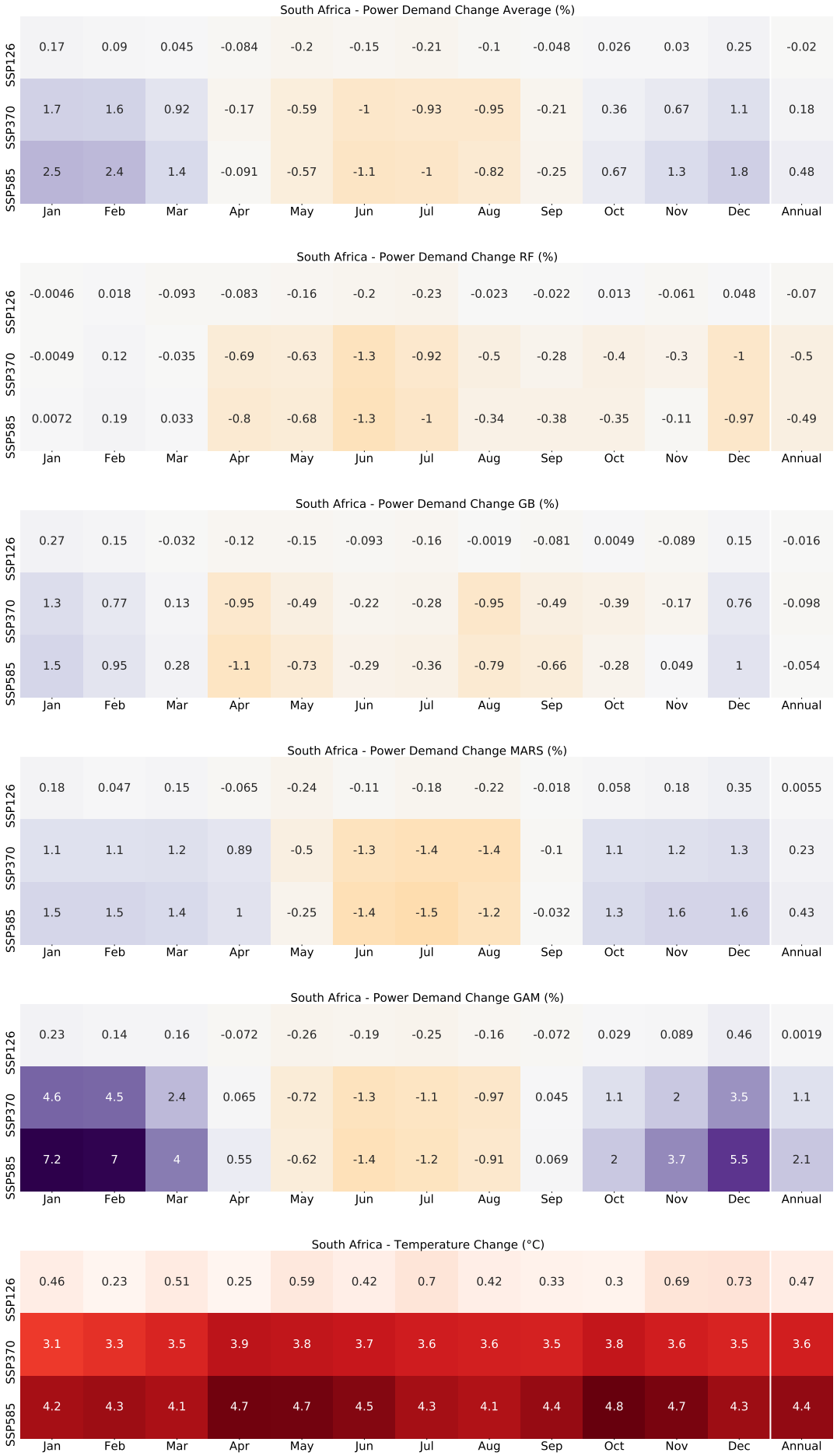

Figure V.10: Monthly power demand difference between 2090-2100 and 2020-2030 for South Africa across ML models in percentage and monthly temperature changes between the same decades in °C.

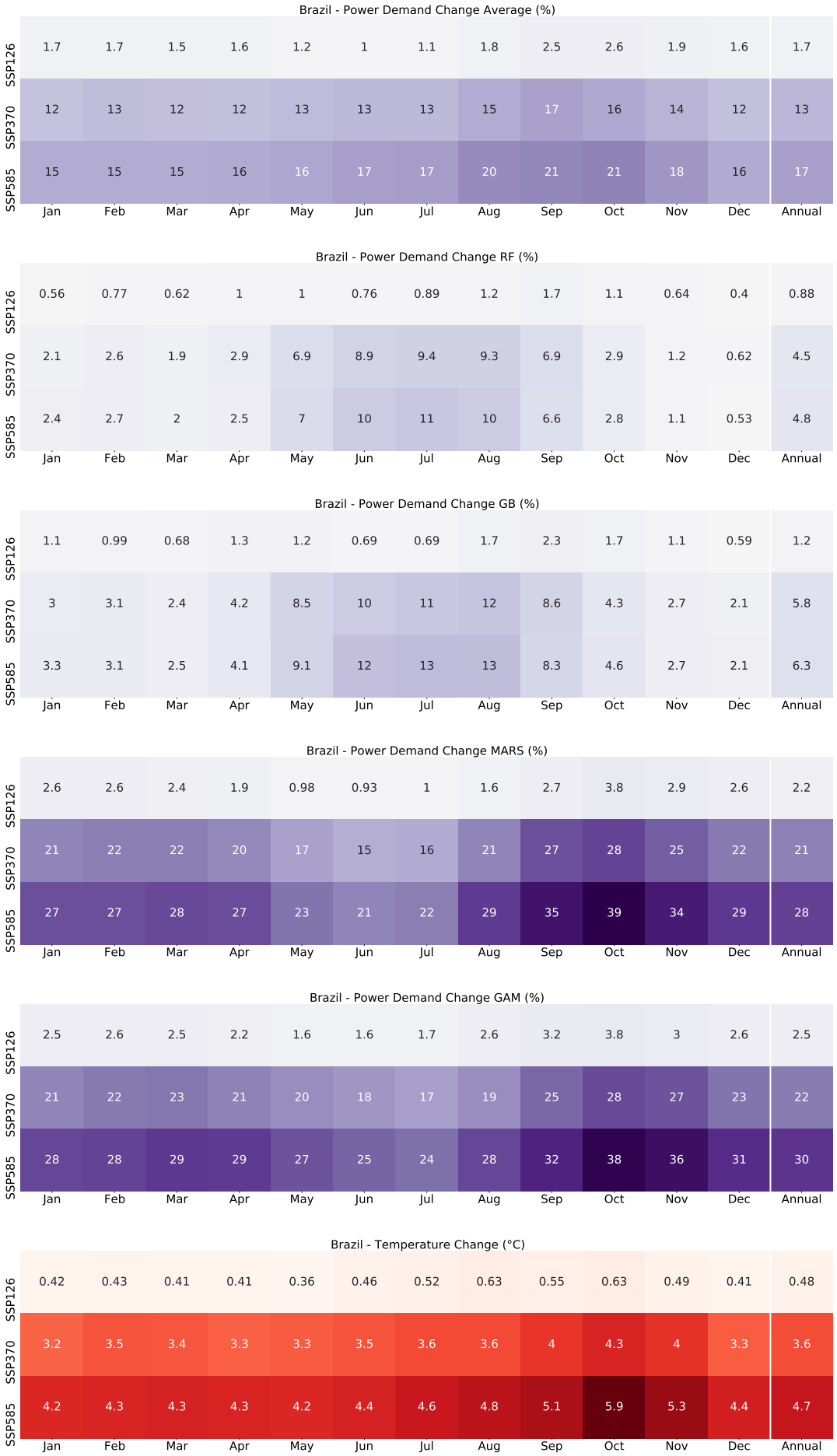

Figure V.11: Monthly power demand difference between 2090-2100 and 2020-2030 for Brazil across ML models in percentage and monthly temperature changes between the same decades in °C.

3 How to Project the National Carbon Intensity of Power Demand Emissions in the Future?

Based on projections of electricity demand, it is possible to calculate the CO_2 emissions resulting from the production of the electricity needed to meet that demand. This requires a projection of the carbon intensity of electricity production. Projections of future annual CO_2 emissions from electricity production (CO_2em) as well as projections of total annual electricity production (TPP) are based on the IMAGE 3.2 model database. Using this database, carbon intensity projection can be calculated from the formula:

$$CI = CO_2em / TPP \tag{V.2}$$

3.1 The IMAGE3.2 Model

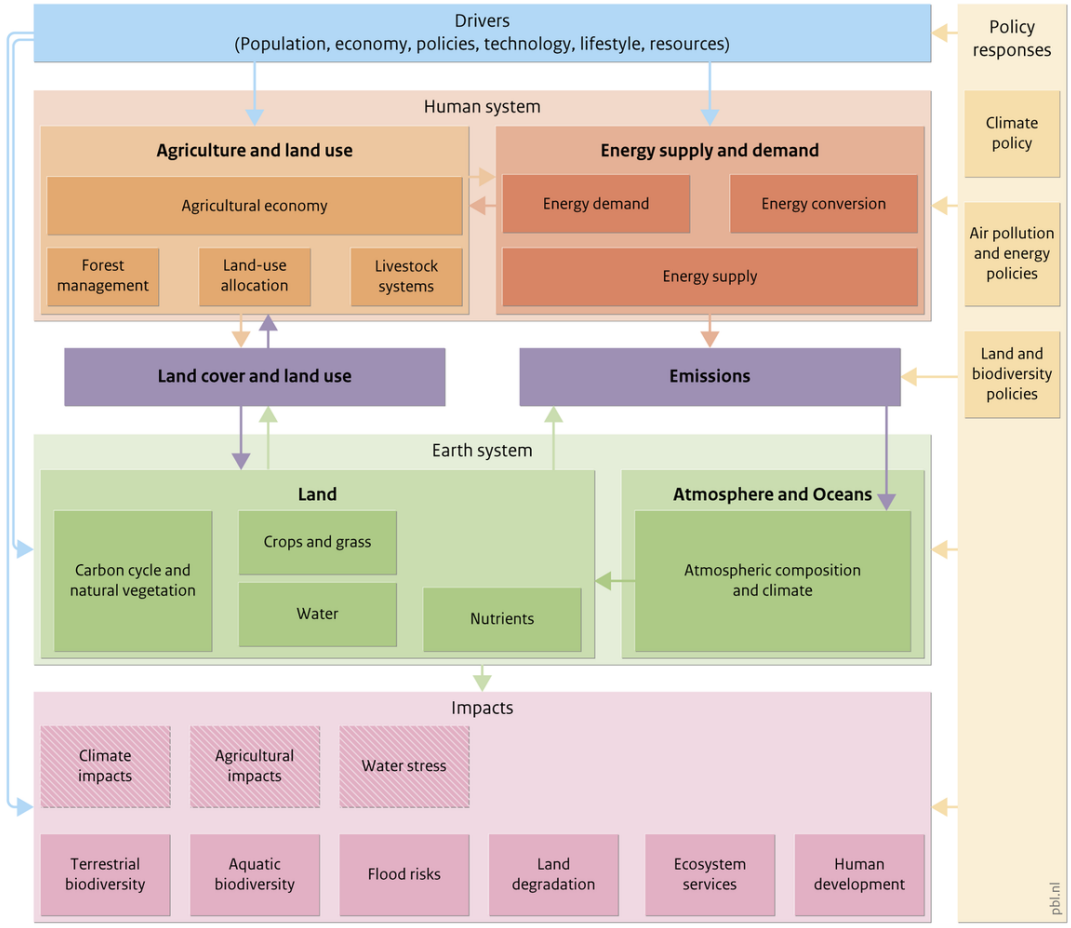

Figure V.12: IMAGE 3.0 framework. *Source: Stehfest et al., 2014*

The IMAGE (Integrated Model to Assess the Global Environment) framework is a widely used and comprehensive Integrated Assessment Model (IAM) developed to analyze and project various aspects of the global environment and human activities. The IMAGE model is designed to provide insights into the interactions between the environment, economy, and society, facilitating assessments of sustainable development, energy, climate change, land use, and other environmental issues. The model framework consists of several interconnected modules, each representing specific components of the global system (Fig. V.12). These modules include:

- Emission Module: This module calculates greenhouse gas emissions and other air pollutants resulting from human activities, such as energy production, industrial processes, transportation, and land use change.
- Energy Module: The energy module focuses on the production, consumption, and trade of different energy sources, such as fossil fuels (coal, oil, natural gas), nuclear, and renewable energy (solar, wind, biomass).
- Land Use Module: This module simulates land use changes, including deforestation, afforestation, urbanization, and agricultural expansion, and their impacts on carbon sequestration and emissions.
- Climate Module: The climate module incorporates climate science to estimate the impacts of greenhouse gas emissions on global temperature, sea level rise, and regional climate patterns.
- Socioeconomic Module: This module represents demographic trends, economic development, and human behavior, influencing energy demand, land use decisions, and emissions.
- Impact Module: The impact module assesses the consequences of environmental changes, such as climate change and land use, on various sectors like agriculture, water resources, and ecosystems.
- Policy Module: This module allows for evaluating different policy scenarios and measures, helping policymakers understand the effectiveness of different interventions in achieving sustainable development goals.

The IMAGE model framework integrates these modules' data, processes, and feedback loops to provide a holistic perspective on complex global environmental issues (Stehfest et al., 2014).

In 2014, the IMAGE 3.0 model was released. In 2017, IMAGE 3.0 was among the six IAMs used to develop the SSPs. The further updated version IMAGE 3.2, which was finalized in

2020, includes essential revisions and improvements to account for recent changes that may influence long-term energy demand projections, greenhouse gas emissions, and other relevant factors (Van Vuuren et al., 2021).

3.2 National and Regional Projections of Carbon Intensity

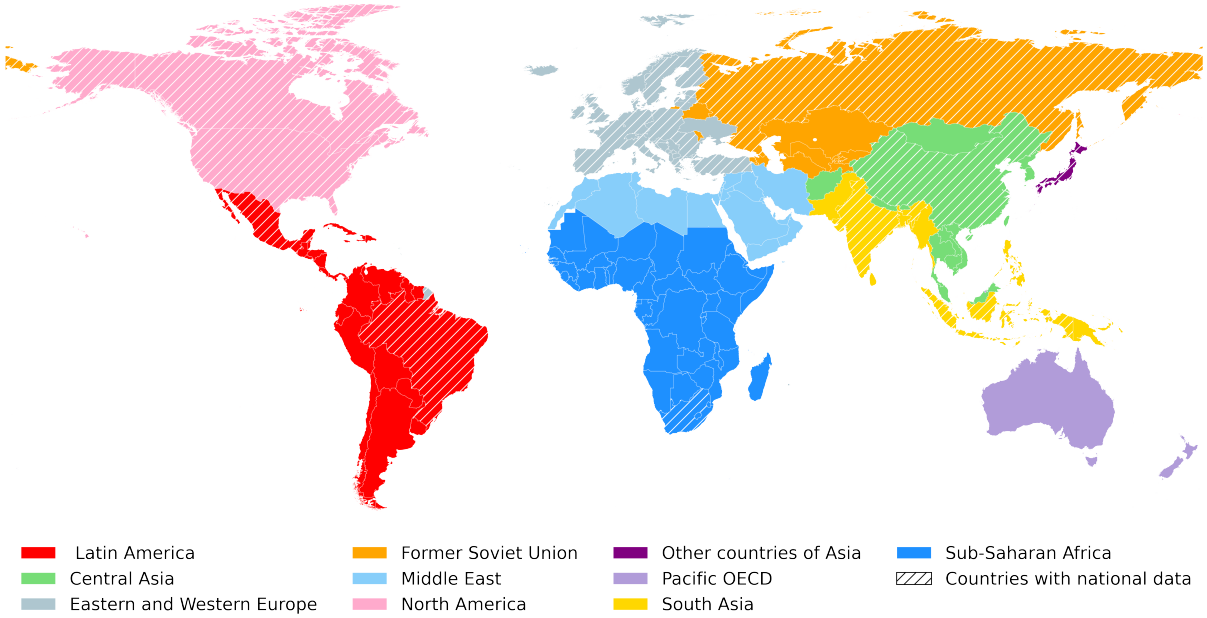

Figure V.13: Geographic coverage of power production and CO_2 emission projections in the IMAGE3.2 Model. The colors indicates the the regional data and the dashed lines the national data availabillity.

Two modules were essential within the IMAGE 3.2 framework to project carbon intensity: the emission module, which provides future CO_2 emissions from power production, and the energy module, which offers power demand projections. These projections are available for different scenarios and were obtained through the AR6 scenario explorer. The data were downloaded for the 2015-2100 period, with a five-year interval, and for three baseline scenarios: SSP1-2.6, SSP3, and SSP5. The projections are available at both regional and national scales. At the regional level, data is available for ten regions, including North America, Latin America, Eastern and Western Europe, the Middle East, Sub-Saharan Africa, the Former Soviet Union, Central Asia, South Asia, and Other countries of Asia, and Pacific OECD. For more detailed insights, data is available at the national level for 12 countries: Canada, United States, Mexico, Brazil, EU27 & UK, Turkey, South Africa, Russia, China, Japan, India, and Indonesia. Some regions, such as Northern Africa, are not individually represented in the available data. These regions were grouped with the closest available region in the dataset to address this limitation. This approach allowed calculating CO_2 emissions from power demand even in areas where

direct data was unavailable. Figure V.13 provides a visualization of the coverage of available data, illustrating the regions and countries for which IMAGE 3.2 data are accessible.

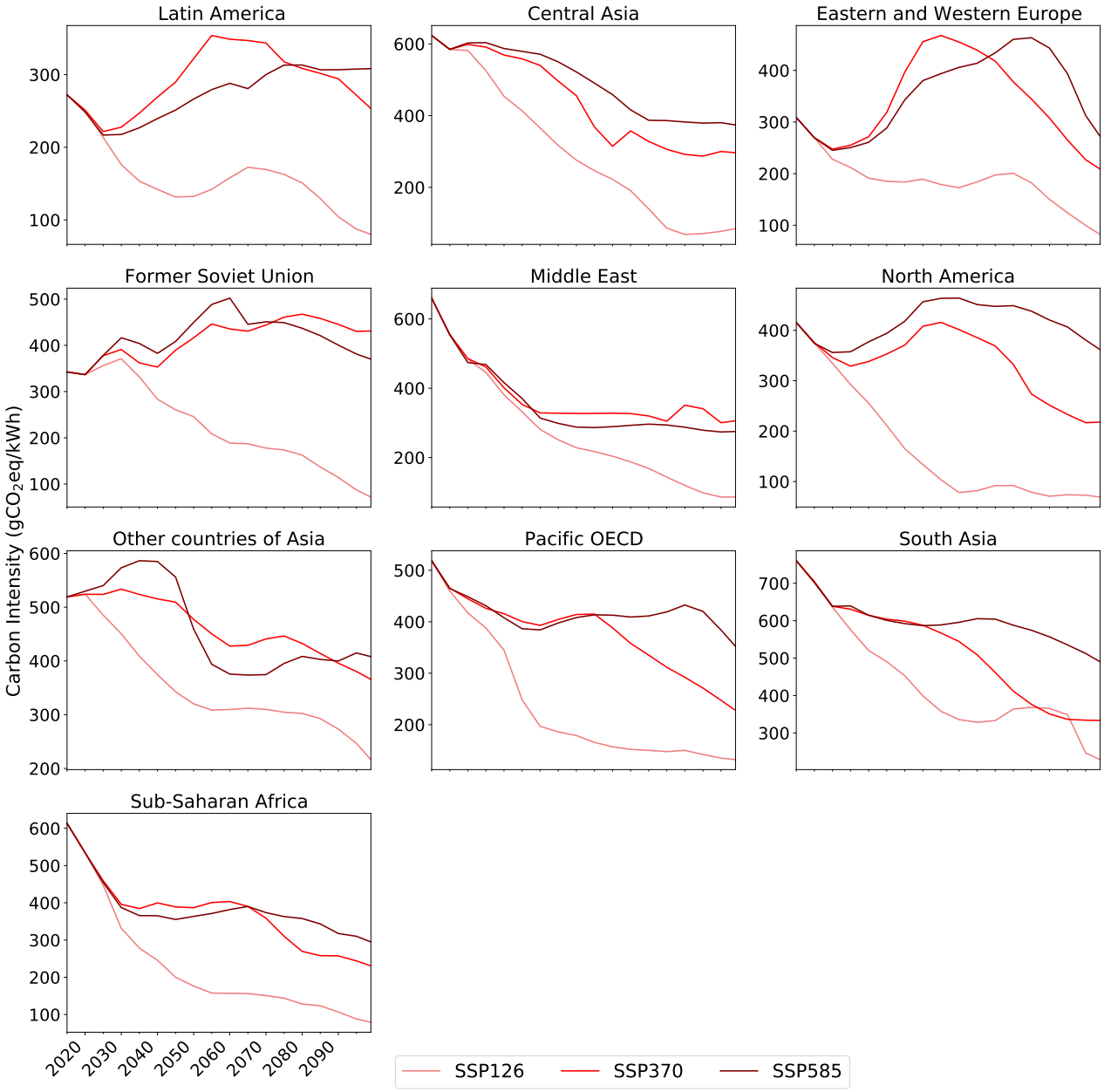

Figure V.14: Regional carbon intensity projections for the power sector calculated from IMAGE 3.2 data.

Using formula V.2, carbon intensity projections at the annual scale are calculated until the end of the century. Given that the data is available with a five-year interval, a one-dimensional linear interpolation method was applied to calculate carbon intensity data for missing years and ensure a continuous dataset. Using this approach, the carbon intensity projections could be extended to cover the entire time range from 2015 to 2100 with consistent and continuous data points. The carbon intensity projections thus obtained (Figs V.14 and V.15) reveal two distinct

types of behavior. In the first scenario, carbon intensity rises until around the middle of the 21st century and then begins to decline. In the second scenario, carbon intensity decreases from the beginning and stabilizes around the middle of the century.

Figure V.15: National carbon intensity projections for the power sector calculated from IMAGE 3.2 data.

The carbon intensity projections within the SSP1-2.6 scenarios predominantly follow the second behavior, characterized by a continuous decrease from the beginning, and differ significantly from the trends observed in the SSP3-7.0 and SSP5-8.5 scenarios. In contrast, the carbon intensity projections under the SSP3-7.0 and SSP5-8.5 scenarios tend to manifest the first behavior outlined, where the carbon intensity experiences an initial increase before gradually

decreasing. Certain regions deviate from this general pattern. Sub-Saharan Africa, for example, shows a consistent decline in carbon intensity across all scenarios from the beginning of the century. Overall, SSPs 3-7.0 and 5-8.5 show remarkably similar behavior, while SSP1-2.6 often diverges with a lower carbon intensity, thus accentuating the differences in carbon intensity dynamics between the different SSPs.

A notable disparity emerges when comparing regions of the Global North and Latin America with other parts of the Global South in the context of SSPs 3-7.0 and 5-8.5. Specifically, regions such as Eastern and Western Europe, North America, the former Soviet Union, and Latin America show a more pronounced escalation in carbon intensity during the first half of the century compared to counterparts in other regions where carbon intensity either declines or shows very modest growth. Some regions, such as Europe, show an anomalous pattern characterized by an initial decline in carbon intensity followed by subsequent growth. To correct for this pattern, it may be useful to reconsider the carbon intensity curves to remove this artifact. Furthermore, some of the projections for SSP3-7.0 and SSP5-8.5 go above pathways reflecting Nationally Determined Contributions (NDCs) and may not be aligned with current policies already implemented.

4 CO_2 Emissions Projections

4.1 Additionnal CO_2 Emissions Due to Climate Change

Combining annual power demand projections with carbon intensity projections, a comprehensive array of annual CO_2 emissions projections for the entire century is generated at the country level. First, the annual electricity demand projections are calculated by summing daily demand values over a year. These projections are then multiplied by the carbon intensity projections. This results in a total of 20 different CO_2 emissions projections for each SSP scenario and country, reflecting the combination of five ESMs and four ML models.

To elucidate the influence of climate change on the evolution of CO_2 emissions stemming from electricity production, a scenario denoted as 'no climate change' has been formulated. Within this 'no climate change' scenario, climatic conditions are kept the same throughout the entire century, mirroring those of 2020. Electricity demand projections under this scenario are computed using the four ML models. Subsequently, CO_2 emissions are calculated for all countries across the three scenarios, as previously described. The resulting projections from the 'no climate change' scenario are then subtracted from the projections under climate change

conditions. These final projections enable us to discern the impact of climate change on the projected CO_2 emissions, as depicted in Figure V.16.

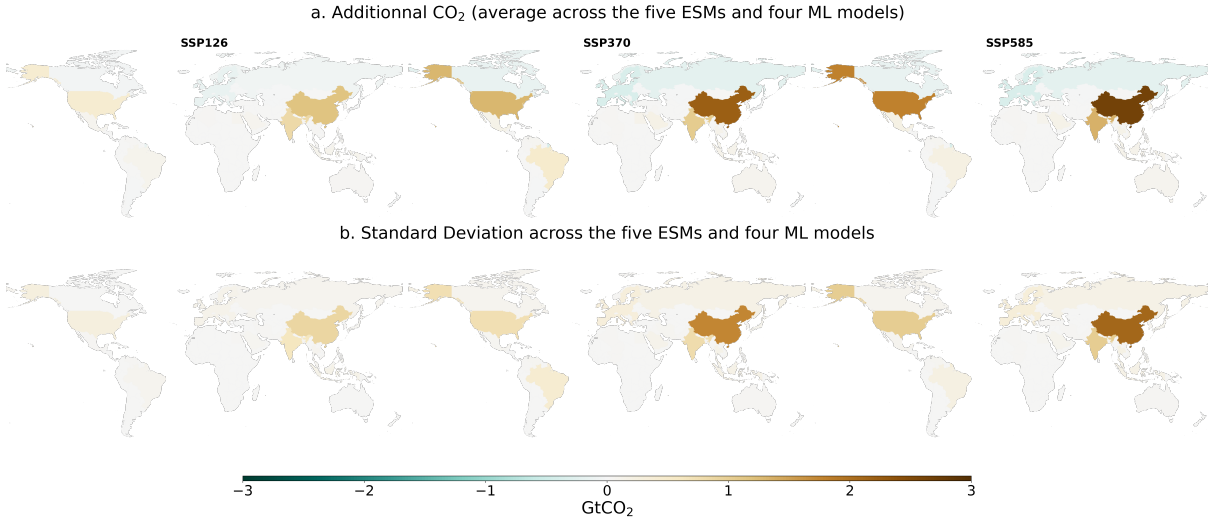

Figure V.16: Cumulative Additional CO_2 emissions over 2020-2100 from power production (averaged over the 20 projections, *i.e.* the combination of the five ESMs and the four ML models) compared to a scenario with no climate change.

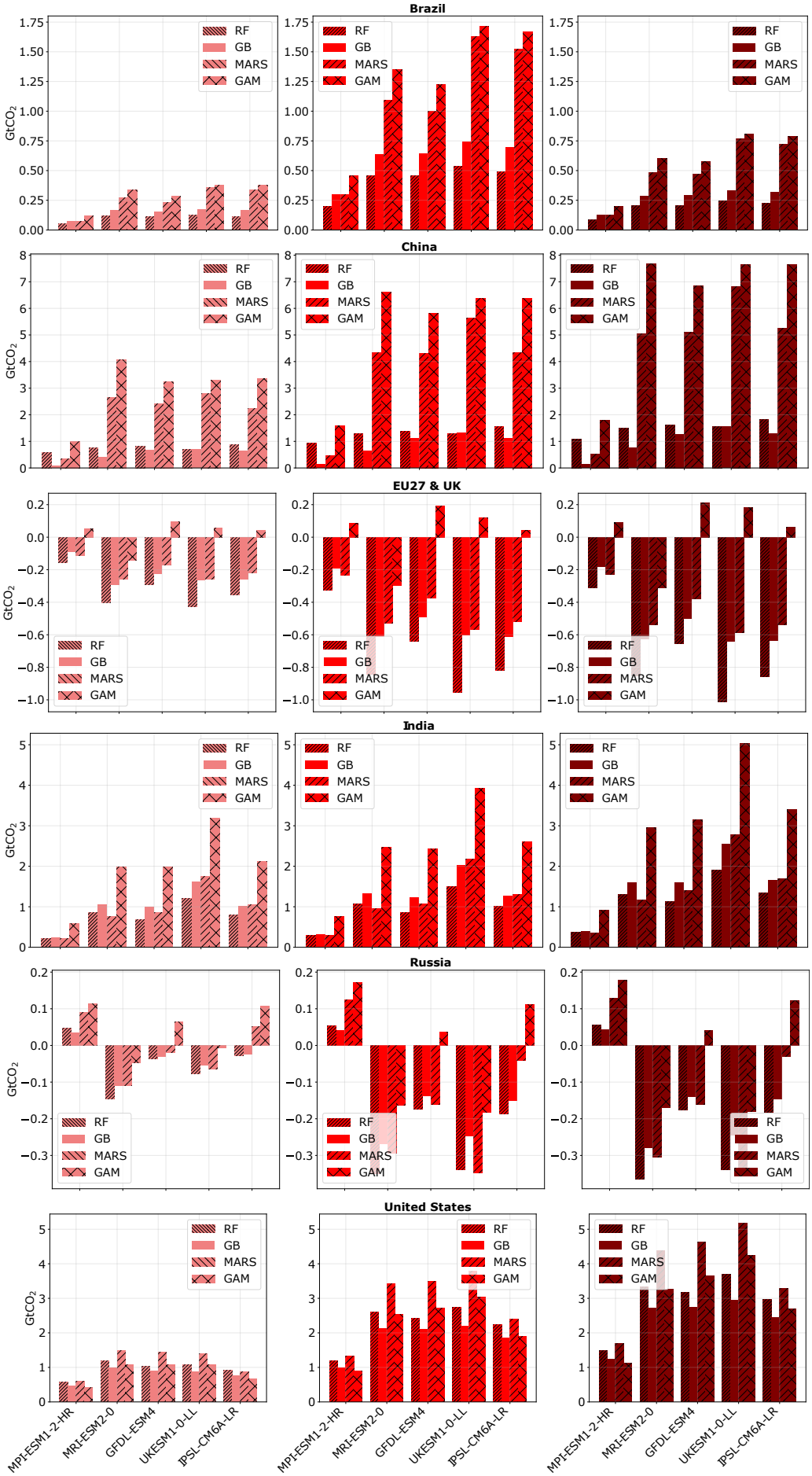

Figure V.17: Cumulative additional CO_2 emissions over the period 2020-2100 induced by climate change alone calculated for the five ESMs and four ML models for Brazil(a), China (b), EU27 & UK (c), India (d), Russia (e), and United States (f).

On the global scale, the overall impact of climate change on CO_2 emissions remains relatively small across all SSPs. However, noteworthy exceptions to this trend emerge, primarily observed in the cases of China, the United States, India, and Brazil, where increases in CO_2 emissions arising from power production due to climate change are discernible. Of these regions, China has the highest cumulative additional CO_2 emissions, with a surplus of more than two gigatonnes (Gt) of CO_2 for SSP5-8.5 over the entire period 2020-2100, averaged over the 20 projections. The United States closely follows China with a cumulative additional CO_2 emission of about 2 $GtCO_2$. In contrast, Europe and Russia undergo an opposite trajectory, manifesting a marginal reduction in CO_2 emissions attributed to climate change, albeit with a lesser degree of intensity. The uncertainty associated with the additional CO_2 emissions (Fig. V.16b) has been quantified by calculating the standard deviation over the 20 projections, as for the electricity demand projections. It is relatively large for the above countries, although lower than the average of the 20 projections.

Figure V.17 offers a comprehensive breakdown of the supplementary CO_2 emissions for the specified countries across the ESMs and ML models. This visual representation underscores the profound influence of climate sensitivity inherent in the ESMs on the magnitude and even the direction of climate change impact, as is particularly evident in the case of Russia, although the absolute magnitudes are small. MPI-ESM1-2-HR consistently exhibits a less pronounced impact of climate change on additional CO_2 emissions in contrast to the other ESMs, irrespective of the ML model considered. Nonetheless, a substantial portion of the disparities among projections can be attributed to the choice of ML models, implying that these models primarily contribute to the substantial standard deviation observed earlier.

Moreover, the figure accentuates the significant role played by UKESM1-0-LL, and, to a somewhat lesser extent, IPSL-CM6A-LR, in generating the most substantial additional CO_2 emissions, especially when coupled with the GAM and MARS models. Conversely, the GB models tend to produce a more moderate effect than the other ML models. CO_2 emissions are forecasted to decline for Europe, except in scenarios where the GAM model is applied, aligning with prior findings regarding electricity demand in Europe. The pattern is similar for Russia, except when the MPI-ESM1-2-HR is used. For the other countries, all projections uniformly agree on an increase in CO_2 emissions attributed to climate change. In some cases, the average additional CO_2 shown in Figure V.16 is much lower than the individual projections. For example, China's projections show an increase of up to +6 $GtCO_2$ over the assessment period, which is significantly higher than the observed average effect.

The insights gained from the maps shown in Figures V.18 and V.19 extend the scope of this analysis to the entire globe. Figure V.18 shows the averaged additional CO_2 emissions

across ESMs for all ML models, while Figure V.19 shows the averaged additional CO_2 emissions across ML models for all ESMs. Aside from the countries previously mentioned, the additional CO_2 emissions are very small for all other countries. For a comprehensive overview of all 20 combinations of ESM and ML models, maps are provided in Appendix C.

Analysis of the maps presented in the previous section (Figures V.6 and V.7) leads to several conclusions. In temperate countries such as China, the projected increase in CO_2 emissions can be attributed to increased electricity demand during the summer. This increase in demand is not adequately offset by a corresponding reduction in electricity demand during the winter months. On the other hand, Brazil and tropical regions in general show a steady increase in electricity demand throughout the year, which accounts for the observed positive additional CO_2 emissions. Regions with negative additional CO_2 emissions are characterised by an overall decrease in demand during the winter months, which is not sufficiently compensated by an increase in demand during the summer. Europe has a more significant impact on the additional CO_2 emissions compared to Russia, although Russia experiences a more pronounced decrease in electricity demand. This difference is mainly due to the carbon intensity of electricity production, which is lower in Europe and is expected to decrease more than in Russia (Figures V.14 and V.15).

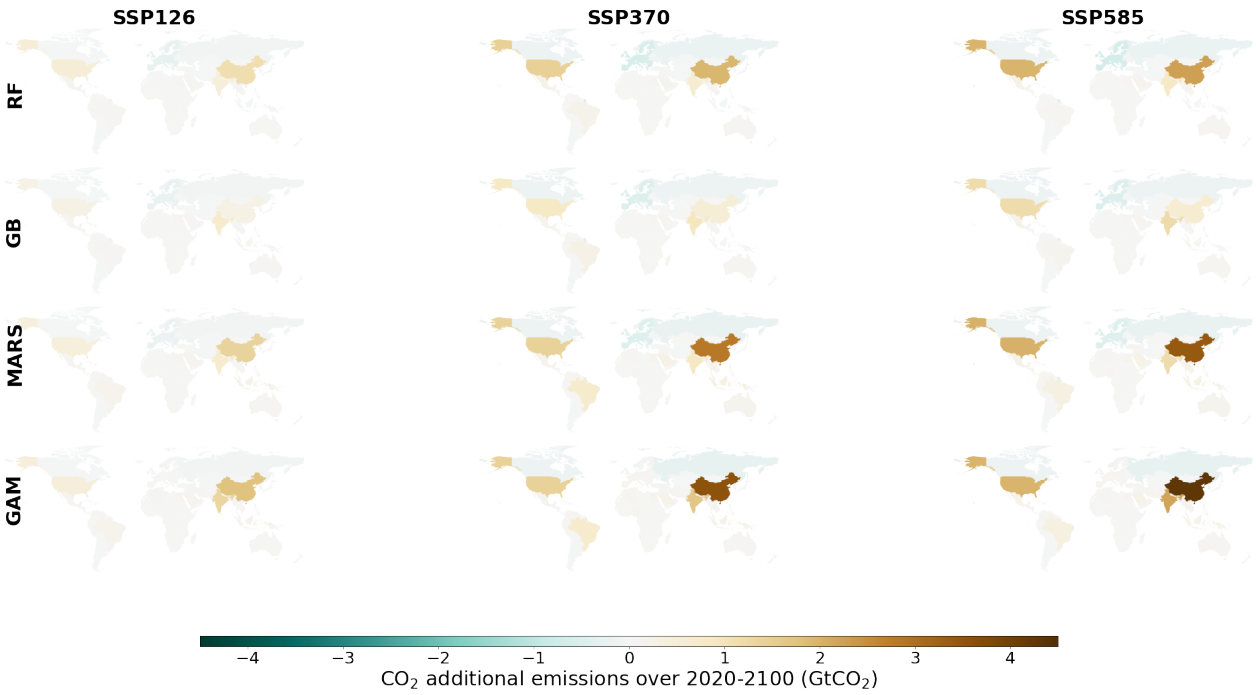

Figure V.18: Additional CO_2 emissions from power production compared to a scenario with no climate change for the different ML models (averaged over the five ESMs).

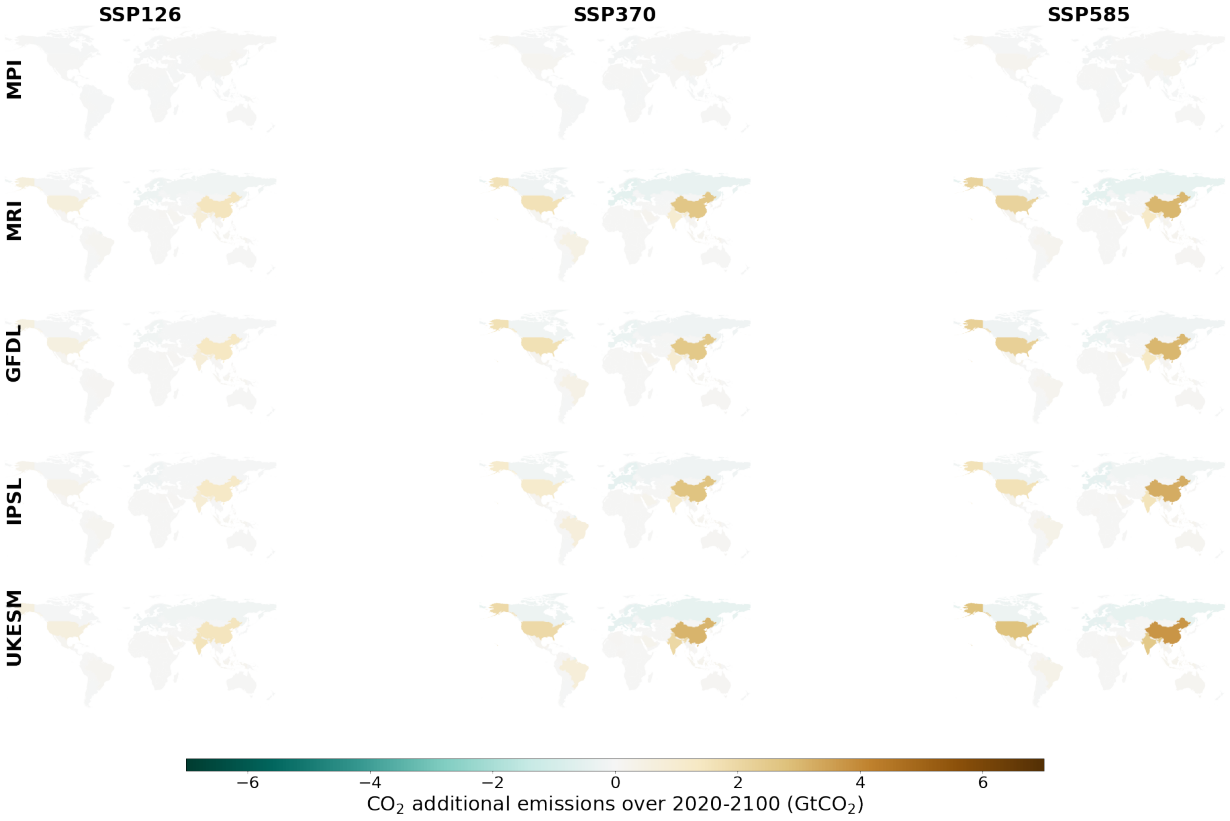

Figure V.19: Additional CO_2 emissions from power production compared to a scenario with no climate change for the different ESMs (averaged over the five ML models).

4.2 Global CO_2 Emissions

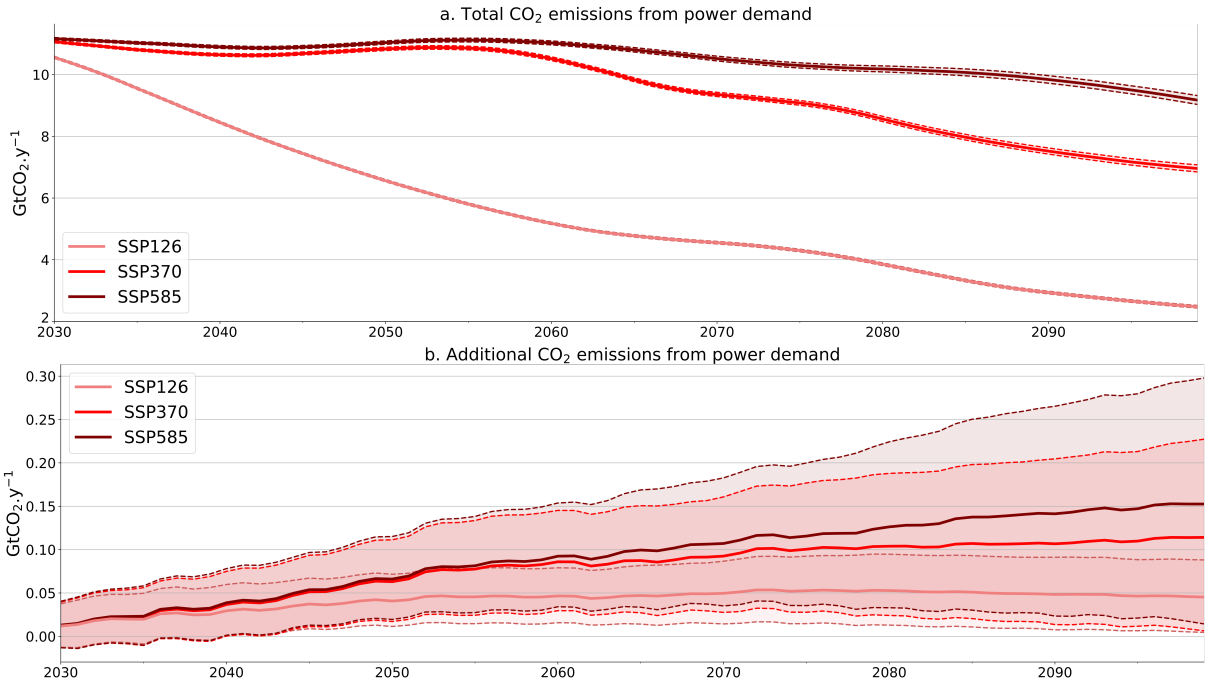

Figure V.20: (a) Global total CO_2 emissions from power production. (b) Additional CO_2 emissions from power production due to climate change. The solid lines represent the average of the 20 projections and the colored area inside the dashed lines is the standard deviation across the 20 projections. The projections were smoothed using a rolling 10-year average.

Figure V.20 shows global annual CO_2 emissions, including the additional CO_2 emissions arising from power demand. Across all SSPs, emissions attributed to power demand are projected to decrease from 2060 at the latest. Notably, SSP3-7.0 and SSP5-8.5 exhibit similar emission trends and intensity. In contrast, SSP1-2.6 shows an earlier decline, starting around 2030, and maintaining lower emissions compared to the other two scenarios.

The standard deviation among the 20 projections is considerably lower than the averaged total CO_2 emissions, allowing a clear differentiation among the three scenarios. However, this is different when examining the additional CO_2 emissions attributed to climate change. Although SSP1-2.6 generally indicates lower additional CO_2 emissions, the differences between the scenarios are less pronounced than for total CO_2 emissions. The standard deviation across all scenarios is greater than the mean, suggesting that the methodology established in this thesis cannot currently determine whether the additional CO_2 emissions due to global warming will be more pronounced in one scenario relative to another. It is also worth noting that the additional CO_2 emissions are relatively small, measured in tenths of $GtCO_2$ per year, compared to the CO_2 emissions from electricity generation, which range from 2 to 10 $GtCO_2$ per year.

4.3 Impact of Carbon Intensity on CO_2 emissions

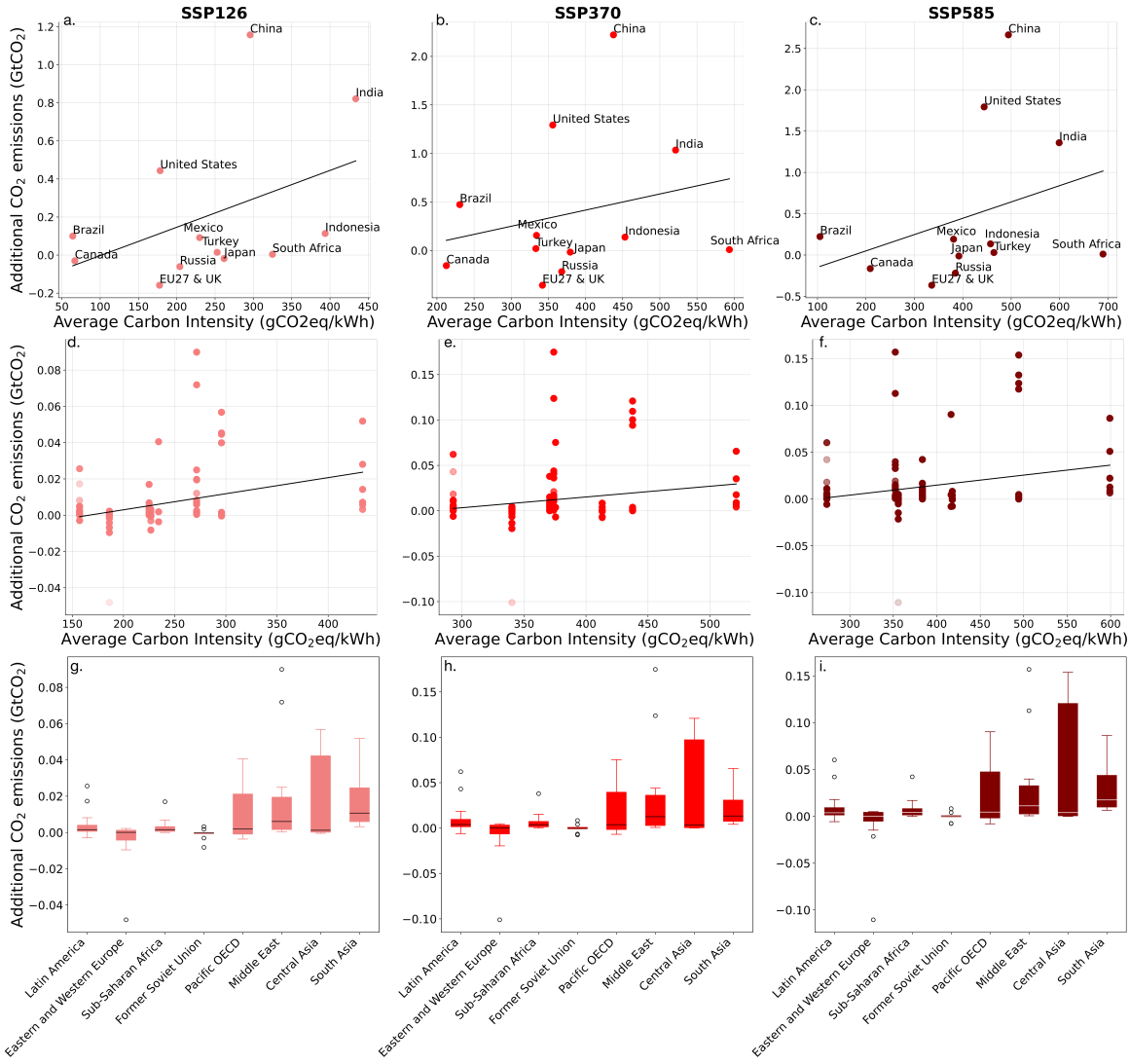

Figure V.21: Scatter plots (a, b, c) display the relationship between additional CO_2 emissions and the average carbon intensity over the period 2020-2100 for countries with specific carbon intensity projections. In contrast, scatter plots (d, e, f) show the same relationship for countries with regional carbon intensity projections. The black lines represent linear regression lines. Boxplots (g, h, i) provide a summary of the data depicted in figures (d, e, f).

Examining the relationship between additional CO_2 emissions and carbon intensity reveals the influence of carbon intensity on the amount of additional CO_2 emissions resulting from global warming (Fig V.21). Although this effect may not be immediately apparent, the trend lines show a positive correlation between average carbon intensity over the projection period and additional CO_2 emissions, a trend that is consistent across different scenarios for countries with available carbon intensity projections (Fig V.21a, b and c). Extending this analysis to all countries shows a similar trend, although with less pronounced effects (Fig V.21, d to i). However, it is important to note that the confidence in this trend is relatively low due to the scatter of the

data points. Significant deviations from the trend lines, as seen in countries such as China, the United States and India, underline the need to consider additional influencing factors such as population size and GDP.

5 Limitations

5.1 Machine Learning Models Extrapolation Assumption

The challenge of extrapolating models when faced with limited or missing data points is the main limitation of this study. These extrapolation challenges are well recognized in the field of load forecasting with ML models, particularly when forecasting electricity demand during extreme events. The dilemma of extending model predictions beyond the scope of available data points can introduce uncertainties and potential inaccuracies, which are particularly evident in scenarios characterized by unusual or extreme conditions, such as COVID-19 or extreme heat waves or cold spells (Cao et al., 2022; Yadav et al., 2021; Yang et al., 2023). This limitation underscores the complexity of forecasting needs in unconventional circumstances and highlights the critical need for advanced techniques to address extrapolation challenges more effectively.

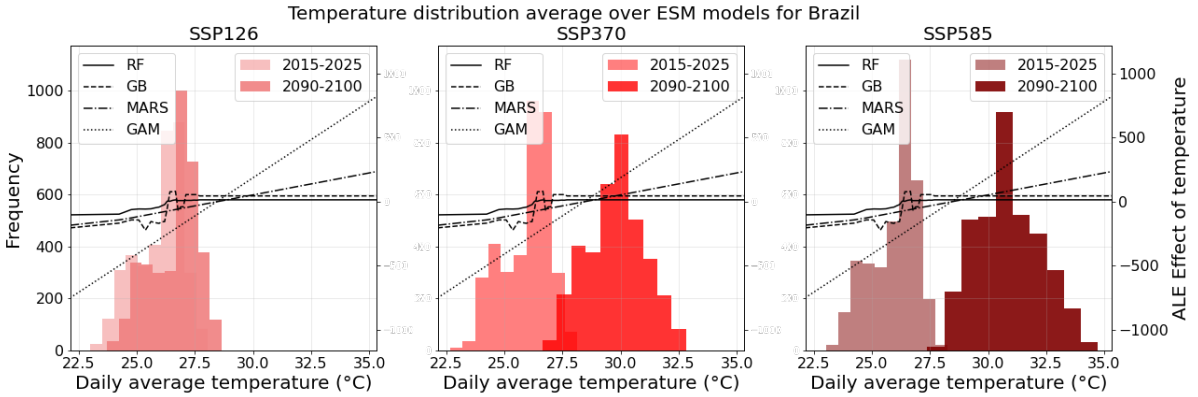

Figure V.22: Histograms representing the temperature distribution in Brazil for the decades 2015-2025 and 2090-2100 for the three SSPs. The black lines represent the Accumulated Local Effect of T2M on power demand for the four ML models over the entire projection period. The ALE effect of RF and GB has been multiplied by ten for comparability with the effects of MARS and GAM.

Examining the case of Brazil in this study highlights the problems of extrapolating machine learning models when data is sparse or absent. The GAM model for Brazil predicting a remarkable 32% annual increase under SSP5-8.5 by the end of the century, in contrast to the small 4.8% increase projected by RF, is a striking example. Indeed, the dichotomy between RF and GB, juxtaposed with GAM and MARS, is evident, with the latter two models forecasting significantly

higher increases in demand (Fig. V.11). A prominent approach to unraveling the mechanics of these models is the Accumulated Local Effects (ALE) plot, particularly the ALE plot for temperature - the main climate variable influencing demand. In Brazil, the temperature histograms for 2015-2025 and 2090-2100 barely overlap, showing a noticeable shift in daily average temperature, particularly pronounced in SSP3-7.0 and SSP5-8.5 (Fig. V.22). This discrepancy means that the machine learning models had to predict demand in temperature ranges beyond their training data, highlighting the critical role of extrapolation assumptions. Different hypotheses emerge from the ALE plots: RF and GB postulate invariant demand beyond 27°C, while MARS and GAM present a linear escalation of demand above 25°C (Fig. V.22). This contrast explains the variance in demand projections for Brazil. The implications are significant and introduce the notable degree of uncertainty observed earlier (Fig. V.2) into our results, leaving the trajectory of demand evolution in Brazil under global warming considerably uncertain and by extrapolation to the other countries where we used the Brazilian model as a reference model.

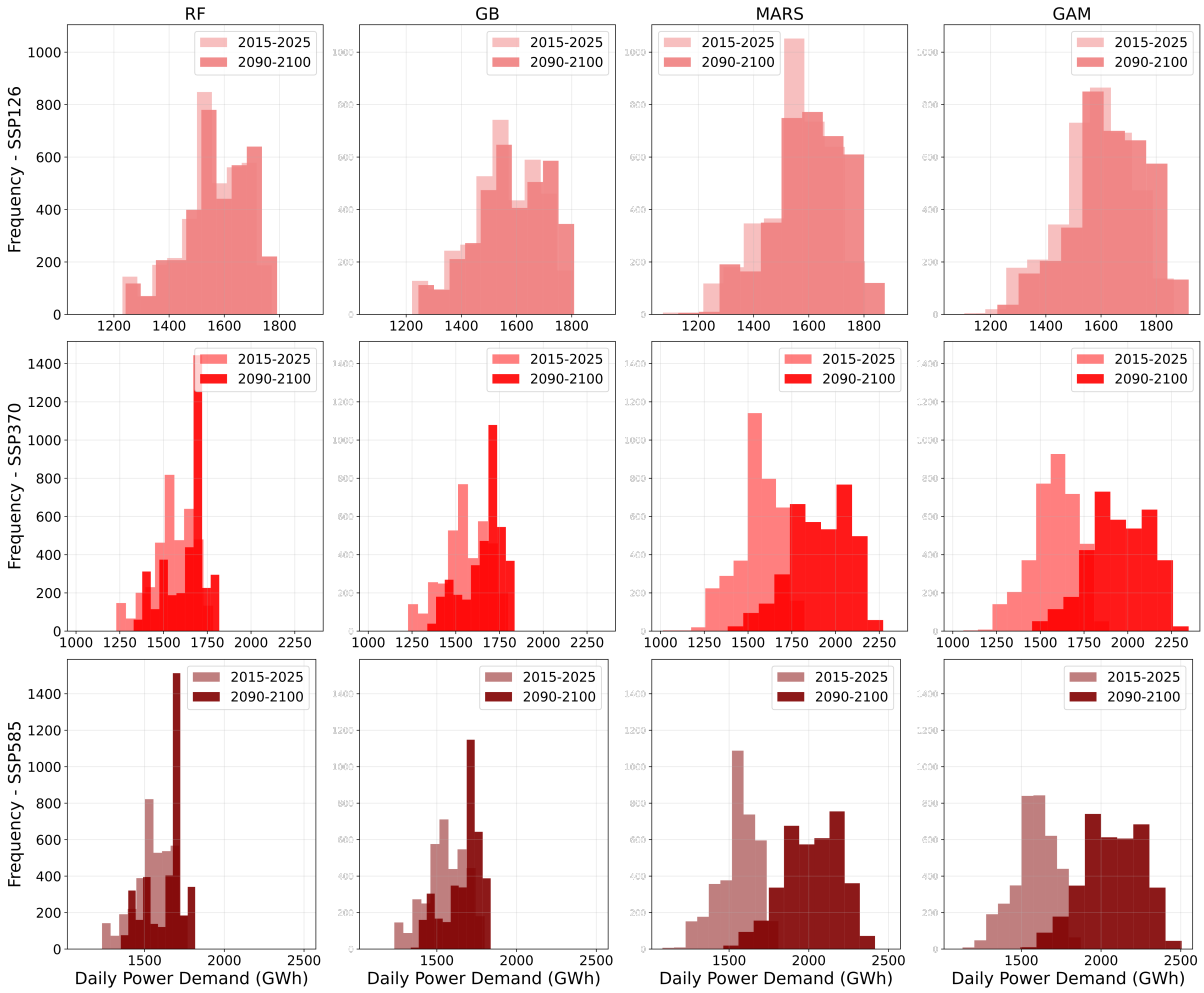

Figure V.23: Histograms representing the distribution of power demand in Brazil for the decades 2015-2025 and 2090-2100 under the three SSPs and across the four ML models, averaged over the five ESMs.

The histogram of electricity demand across the different ML models, as shown in Fig-

ure V.23, does indeed reveal distinct patterns. In particular, in the case of MARS and GAM, a notable deviation is observed, characterized by a shift towards elevated daily power demand levels projected for the end of the century. These projections indicate unprecedented demand levels, reaching as high as 2400 GWh per day. This starkly contrasts with the pre-2025 period, during which the highest recorded demand did not exceed 1800 GWh. In contrast, the 2090-2100 decade projections for both RF and GB models consistently fall within the historical range of daily power demand. In light of the ALE plots for temperature, the discernible disparities in these projections can be attributed to the inherent extrapolation assumptions embedded within the ML models.

While Brazil serves as an illustrative example, it's important to acknowledge that the limitation discussed here applies universally to all models when confronted with the task of projecting demand based on previously unobserved climatic conditions. This inherent challenge transcends geographical boundaries and pertains to the broader context of machine learning applications on unknown conditions.

5.2 Lack of Data to Predict Cooling Demand

In the European context, the constraints associated with extrapolation assumptions are compounded by another significant limitation. There is currently a lack of data that can adequately capture the highly probable future increase in demand for air conditioning. This emerging demand trend, which is expected to result from the increasing prevalence of warmer temperatures, poses a significant challenge to the accurate representation and forecasting of electricity consumption patterns.

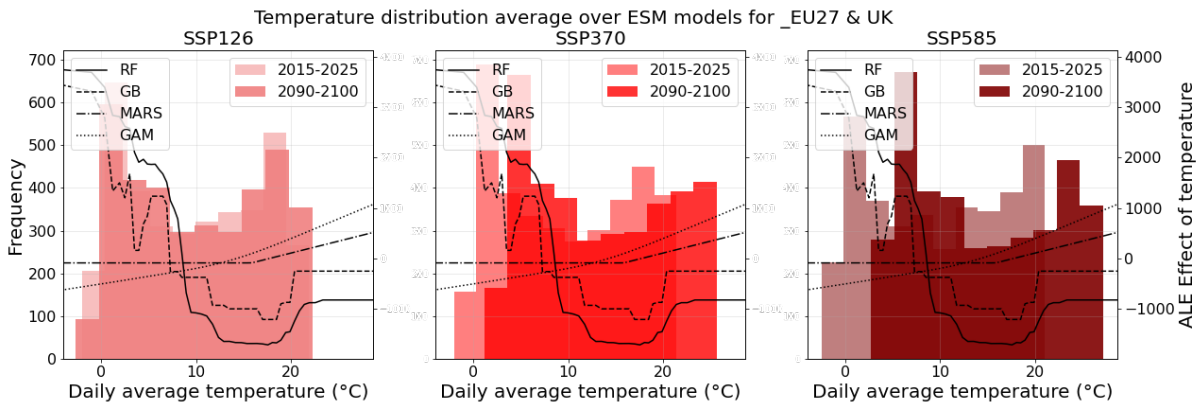

Figure V.24: Histograms representing the temperature distribution in the European Union for the decades 2015-2025 and 2090-2100 for the three SSPs. The black lines represent the Accumulated Local Effect of T2M on power demand for the four ML models over the entire projection period. The ALE effect of RF and GB has been multiplied by ten for comparability with the effects of MARS and GAM.

Indeed, the complexity of model extrapolation is also a challenge for the European case. Even when ML models show a high degree of consistency and similar seasonal patterns of demand evolution (Fig. V.8), uncertainties remain due to the extrapolation assumptions. In the European context, we also observe nuanced differences in the ALE plots of RF and GB compared to those of MARS and GAM in their extrapolations using temperature data with limited or no historical record. This disparity mirrors the scenario observed in Brazil, illustrating a two-fold divergence. The RF and GB models predict a steady demand that remains virtually unchanged above 20 degrees Celsius, while MARS and GAM predict a linear increase in demand with rising temperatures (Fig. V.24). However, the reasons for the uncertainty surrounding Europe's projections diverges from the Brazilian case. In Europe, the primary source of uncertainty stems from the challenge of comprehensively accounting for the influence of residential air conditioning demand. In contrast to regions such as the United States or Japan, where a substantial proportion of households possess air conditioning systems, Europe has not experienced a similar level of adoption. A closer examination of the electricity demand histograms (Fig. V.25) reveals that the demand range between 2090-2100 is even narrower than that observed between 2015 and 2025, despite the anticipated increase in extreme heat events. This incongruity suggests that the current extrapolation assumptions inadequately capture the likely future demand for air conditioning in the region.

This question becomes even more relevant in light of the expected increase in heatwaves across Europe under different climate scenarios, as shown in Figure V.26. In particular, European countries using models derived from the US or Japan, such as Switzerland or countries in the Balkans, show a much more pronounced projected increase in demand. This is in stark contrast to the countries relying on the European model for their demand projections (Fig. V.2). These discrepancies highlight the key influence of regional differences in household equipment, especially air conditioning, and their potential impact on demand projections and resulting CO_2 emissions.

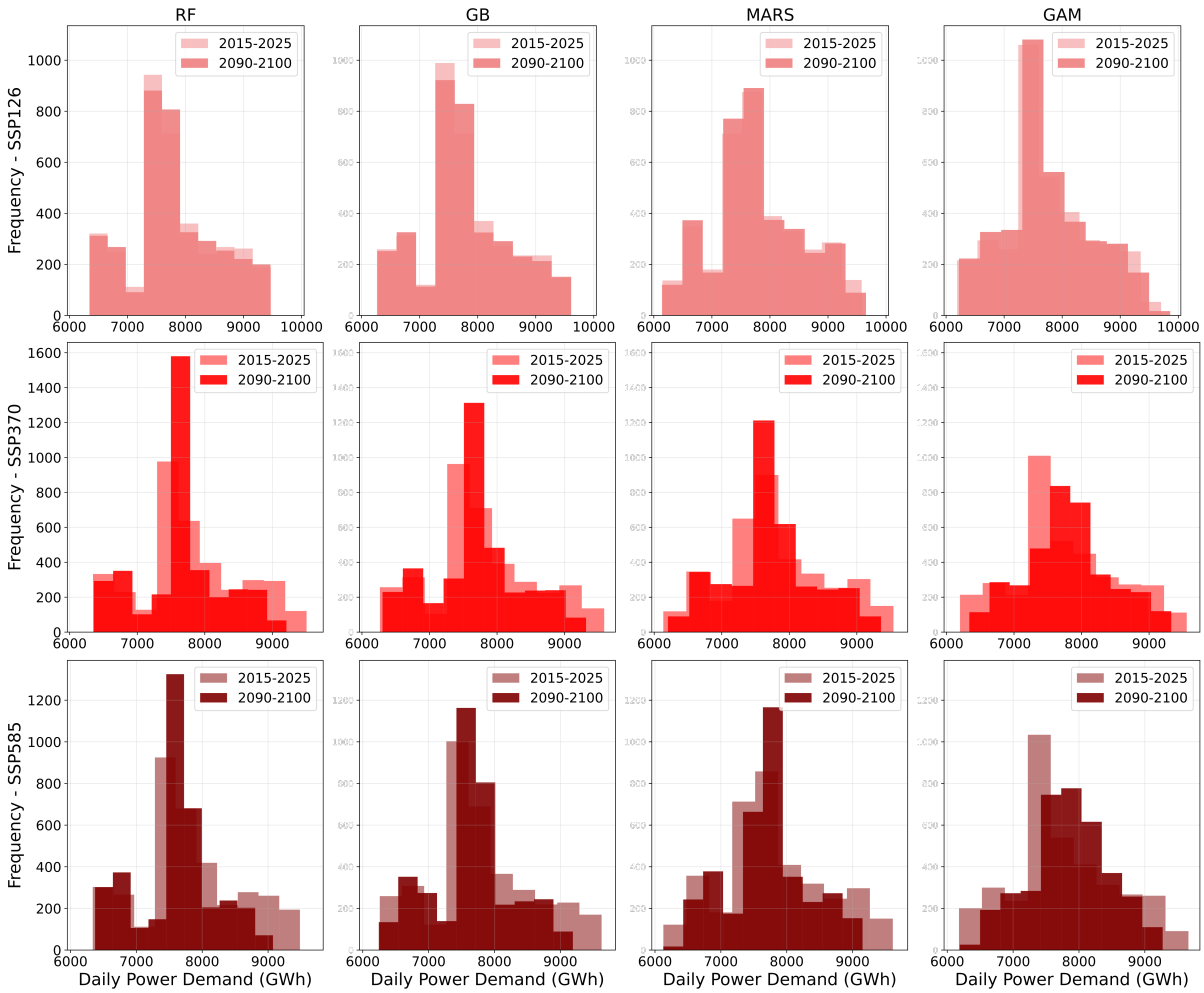

Figure V.25: Histograms representing the distribution of power demand in the European Union for the decades 2015-2025 and 2090-2100 under the three SSPs and across the four ML models, averaged over the five ESMs.

5.3 Major Energy Data Gaps

The difficulty of obtaining accurate data on electricity demand in Africa is a major obstacle to research efforts. Due to the limited availability of reliable data, models from other regions have been used for the majority of African countries. Although a sophisticated k-means clustering approach was used to assign reference countries to these regions, this methodology can only partially alleviate the problem, resulting in significant uncertainties in electricity demand projections. In addition, Africa is currently undergoing a major transformation characterized by the potential for rapid population and GDP growth. For example, the future adoption of household air conditioning has the potential to change the electricity demand landscape significantly. This, combined with the expectation of significant heat waves in the region (Marcotullio et al., 2021; Weber et al., 2020), introduces an additional layer of uncertainty into projections. The complex interplay of these factors underscores the urgent need for further research

and methodological refinement to gain a more comprehensive understanding and anticipatory insight into electricity demand dynamics in Africa.

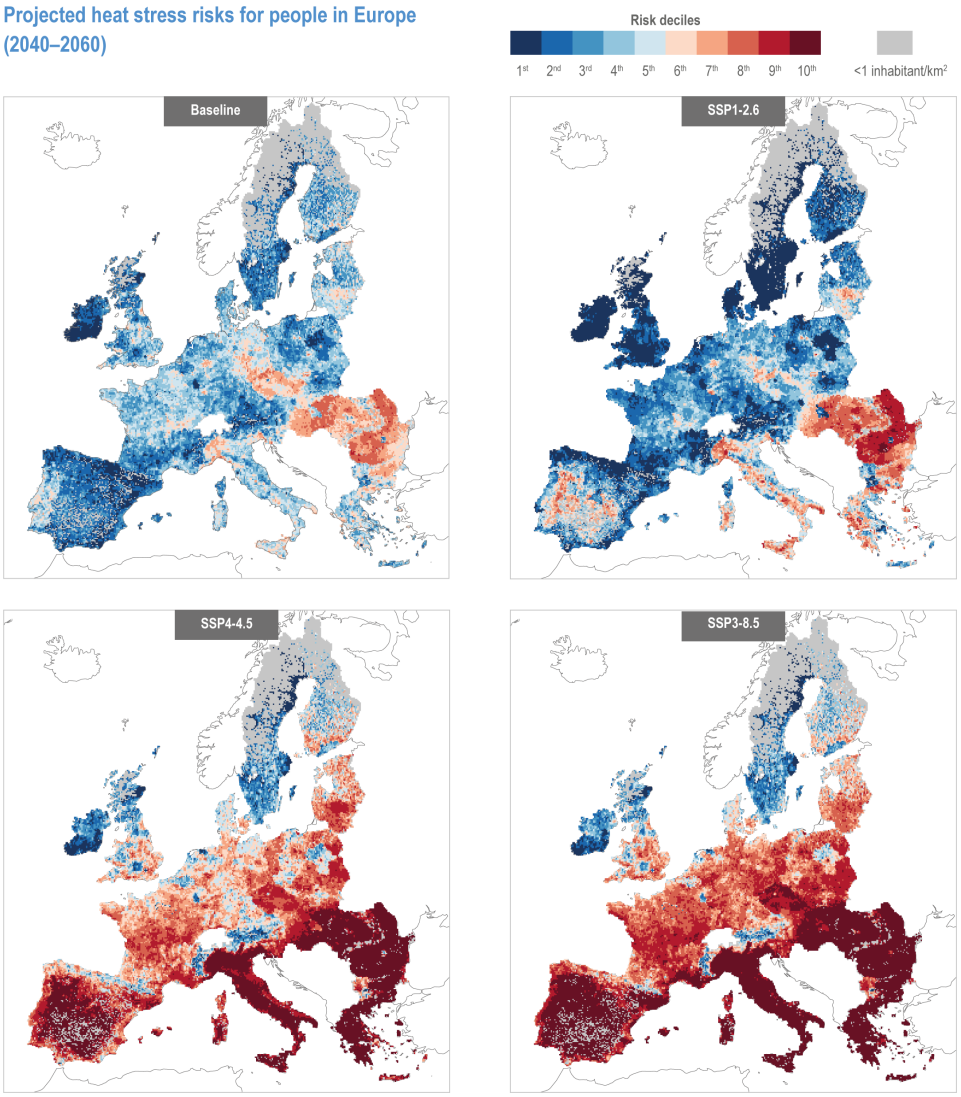

Figure V.26: Heat stress risk scenarios for both the baseline period of 1986–2005 and the 2040–2060 period, considering various SSP–RCP combinations. The calculation combines heatwave days, population vulnerability, and exposure. *Source*: (Bednar-Friedl et al., 2022).

References

Bednar-Friedl, B., Biesbroek, R., Schmidt, D. N., Alexander, P., Børsheim, K. Y., Carnicer, J., Georgopoulou, E., Haasnoot, M., Le Cozannet, G., Lionello, P., Lipka, O., Möllmann, C., Muccione, V., Mustonen, T., Piepenburg, D., & Whitmarsh, L. (2022). Europe. In *Climate change 2022: Impacts, adaptation and vulnerability* (pp. 1817–1927). Cambridge University Press. https://doi.org/10.1017/9781009325844.015

Cannon, A. J. (2018). Multivariate quantile mapping bias correction: An n-dimensional probability density function transform for climate model simulations of multiple variables. *Climatic Dynamics*, *50*, 31–49. https://doi.org/10.1007/s00382-017-3580-6

Cao, D., Zhao, J., Hu, W., Zhang, Y., Liao, Q., Chen, Z., & Blaabjerg, F. (2022). Robust deep gaussian process-based probabilistic electrical load forecasting against anomalous events. *IEEE Transactions on Industrial Informatics*, *18*(2), 1142–1153. https://doi.org/10.1109/TII.2021.3081531

Cucchi, M., Weedon, G., Amici, A., Bellouin, N., Lange, S., Müller Schmied, H., Hersbach, H., & Buontempo, C. (2020). Wfde5: Bias-adjusted era5 reanalysis data for impact studies. *Earth Syst. Sci. Data*, *12*, 2097–2120.

Lange, S. (2019). Trend-preserving bias adjustment and statistical downscaling with isimip3basd (v1.0). *Geoscientific Model Development*, *12*(7), 3055–3070. https://doi.org/10.5194/gmd-12-3055-2019

Lange, S. (2021). Isimip3b bias adjustment fact sheet. https://www.isimip.org/documents/413/ISIMIP3b_bias_adjustment_fact_sheet_Gnsz7CO.pdf

Lange, S., Menz, C., Gleixner, S., Cucchi, M., Weedon, G. P., Amici, A., Bellouin, N., Müller Schmied, H., Hersbach, H., Buontempo, C., & Cagnazzo, C. (2021). Wfde5 over land merged with era5 over the ocean (w5e5 v2.0) [GFZ Data Services]. https://doi.org/10.48364/ISIMIP.342217

Marcotullio, P., Keßler, C., & Fekete, B. (2021). The future urban heat-wave challenge in africa: Exploratory analysis. *Global Environmental Change*, *66*, 102190. https://doi.org/10.1016/j.gloenvcha.2020.102190

Stehfest, E., Vuuren, D., Kram, T., Bouwman, A., Alkemade, R., Bakkenes, M., Biemans, H., Bouwman, A., Elzen, M., Janse, J., Lucas, P., van Minnen, J., Müller, M., & Prins, A. (2014). *Integrated assessment of global environmental change with image 3.0. model description and policy applications*.

Van Vuuren, D., Stehfest, E., Gernaat, D., & et al. (2021). *The 2021 ssp scenarios of the image3.2 model* (tech. rep. No. 4740). PBL Netherlands Environmental Assessment Agency. https://doi.org/10.31223/X5CG92

Weber, T., Bowyer, P., Rechid, D., Pfeifer, S., Raffaele, F., Remedio, A. R., Teichmann, C., & Jacob, D. (2020). Analysis of compound climate extremes and exposed population in africa under two different emission scenarios. *Earth's Future*, *8*(9), e2019EF001473. https://doi.org/10.1029/2019EF001473

WorldBank. (2023). World development indicators. https://databank.worldbank.org/source/world-development-indicators#

Yadav, S., Jain, A., Sharma, K. C., & Bhakar, R. (2021). Load forecasting for rare events using lstm. *2021 9th IEEE International Conference on Power Systems (ICPS)*, 1–6. https://doi.org/10.1109/ICPS52420.2021.9670200

Yang, L., Ren, R., Gu, X., & Sun, L. (2023). Interactive generalized additive model and its applications in electric load forecasting. *Proceedings of the 29th ACM SIGKDD Conference on Knowledge Discovery and Data Mining*, 5393–5403. https://doi.org/10.1145/3580305.3599848

CHAPTER VI

CONCLUSION AND PERSPECTIVES

1 Perspective

1.1 Multi-Country Models: a Possible Solution to Adress Data Limitation

The lack of comprehensive data on the use of air conditioning in parts of the world where it is not yet widespread is one of the main challenges of the study, as discussed previously for Europe. This limitation hinders the accurate modeling of future power demand under extreme heat conditions, which are becoming more frequent due to climate change. The development of multi-country models could help to reduce this data gap issue.

The concept behind multi-country models is relatively simple but has the potential to improve the accuracy of our predictions significantly. The idea is to use the power demand model developed for Europe when temperatures are below a certain threshold, reflecting typical weather conditions in the region. However, when temperatures exceed this threshold, which typically leads to increased air conditioning use, we propose using models from other countries where air conditioning use is already widespread.

Preliminary experiments have been carried out assuming that the EU has the same level of air conditioning as the US. These experiments were conducted by applying the US model to European predictor functions when the average daily temperature exceeds 15°C (Fig. VI.1). All features were normalised to avoid scalability problems. These initial results suggest that

this approach has the potential to compensate for the lack of cooling-related information in Europe. When using the multi-country model, the power demand predictions at temperatures above 15°C become significantly more important, especially for the RF, GB and MARS models. The multi-country model combined with the GAM model showed a more pronounced effect of temperature on electricity demand for May, June, September, and October, although the GAM model initially predicted an increase in electricity demand at temperatures above 15°C.

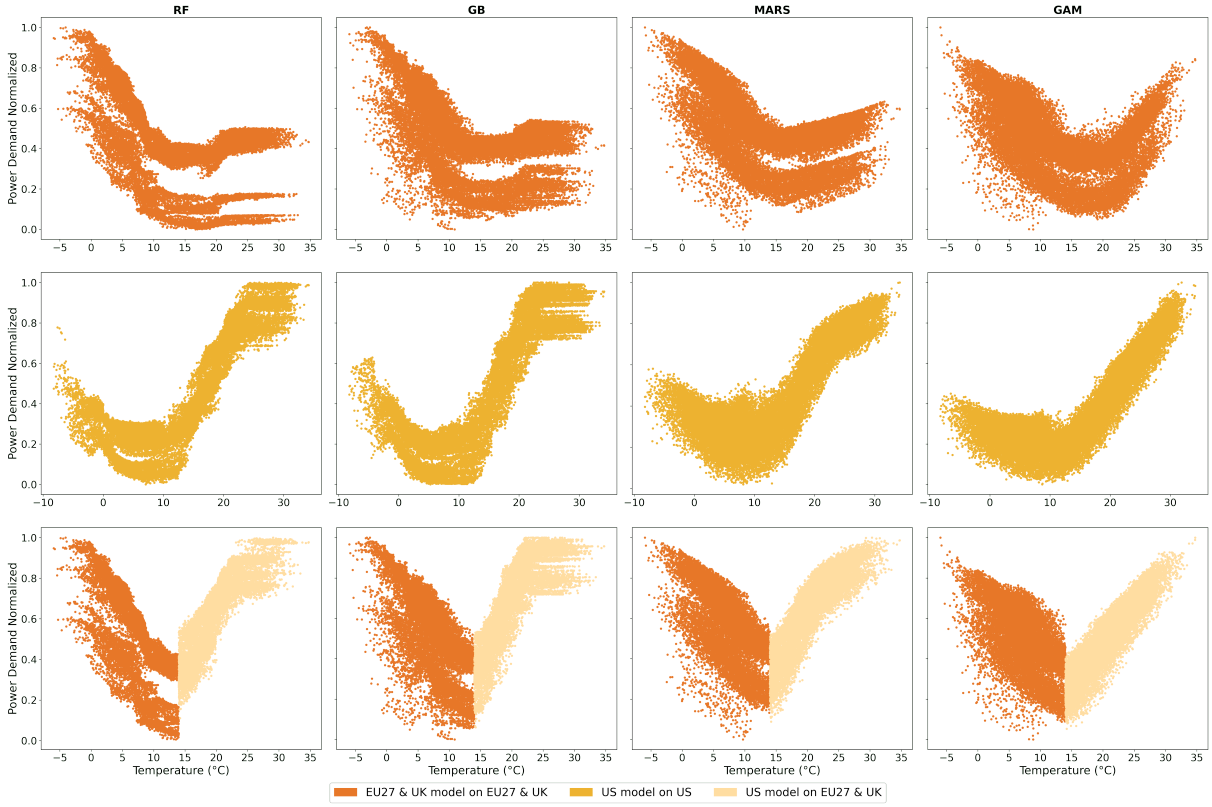

Figure VI.1: Normalized Daily power demand projected with RF, GB, MARS, and GAM versus daily average temperature.

When comparing the monthly power demand projections generated by the multi-country models to those produced by the Europe-only model, a distinct pattern shift emerges for RF, GB, and MARS (Fig.VI.2). The warmest month exhibits a substantial increase in power demand by the end of the century in the case of SSP1-2.6 and SSP5-8.5, whereas the variations in the coldest month remain relatively consistent between the two approaches. This leads to a positive annual change in power demand for the multi-country model, in contrast to the negative change observed for the Europe-only model.

However, a challenge arises at the transition between the EU and US models, i.e., at 15°C, when applied to the European region, particularly for the RF model, where demand becomes more important. Furthermore, unlike Europe the US model does not show two very different behaviors regarding power demand for weekends and working days. This issue underlines

the need to make a well-informed decision on which countries to include in a multi-model framework. In this context, identifying similarities in power consumption across countries and considering adding exogenous features such as other socioeconomic indicators or panel data to capture power demand characteristics better are promising research avenues.

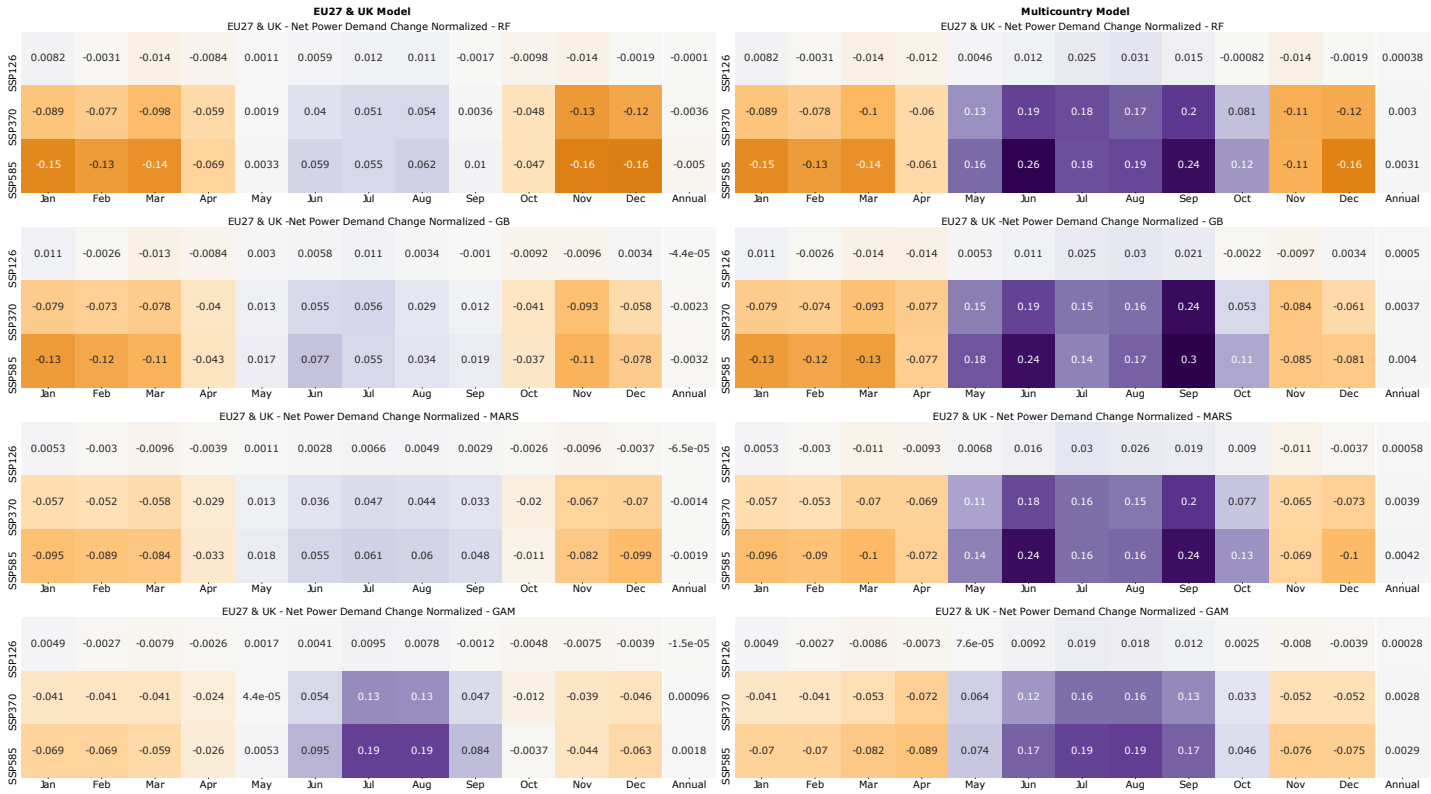

Figure VI.2: Net changes in normalized monthly power demand for EU27 & UK projections of power demand made with only the EU27 & UK model and with the combination of EEU27 & UK and US model.

1.2 Power Demand Extreme Events Models

Another promising avenue for further research is the development of power demand extreme event models. Climate change has a profound impact on the behavior of extreme weather events, in particular heat and cold waves, which can have a significant impact on various sectors, including energy demand and infrastructure resilience. To address this challenge, advanced machine learning methods tailored to extreme event modeling have great potential.

Extensive research has already been conducted in the field of extreme event modeling, particularly in the area of quantile regression. Recent studies such as Fasiolo et al., 2021, Velthoen et al., 2022, and Gnecco et al., 2023, have explored novel ML approaches to improve our under-

standing and prediction of extreme quantiles, which are crucial for assessing and mitigating the impacts of climate-related extreme events.

The application of specifically designed ML methods to power demand extreme event modeling can offer several advantages. It allows for a more nuanced and accurate characterization of power demand during extreme events, enabling better quantification of their probabilities, durations, and intensities.

1.3 Calculate the Potential Feedback of the Additional CO_2 Emissions from Power Production on Global Temperature

The Aggregated Carbon Cycle, Atmospheric Chemistry, and Climate model (ACC2) was used to explore the interaction between power demand and global climate (Tanaka et al., 2007; Tanaka et al., 2018). ACC2, a simple climate model operating on a global annual mean basis, encompasses three key components to represent the carbon cycle, atmospheric chemistry, and climate dynamics. This versatile model allows for examining different scenarios and offers projections for global annual temperatures.

Preliminary calculations were made using ACC2 by adding the additional CO_2 emissions in the previous Chapter to the baseline annual CO_2 emissions. ACC2 was then used to compute the corresponding temperature projections, accounting for the impact of the cumulative additional CO_2 released in the atmosphere. These preliminary results revealed a minimal effect, with a temperature increase of approximately +0.01°C observed across all scenarios. However, it is imperative to interpret these outcomes in light of certain limitations.

First, in these preliminary calculations, the power demand models and ACC2 were not fully coupled, meaning that they did not consider the feedback between them. This simplification might underestimate the cumulative feedback effects that can develop over time.

Second, the additional CO_2 projections used were calculated based on power demand projections obtained with the EU-specific power demand model rather than incorporating the multi-country model suggested earlier. This may result in the omission of potential increased power demand during hot periods, which might result in conservative estimates of CO_2 emissions. Furthermore, the carbon intensity projections could be the subject of further work, as was done for the Qatar study, which could significantly impact the additional CO_2 emissions.

Lastly, these preliminary calculations relied on the average additional CO_2 emissions across

all projection scenarios, encompassing the four ML models and five Earth System Models (ESMs). Given the variance in these projections, different runs could be realized with the different projections. Also, tuning the climate sensitivity in ACC2 to adapt to that of each ESMs could yield more pronounced effects.

While these results are preliminary, they open avenues for future research. The coupling of energy demand models with ACC2 in more comprehensive analyses has the potential to yield more realistic assessments of the feedback loops between energy usage and climate change (Gaucher et al., 2023). Further refinements, including multi-country models and customized adjustments for climate sensitivity, promise to enhance our predictions' accuracy. Nevertheless, it remains unlikely that the feedback loop's impact on global temperature will be substantial.

2 General Conclusion

My Ph.D. research employed machine learning techniques to develop data-driven models capable of simulating daily power demand at regional or national scales. These power demand models relied on predictive features, including climate variables and indicators of human activity, and incorporated a variety of machine learning algorithms of varying complexity. The power demand models were rigorously tested for validity within a comprehensive framework.

Once successfully validated, the power demand models were used to project daily power demand trends up to 2100. These projections were based on the CMIP6 climate projections and included different global warming and socioeconomic scenarios, enabling an assessment of the impact of global warming on future power demand. Detailed examination of these forecasts at a seasonal scale underscored the significance of seasonal variations, especially in temperate regions.

For nations experiencing cold winters, our models projected a decline in electricity demand during winter, primarily attributed to reduced heating demand. In contrast, the forecasts indicated an increase in demand during the summer months, driven by the growing need for air conditioning. On an annual basis, the results exhibited three primary trends across countries.

First, potential annual increases of up to +20% were identified in countries with significant projected increases in electricity demand. This upward trend is mainly due to increasing demand for air conditioning in response to rising temperatures, particularly in hot climate countries in tropical regions. Second, we identified a projected decrease in electricity demand for some countries, typically those at higher latitudes with colder climates. This decline was asso-

ciated with a larger reduction in winter heating demand compared to the increase in summer electricity demand. Finally, countries with relatively stable or slightly fluctuating electricity demand patterns were identified, mainly influenced by increasing demand for air conditioning, offset by decreasing demand for heating.

Drawing from the electricity demand projections, calculations were conducted to quantify the CO_2 emissions originating from electricity generation necessary to fulfill this demand. This involved assessing the carbon intensity associated with electricity production, enabling us to estimate the additional CO_2 emissions attributable to global warming effects. Only a select few countries displayed notable increases in CO_2 emissions due to global warming. These nations, including China, India, the United States, and Brazil, saw a collective increase in the order of several gigatonnes over the entire projection period.

Conversely, Russia and Europe demonstrated decrease in CO_2 emissions resulting from global warming. Nevertheless, the additional CO_2 emissions, whether positive or negative, remained relatively modest when contrasted with the total annual CO_2 emissions stemming from electricity generation activities. Consequently, the effect of these additional CO_2 emissions on global temperature remains negligible.

Two case studies, Qatar and Japan, played a pivotal role in shaping the overarching methodology adopted for all countries. These case studies not only served as initial use cases but also served as exemplars of the potential applications of our data-driven approach. In particular, the Japanese case study illustrated the possibility of exploring the day-to-day variations in carbon intensity.

Nevertheless, it is imperative to acknowledge several limitations in this research, mainly due to the limited data availability. It is therefore important to treat the projections generated by our models with a degree of caution. Exploratory approaches such as multi-country modeling, collecting data from regions with large data gaps, improving the accuracy of carbon intensity projections as demonstrated in the case of Qatar, or improving the accuracy of extreme event models are promising ways to increase the reliability and confidence of electricity demand and CO_2 emission projections obtained with the approach developed for this thesis.

References

Fasiolo, M., Wood, S. N., Zaffran, M., Nedellec, R., & Goude, Y. (2021). Fast calibrated additive quantile regression. *Journal of the American Statistical Association*, *116*(535), 1402–1412. https://doi.org/10.1080/01621459.2020.1725521

Gaucher, Y., Tanaka, K., Johansson, D., Goll, D., & Ciais, P. (2023). Leveraging ecosystems responses to enhanced rock weathering in mitigation scenarios. *PREPRINT (Version 1) available at Research Square*. https://doi.org/https://doi.org/10.21203/rs.3.rs-3145606/v1

Gnecco, N., Terefe, E. M., & Engelke, S. (2023). Extremal random forests.

Tanaka, K., Kriegler, E., Bruckner, T., Hooss, G., Knorr, W., & Raddatz, T. (2007). Aggregated carbon cycle, atmospheric chemistry, and climate model (acc2) – description of the forward and inverse modes. *Reports on Earth System Science*, *40*, Max Planck Institute for Meteorology, Hamburg.

Tanaka, K., & O'Neill, B. (2018). The paris agreement zero-emissions goal is not always consistent with the 1.5 and 2°c temperature targets. *Nature Climate Change*, *8*, 319–324. https://doi.org/10.1038/s41558-018-0097-x

Velthoen, J., Dombry, C., Cai, J.-J., & Engelke, S. (2022). Gradient boosting for extreme quantile regression.

APPENDIX A: CASE STUDY ARTICLES

1 Supplementary Material of Article 1

Supplementary Material

Validation of the model

To evaluate the model, we applied it to the 2016 daily mean temperature data and recalculated the demand. We then compared the modeled electricity demand with the observed one. There is a very strong correlation coefficient for the linear regressions between the electricity demand modeled and observed (r^2 = 0.95 and RMSEn = 0.055 for daily total load and r^2 = 0.96 and RMSEn = 0.053 for daily maximum hourly load, cf. Figure S1).

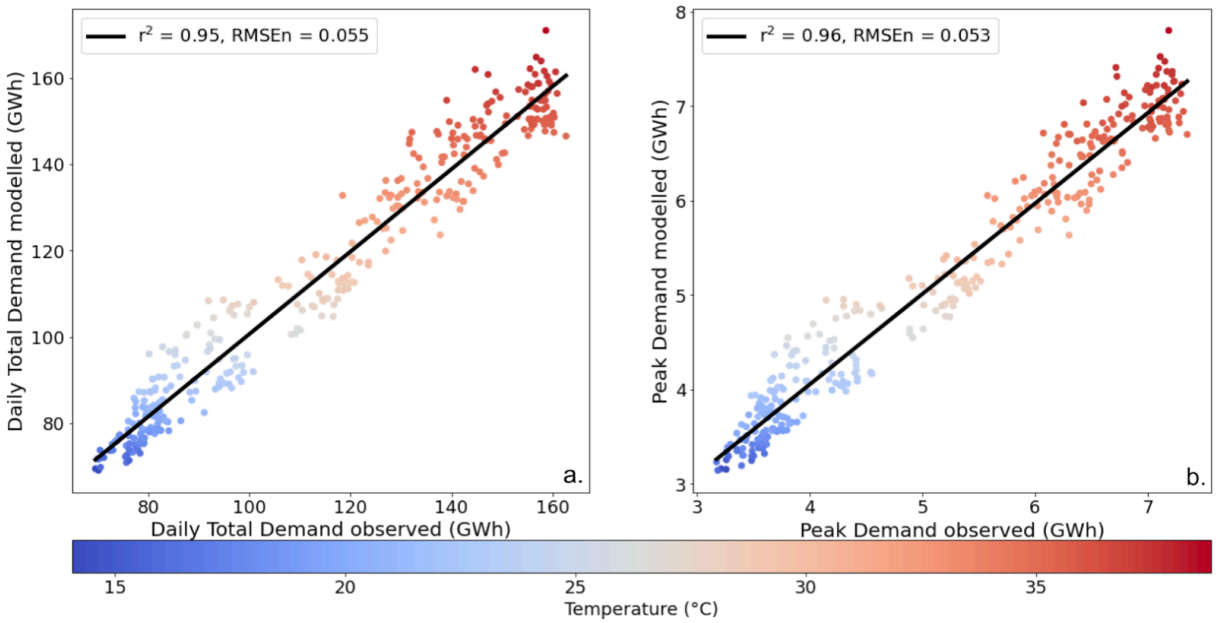

Figure S1. *Actual electricity demand modeled versus electricity demand observed in Qatar for the year 2016 for daily total demand (a) and peak demand (b). Colors indicate the daily average temperature in Qatar.*

Few official data are available to compare our results with observation but the state-owned Qatari company Kahramaa, the sole producer of electricity in Qatar, published reports on its activity[28]. In particular, they released figures for the annual electricity generation in Qatar for the years 2015 to 2019, with the average for these 5 years at 45,430 GWh. The order of magnitude is consistent with our estimate. In 2014 Qatar's government also published its monthly statistics report in which they released their monthly electricity generation[29]. We did a cross-validation of our results by aggregating them by month and comparing them to the government's data (cf. Figure S2). We model well the seasonal variability and our orders of magnitude are accurate. Visually it seems that our results are closer to the observations when we take into account only the effect of temperature and not the population and the GDP. The difference between our results and the observations seems to be slightly overestimated for the warmest (June, July, August) and coldest (November, December, January)months, respectively. Biases have been quantified for these two categories of months and for the simulation temperature only and the simulation temperature + population + GDP (Table S1).

	Temperature only	Temperature + population + GDP
Cold months	-0.4%	0.6%
Hot months	-1.9%	4.1%

Table S1. *Biases for cold and hot months (November, December, January and June, July, August, respectively) for the simulation with only the effect of temperature on the demand and the one with the effect of temperature, population, and GDP expressed in percentage of difference with the government data.*

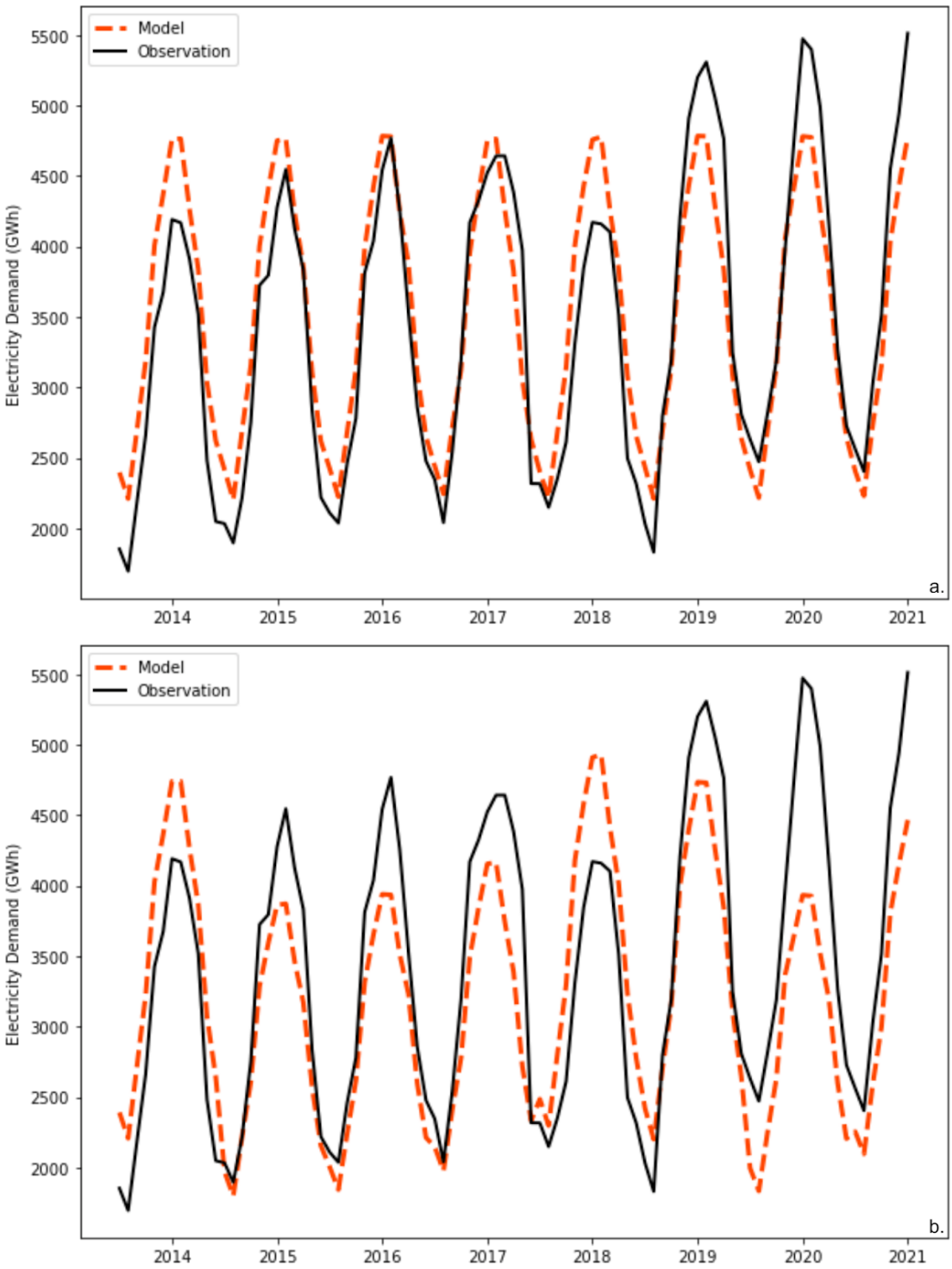

Figure S2. *Comparison of monthly electricity demand reported by the Qatari government (black curves) and modeled monthly demand (dashed red curves) with the effect of (a) temperature and (b) temperature, GDP, and population. The years indicate the month of June.*

We have defined two categories of days: extremely cold days with an average temperature under 14.1°C, the 2016 minimal average daily temperature, and extremely hot days above 38.8°C, the 2016 maximum daily average temperature. The values of the electricity demand calculated with our model for these days are to be taken with precaution, as they are extrapolated to a domain without data. Table S2 shows the percentage these days represent for the period 1980 - 2100. We can see that for all SSP, there are many more extremely hot days than extremely cold days, and the number of extremely cold days stays constant (around 0.2%). In contrast, the number of extremely hot days increases with the radiative forcing and goes from 1.2% for SSP126 to 11.5% for SSP585.

	SSP 126	SSP 245	SSP 370	SSP 585
Extremely cold days	0.27%	0.21%	0.22%	0.20%
Extremely hot days	1.2%	7.6%	9.3%	11.5%

Table S2. *Percentage of extremely cold days (under 2016 minimal daily average temperature, i.e., 14.1°C) and extremely hot days (above 2016 maximum daily average temperature, i.e., 38.8°C) for the different SSP for the whole period of study (1980 - 2100).*

The model presented in this study is a statistical model based on electricity demand and temperature data. To develop this model, we only had electricity consumption data for one year, which was sufficient to produce a very robust relationship between electricity demand and temperature (r^2 = 0.95, RMSEn = 0.057). On the other hand, we do not have enough data on electricity demand during hot or cold waves if we want to look more closely at the response of the electricity demand to extreme temperature events, which is why in our study of extreme annual temperature and electricity demand (section 3.1.2) we took the 5% highest and lowest temperatures and not only the highest or lowest temperature of the year. Little data is available to validate the electricity demand model. By aggregating our results by year and by month, we were able to compare them to the limited data on electricity demand disclosed by the government and the company Kahramaa which allowed us to validate our model, at least in terms of order of magnitude with a mean bias of ±4.1% by year (section 3.1.1). But for the study of extreme temperature and the calculation of CO_2 emissions associated with the production of electricity in Qatar, it would seem that this study is the first of its kind.

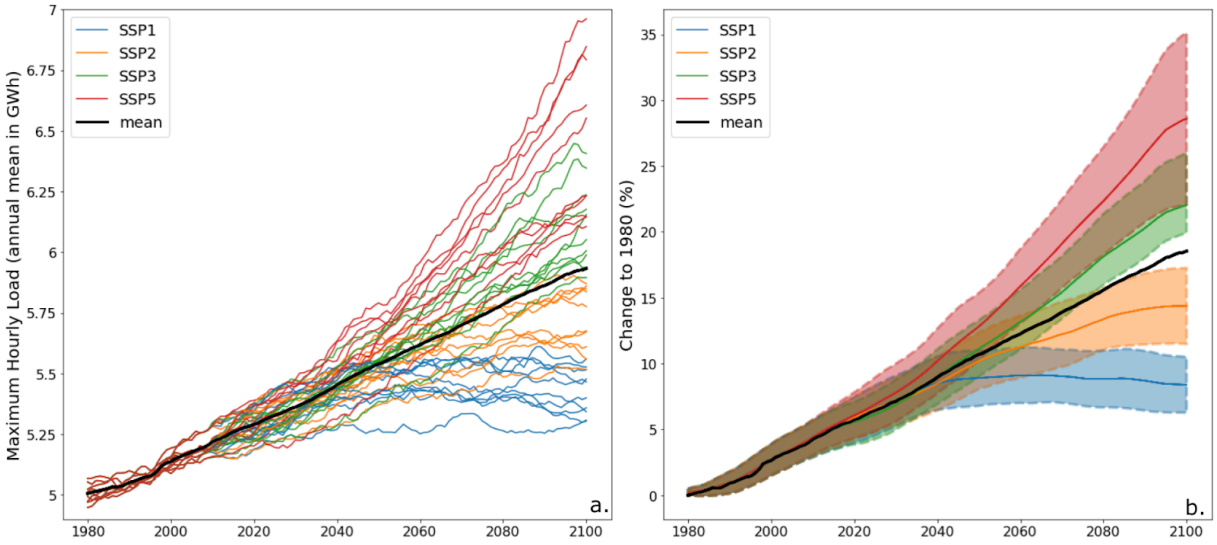

Figure S3. *Daily maximum hourly demand (annual average) calculated with the quadratic model (cf. equation 3) that simulates the effect of temperature on the demand. On panel a, each curve represents the results obtained with one of the 10 models for each SSP with10-year rolling average. On panel b, it is the change in demand compared to the year 1980 (in percentage) that is represented. The thick colored lines show the average of the different SSP and the colored areas the interval in which the 1- error is included.*

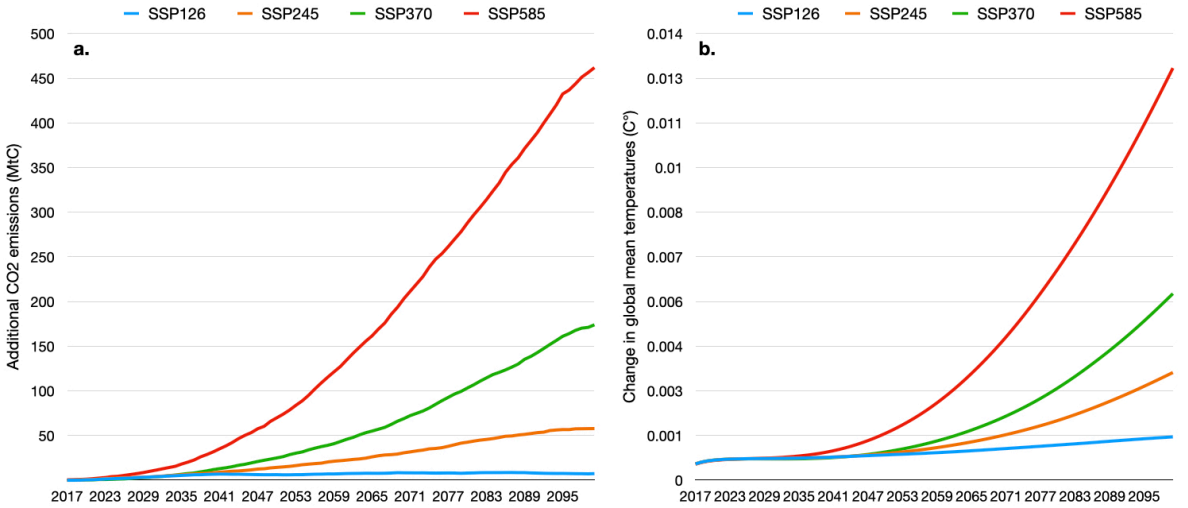

Figure S4. *Additional CO_2 emissions (a) and the resulting global temperature change (b) obtained when we add the temperature feedback on electricity demand compared to a baseline scenario with no effect of temperature on the demand. The additional CO_2 emissions are obtained by taking the difference between the CO_2 emissions calculated with the method described in the article, i.e., by taking into account the effect of the variation over time of the 4 factors (temperature, population, GDP, and carbon intensity) and the CO_2 emissions calculated in the same way but by keeping the temperature at the 2016 level. The additional temperature change is obtained by using the simple climate model ACC2 with these additional CO_2 emissions (see main text).*

2 Supplementary Material of Article 2

Supplementary Materials

S1. Human climate exposure indices (Thom 1959, Sohar et al. 1963, Epstein et al. 2006, Buzan et al. 2014, Maia-Silva et al. 2020)

- Dew point temperature: $T_d = T - (\frac{100 - RH}{5})$, where T is the ambient air temperature and RH the relative humidity
- Wet bulb temperature :
  $T_w = T \times arctan(0.151977 \times (RH + 8.313659)^{1/2}) + arctan(T + RH)$
  $-arctan(RH - 1.676331) + 0.00391838 \times j^{3/2} \times arctan(0.023101 \times j) - 4.686035$
- Discomfort Index with T in degrees Celsius: $DI = 0.5T_w + 0.5T$
- Humidex : $Hx = T + \frac{5}{9}(\frac{e_{RH}}{100} - 10)$
- Heat Index :
  $-42.379 + 2.04901523 \times T_f + 10.14333127 \times RH - 0.22475541 \times T_f \times RH$
  $-6.83783 \times 10^{-3} \times T_f^2 - 5.481717 \times 10^{-2} \times RH^2 + 1.22874 \times 10^{-3} \times T_f^2 \times RH$
  $+8.5282 \times 10^{-4} \times T_f \times RH^2 - 1.99 \times 10^{-6} \times T_f^2 \times RH^2$ Where T_f is the ambient air temperature in Fahrenheit degrees

S2. Table referencing power companies in Japan

Region	Company	Website	Type of energy supply
Hokkaido	Hokkaido Electric Power Co., Inc.	http://www.hepco.co.jp/english/	Fossil fuel, Biothermal, Photovoltaic, Wind Hydroelectricity, Geothermal, PSH
Tohoku	Tohoku Electric Power Co., Inc	https://www.tohoku-epco.co.jp/english/	Fossil fuel, Biothermal, Photovoltaic, Wind Hydroelectricity, Geothermal, PSH
Tokyo	Tokyo Electric Power Company Holdings	https://www.tepco.co.jp/en/hd/index-e.html	Fossil fuel, Biothermal, Photovoltaic, Wind Hydroelectricity, PSH
Hokuriku	Hokuriku Electric Power Company	https://www.rikuden.co.jp/english/	Fossil fuel, Biothermal, Photovoltaic, Wind Hydroelectricity, PSH
Kansai	Kansai Electric Power Co., Inc.	https://www.kepco.co.jp/english/	Fossil fuel, Photovoltaic, Wind Hydroelectricity, PSH, Nuclear

Region	Company	Website	Type of energy supply
Chubu	CHUBU Electric Power, Inc.	https://www.chuden.co.jp/english/	Fossil fuel, Photovoltaic, Wind Hydroelectricity, PSH
Shikoku	YONDEN Shikoku Electric Power CO.,Inc.	https://www.yonden.co.jp/english/index.html	Fossil fuel, Biothermal, Photovoltaic, Wind Hydroelecitricty, PSH, Nuclear
Chugoku	The Chugoku Electric Power co.,inc	https://www.energia.co.jp/e/	Fossil fuel, Biothermal, Photovoltaic, Wind Hydroelectricity, PSH
Kyushu	KYUSHU ELECTRIC POWER CO., INC.	https://www.kyuden.co.jp/english_index.html	Fossil fuel, Biothermal, Photovoltaic, Wind Hydroelectricity, Geothermal, PSH, Nuclear
Okinawa	The Okinawa Electric Power Company, Inc.	http://www.okiden.co.jp/en/	Fossil fuel, Biothermal, Photovoltaic, Wind Hydroelectricity

Table S1. List of power companies in Japan and their website. PSH = Pumped Storaged Hydroelectricity

S3. Model development and selection

	In-R2	Out-R2	In-MAPE	Out-MAPE	In-RMSE	Out-RMSE
Power Demand (MWh)						
Random Forest	0.98	0.83	0.01	0.04	5041	13762
Gradient Boosting	0.79	0.76	0.05	0.05	15648	16773
MARS	0.97	0.84	0.01	0.04	5264	13579
Carbon Intensity (gCO_2eq/kWh)						
Random Forest	0.91	0.32	0.03	0.07	17	45
Gradient Boosting	0.38	0.31	0.07	0.07	44	45
MARS	0.91	0.26	0.03	0.07	17	46

Table S2. Algorithm evaluation metric, average of the ten regions. "In" are for the training dataset and "Out" for the test dataset.

Note that the average daily power demand per inhabitant varies from 10 to 50 kWh across months and regions, and the carbon intensity from 400 to 700 gCO2eq/kWh.

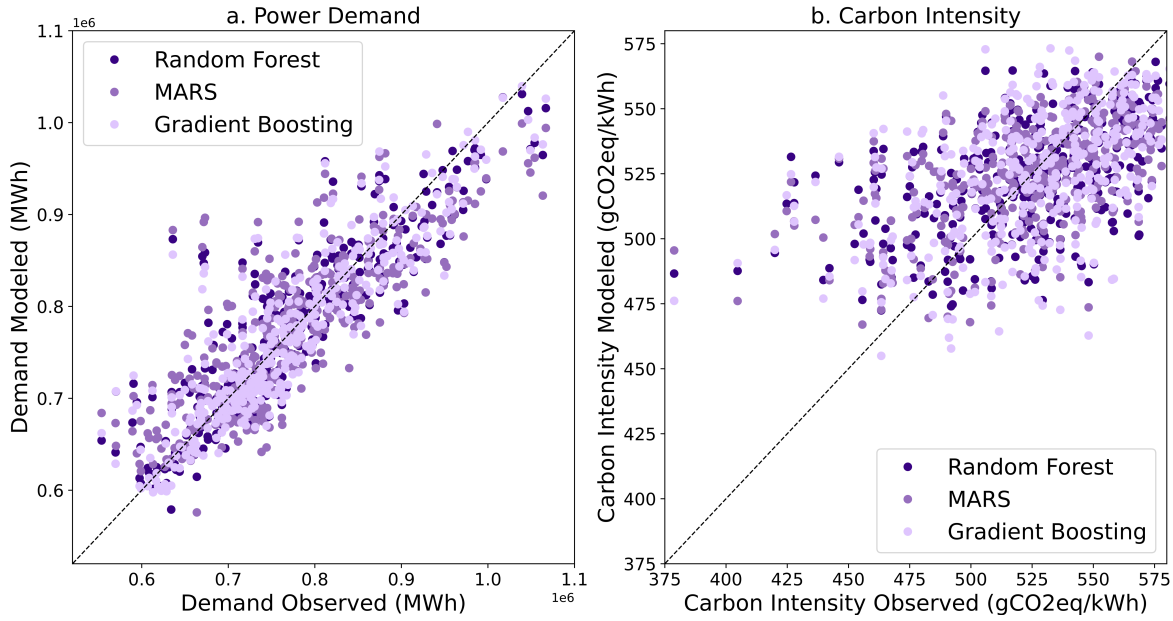

Figure S1. Scatter plots of power demand (a) and carbon intensity (b) modeled as a function of the demand observed for the test sample. Blue circles represent the results obtained with the random forest method, orange with the MARS, and green with the gradient boosting. The results shown here are for the Tokyo region.

S4. Calculation of carbon intensity projection

The carbon intensity of power generation was calculated by dividing the CO_2 emissions from power generation by the power generation from the IMAGE 3.2 model (Van Vuuren et al. 2021). The regional carbon intensity projections were also obtained, assuming the current ratios will hold over this century. For SSP370 and SSP585, we use the projections for the baseline scenarios since the forcing reaches a very high level at the end of this century. For SSP1, we use the average of four scenarios from the IMAGE 3.2 model: SSP1_SPA1_26l_D, SSP1_SPA1_26l_LI, SSP1_SPA1_26l__RE, and SSP1_SPA1_26l_LIRE. These four scenarios integrate negative emissions from carbon sequestration with BECCS (BioEnergy with Carbon Capture and Storage). As we do not assume BECCS implementation in our SSP126 scenario, we calculate the carbon intensity of power generation without considering the negative emissions. Assuming linear relationships between power demand and population and between power demand and GDP, we independently calculated the evolution of demand related to the evolution of these two factors.

S5. ERA5 and ISIMIP models intercomparison.

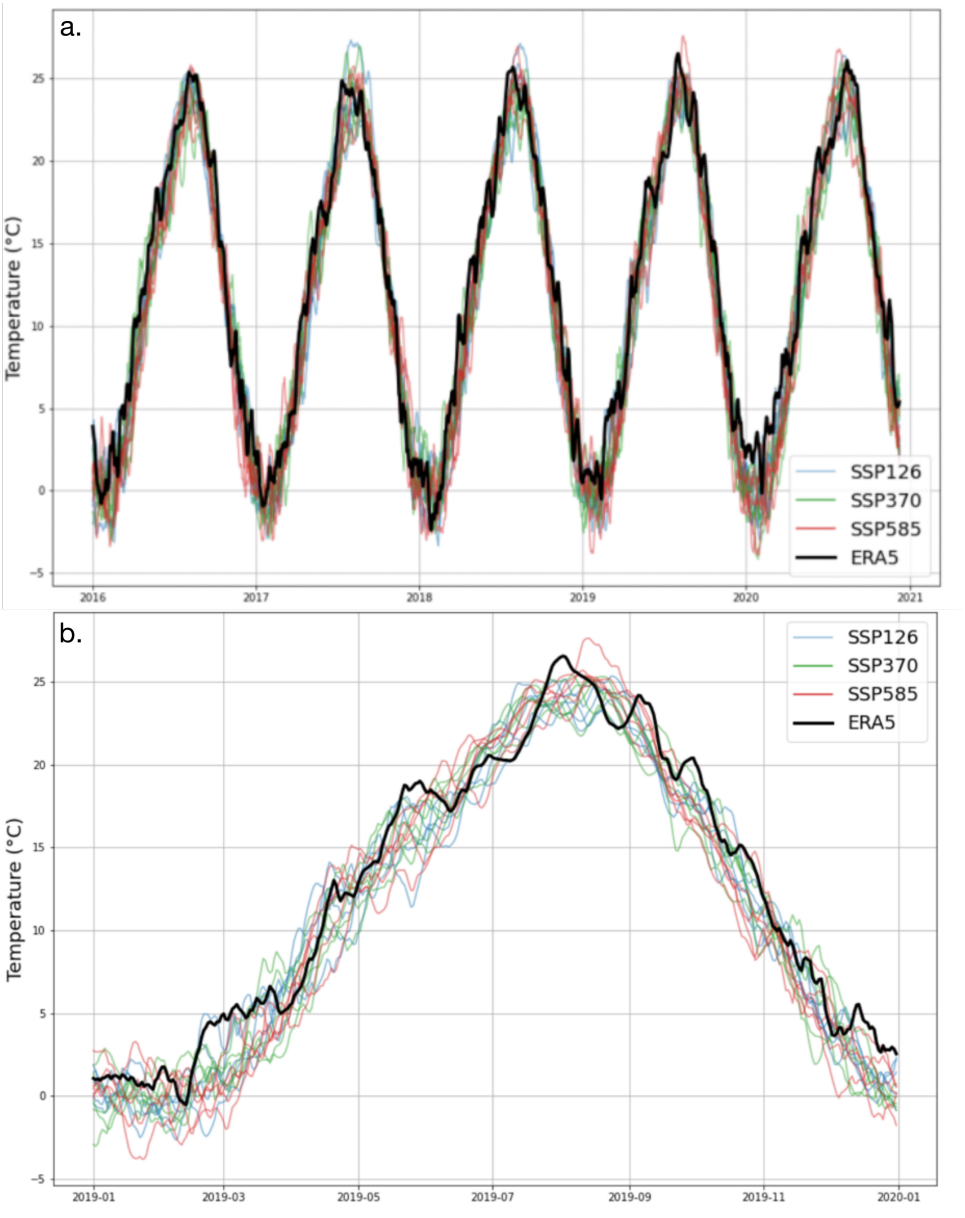

Figure S2. (a) Averaged daily temperature over Japan from 2016 to 2020. The ERA5 reanalysis data is represented by the black thick line, while the five ISIMIP models are depicted by thin colored lines, with each color representing a different SSP. (b) Averaged daily temperature over Japan for the year 2019. The ERA5 reanalysis data is shown by the black thick line, and the five ISIMIP models are indicated by thin colored lines, with each color corresponding to a specific SSP.

S6. Partial dependence plots and Shapley Values for all regions

S3a. Hokkaido

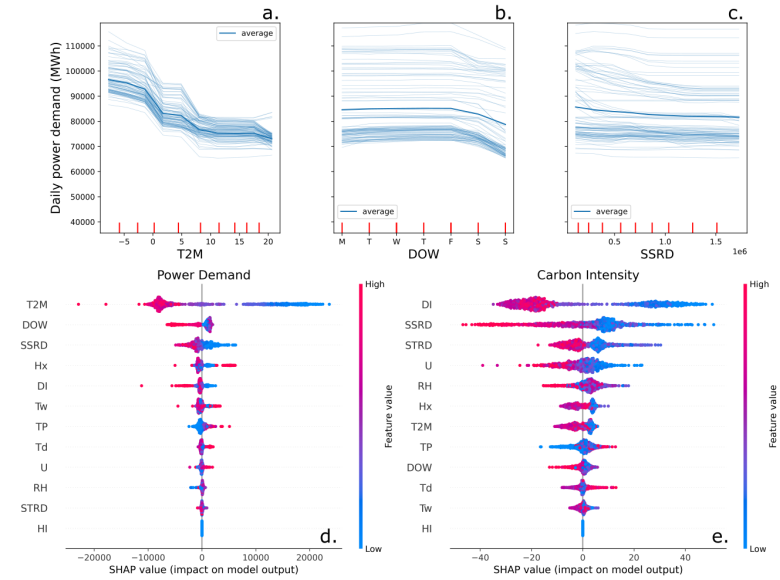

S3b. Tohoku

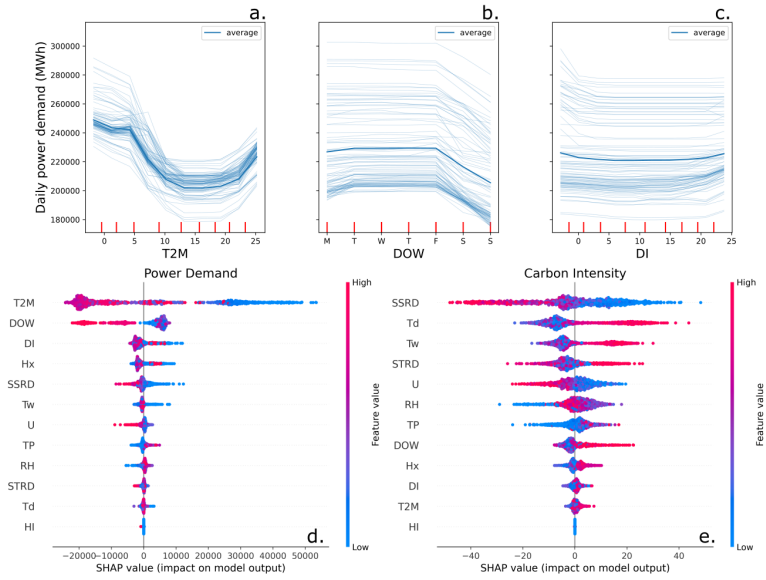

S3c. Hokuriku

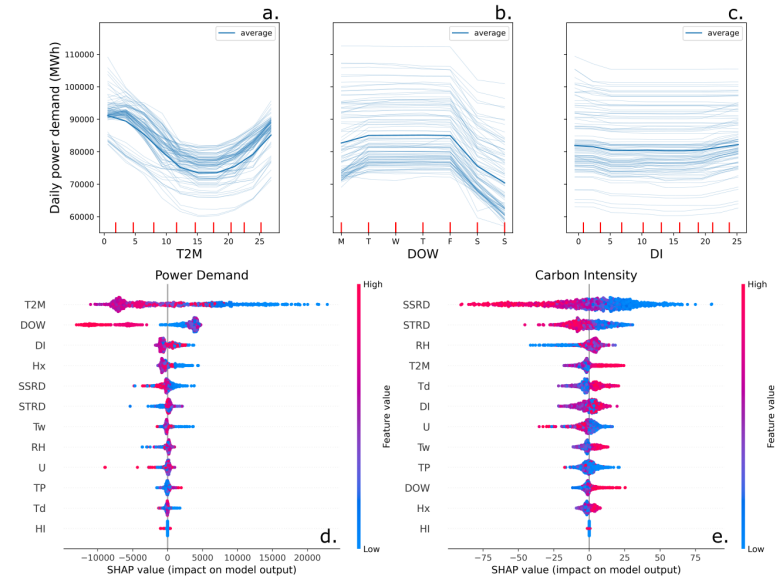

S3d. Tokyo

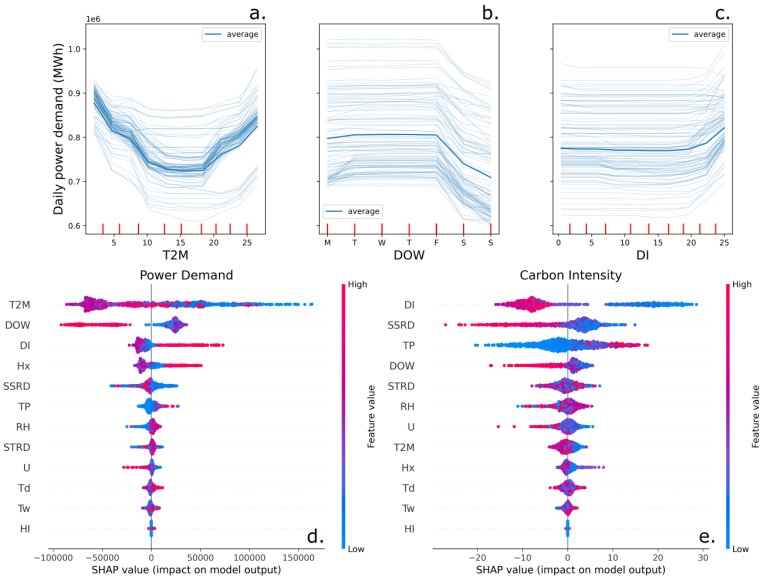

S3e. Chubu

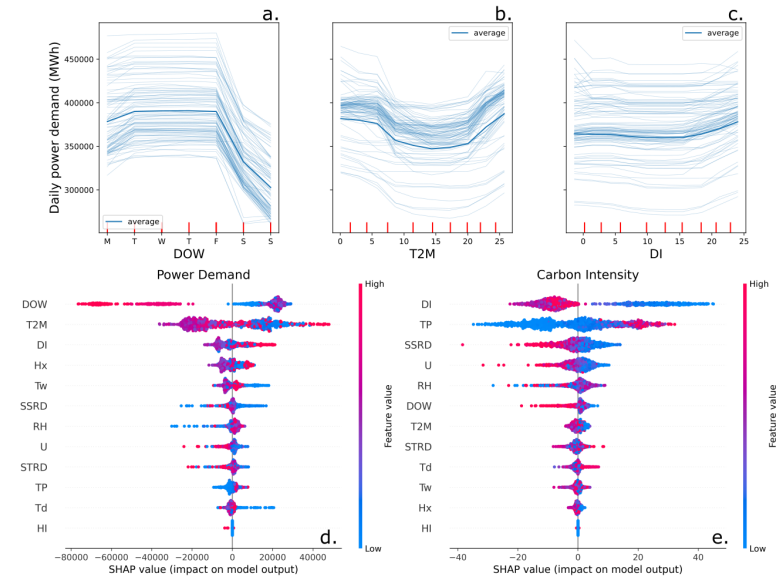

S3f. Kansai

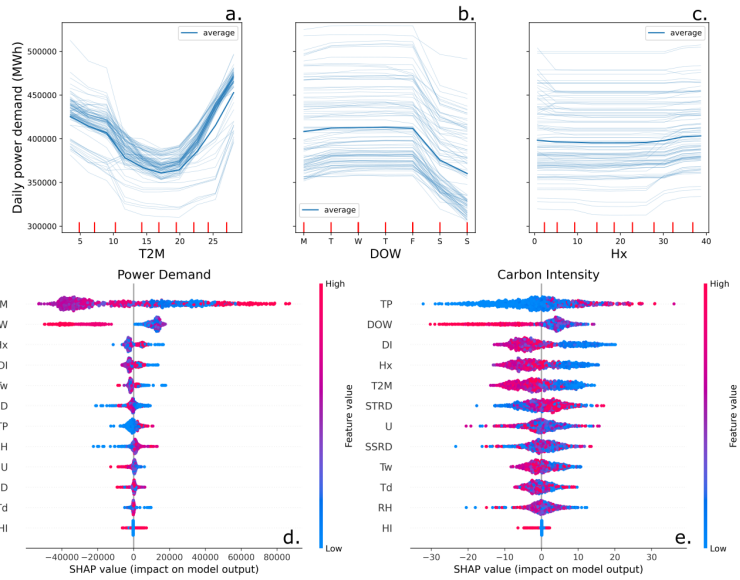

S3g. Chugoku

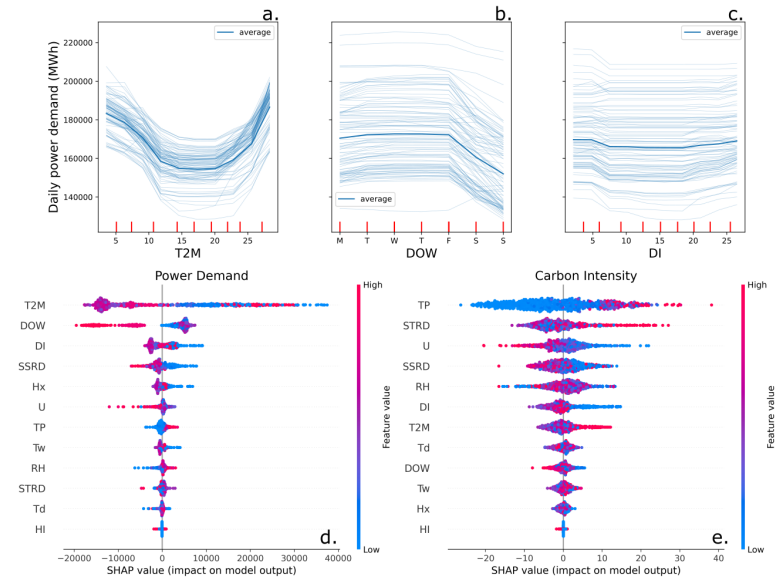

S3h. Shikoku

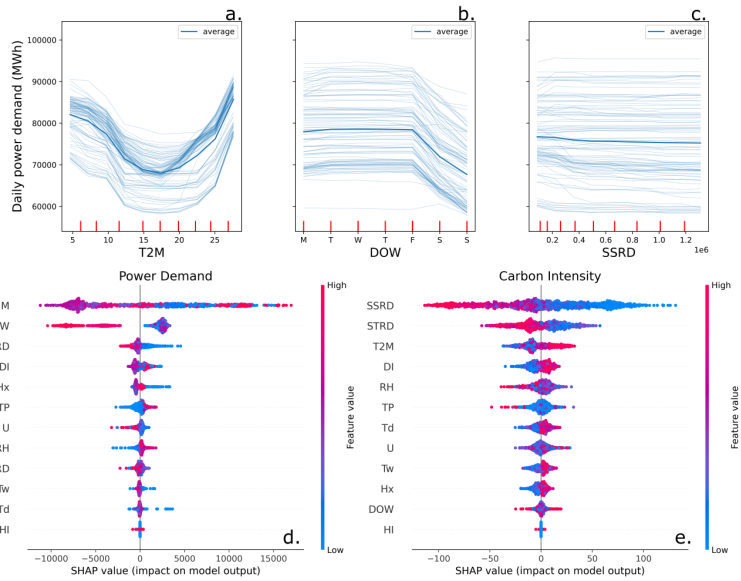

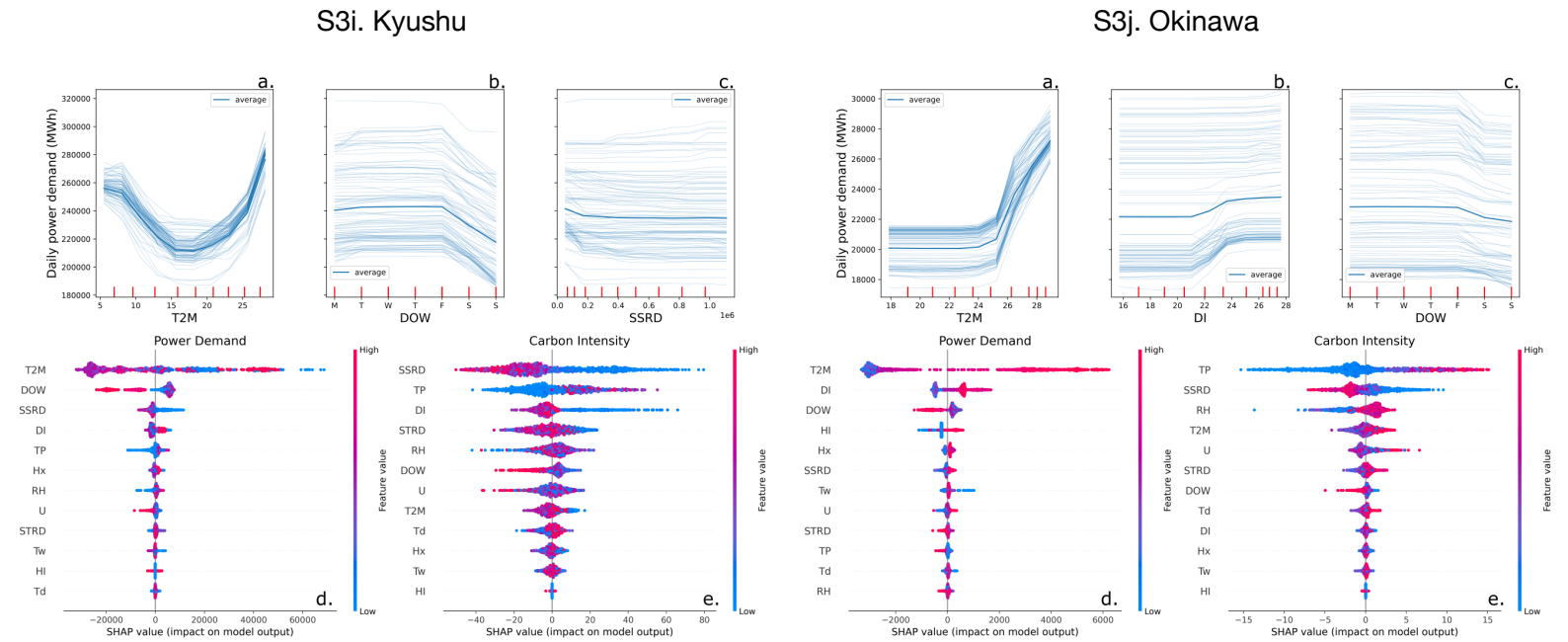

Figure S3a-j. Partial dependence plot (thick line) and Individual Conditional Expectation plots (thin lines) for 100 observations for the three main predictors explaining the power demand in the ten studied regions. For the predictor DOW, the letters indicate the days of the week. The vertical red bars show the dataset's predictor values distribution. The lower panels represent the Shapley values for each predictor and each observation for power demand (d) and carbon intensity (e) for all regions.

S7. CO_2 emissions with and without climate change effect

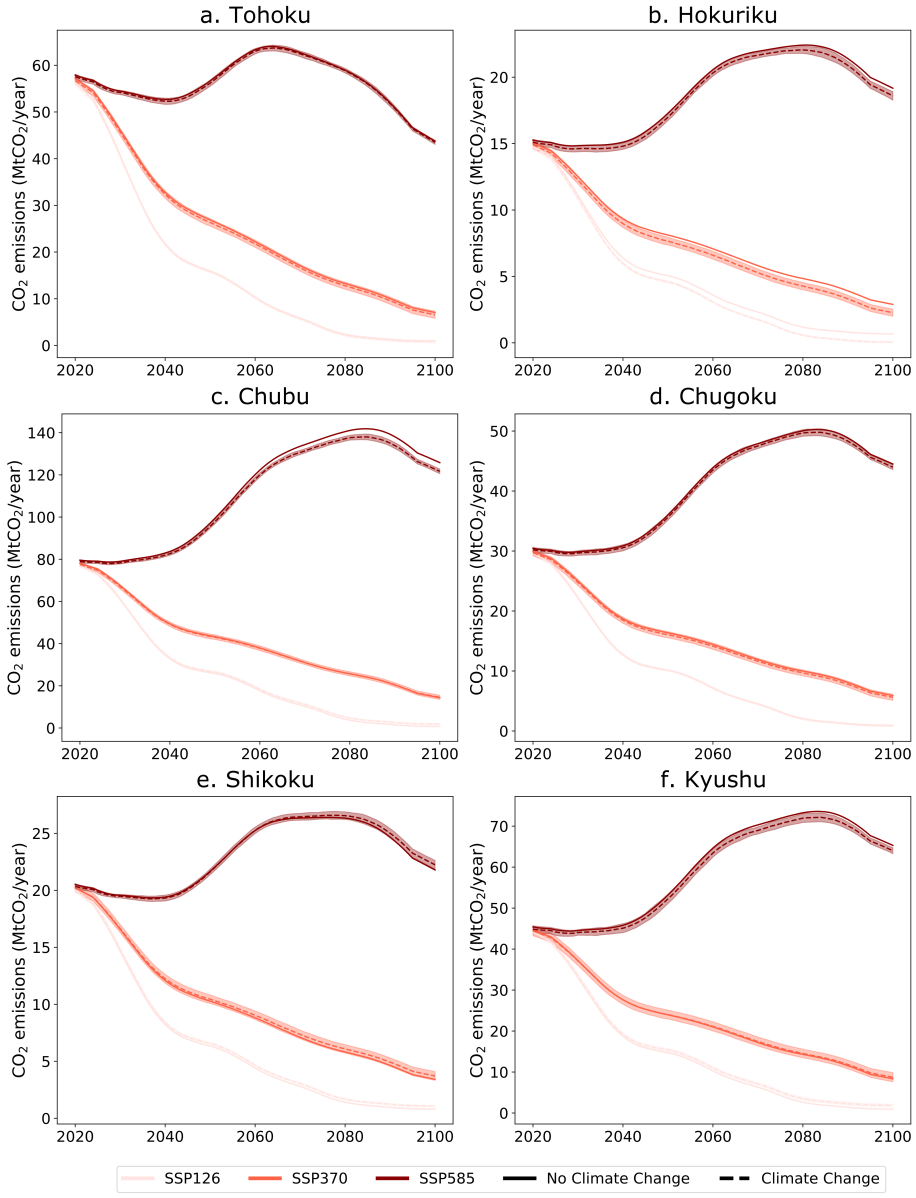

Figure S4. Annual CO_2 emissions from power production under SSP126, SSP370, and SSP585, after taking into account the effect of socio-economic factors with (dashed line) and without (direct line) the effect of climate change for six regions: Tohoku (a), Hokuriku (b), Chubu (c), Chugoku (d), Shikoku (e) and Kyushu (f). The shaded area represents the 1-sigma standard deviation from the five climate models for the climate-change effect curves.

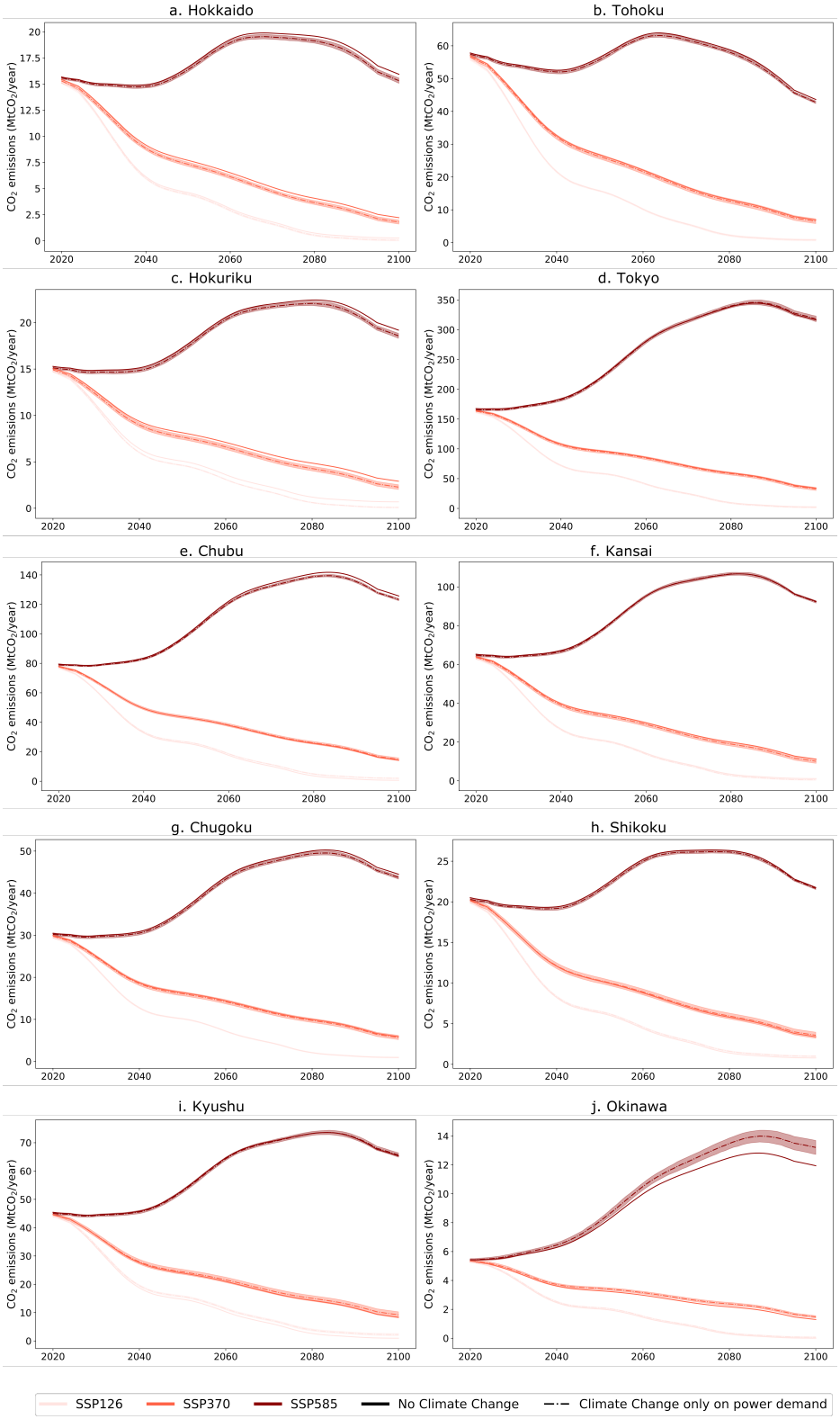

Figure S5. Annual CO_2 emissions from power production under SSP126, SSP370, and SSP585, after taking into account the effect of socio-economic factors with the effect of climate change only on power (dashed line) and without climate change (direct line). The shaded area represents the 1-sigma standard deviation from the five climate models for the climate-change effect curves.

S8. Effect of hot and cold periods on the demand

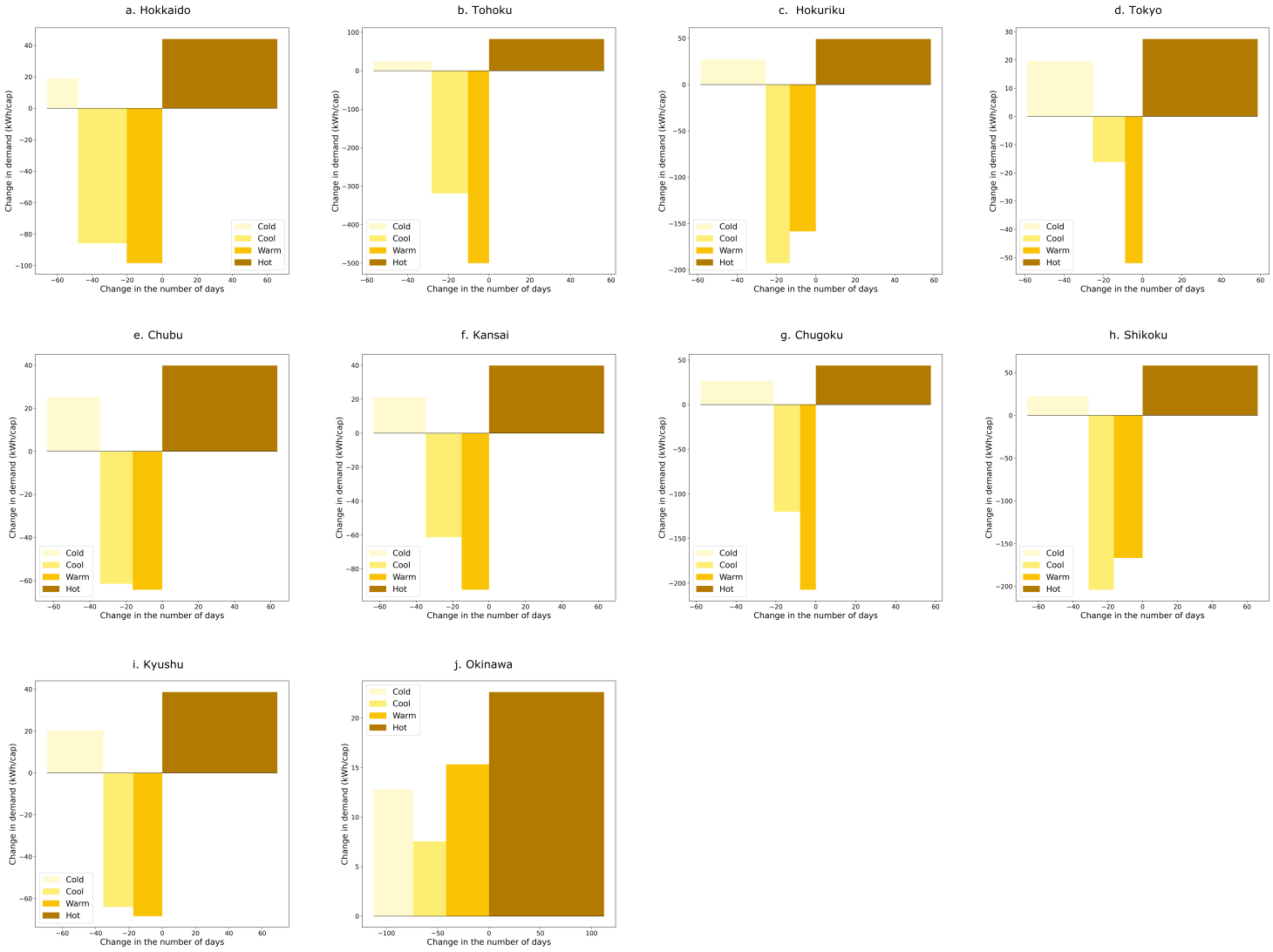

Figure S6. Contribution of cold, cool, warm, and hot days to the change in power demand per capita between the years 2020-2030 and 2090-2100 in four regions (a.) Hokkaido, (b.) Tokyo, (c.) Kansai, and (d.) Okinawa. We represent here the annual average. Cold days are when the temperature is below the 5th percentile. Cool days are when it is between the 5th and the 50th percentile. Warm days are between the 50th and the 95th percentile. Hot days are when it is above the 95th percentile. The percentiles are calculated for each region with their 2016-2020 temperature distribution. The x-axis is the change in the number of days in the four categories, and the y-axis represents the daily change in power demand per capita between the two periods. The area of each rectangle is the average absolute contribution of each category of days to the change in demand. The black dotted line represents the total change in power demand between the two periods.

S9. Monthly change in power demand and carbon intensity

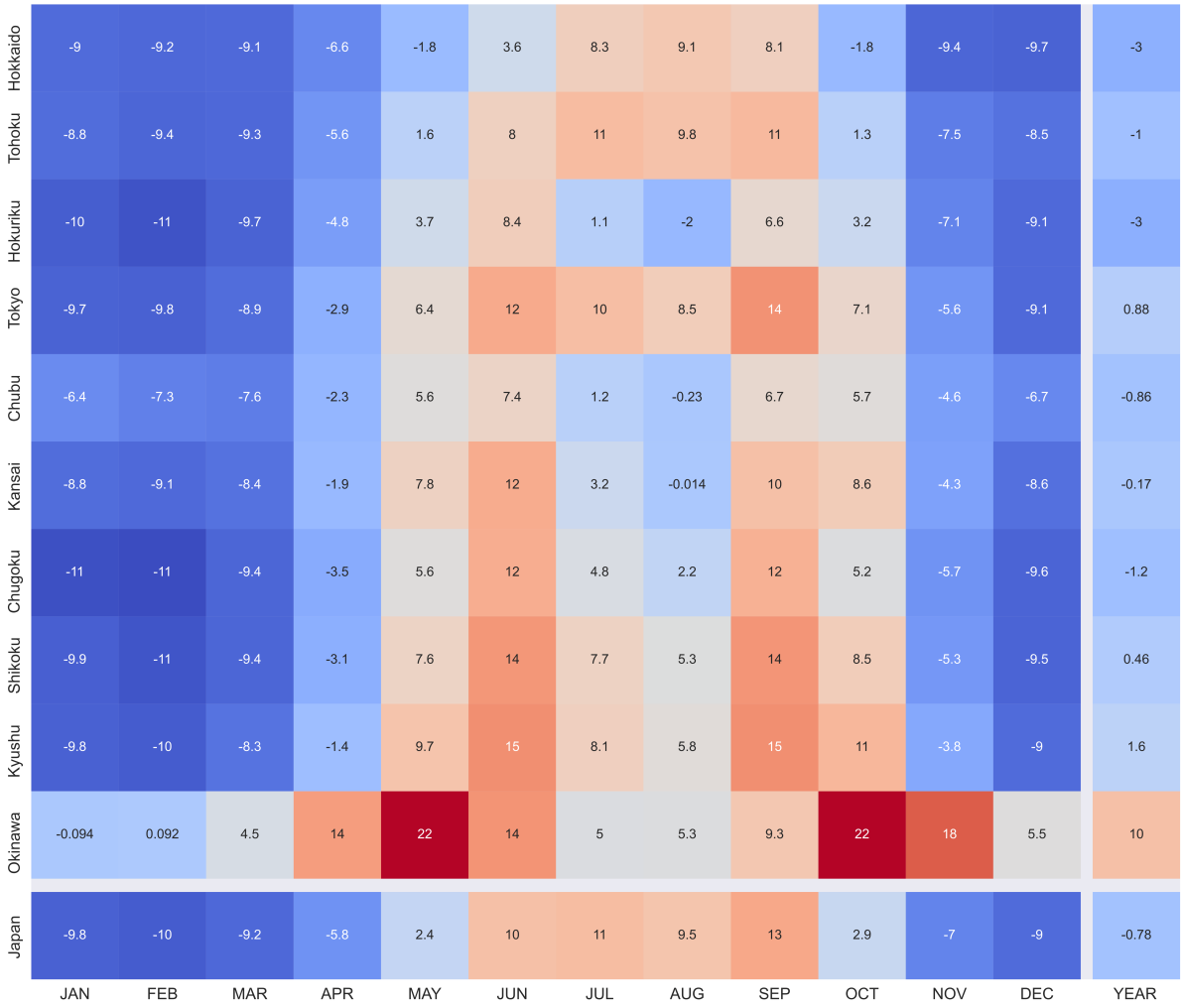

Figure S7a. Monthly and regional changes (in percentage) in power demand between 2020-2030 and 2090-2100 due to climate impacts on future power generation. The mean results of the five models for SSP585 are shown.

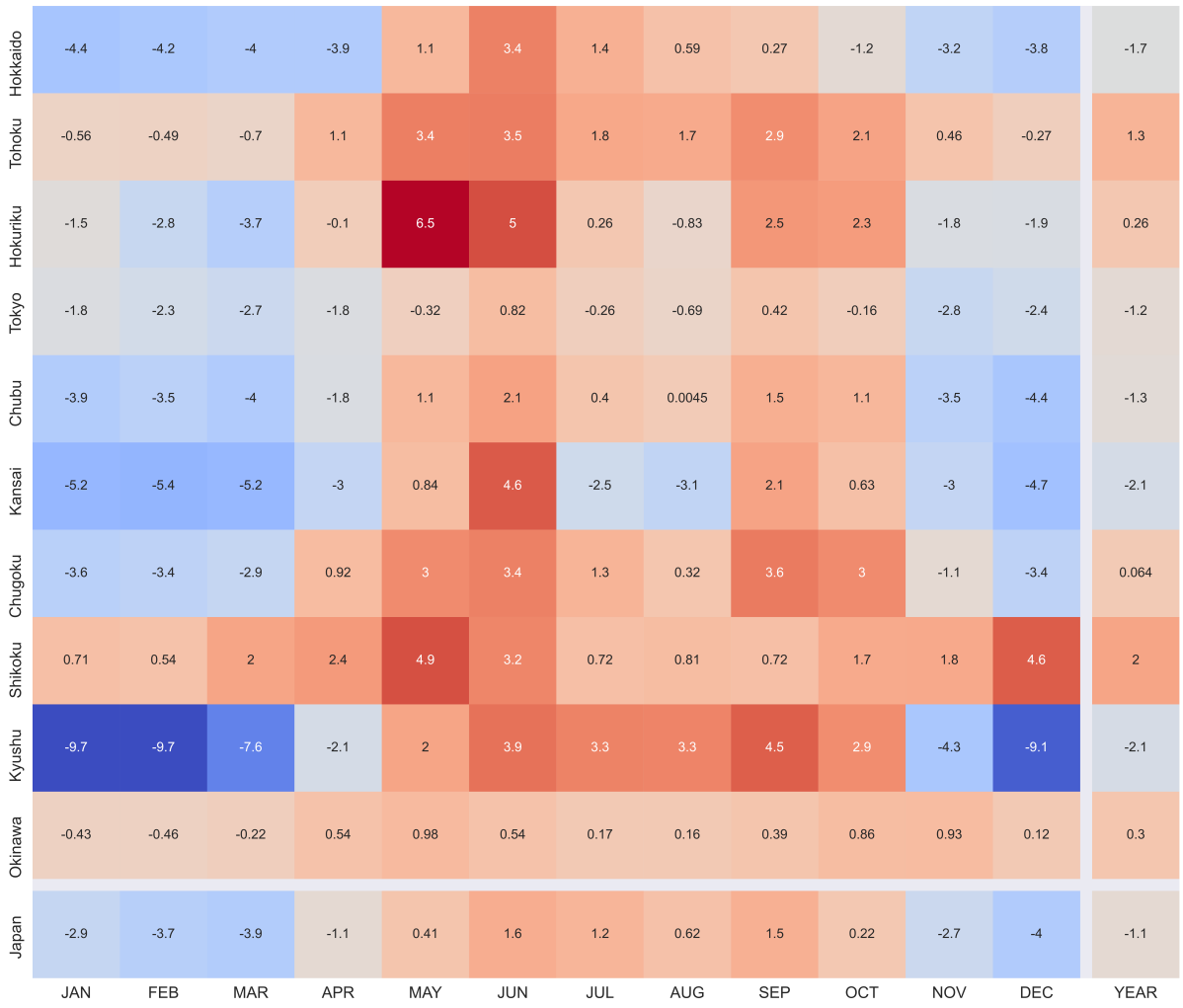

Figure S7b. Monthly and regional changes (in percentage) in carbon intensity between 2020-2030 and 2090-2100 due to climate impacts on future power generation. The mean results of the five models for SSP585 are shown.

APPENDIX B

APPENDIX B - POWER MODELS ARTICLE

1 Supplementary Material of Article 3

Supplementary Materials

S1 Description of the hyperparameters optimized through the grid search process

S1.1 Random Forest

Random forest is an ensemble learning algorithm that combines multiple decision trees to make predictions. The principle behind random forest is to create a diverse set of decision trees that are trained on different subsets of the training data and features.

At each node of each tree, a random subset of features is considered for splitting, which introduces randomness into the model and reduces the variance of the individual trees. The final prediction of the random forest is the majority vote of the predictions made by all the trees in the forest.

Max depth: It controls the complexity of the individual trees in the ensemble by limiting the number of levels in each tree, which in turn limit the number of splits a leaf can make.

Min Samples Leaf: It specifies the minimum number of samples that should be present in a leaf node of a tree. It controls the granularity of the splits made by the tree, and thus, it affects the complexity of the tree.

Min Samples Split: It specifies the minimum number of samples that should be present in an internal node before it can be split. It controls the overall structure of the tree and affects the degree of generalization of the tree.

N Estimator: It specifies the number of trees in the forest

S1.2 Gradient Boosting

Gradient boosting is an ensemble learning algorithm that builds a sequence of decision trees to make predictions. The principle behind gradient boosting is to sequentially add decision trees to the ensemble that corrects the errors made by the previous trees.

At each iteration, the algorithm fits a decision tree to the residuals or gradients of the previous model's predictions. The residuals represent the difference between the true labels and the current model's predictions, while the gradients represent the first-order derivatives of the loss function with respect to the model's predictions. By fitting trees to the residuals or gradients, the algorithm can focus on the examples that are difficult to predict and improve the overall performance of the model.

Max Depth: It controls the maximum depth of each decision tree in the ensemble. It specifies the maximum number of levels that a tree can have, and it can be used to control the complexity of the model and prevent overfitting.

Learning Rate: It controls the contribution of each tree in the ensemble to the final prediction. It specifies the amount by which the predictions of the new trees are scaled before being added to the ensemble.

Max Iter: It controls the maximum number of trees in the ensemble. It specifies the number of boosting iterations that the model will fit to the data.

Max Leaf Nodes: It specifies the maximum number of terminal nodes or leaves that a tree can have, and it can be used to control the complexity of the model and prevent overfitting.
Min Samples Leaf: It specifies the minimum number of samples that should be present in a leaf node of a tree. It controls the granularity of the splits made by the tree, and thus, it affects the complexity of the tree.
L2 Regularization: It is a technique used to prevent overfitting by adding a penalty term to the objective function. The L2 penalty term is proportional to the sum of the squares of the model's parameters, and it encourages the model to choose smaller values for the parameters.

S1.3 MARS

The Multivariate Adaptive Regression Splines (MARS) model is a flexible non-parametric regression technique that can capture complex nonlinear relationships between predictors and a response variable. MARS is a form of regression that constructs a piecewise linear model by breaking the predictor space into smaller subspaces and fitting a linear regression model to each subspace.
The MARS model builds upon the basic concept of linear regression by introducing nonlinear features and interactions between variables. It works by iteratively identifying breakpoints or knots in the predictor variables and fitting linear regression models to each segment between the breakpoints.
MARS is designed to handle both continuous and categorical variables and can automatically detect interactions between them. The model starts by creating simple linear models for each predictor and then combines them to form a more complex model. The model uses a forward selection approach to determine which variables to include in the model and where to place the breakpoints.

Max Degree: It is the maximum degree of terms generated by the forward pass.
Penalty: The MARS algorithm constructs a model by building basis functions that are combinations of simple functions such as linear, hinge, or threshold functions. Each basis function is a product of one or more simple functions, and the number of basis functions can quickly grow with the number of predictors and interactions considered. To avoid overfitting and improve the model's generalization performance, the MARS model uses a regularization penalty that penalizes the complexity of the model. The regularization penalty term is added to the objective function of the model, and it is typically a function of the sum of the absolute values of the coefficients or weights of the basis functions. The penalty encourages the MARS algorithm to choose simpler models with fewer basis functions and smaller coefficients, thereby avoiding overfitting.

S1.4 GAM

GAM stands for Generalized Additive Models. It is a statistical model that extends the linear model by allowing for non-linear relationships between the dependent variable and one or more independent variables. The principle of GAM is based on the idea that a complex relationship between the response variable and the predictor variables can be modeled as a sum of smooth functions of the predictors.

The model assumes that the response variable is a function of the predictor variables, which can be modeled using a combination of smooth functions. These smooth functions can be linear, non-linear, or a combination of both, and can be modeled using a variety of techniques, such as cubic splines or smoothing splines.
The key principle of GAM is to use these smooth functions to capture the non-linear relationship between the dependent and independent variables, without imposing any specific functional form on the relationship. GAM models can be used for both regression and classification problems, and they are particularly useful for analyzing complex relationships that cannot be modeled using linear models.

Lambda: lambda refers to the smoothing parameter that controls the amount of smoothing applied to the smooth functions. Lambda is the parameter that determines the amount of smoothing applied to the smooth functions. A small value of lambda will result in less smoothing and a more complex, wiggly fit to the data, whereas a large value of lambda will result in more smoothing and a simpler, smoother fit to the data.

N Splines: Splines are flexible functions that can approximate a wide range of non-linear relationships between variables. N splines refer to the number of spline basis functions used to model a smooth function in GAM. A spline basis function is a mathematical function that defines the shape of the spline. A spline function is a linear combination of these basis functions.

S2. Outputs of the models for all the countries considered in this study.

EU27 & UK: ALE plots not shown in the main text

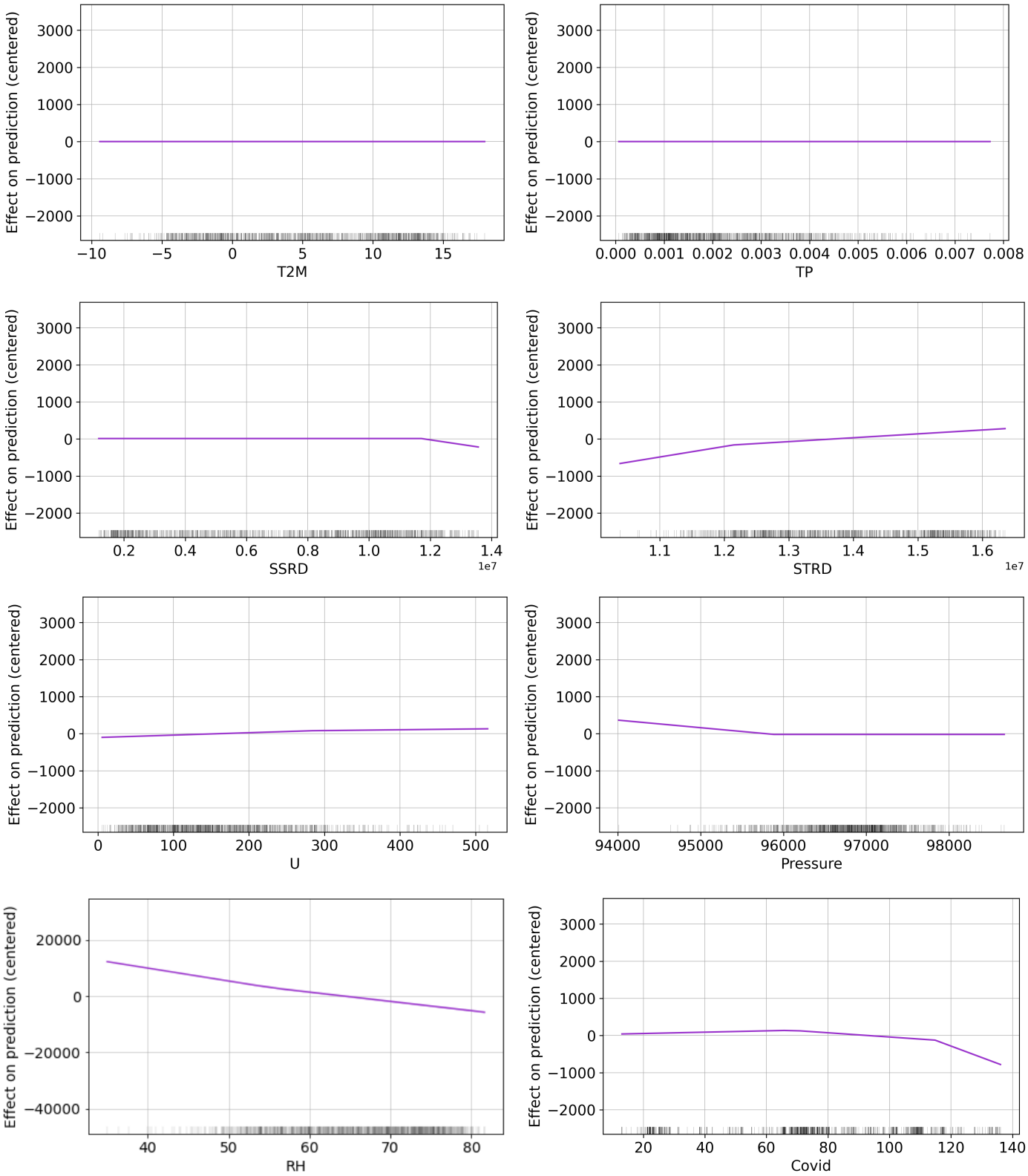

Figure S1. ALE plots depicting the effect of different predictive features on the target variable. The features are divided into two categories: (a) climate features and (b) human activity features. Each ALE plot shows the partial dependence of the target variable on a single feature while controlling for the effects of all other features. The x-axis represents the range of values for each feature, and the y-axis represents the corresponding change in the predicted value of the target variable. The shaded areas represent the 95% confidence intervals for each ALE curve.

EU27 & UK: Validation Curves

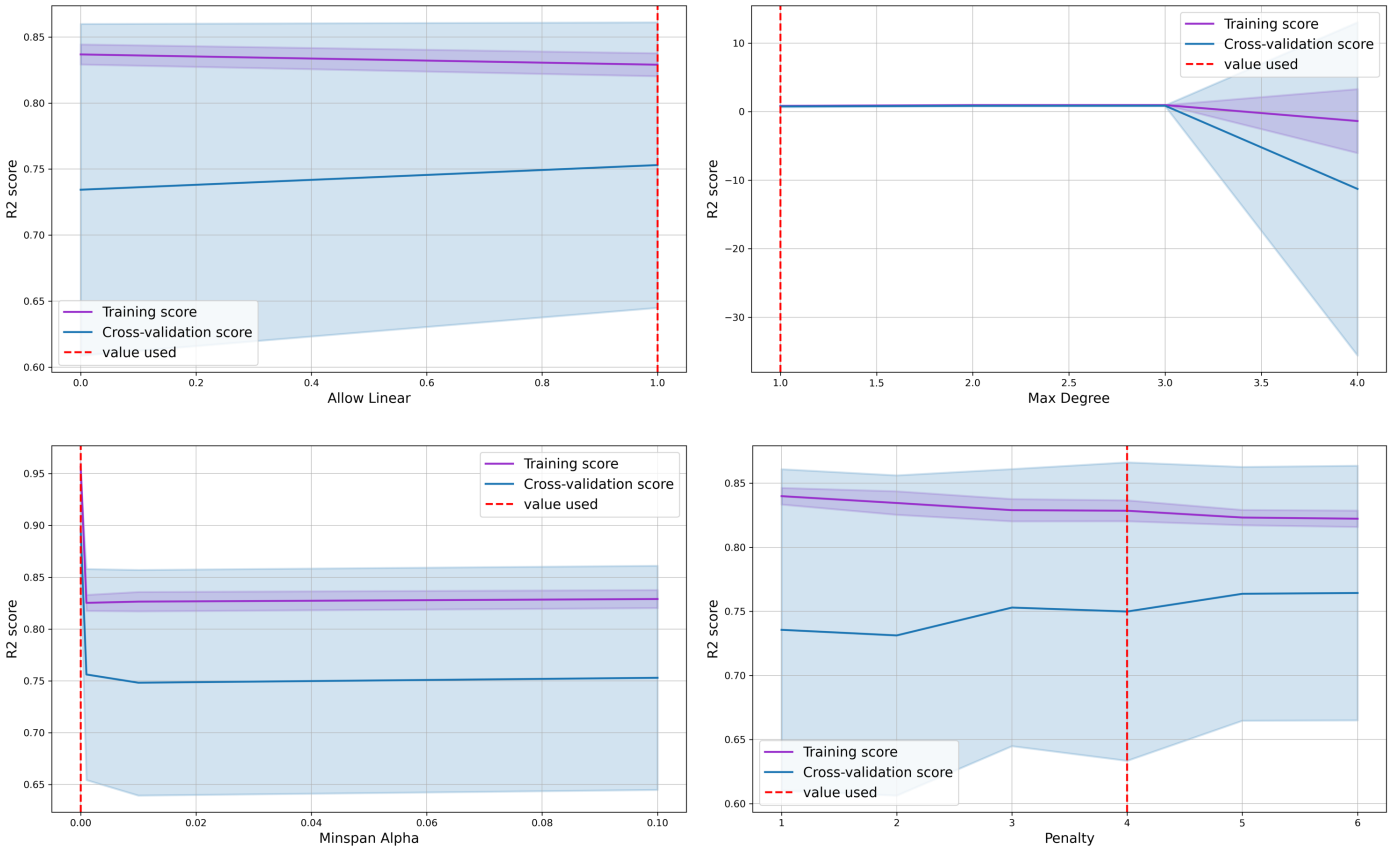

Figure S2. This figure displays validation curves for the hyperparameter of the MARS, which is the best model EU27 & UK. The curves demonstrate how changes in the values of the hyperparameters affect the performance of the model, as measured by the R^2 score. The x-axis represents the range of values for the hyperparameter, and the y-axis shows the mean R^2 cross-validation score and R^2 training score. The validation and training scores are averaged over five scores calculated through cross-validation. The shaded areas represent the 95% confidence intervals for each curve. The red dashed line indicates the value of the hyperparameter selected during the grid-search process.

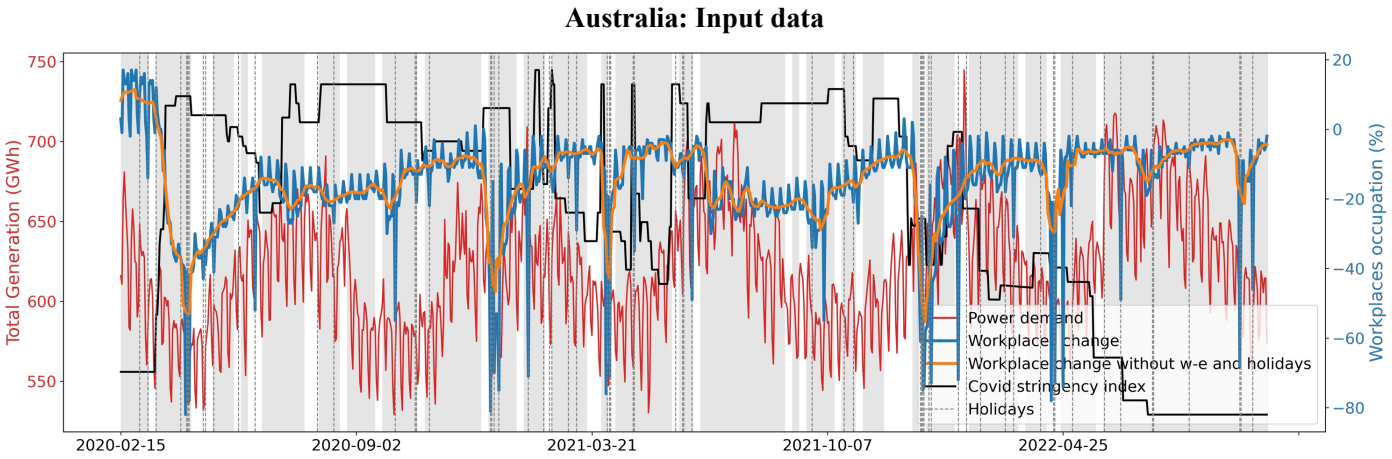

Figure S3. Evolution of human activity predictive features and power demand over the model training and testing period. Shaded area represents the train periods, blank area the test periods.

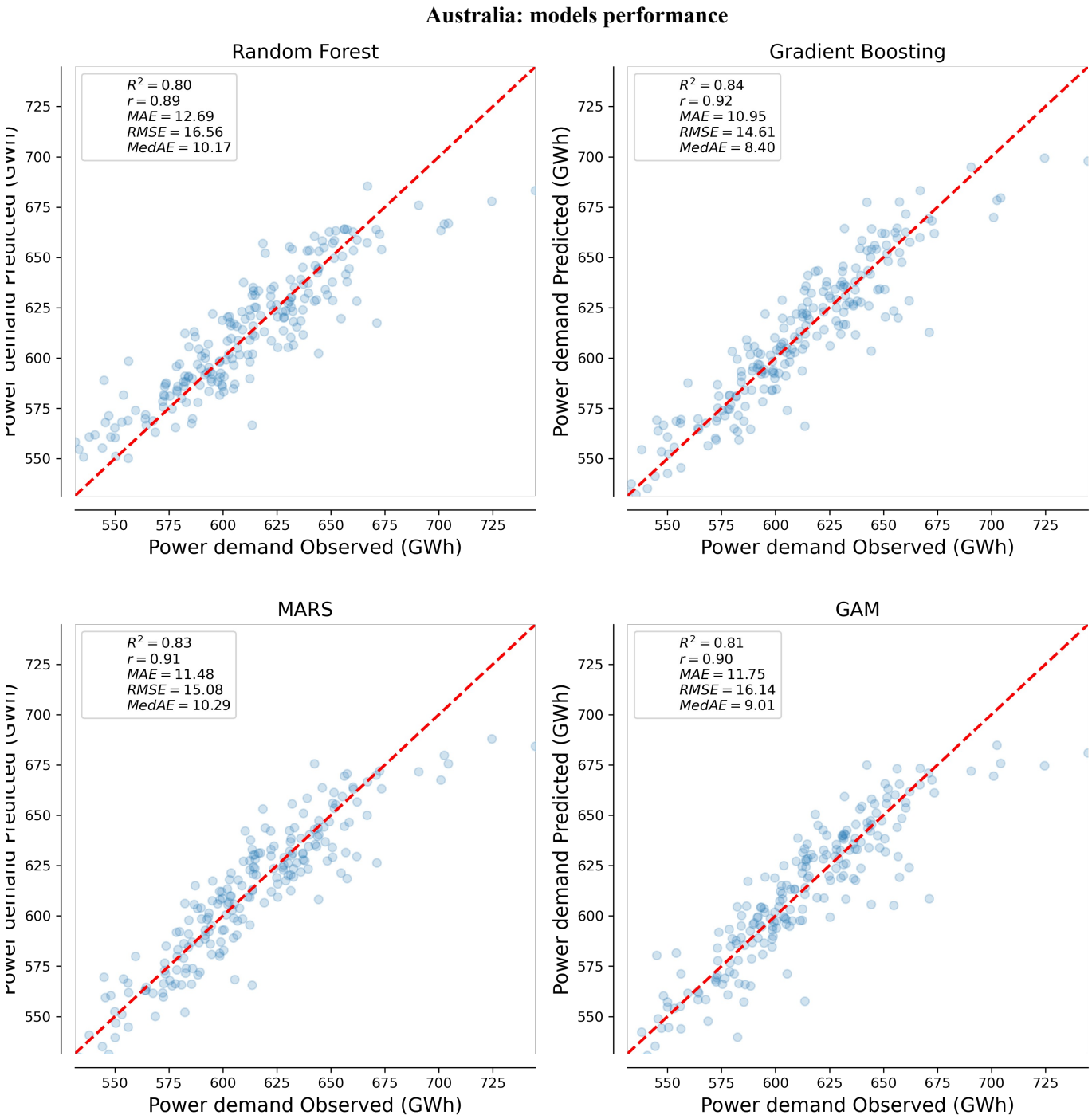

Figure S4. Comparison of machine learning model performance: predicted power demand plotted against observed power demand (blue points). The red dashed line represents the 1:1 line of perfect agreement between predictions and observations.

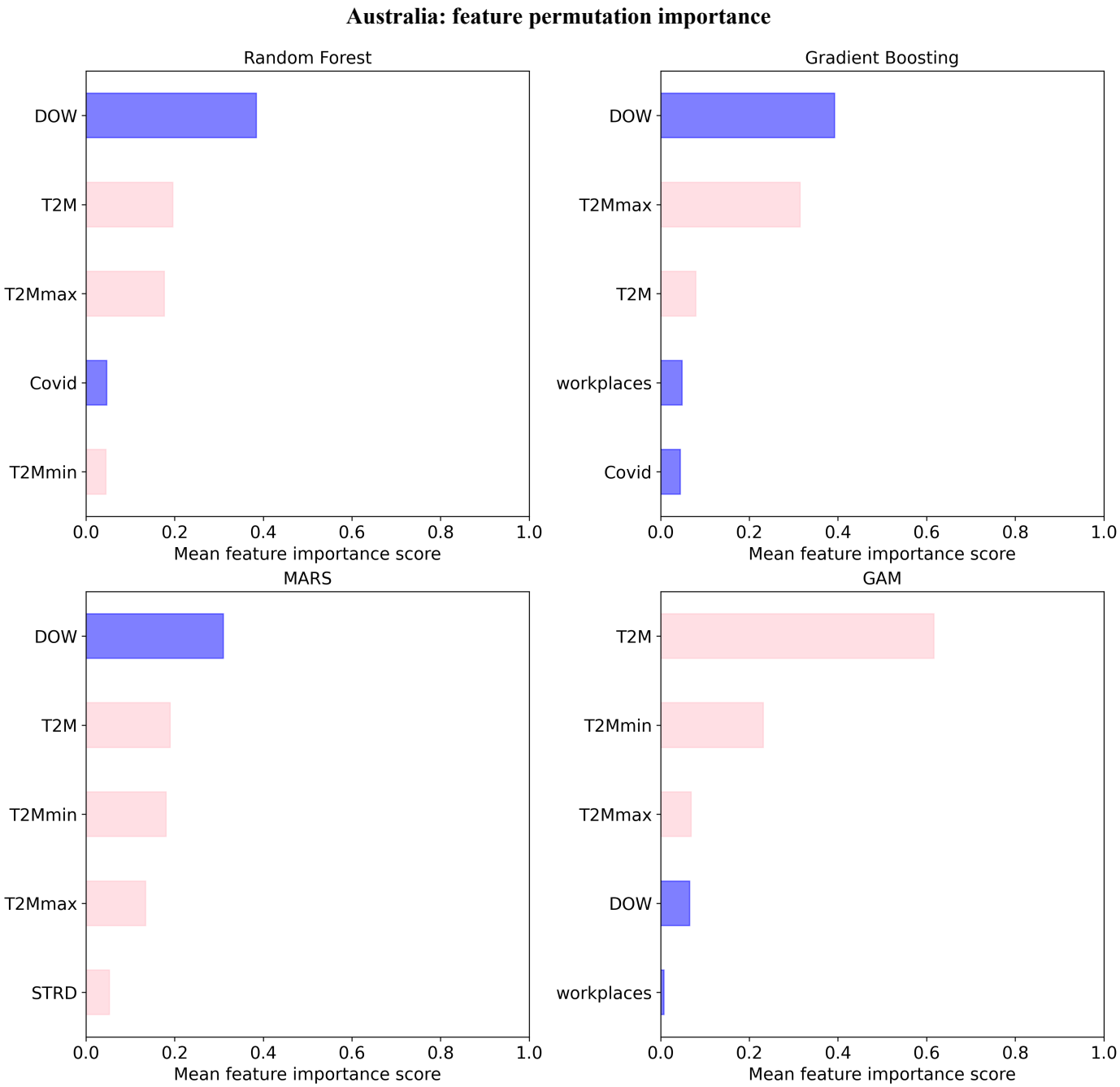

Figure S5. Permutation feature importance scores for the five most important predictive features for four different machine learning models: Random Forest, Gradient Boosting, Multivariate Adaptive Regression Splines (MARS), and Generalized Additive Models (GAM). The x-axis represents the countries, and the y-axis the different predictive features used in the models.

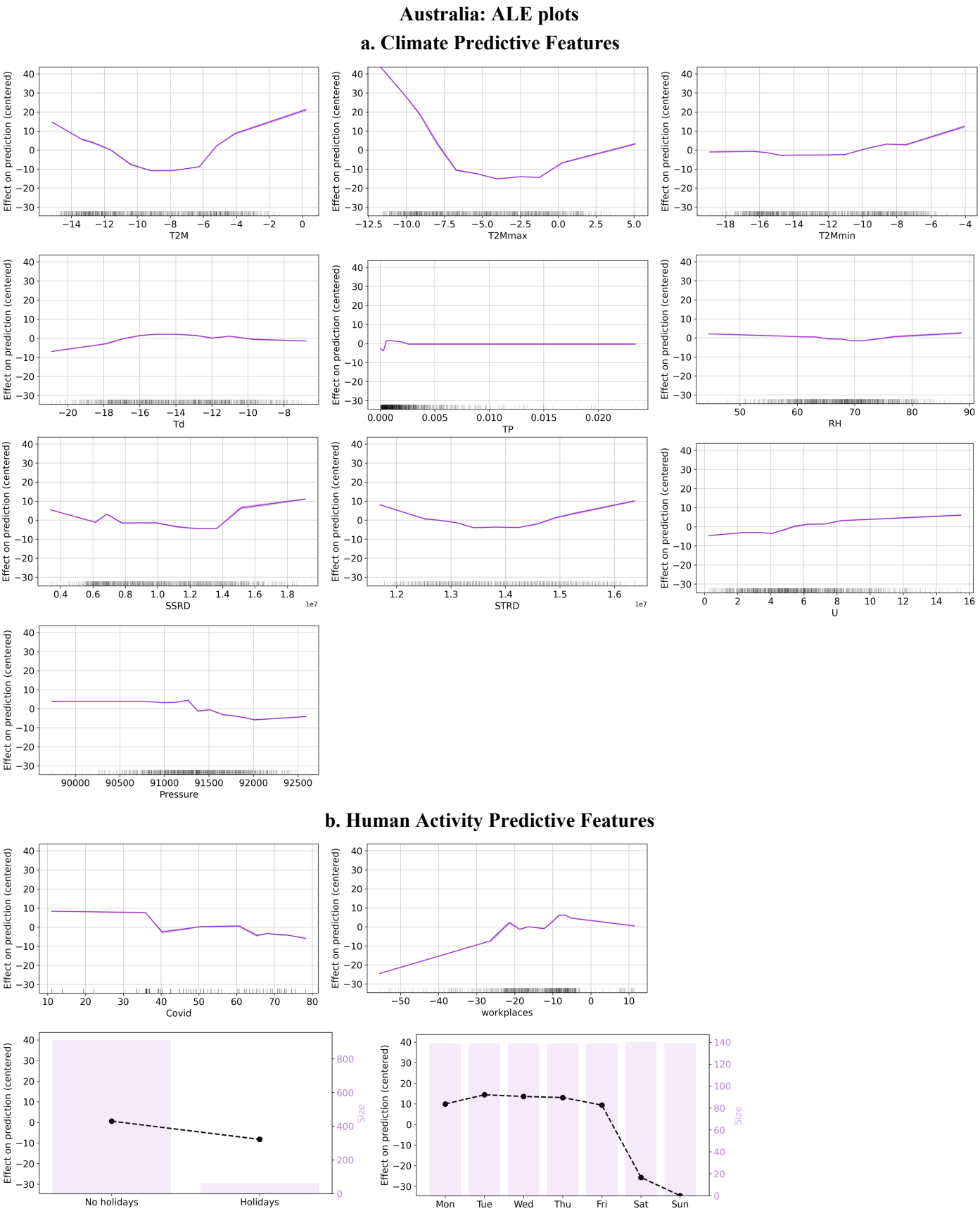

Figure S6. ALE plots depicting the effect of different predictive features on the target variable. The features are divided into two categories: (a) climate features and (b) human activity features. Each ALE plot shows the partial dependence of the target variable on a single feature while controlling for the effects of all other features. The x-axis represents the range of values for each feature, and the y-axis represents the corresponding change in the predicted value of the target variable. The shaded areas represent the 95% confidence intervals for each ALE curve.

Australia: Validation curves

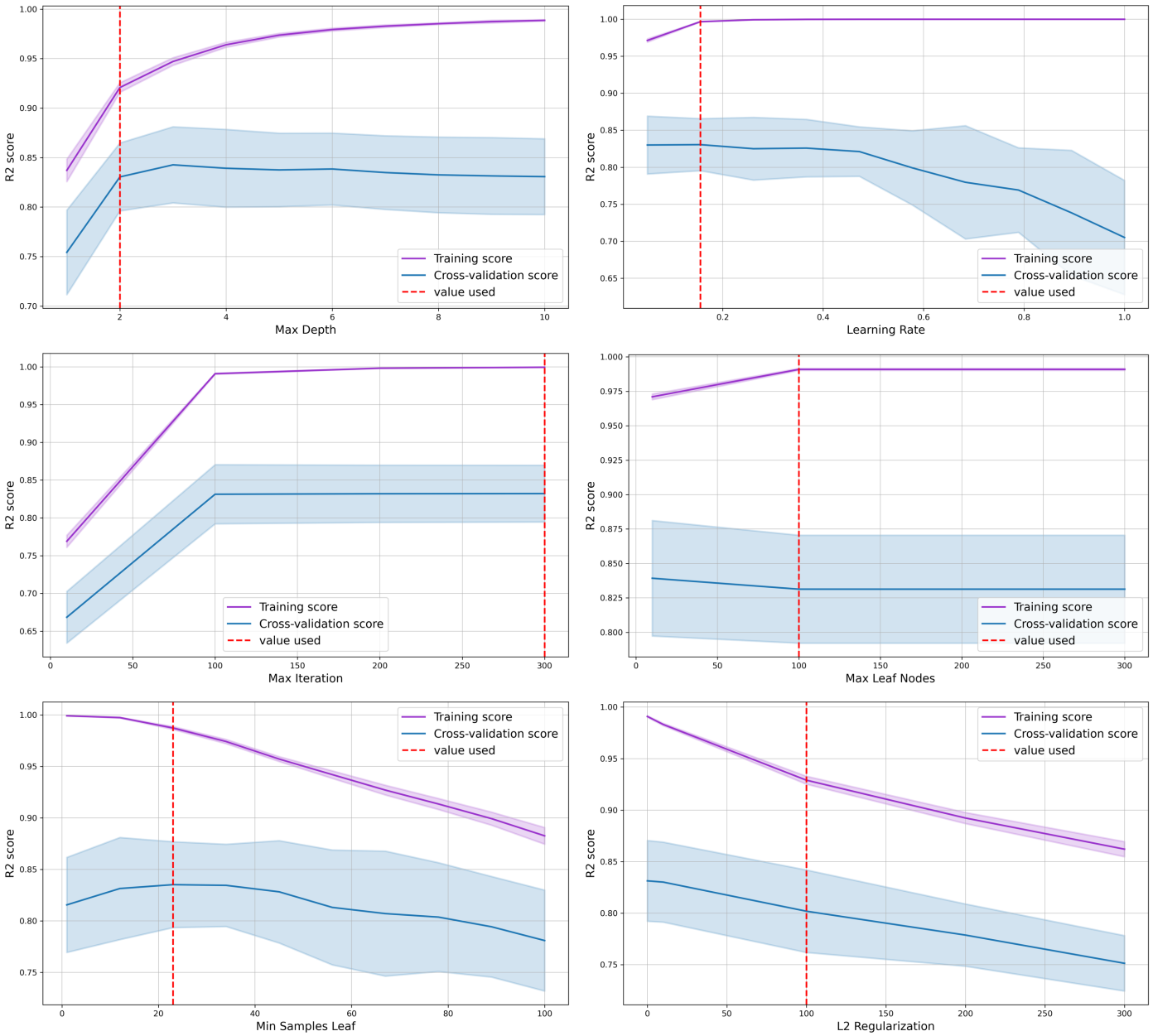

Figure S7. This figure displays validation curves for the hyperparameter of the Gradient Boosting, which is the best model in Australia. The curves demonstrate how changes in the values of the hyperparameters affect the performance of the model, as measured by the R^2 score. The x-axis represents the range of values for the hyperparameter, and the y-axis shows the mean R^2 cross-validation score and R^2 training score. The validation and training scores are averaged over five scores calculated through cross-validation. The shaded areas represent the 95% confidence intervals for each curve. The red dashed line indicates the value of the hyperparameter selected during the grid-search process.

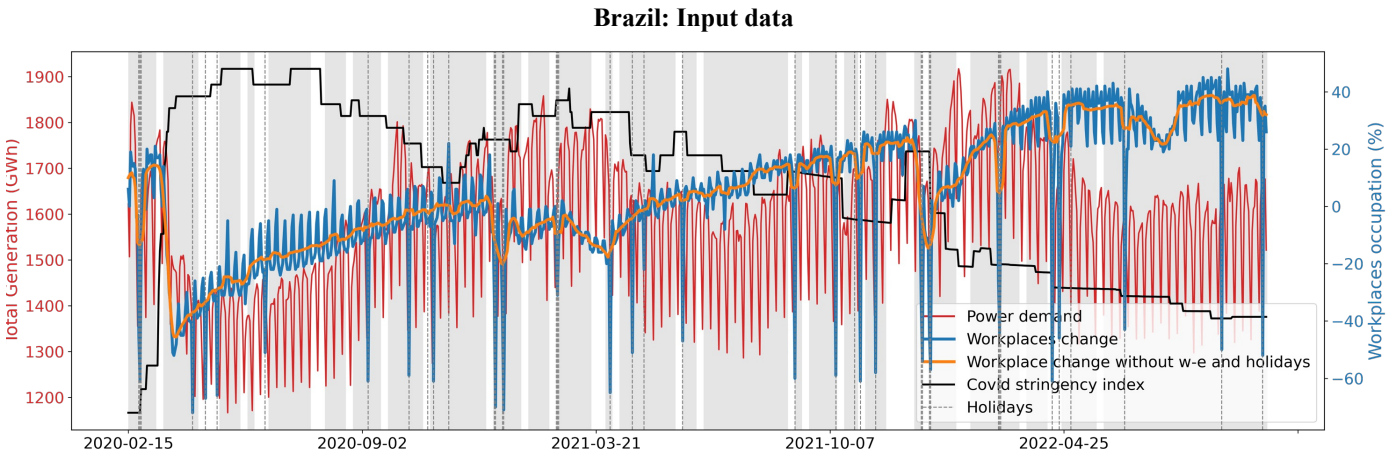

Figure S8. Evolution of human activity predictive features and power demand over the model training and testing period. Shaded area represents the train periods, blank area the test periods.

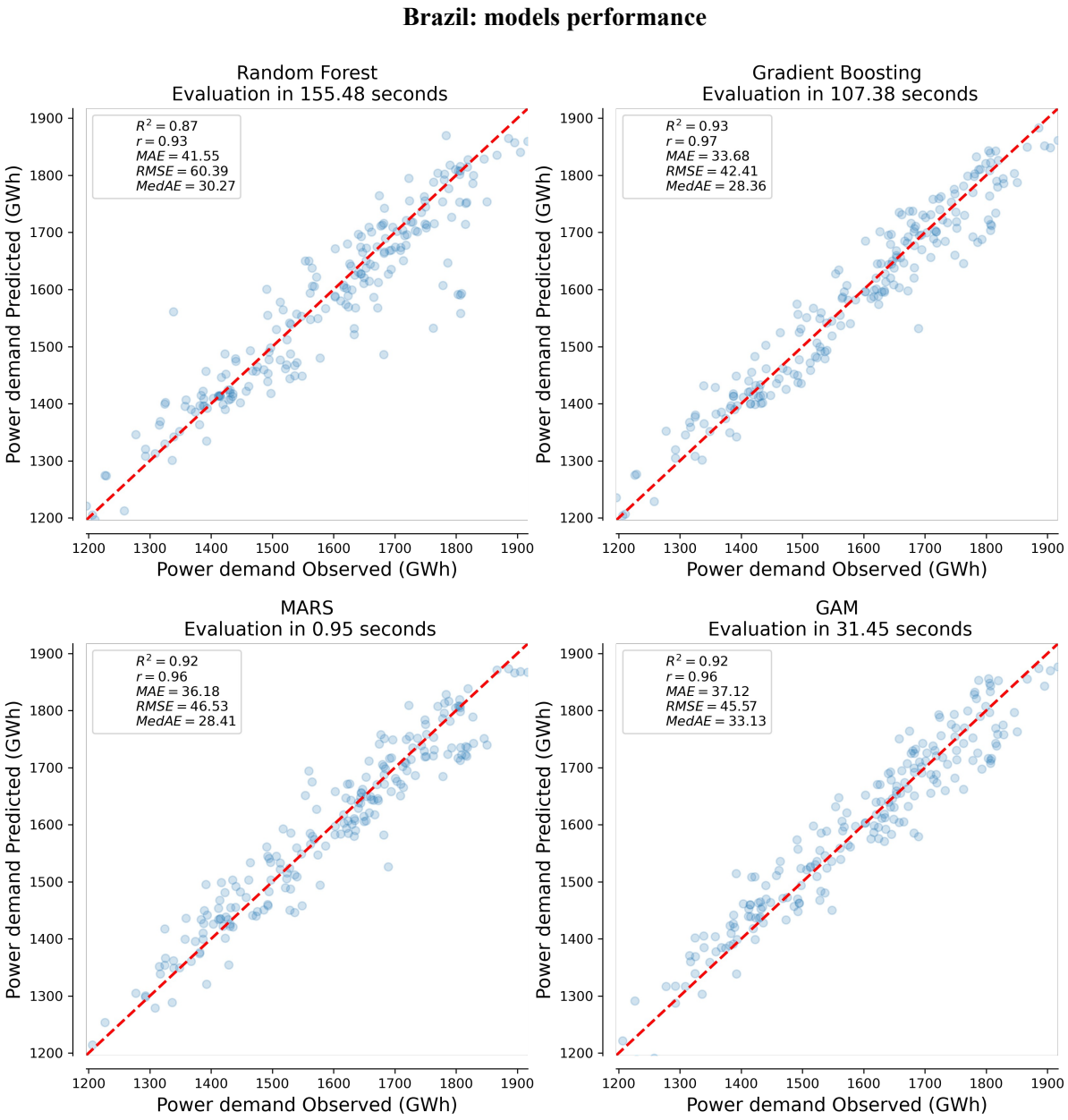

Figure S9. Comparison of machine learning model performance: predicted power demand plotted against observed power demand (blue points). The red dashed line represents the 1:1 line of perfect agreement between predictions and observations.

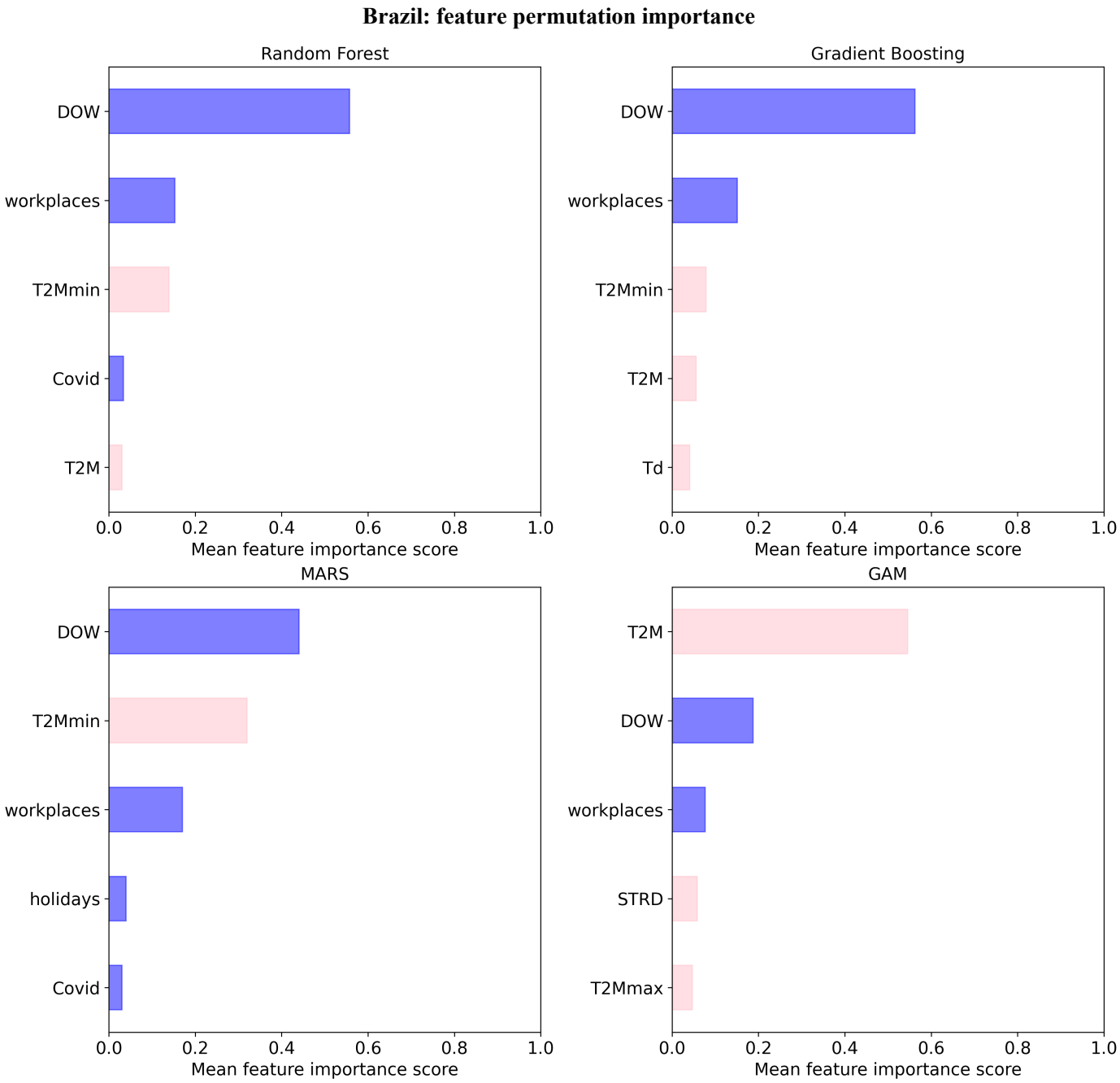

Figure S10.Permutation feature importance scores for the five most important predictive features for four different machine learning models: Random Forest, Gradient Boosting, Multivariate Adaptive Regression Splines (MARS), and Generalized Additive Models (GAM). The x-axis represents the countries, and the y-axis the different predictive features used in the models.

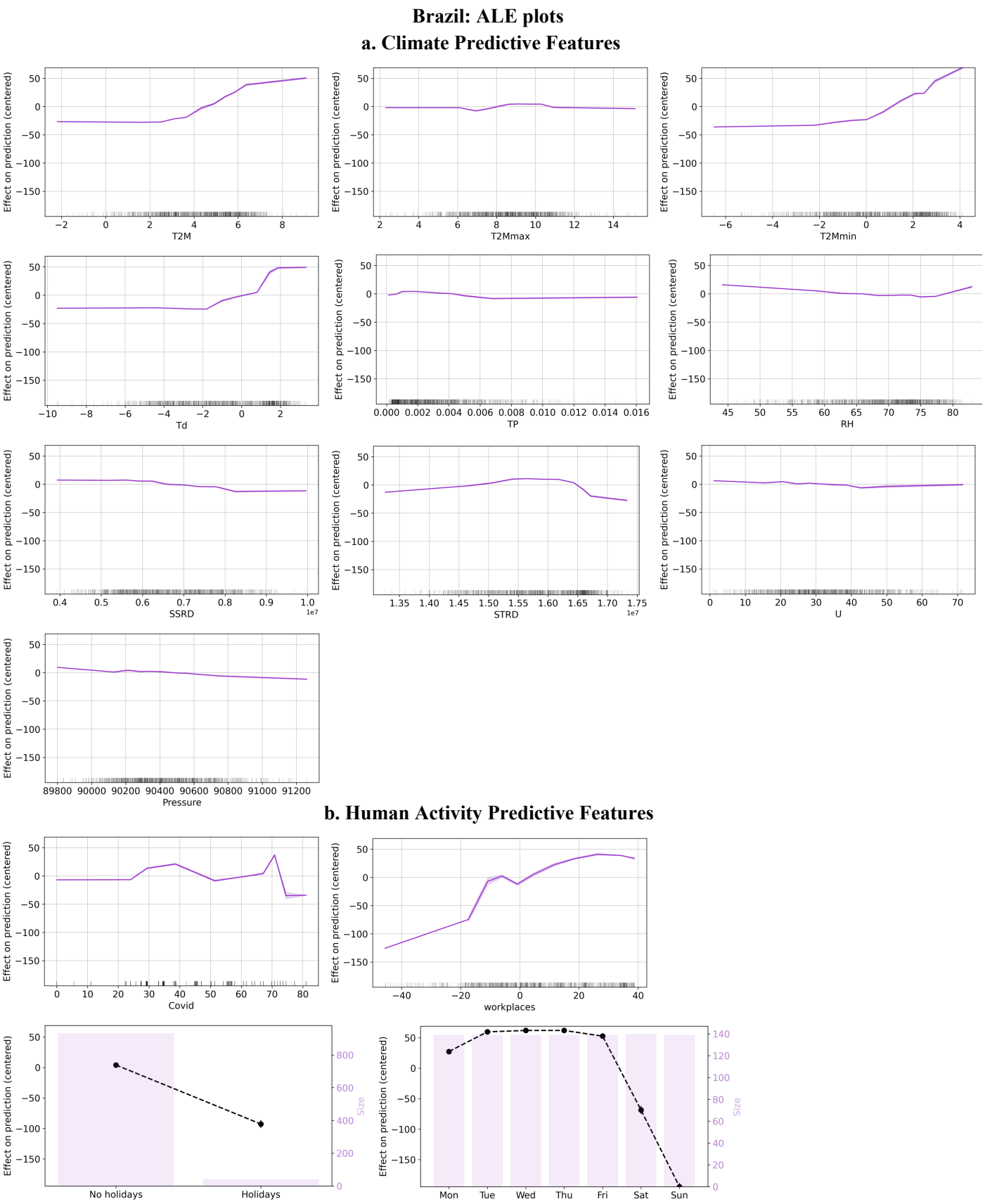

Figure S11. ALE plots depicting the effect of different predictive features on the target variable. The features are divided into two categories: (a) climate features and (b) human activity features. Each ALE plot shows the partial dependence of the target variable on a single feature while controlling for the effects of all other features. The x-axis represents the range of values for each feature, and the y-axis represents the corresponding change in the predicted value of the target variable. The shaded areas represent the 95% confidence intervals for each ALE curve.

Brazil: Validation curves

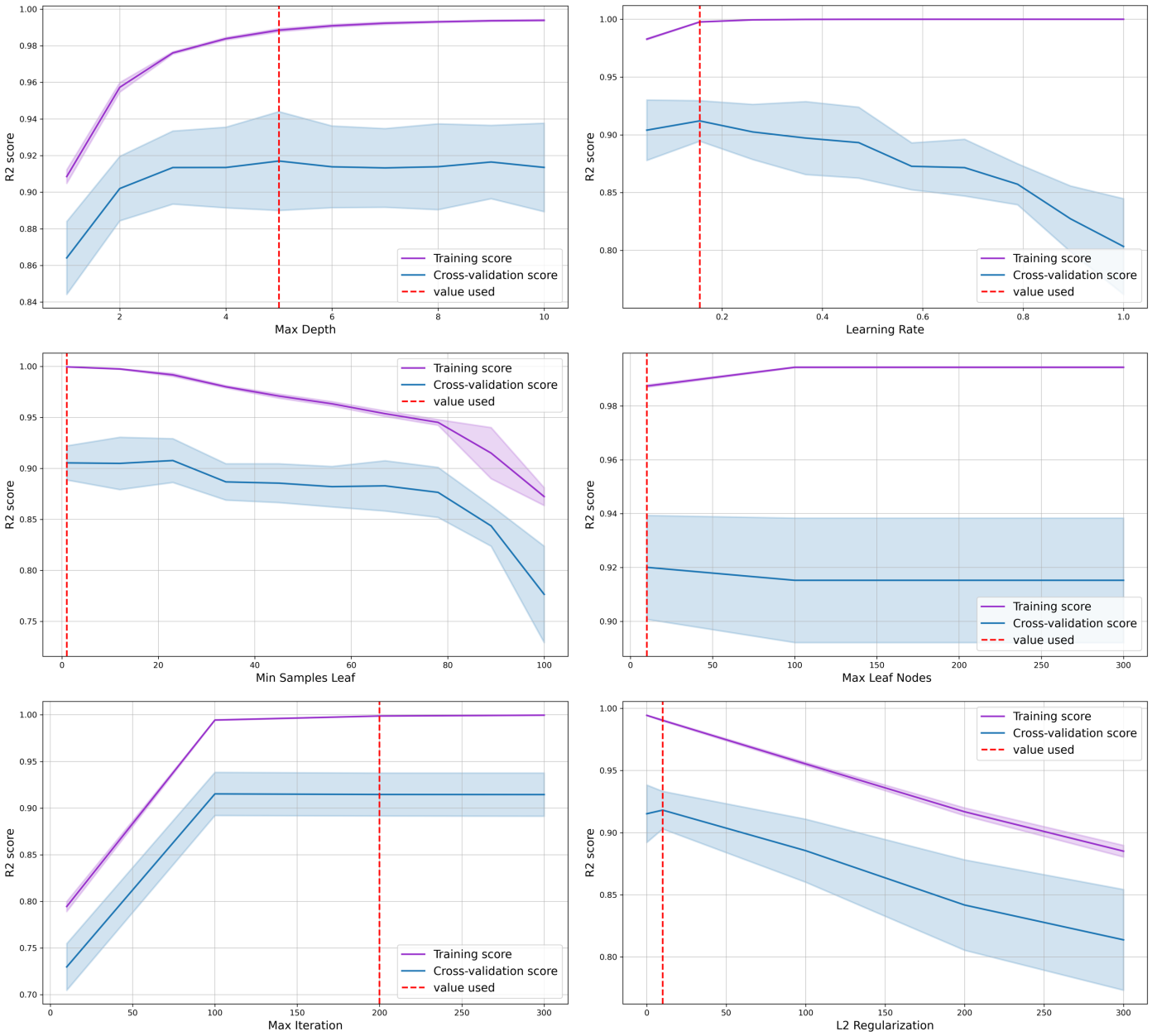

Figure S12. This figure displays validation curves for the hyperparameter of the gradient boosting model, which is the best model in Brazil. The curves demonstrate how changes in the values of the hyperparameters affect the performance of the model, as measured by the R^2 score. The x-axis represents the range of values for the hyperparameter, and the y-axis shows the mean R^2 cross-validation score and R^2 training score. The validation and training scores are averaged over five scores calculated through cross-validation. The shaded areas represent the 95% confidence intervals for each curve. The red dashed line indicates the value of the hyperparameter selected during the grid-search process.

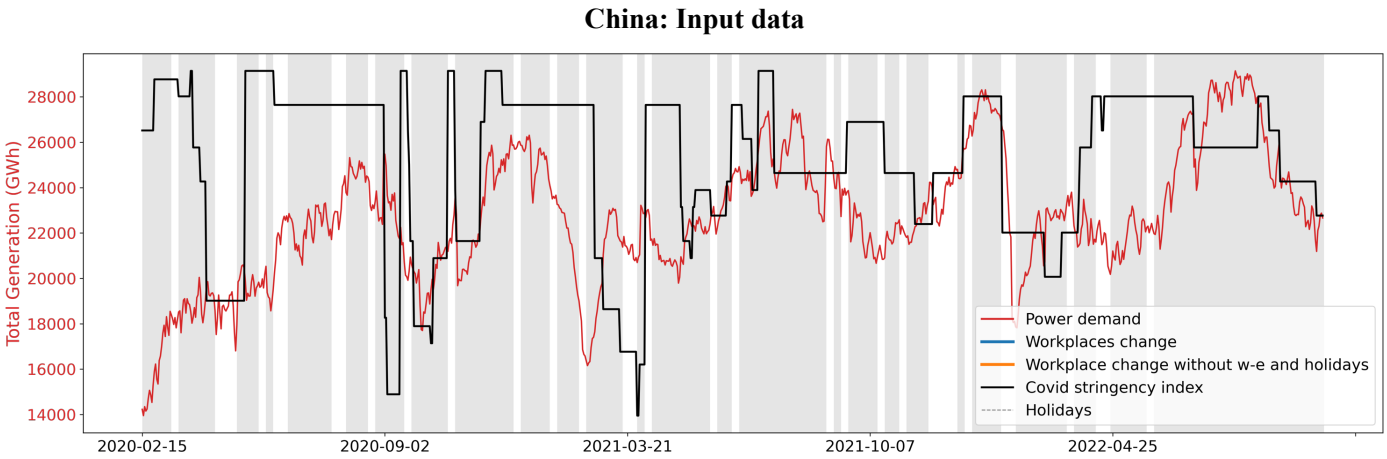

Figure S13. Evolution of human activity predictive features and power demand over the model training and testing period. Shaded area represents the train periods, blank area the test periods.

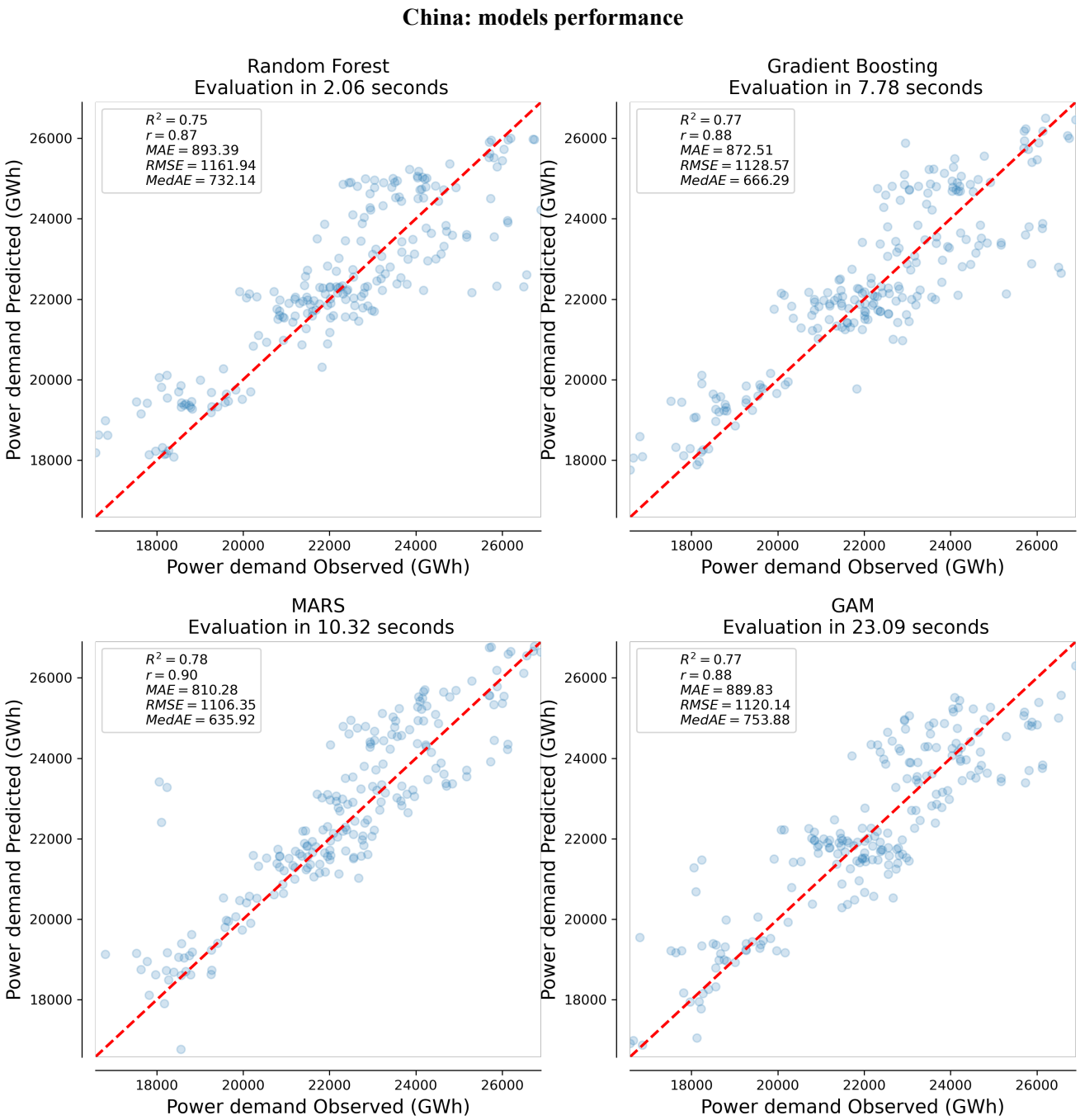

Figure S14. Comparison of machine learning model performance: predicted power demand plotted against observed power demand (blue points). The red dashed line represents the 1:1 line of perfect agreement between predictions and observations.

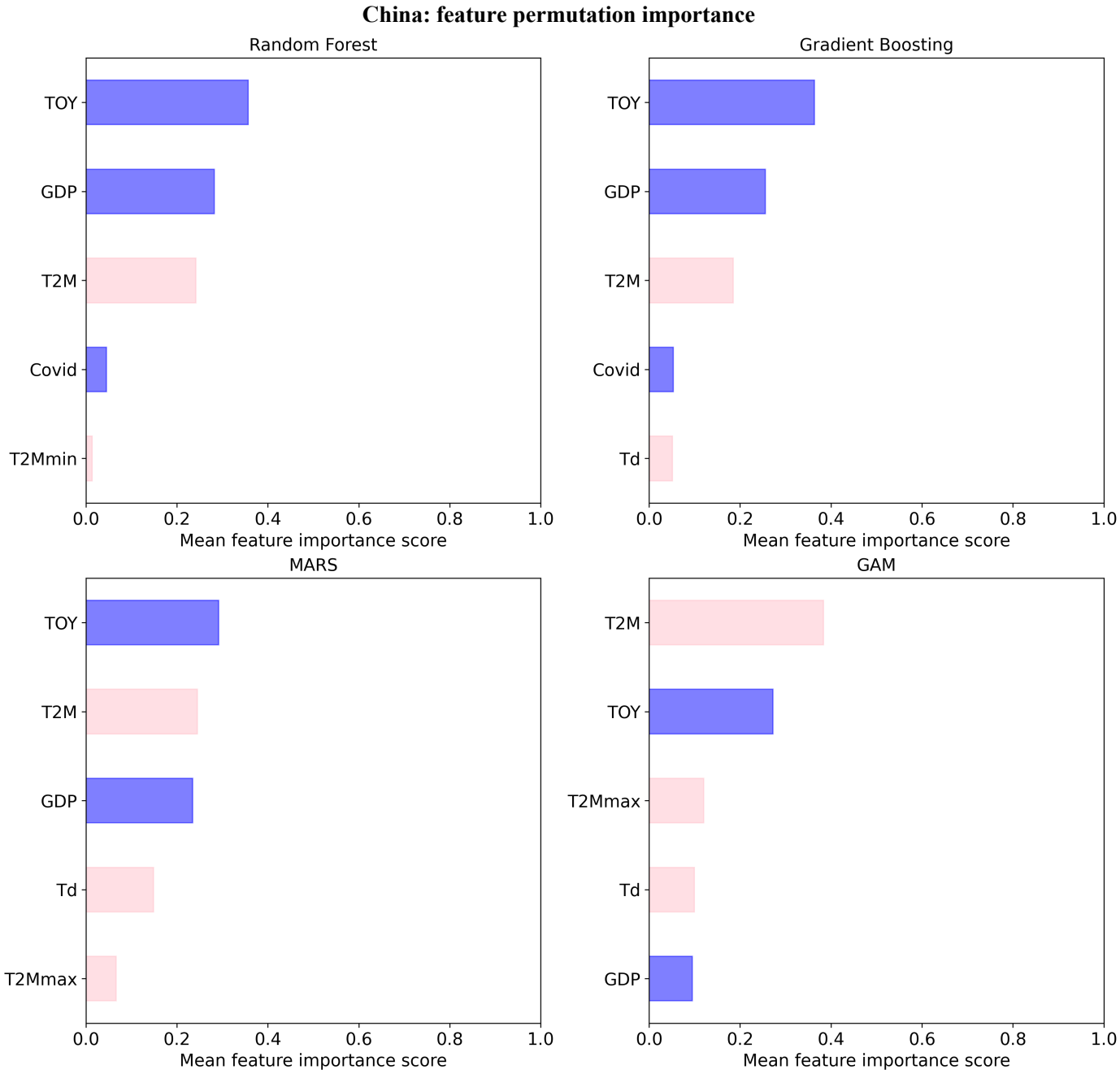

Figure S15. Permutation feature importance scores for the five most important predictive features for four different machine learning models: Random Forest, Gradient Boosting, Multivariate Adaptive Regression Splines (MARS), and Generalized Additive Models (GAM). The x-axis represents the countries, and the y-axis the different predictive features used in the models.

Figure 16. ALE plots depicting the effect of different predictive features on the target variable. The features are divided into two categories: (a) climate features and (b) human activity features. Each ALE plot shows the partial dependence of the target variable on a single feature while controlling for the effects of all other features. The x-axis represents the range of values for each feature, and the y-axis represents the corresponding change in the predicted value of the target variable. The shaded areas represent the 95% confidence intervals for each ALE curve.

China: Validation curves

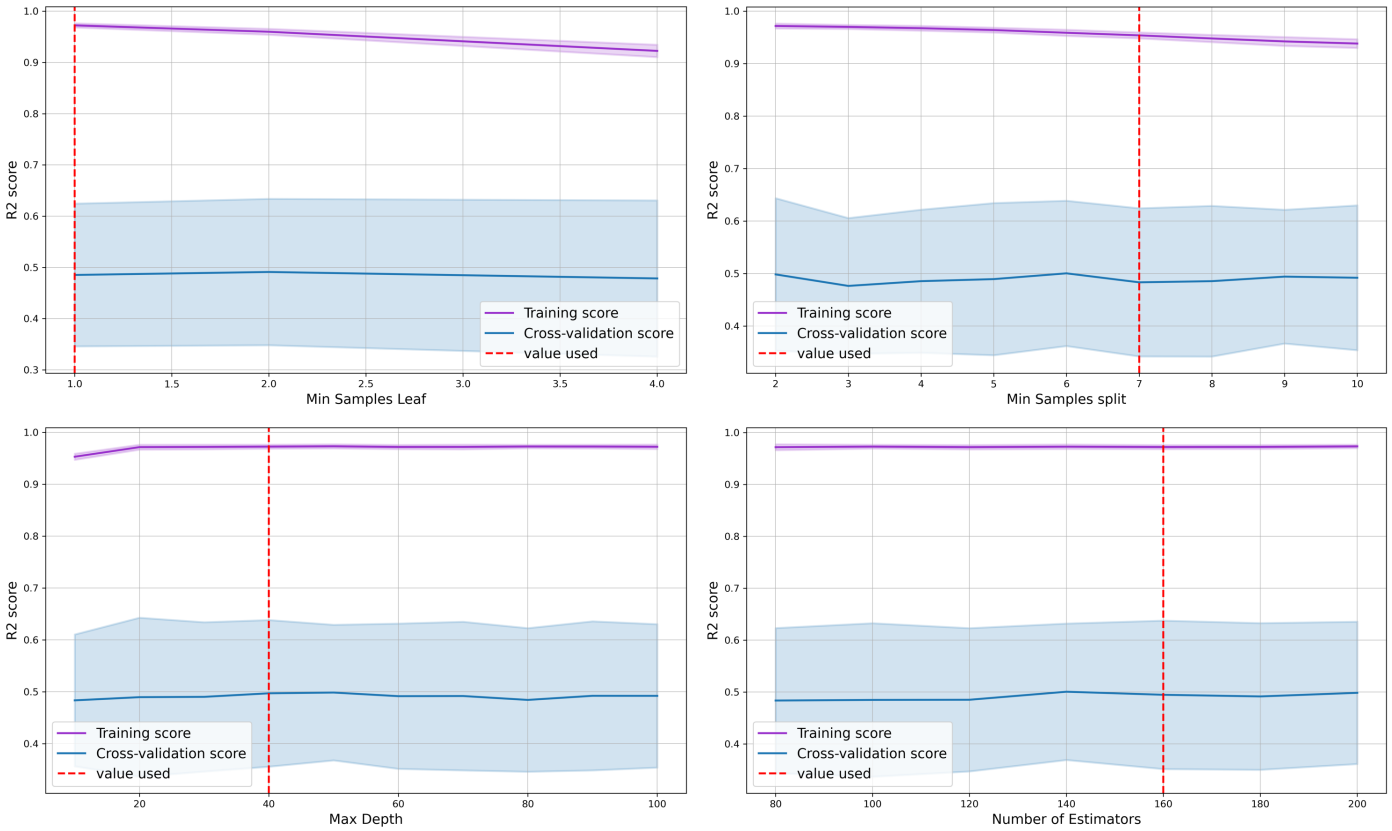

Figure S17. This figure displays validation curves for the hyperparameter of the MARS, which is the best model in China. The curves demonstrate how changes in the values of the hyperparameters affect the performance of the model, as measured by the R^2 score. The x-axis represents the range of values for the hyperparameter, and the y-axis shows the mean R^2 cross-validation score and R^2 training score. The validation and training scores are averaged over five scores calculated through cross-validation. The shaded areas represent the 95% confidence intervals for each curve. The red dashed line indicates the value of the hyperparameter selected during the grid-search process.

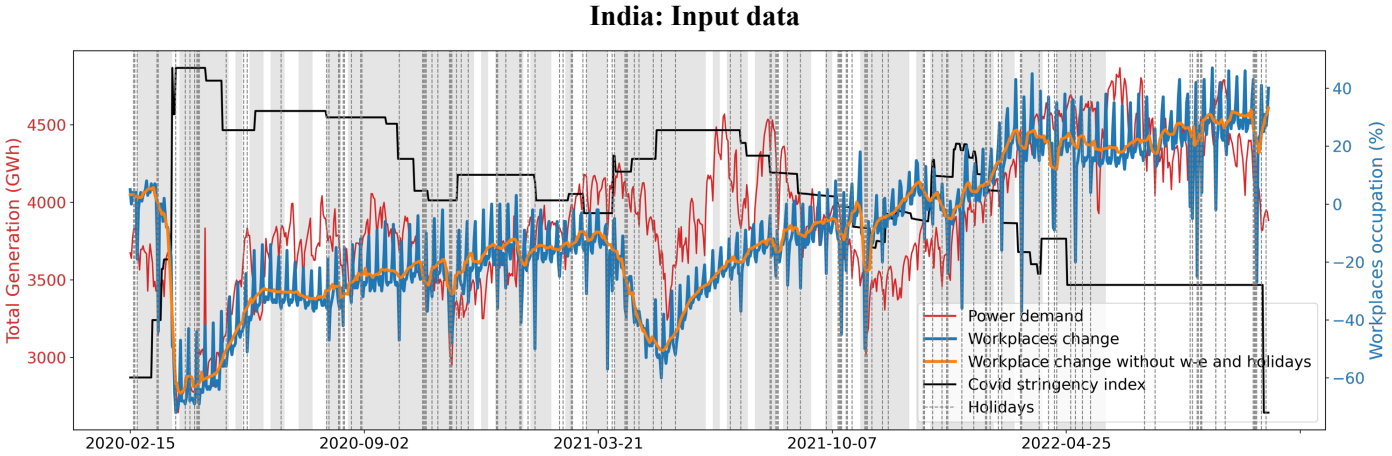

Figure 18. Evolution of human activity predictive features and power demand over the model training and testing period. Shaded area represents the train periods, blank area the test periods.

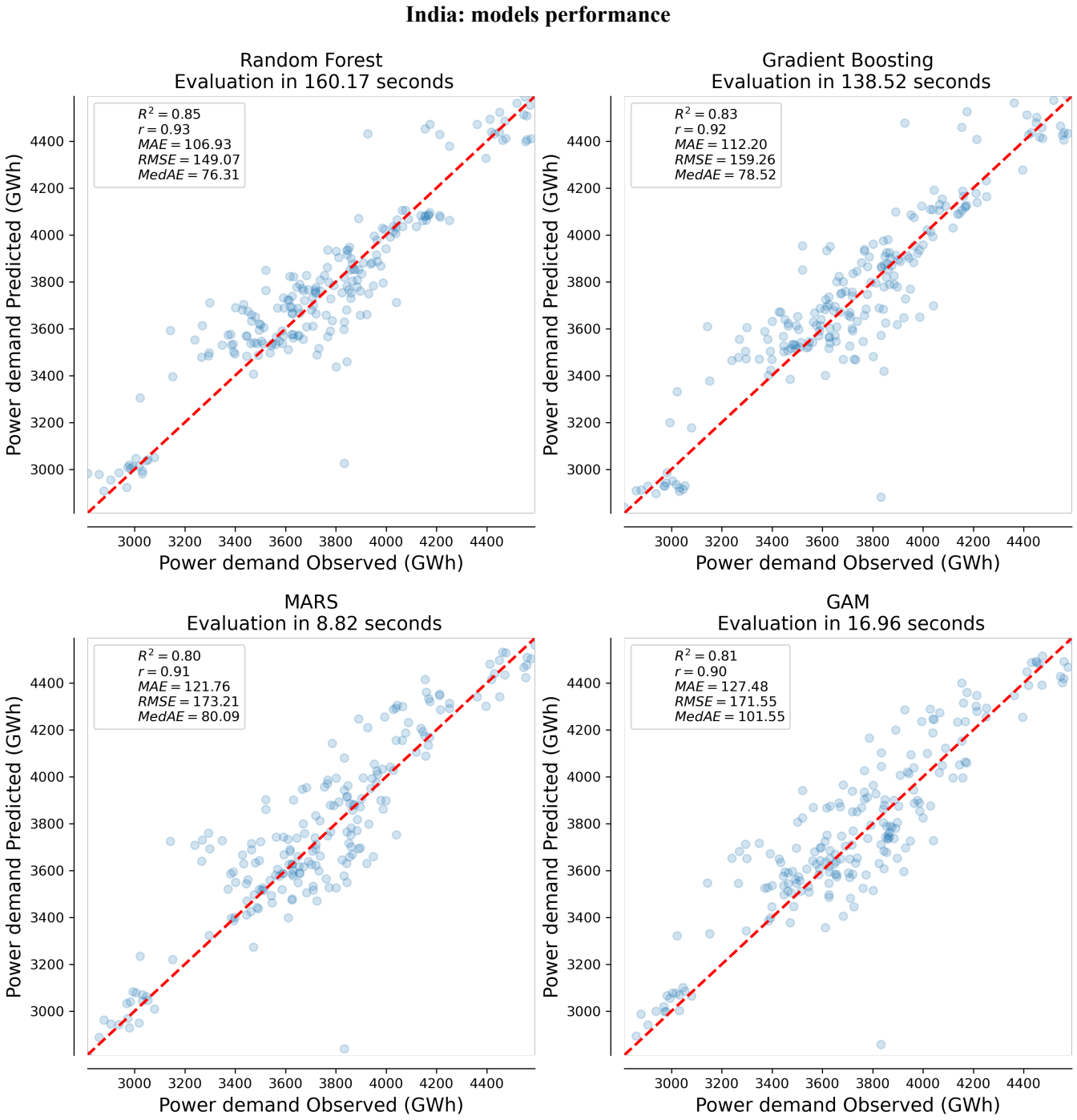

Figure S19. Comparison of machine learning model performance: predicted power demand plotted against observed power demand (blue points). The red dashed line represents the 1:1 line of perfect agreement between predictions and observations.

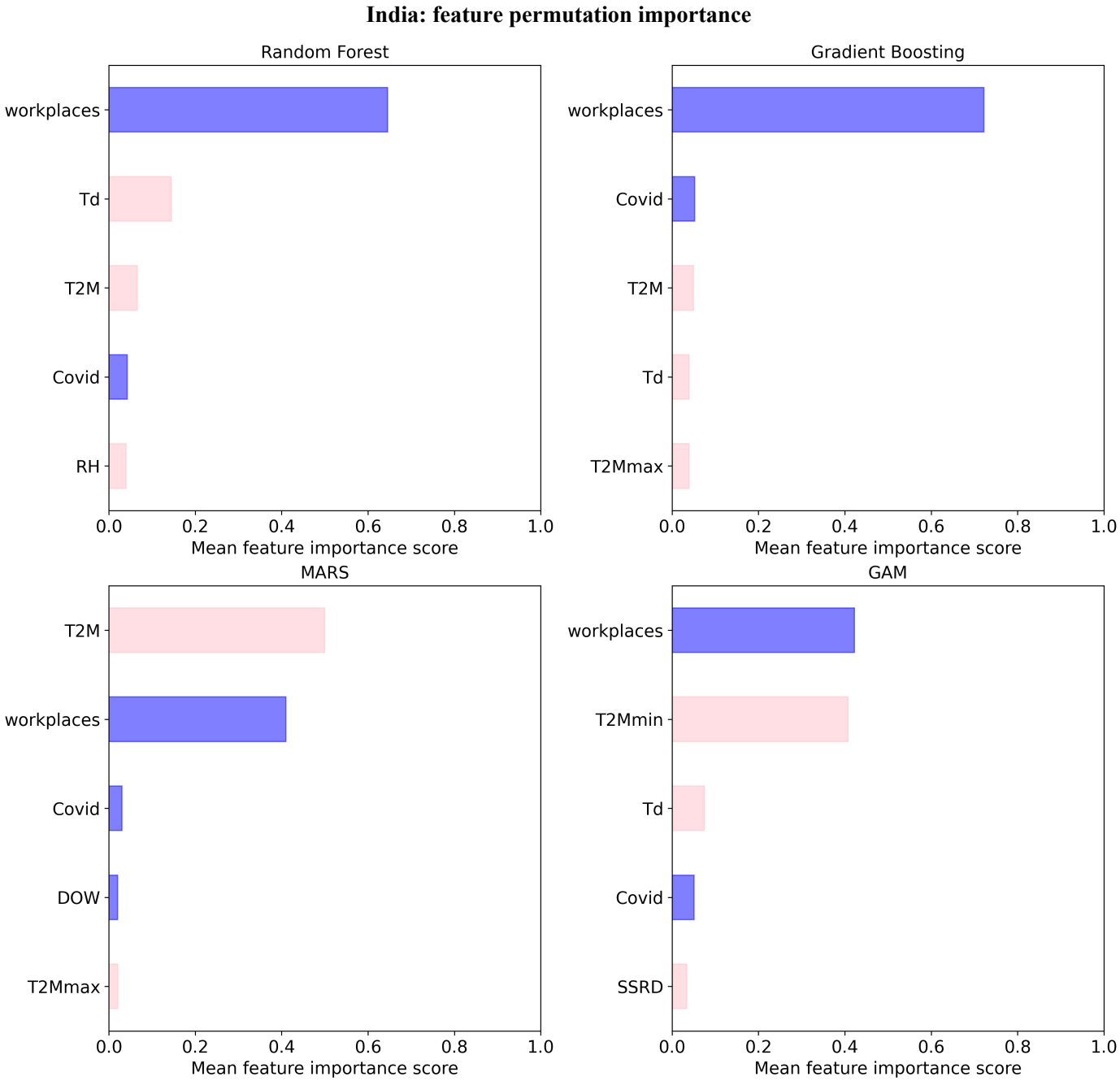

Figure S20. Permutation feature importance scores for the five most important predictive features for four different machine learning models: Random Forest, Gradient Boosting, Multivariate Adaptive Regression Splines (MARS), and Generalized Additive Models (GAM). The x-axis represents the countries, and the y-axis the different predictive features used in the models.

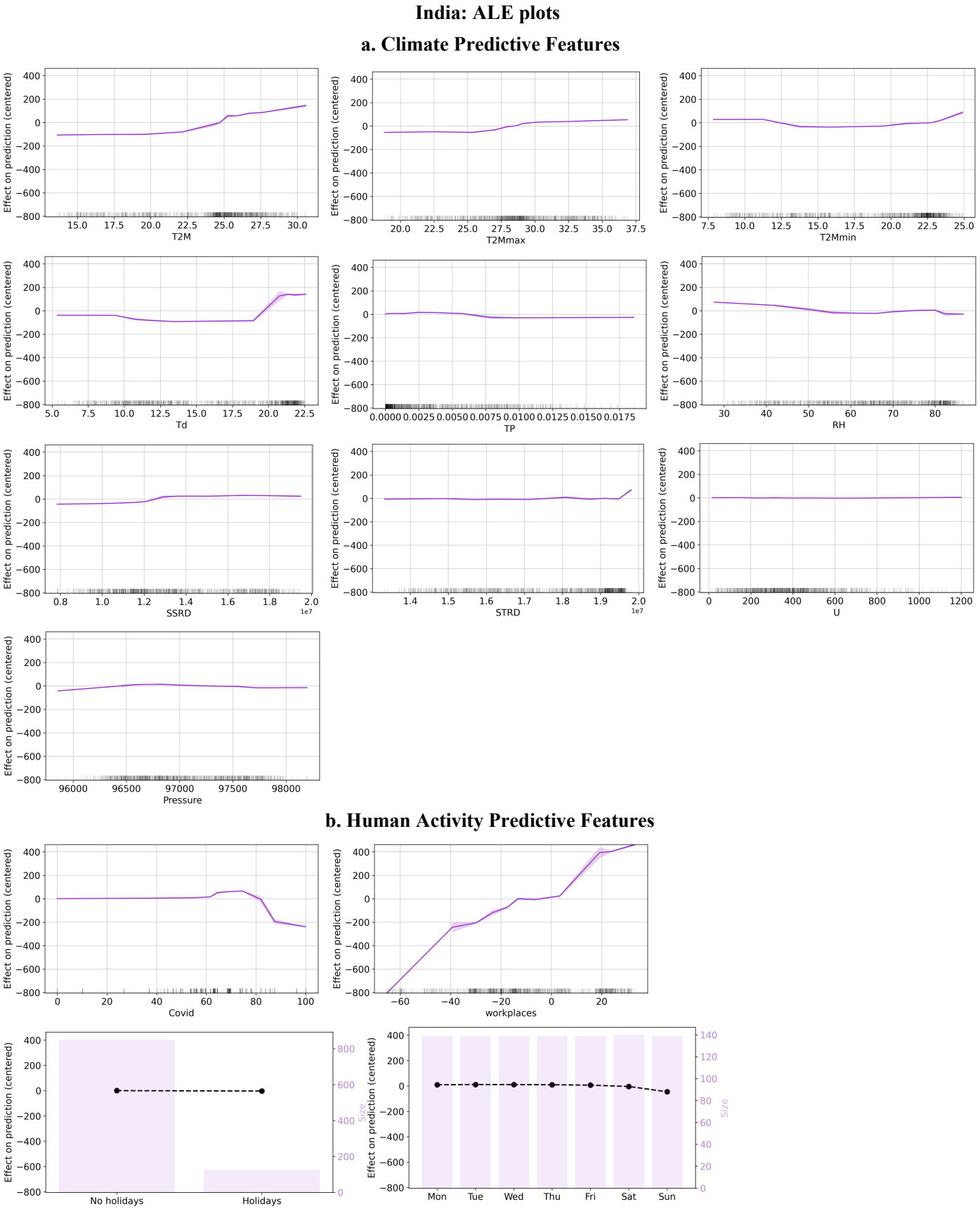

Figure S21. ALE plots depicting the effect of different predictive features on the target variable. The features are divided into two categories: (a) climate features and (b) human activity features. Each ALE plot shows the partial dependence of the target variable on a single feature while controlling for the effects of all other features. The x-axis represents the range of values for each feature, and the y-axis represents the corresponding change in the predicted value of the target variable. The shaded areas represent the 95% confidence intervals for each ALE curve.

India: Validation curves

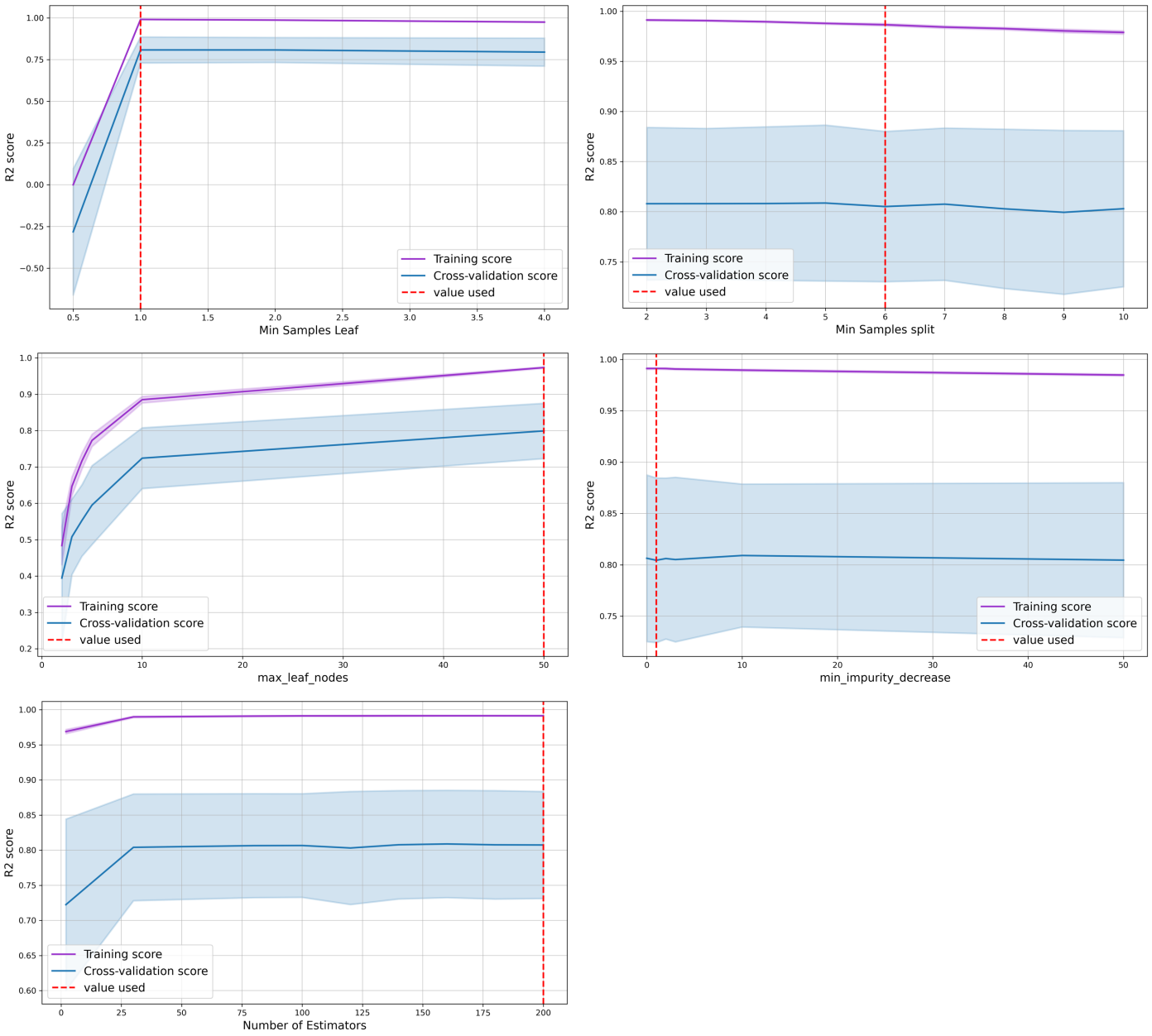

Figure S22. This figure displays validation curves for the hyperparameter of the Random Forest, which is the best model in India. The curves demonstrate how changes in the values of the hyperparameters affect the performance of the model, as measured by the R^2 score. The x-axis represents the range of values for the hyperparameter, and the y-axis shows the mean R^2 cross-validation score and R^2 training score. The validation and training scores are averaged over five scores calculated through cross-validation. The shaded areas represent the 95% confidence intervals for each curve. The red dashed line indicates the value of the hyperparameter selected during the grid-search process.

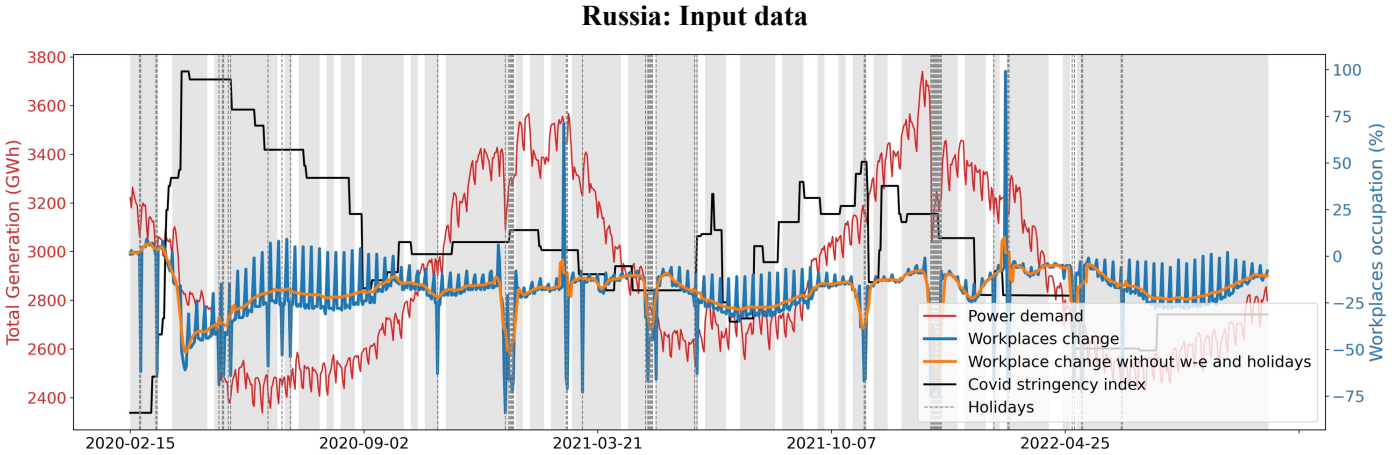

Figure S23. Evolution of human activity predictive features and power demand over the model training and testing period. Shaded area represents the train periods, blank area the test periods.

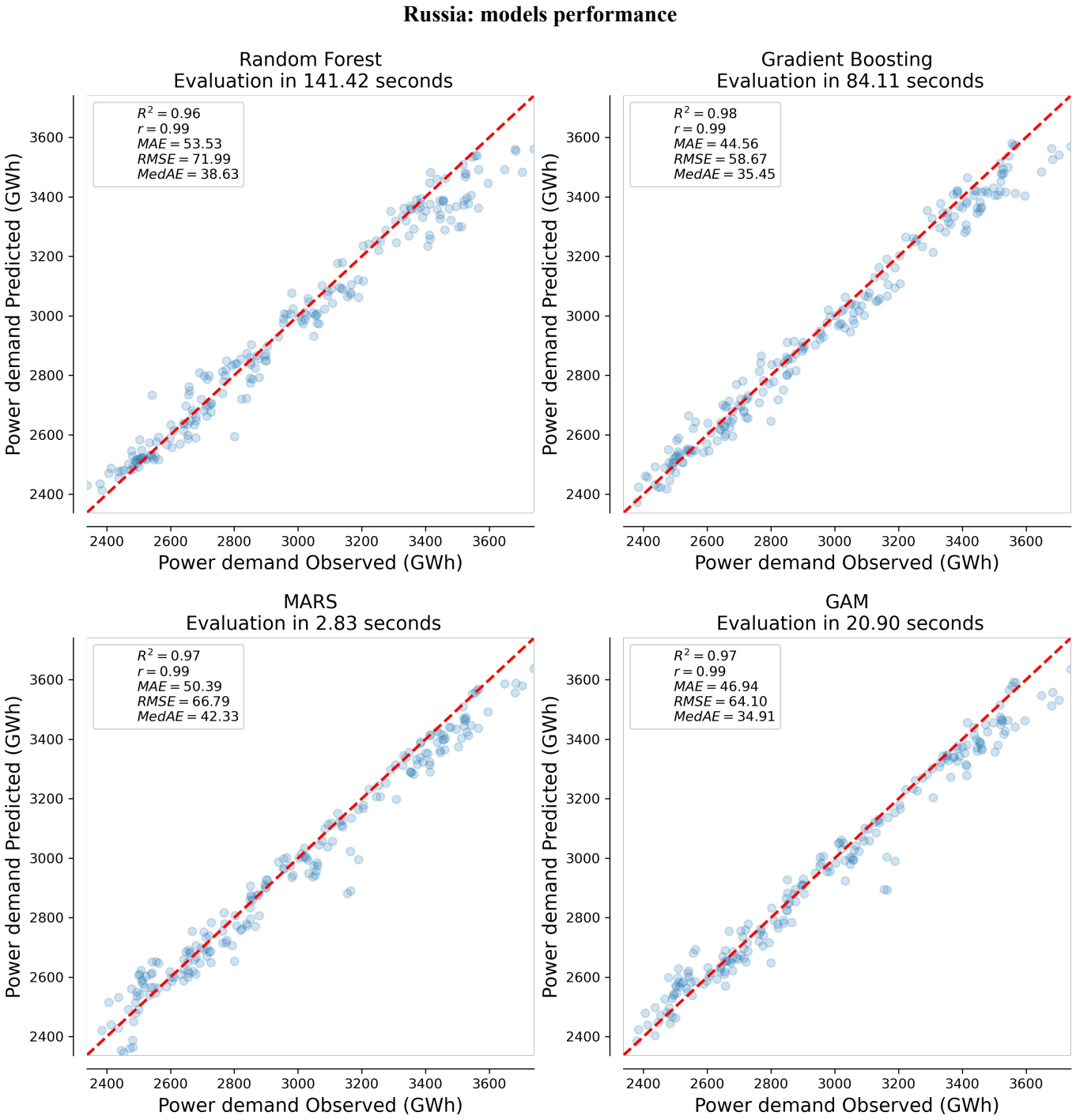

Figure S24. Comparison of machine learning model performance: predicted power demand plotted against observed power demand (blue points). The red dashed line represents the 1:1 line of perfect agreement between predictions and observations.

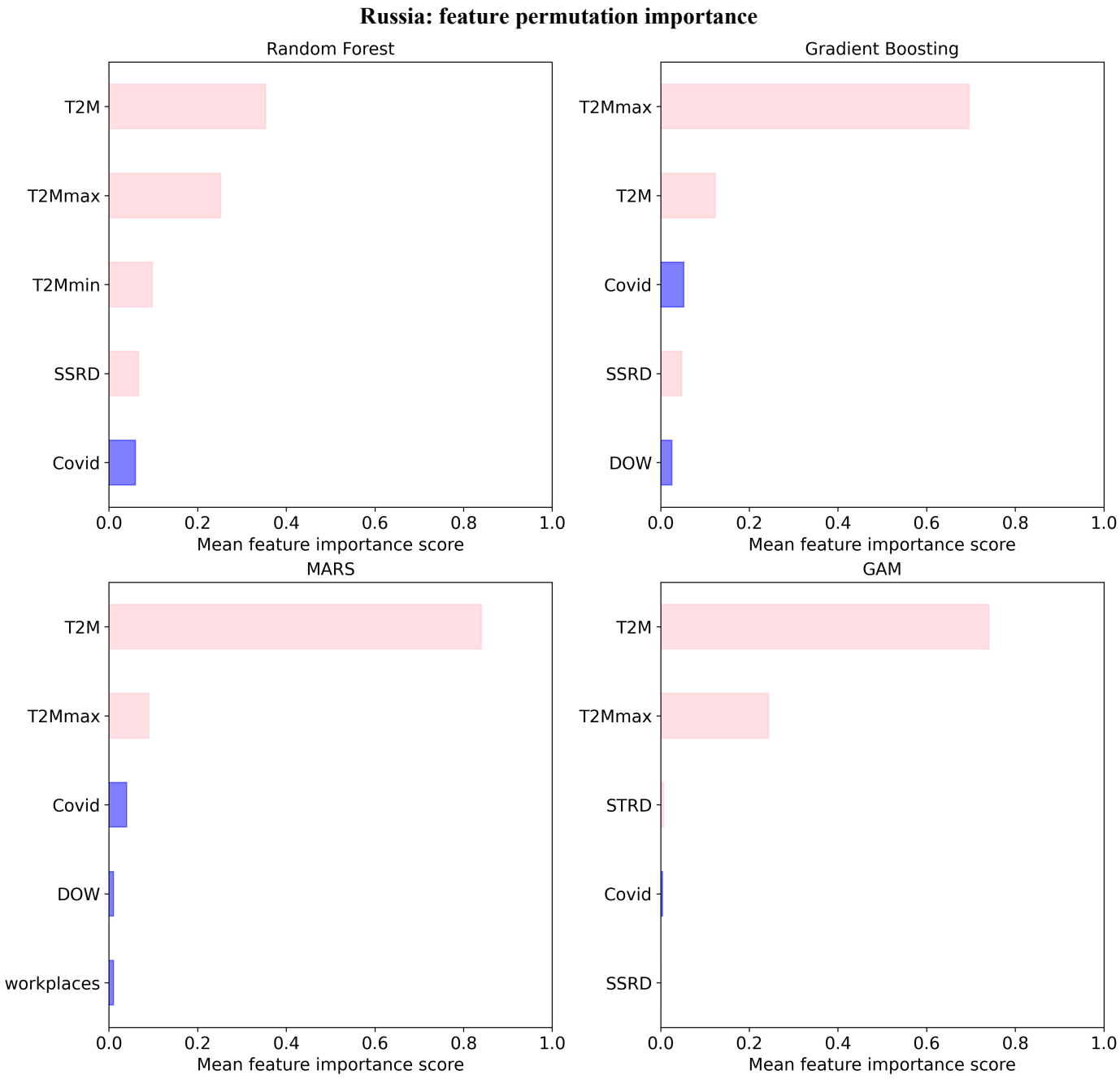

Figure S25. Permutation feature importance scores for the five most important predictive features for four different machine learning models: Random Forest, Gradient Boosting, Multivariate Adaptive Regression Splines (MARS), and Generalized Additive Models (GAM). The x-axis represents the countries, and the y-axis the different predictive features used in the models.

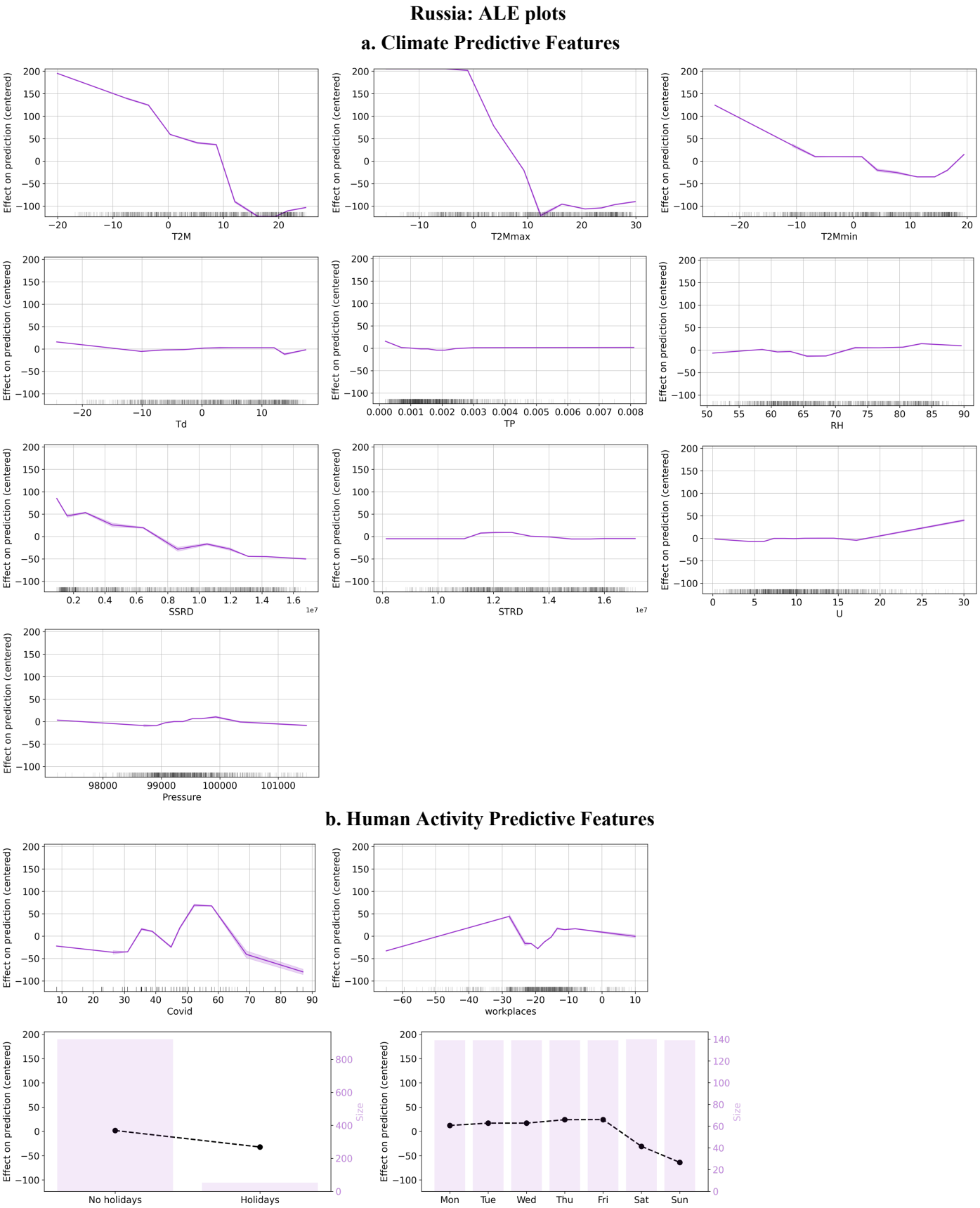

Figure S26. ALE plots depicting the effect of different predictive features on the target variable. The features are divided into two categories: (a) climate features and (b) human activity features. Each ALE plot shows the partial dependence of the target variable on a single feature while controlling for the effects of all other features. The x-axis represents the range of values for each feature, and the y-axis represents the corresponding change in the predicted value of the target variable. The shaded areas represent the 95% confidence intervals for each ALE curve.

Russia: Validation curves

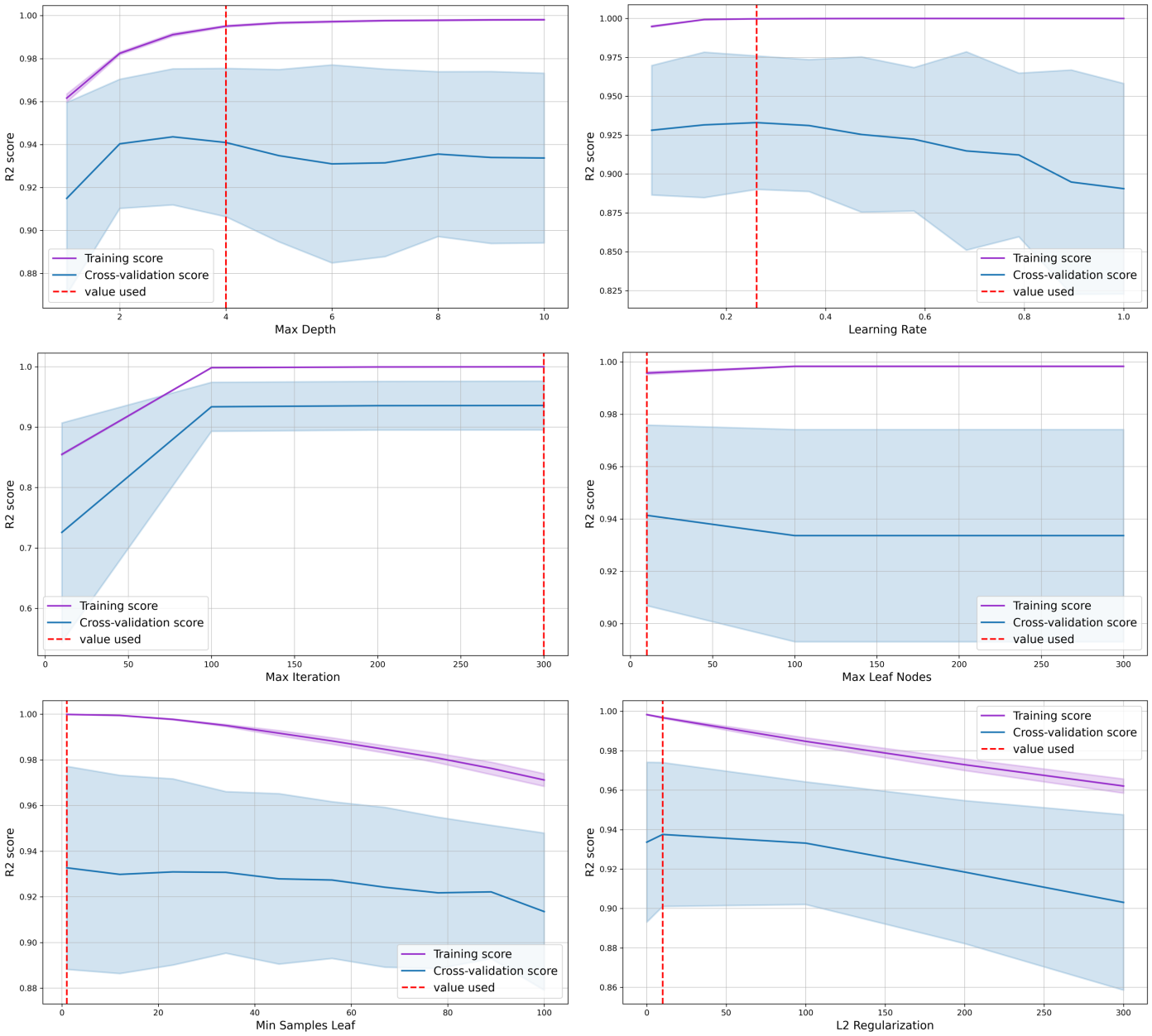

Figure S27. This figure displays validation curves for the hyperparameter of the Gradient Boosting, which is the best model in Russia. The curves demonstrate how changes in the values of the hyperparameters affect the performance of the model, as measured by the R^2 score. The x-axis represents the range of values for the hyperparameter, and the y-axis shows the mean R^2 cross-validation score and R^2 training score. The validation and training scores are averaged over five scores calculated through cross-validation. The shaded areas represent the 95% confidence intervals for each curve. The red dashed line indicates the value of the hyperparameter selected during the grid-search process.

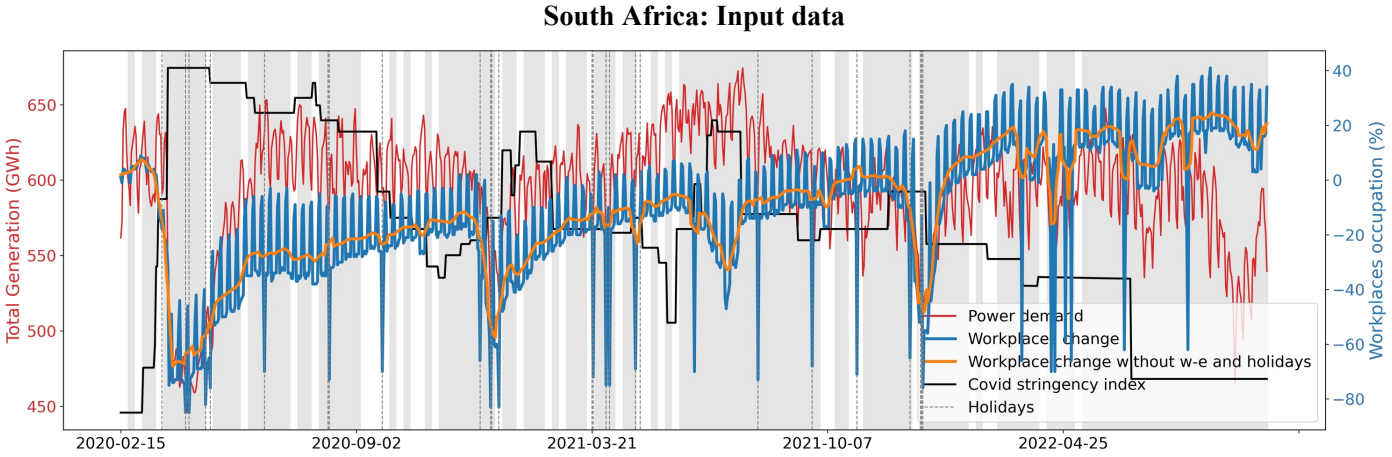

Figure S28. Evolution of human activity predictive features and power demand over the model training and testing period. Shaded area represents the train periods, blank area the test periods.

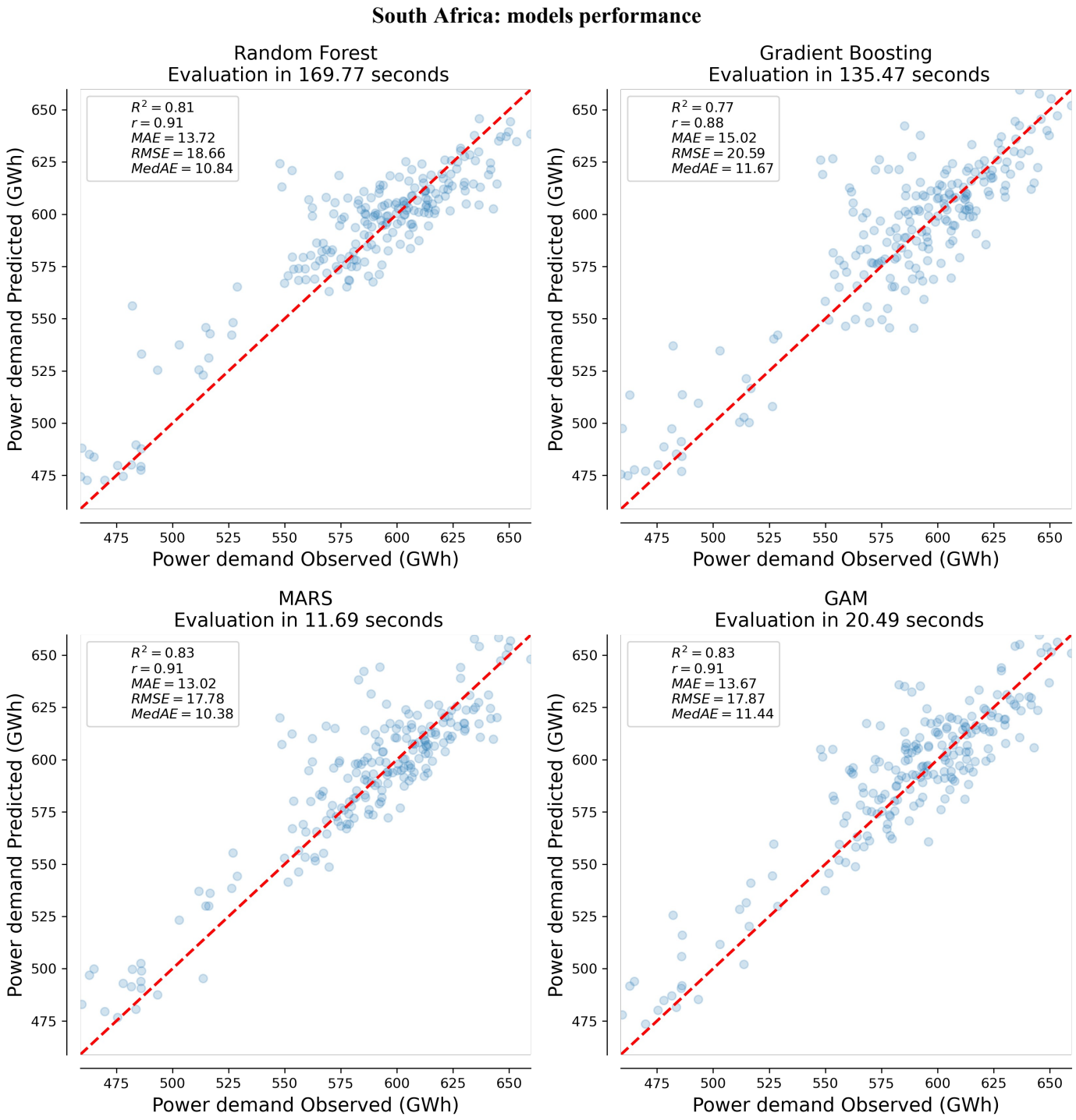

Figure S29. Comparison of machine learning model performance: predicted power demand plotted against observed power demand (blue points). The red dashed line represents the 1:1 line of perfect agreement between predictions and observations.

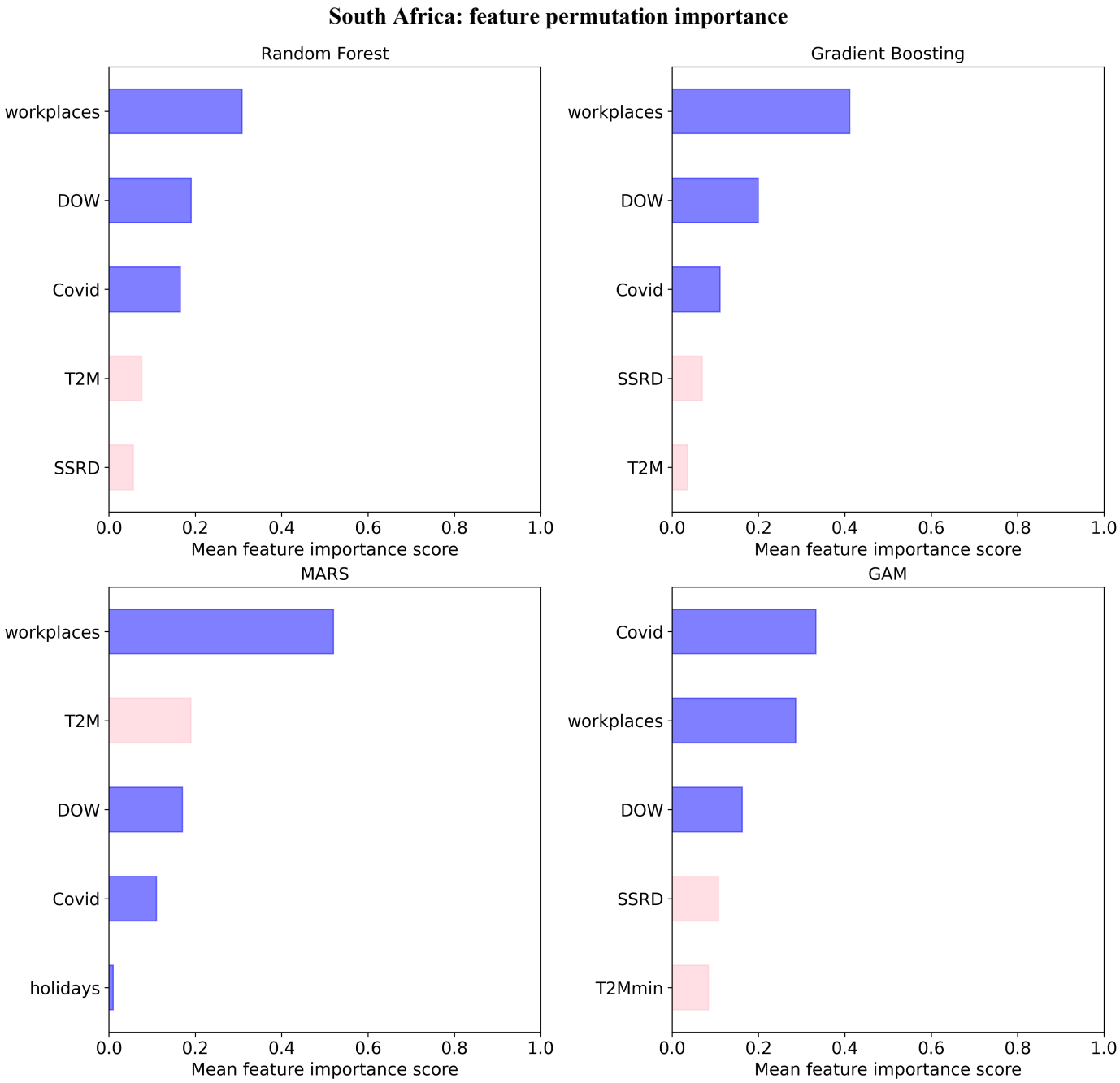

Figure S30. Permutation feature importance scores for the five most important predictive features for four different machine learning models: Random Forest, Gradient Boosting, Multivariate Adaptive Regression Splines (MARS), and Generalized Additive Models (GAM). The x-axis represents the countries, and the y-axis the different predictive features used in the models.

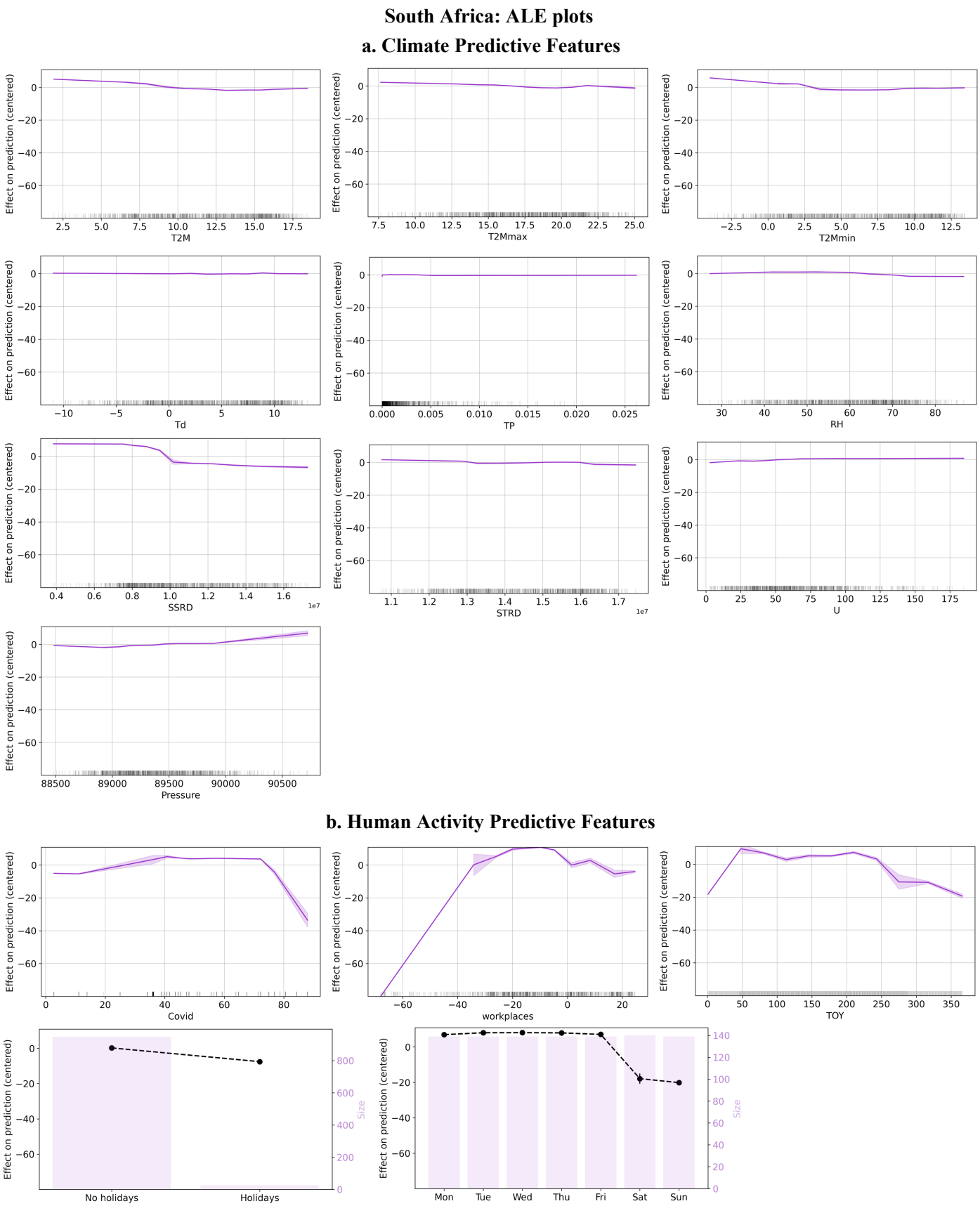

Figure S31. ALE plots depicting the effect of different predictive features on the target variable. The features are divided into two categories: (a) climate features and (b) human activity features. Each ALE plot shows the partial dependence of the target variable on a single feature while controlling for the effects of all other features. The x-axis represents the range of values for each feature, and the y-axis represents the corresponding change in the predicted value of the target variable. The shaded areas represent the 95% confidence intervals for each ALE curve.

South Africa: Validation curves

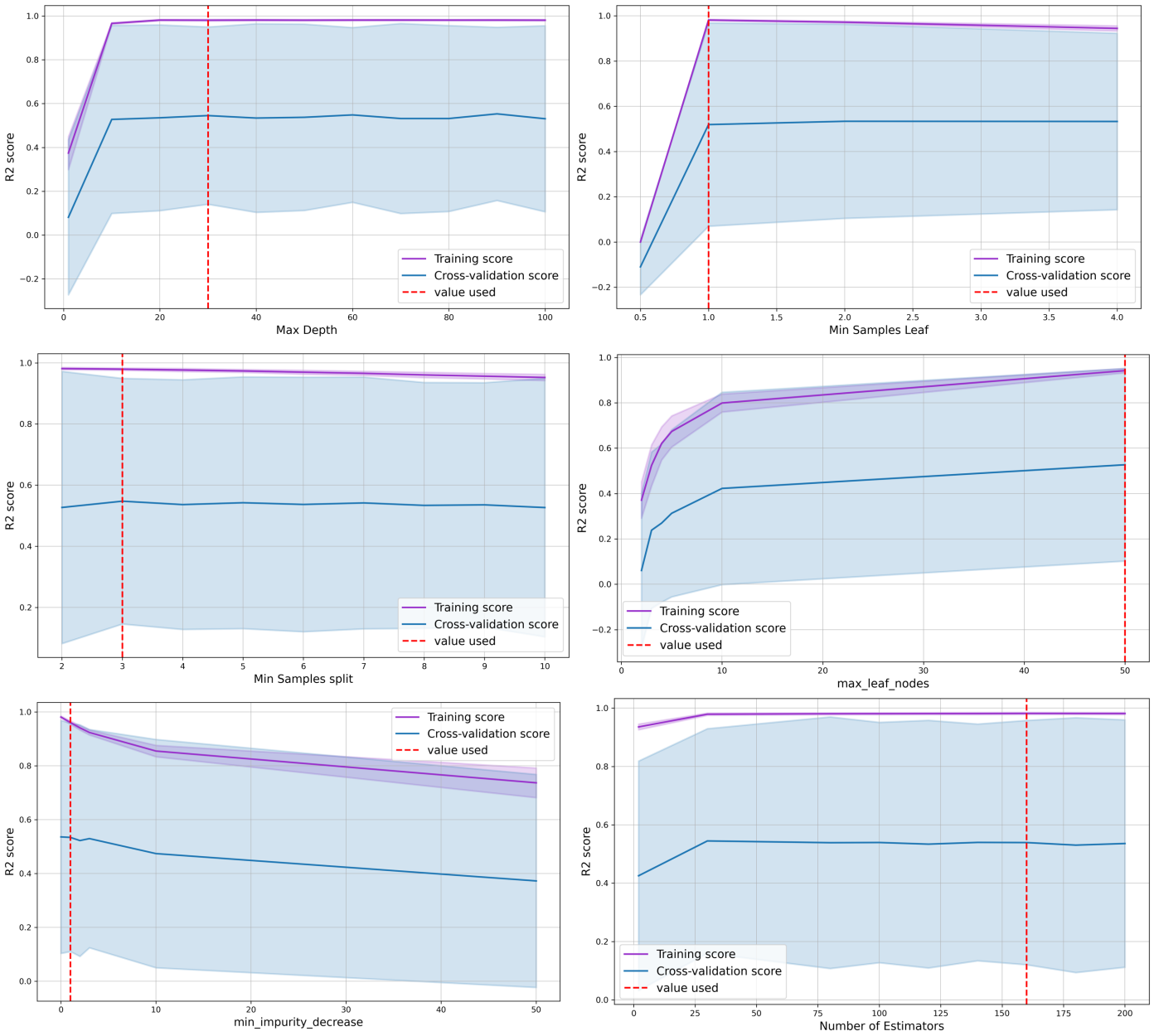

Figure S32. This figure displays validation curves for the hyperparameter of the GAM model, which is the best model in South Africa. The curves demonstrate how changes in the values of the hyperparameters affect the performance of the model, as measured by the R^2 score. The x-axis represents the range of values for the hyperparameter, and the y-axis shows the mean R^2 cross-validation score and R^2 training score. The validation and training scores are averaged over five scores calculated through cross-validation. The shaded areas represent the 95% confidence intervals for each curve. The red dashed line indicates the value of the hyperparameter selected during the grid-search process.

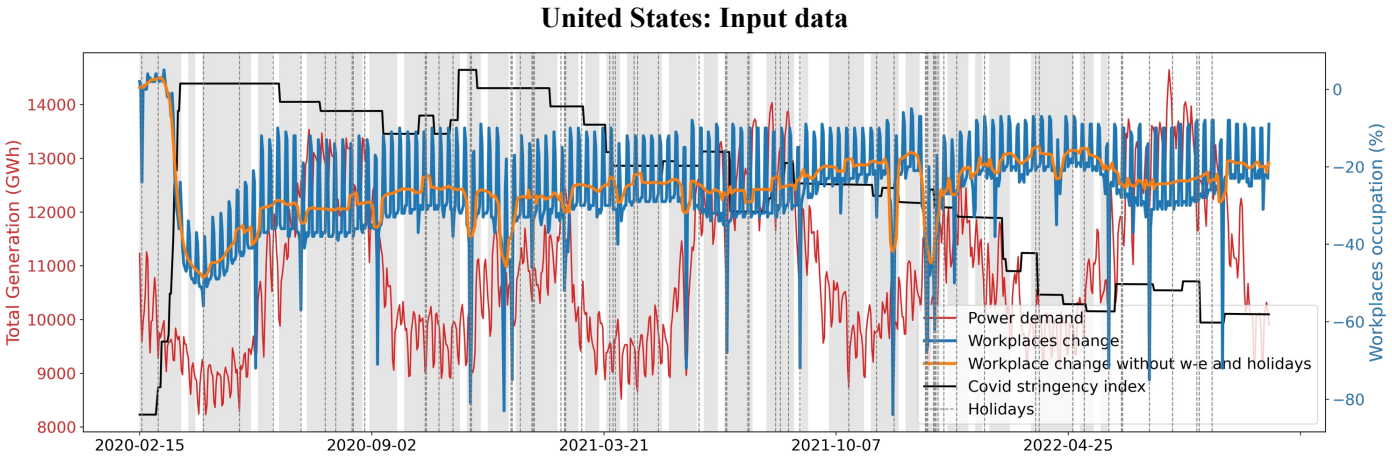

Figure S33. Evolution of human activity predictive features and power demand over the model training and testing period. Shaded area represents the train periods, blank area the test periods.

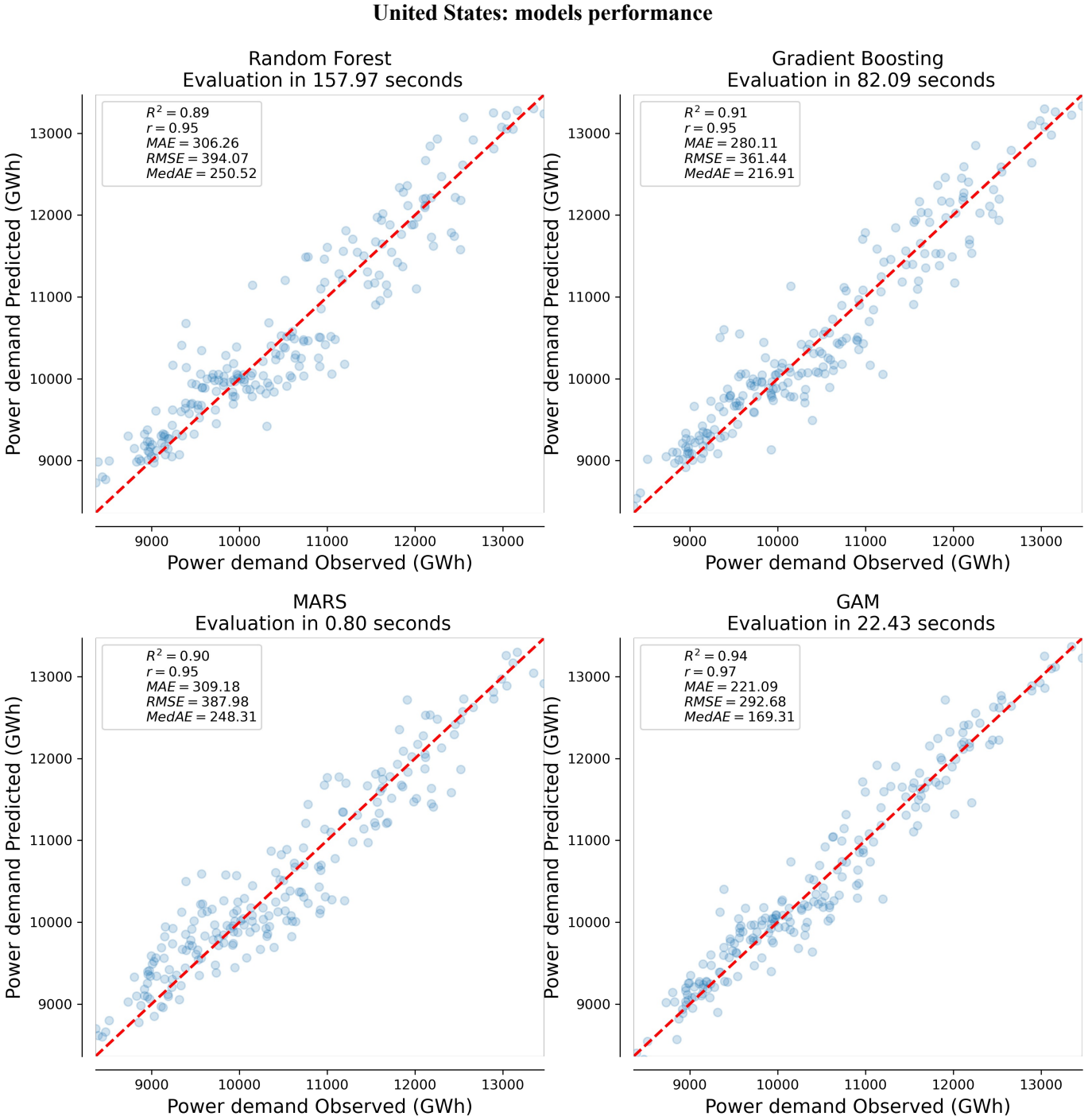

Figure S34. Comparison of machine learning model performance: predicted power demand plotted against observed power demand (blue points). The red dashed line represents the 1:1 line of perfect agreement between predictions and observations.

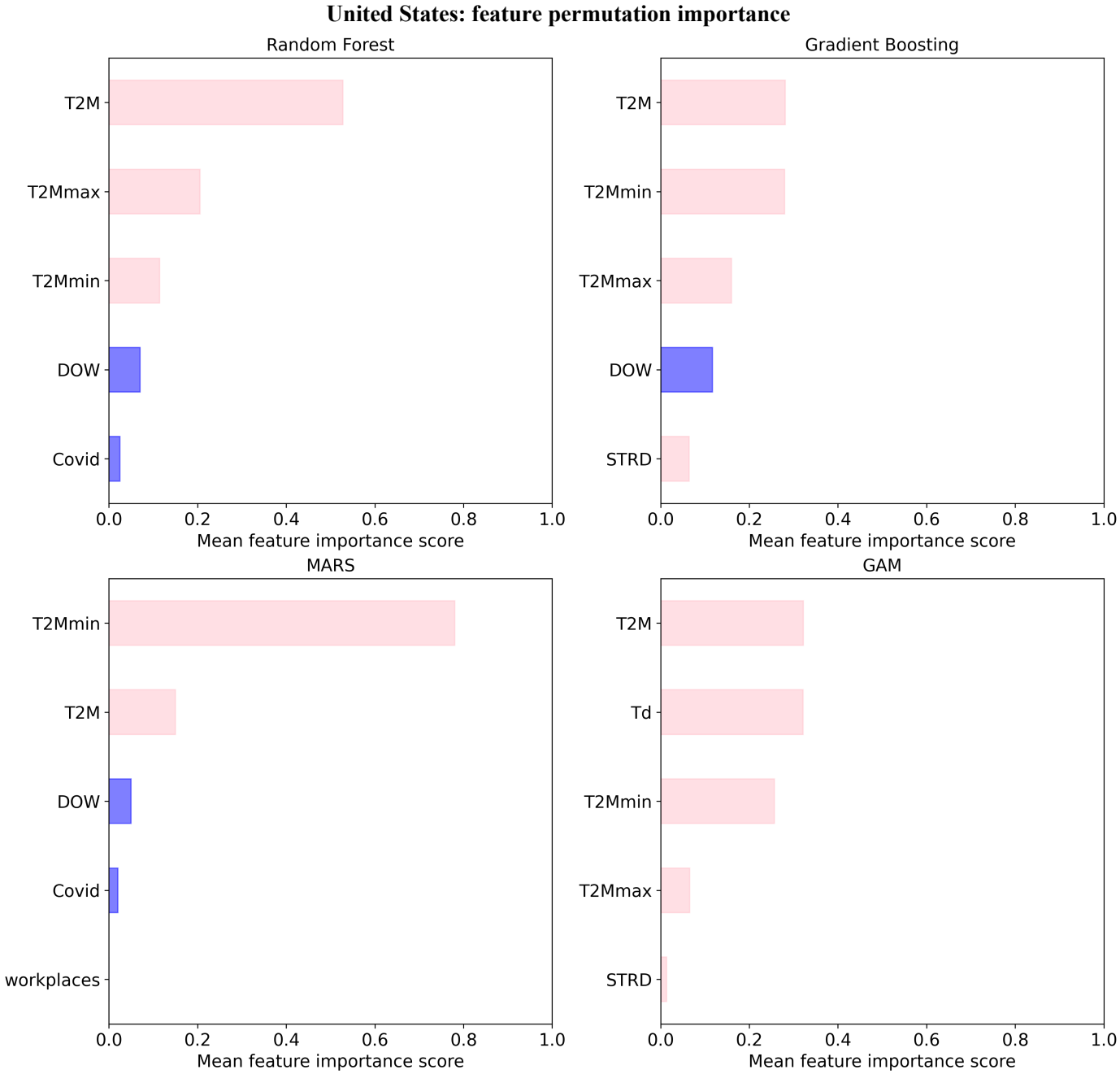

Figure S35. Permutation feature importance scores for the five most important predictive features for four different machine learning models: Random Forest, Gradient Boosting, Multivariate Adaptive Regression Splines (MARS), and Generalized Additive Models (GAM). The x-axis represents the countries, and the y-axis the different predictive features used in the models.

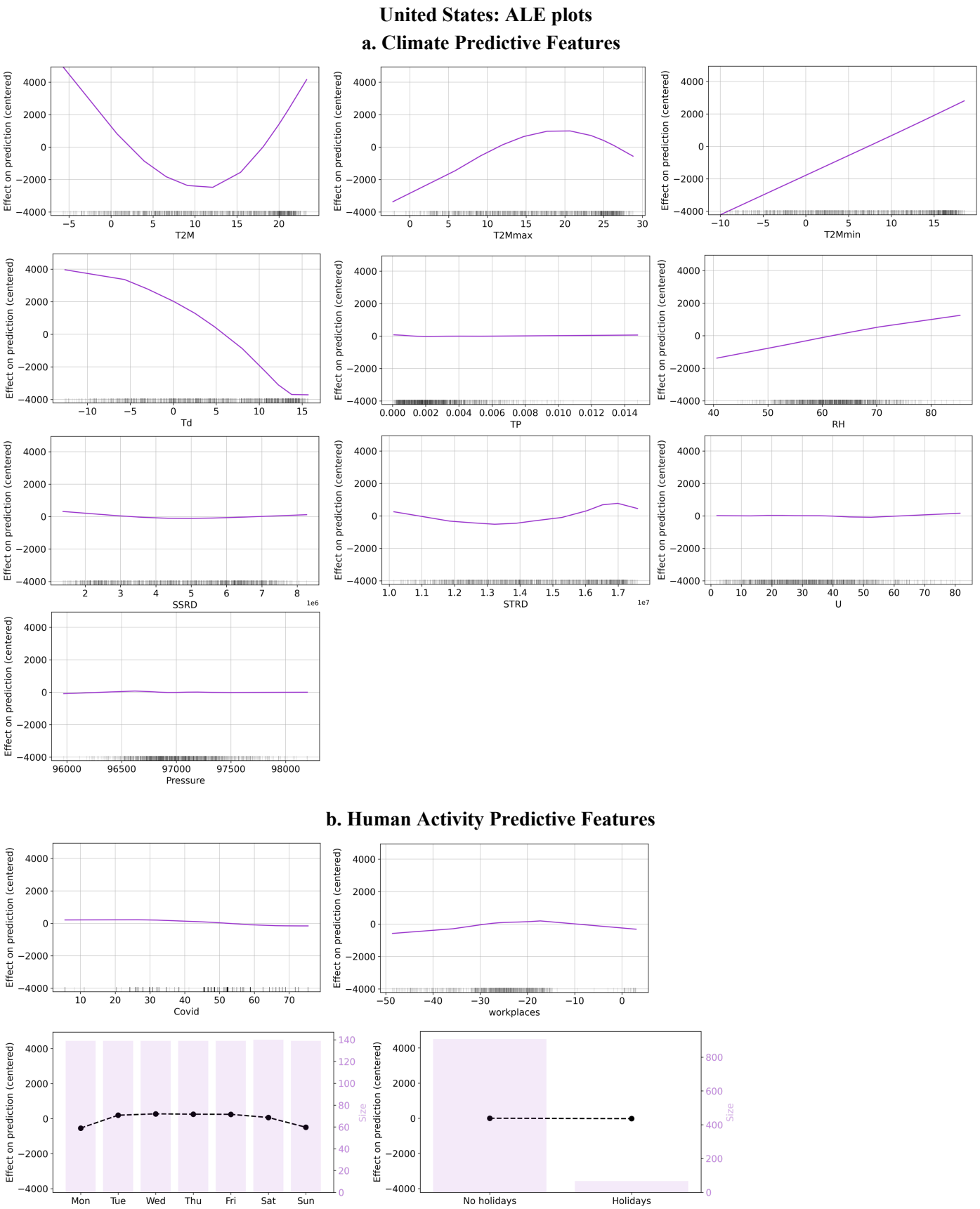

Figure S36. ALE plots depicting the effect of different predictive features on the target variable. The features are divided into two categories: (a) climate features and (b) human activity features. Each ALE plot shows the partial dependence of the target variable on a single feature while controlling for the effects of all other features. The x-axis represents the range of values for each feature, and the y-axis represents the corresponding change in the predicted value of the target variable. The shaded areas represent the 95% confidence intervals for each ALE curve.

APPENDIX C

APPENDIX C - ADDITIONAL CO_2 MAPS

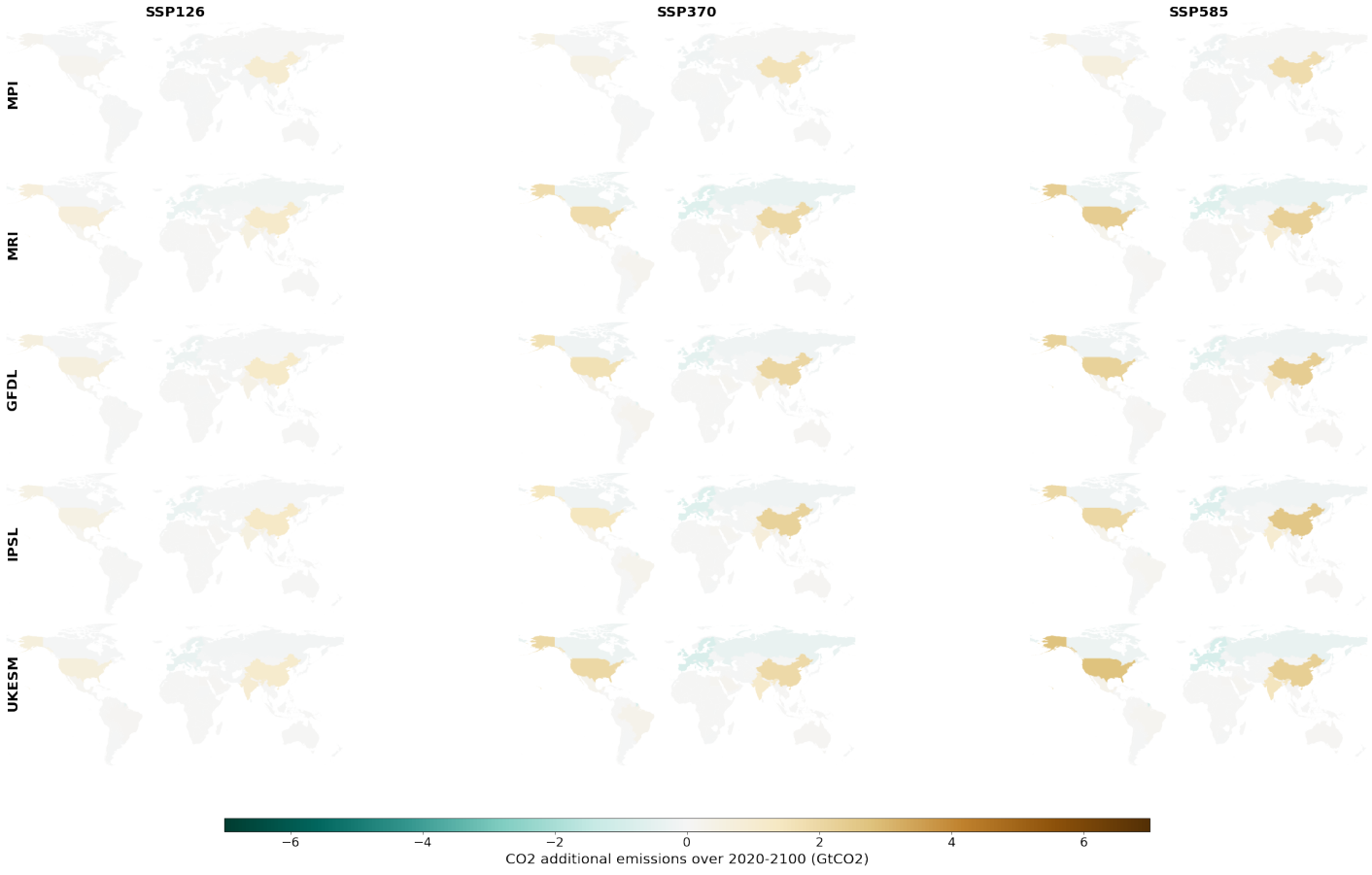

Figure C.1: Additional CO_2 emissions from power production compared to a scenario with no climate change for the five ESMs and Random Forest.

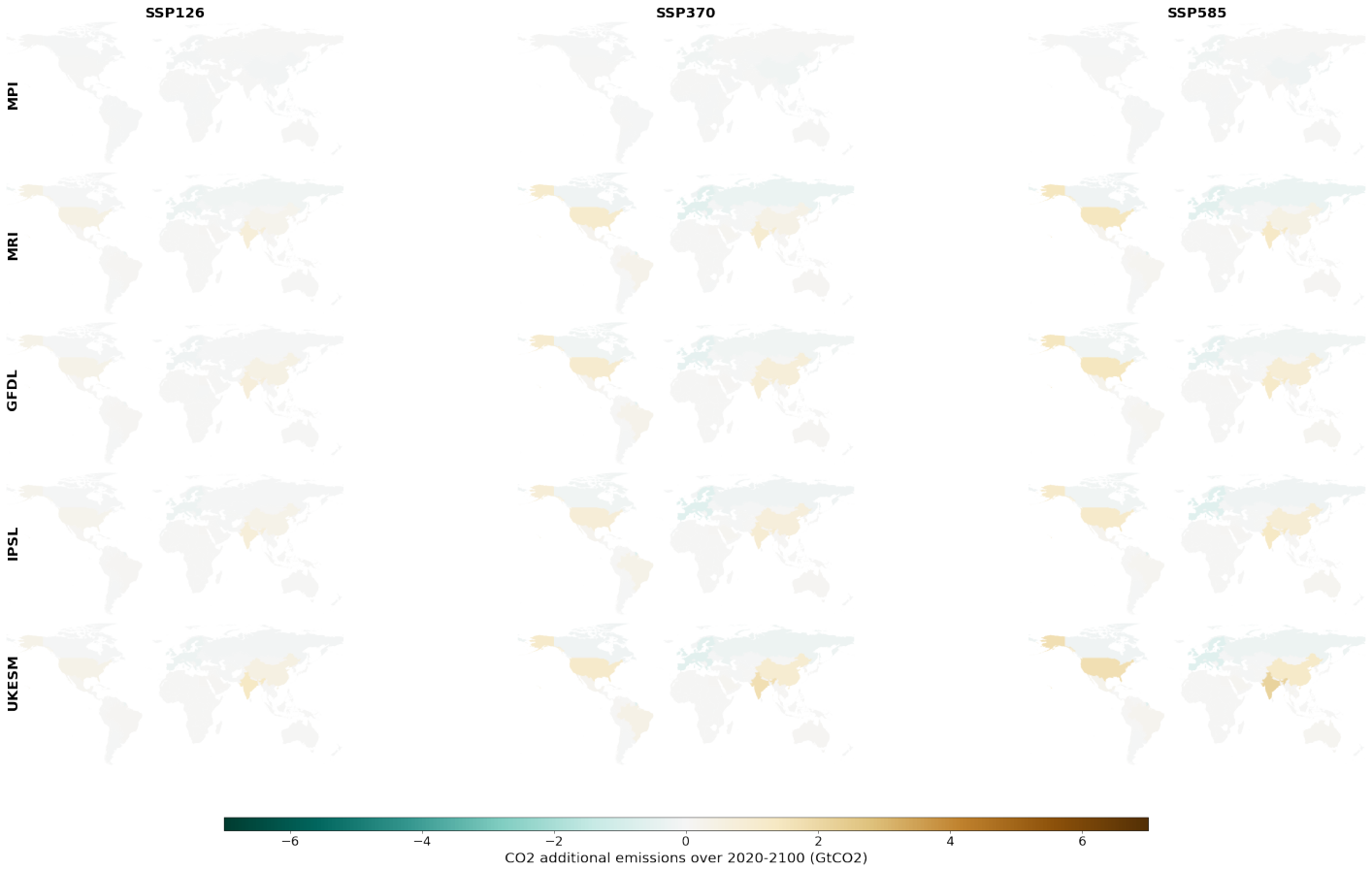

Figure C.2: Additional CO_2 emissions from power production compared to a scenario with no climate change for the five ESMs and Gradient Boosting.

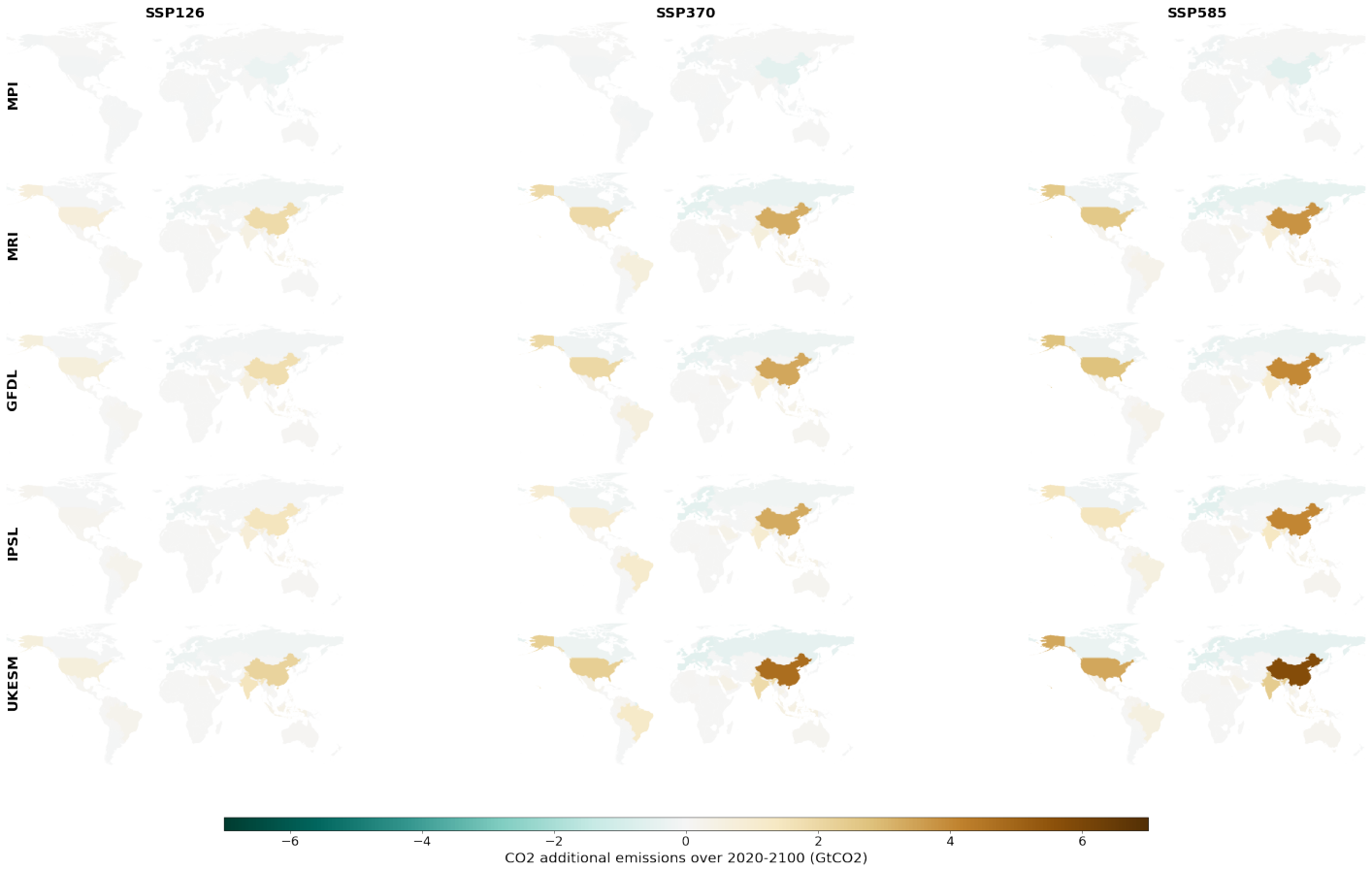

Figure C.3: Additional CO_2 emissions from power production compared to a scenario with no climate change for the five ESMs and MARS.

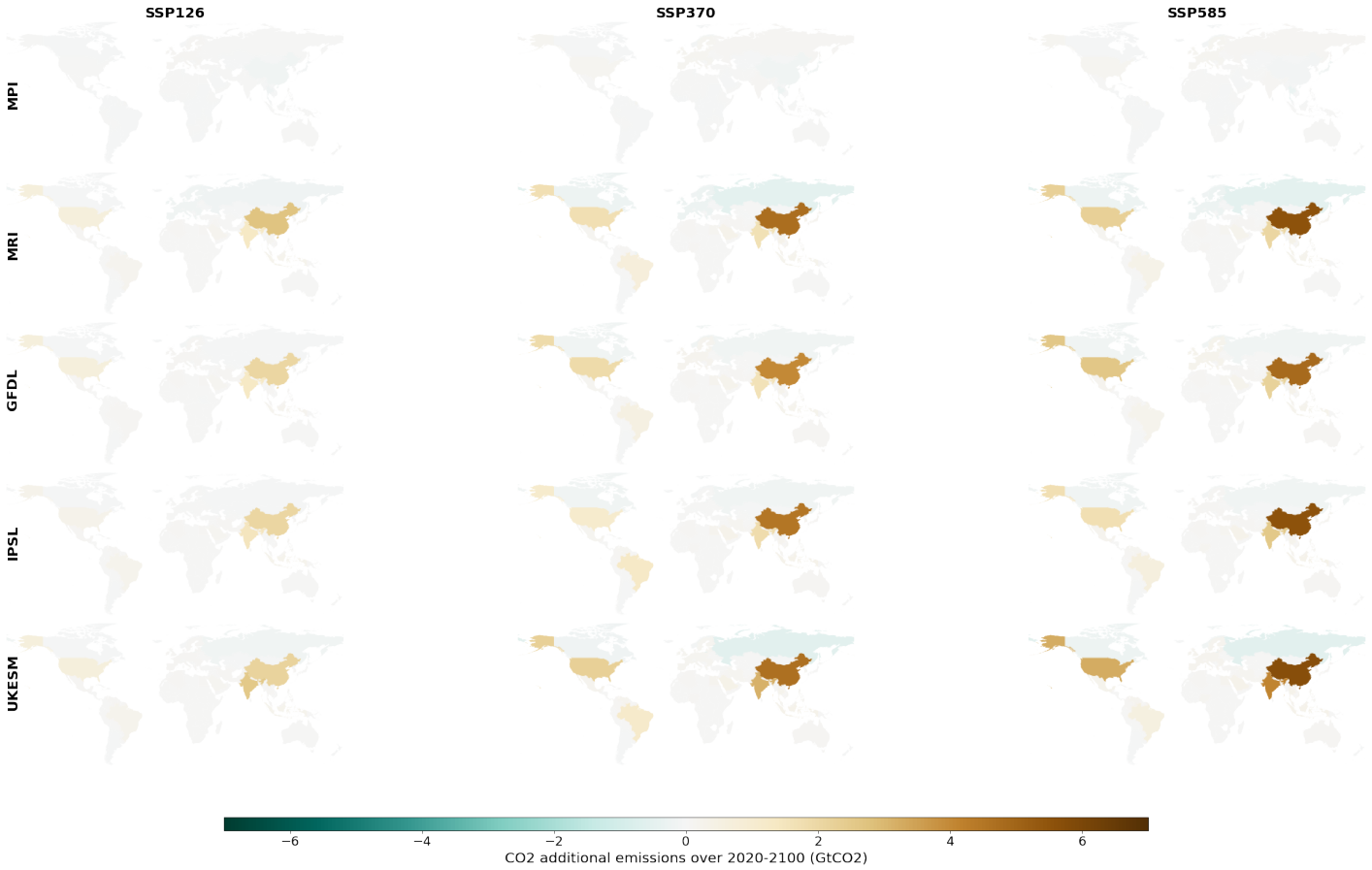

Figure C.4: Additional CO_2 emissions from power production compared to a scenario with no climate change for the five ESMs and GAM.